Oscillatory boundary layers without and with currents

Author:
You, Zai-Jin

Publication Date:
1992

DOI:
https://doi.org/10.26190/unsworks/18355

Oscillatory Boundary Layers without and with Currents

You Zai-Jin

A thesis submitted in fulfillment of the requirements

for the Degree of Doctor of Philosophy

UNIVERSITY OF NEW SOUTH WALES

Department of Water Engineering

School of Civil Engineering

Kensington N.S.W 2033

AUSTRALIA

March, 1992

ACKNOWLEDGMENTS

The author wishes to express his deepest appreciation to Professor David Wilkinson for his advice, kind guidance and encouragement during the experimental study and for his final review of this manuscript.

The author is greatly indebted to Dr. Peter Nielsen for his kind guidance, encouragement and many helpful discussions throughout this research work and for his careful review of this manuscript.

The staff of the Water Research Laboratory of University of New South Wales is thanked for providing assistance during the construction and maintenance of the experimental set-up.

Finally, the author offers special thanks to his parents for providing kind guidance and encouragement during the formative years of his life.

TABLE OF CONTENTS

LIST OF FIGURES

LIST OF TABLES

NOTATION

a	[m]	Wave height amplitude
A	[m]	Semi–excursion of the free stream velocity
$A\omega$	[m/s]	Amplitude of the the free stream velocity
C	[m/s]	Wave celerity
d	[m]	Mean grain diameter of bed material
d_c	[m]	A reference elevation from the bed.
D_1	[m]	Elevation of the upper edge of the inner layer
D_2	[m]	Elevation of the upper edge of the overlap layer
$D(z)$		Nondimensional velocity defect
e		Base of the natural logarithm (=2.718..)
f_w		Wave friction factor
f_c		Current friction factor
h	[m]	Water depth
h_b	[m]	Water depth of breaking waves
H	[m]	Wave height
H_b	[m]	Breaking wave height
K_1	[m]	Apparent roughness
Ker x		Kelvin function
Kei x		Kelvin function
K_N	[m]	Nikuradse roughness
K_o		Wave damping coefficient
K_1	[m]	Apparent roughness
K_∞		Constant value defined in Eq.(3.30)
l	[m]	Mixing length
L	[m]	Wave length
$\bar{p}_b$	[N/m^2]	Bed Shear stress related to the steady component
$\tilde{p}_b$	[N/m^2]	Bed shear stress related to the periodic component
P	[N/m^2]	Pressure
$\bar{P}$	[N/m^2]	Pressure related to steady flow
$\tilde{P}$	[N/m^2]	Pressure related to wave motion

t	[s]	Time
$\bar{u}$	[m/s]	Eulerian time mean velocity
T	[s]	Wave period
U	[m/s]	Horizontal velocity component
$\bar{U}$	[m/s]	Steady or time–averaged horizontal velocity component
$\tilde{U}$	[m/s]	Periodic or phase–averaged horizontal velocity component
u'	[m/s]	Random horizontal velocity component
$\tilde{U}_d$	[m/s]	Velocity defect
$\bar{U}_{dc}$	[m/s]	A reference current velocity at $z = d_c$
$\bar{U}_M$	[m/s]	Measured mass transport velocity
$\bar{U}_L$	[m/s]	Mass transport velocity given by Longuet–Higgins (1953)
$U_\infty(t)$	[m/s]	Free stream velocity outside the boundary layer
$\lvert U \rvert$	[m/s]	Velocity amplitude
$\bar{U}^*$	[m/s]	Current friction velocity at the bed
$\hat{U}_w^*$	[m/s]	Wave friction velocity at the bed
$\hat{U}_{cw}^*$	[m/s]	Friction velocity at the bed related to waves and currents
$\bar{W}$	[m/s]	Vertical steady velocity component
$\tilde{W}$	[m/s]	Vertical periodic velocity component
w'	[m/s]	Vertical random velocity component
x	[m]	Horizontal distance
y	[m]	Vertical coordinate located at mean water level upwards
z	[m]	Vertical coordinate located at the bed upwards
z_o	[m]	$z_o = 30K_N$
z_1	[m]	$z_1 = 30K_1$
z_A	[m]	Bed level
β		Defined in Eq.(2.135)
δ	[m]	Thickness of the boundary interaction zone
δ_1	[m]	Boundary layer thickness after Jonsson & Carlsen (1976)
δ_o	[m]	$\delta_o = 0.4\delta_1$

δ_d	[m]	Thickness of the boundary layer after Kajiura (1968)
δ_s	[m]	Thickness of the boundary layer after Sleath (1987)
δ_w	[m]	Thickness of the wave boundary layer
δ_y	[m]	Thickness of the boundary layer predicted
$\varDelta$	[m]	Thickness of a sand layer
ε	[m^2/s]	Eddy viscosity induced in the boundary layer
ε_c	[m^2/s]	Eddy viscosity for steady flow
ε_w	[m^2/s]	Eddy viscosity for wave motion
η	[m]	Ripple height
$\overline{\eta}$	[m]	Mean current water level
θ	[rad.]	Wave phase [$\theta = \omega t - Kx$]
$\varkappa$		von Karman constant (≈ 0.4)
λ	[m]	Ripple length
ν	[m^2/s]	Kinematic viscosity of water
ξ		A variable defined in Eq.(2.134)
ζ_x	[m]	Horizontal displacement of a water particle
ζ_y	[m]	Vertical displacement of a water particle
ω	[rad./s]	Angular frequency
ϕ	[rad.]	Velocity phase shift in the boundary layer
ϕ_d	[rad.]	Phase shift of defect velocity in the boundary layer
$\varPhi$	[rad.]	An angle between current and direction of wave propagation
π		=3.14159 ...
ϱ	[Kg/m^3]	Fluid density
τ	[N/m^2]	Horizontal shear stress
$\bar{\tau}$	[N/m^2]	Shear stress due to steady flow
$\bar{\tau}_b$	[N/m^2]	Bed shear stress due to steady flow
$\tilde{\tau}$	[N/m^2]	Shear stress due to wave motion
$\hat{\tau}_{wb}$	[N/m^2]	Bed shear stress due to wave motion
$\hat{\tau}_b$	[N/m^2]	Horizontal shear stress at the bed

CHAPTER 1

INTRODUCTION

§1.1 SPECIFIC AIMS OF THE PRESENT STUDY

The specific objective of the present study is to investigate turbulent oscillatory boundary layers without and with currents, and the effect of the bed roughness on the mass transport velocity near the bed due to progressive waves. The detailed objectives of the present study can be divided into three parts as follows:

The first objective is to qualitatively and quantitatively study the eddy viscosity in turbulent oscillatory boundary layers without currents, and then to develop an eddy viscosity model to predict the velocity distribution and wave friction factor. The reason for this is that the concept of eddy viscosity in turbulent oscillatory boundary layers has not been fully understood, for example, some investigators [Kajiura (1968), Brevik (1981) and Myrhaug (1982)] assumed a time–independent eddy viscosity to model turbulent oscillatory boundary layers whereas other investigators [Horikawa & Watanabe (1968) and Trowbridge & Madsen (1984)] argued that the eddy viscosity should be considered to be time–dependent, and that on the other hand, eddy viscosity or momentum diffusion coefficient, the velocity distribution and wave friction factor in turbulent oscillatory boundary layers are important factors in determining the rate of sediment transport.

The second objective of the study is to experimentally examine the effect of bed roughness and wave height on the mass transport velocity or drift velocity near the bed due to progressive waves. Longuet–Higgins (1956) theoretically derived that the mass transport velocity was proportional to the square of the wave height H^2 and possibly not affected by bed roughness even in turbulent boundary layers. On the other hand, Brebner (1966) found experimentally that in the smooth laminar boundary layer the mass transport velocity near the bed increased with increasing bed roughness while in the turbulent boundary layer the mass transport velocity decreased with increasing the bed roughness and was proportional to $H^{1.2}$ rather than H^2 predicted by Longuet Higgins (1956).

The final objective is to develop a model which distinguishes between the eddy viscosities for the steady component and the periodic component of combined wave–current flows, and to use this model to predict the velocity distributions of combined wave–current flows and bed friction factors.

§1.2 SUMMARY OF CONTENTS

In Chapter 2, based on the equation of motion and the definition of eddy viscosity, we will derive a formula to qualitatively examine whether the eddy viscosity is time dependent or time independent when only the first harmonic component is considered, and then according to the formula provided, the eddy viscosity in the boundary layer will be calculated from experimental data, and finally based on the calculated eddy viscosity data we will develop an analytical model and compare it with the models of Kajiura (1968) and Myrhaug (1982) and with the experimental data such as Jonsson & Carlsen (1976) Test No.1 and Test No.2, van Doorn (1981) V00RA, van Doorn (1982) S00RAL and M00RAL, Sleath (1982) Test–3, Test–4, Test–5, Test–9 and Test–10, and Jensen (1989) Test–12 and Test–13.

Chapter 3 describes an experimental study of the variation of the maximum mass transport velocity or drift velocity near the bed with bed roughness due to progressive waves. Maximum drift velocities are measured over three different bed configurations;

a smooth bed, sand bed and gravel bed to examine whether the bed roughness increases the mass transport velocity as Brebner (1966) experimentally found, or has no effect on it as postulated by the theory of Longuet–Higgins (1956).

In Chapter 4, based on the equation of motion for the steady flow and the wave motion in the combined flow we will derive the formulas to calculate the eddy viscosities of waves and currents, and then according to the calculated eddy viscosity data we will quantitatively discuss whether the eddy viscosity for the steady flow is different from that for the wave motion. Finally we will develop an analytical model and compare it with experimental data such as van Doorn (1981) V10RA & V20RA and van Doorn (1982) S10RAL, S20RAL, M10RAL & M20RAL

Chapter 5 gives a simple example to demonstrate how to calculate wave friction factor and the current velocity profile in the combined wave–current flow.

In Chapter 6, the conclusions of the present study will be summarized, and suggestions are offered for further research.

CHAPTER 2

OSCILLATORY BOUNDARY LAYERS WITHOUT CURRENTS

§2.1 INTRODUCTION

§2.1.1 OSCILLATORY BOUNDARY LAYERS

The aim of the present section is to give a general idea about what the oscillatory boundary layer is, and to answer these questions why the boundary layer needs to be studied and what kinds of problems will need investigating in the oscillatory boundary layer.

The bottom boundary layer is intuitively defined as a layer in which the flow is significantly influenced by the bed. The thickness of the layer has been defined in various ways, and the different definitions will lead to somewhat different results, e.g. one of the formulas for estimation of the thickness of the boundary layer is

$$\delta_w \quad \propto \quad \sqrt{\varepsilon \; T} \tag{2.1}$$

in which ε is the eddy viscosity in the boundary layer, and T the period of oscillation. Thus, based on Eq.(2.1) the thickness of the boundary layer for tidal flow with a period of 12 hours will be approximately 66 times thicker than that of the wave motion with a period of 10 seconds. Therefore, the tidal boundary layer thickness is often equal to the mean water depth while the wave boundary layer thickness is only a small fraction of the mean water depth, e.g. a few millimetres over a smooth solid bed, and a few centimetres over a flat mobile sand bed. Although the water motion induced by natural waves is generally not simple harmonic, it is instructive and useful to study a simple harmonic case, and to use it as an approximation to natural wave boundary layers.

For general wave fields, the orbital motion of a water particle is circular in deep water, and elliptical in intermediate and shallow water. If the wave is small and with long period, based on linear or Airy wave theory the horizontal and vertical displacements of a water particle from its mean position (x, y) are respectively

$$\zeta_x = \frac{H}{2}\frac{\cosh k(y+h)}{\sinh kd}\sin(\omega t - kx) \tag{2.2}$$

$$\zeta_y = \frac{H}{2}\frac{\sinh k(y+h)}{\sinh kd}\cos(\omega t - kx) \tag{2.3}$$

where

H : Wave Height,

k : Wave number ($= \frac{2\pi}{L}$),

L : Wave length,

T : Wave period,

ω : Angular frequency ($= \frac{2\pi}{T}$),

y : Elevation measured upward from the mean water level,

x : Horizontal distance,

t : Time variable.

From Eqs.(2.2) and (2.3), the horizontal and vertical local fluid velocities can be determined as

$$U(x,y,t) = \frac{\partial \zeta_x}{\partial t} = \frac{H\omega}{2}\frac{\cosh k(y+h)}{\sinh kd}\cos(\omega t - kx) \tag{2.4}$$

$$W(x,y,t) = \frac{\partial \zeta_y}{\partial t} = -\frac{H\omega}{2}\frac{\sinh k(y+h)}{\sinh kd}\sin(\omega t - kx) \tag{2.5}$$

and the horizontal and vertical semi−orbital amplitudes of the particle in motion from its mean position (x, y) are given respectively by

$$A(y) = \frac{H}{2}\frac{\cosh k(y+h)}{\sinh kd} \tag{2.6}$$

$$B(y) = \frac{H}{2}\frac{\sinh k(y+h)}{\sinh kd} \tag{2.7}$$

Eqs.(2.6) and (2.7) indicate that $A(y)$ and $B(y)$ both decrease with decreasing elevation, but $A(y)$ decreases more slowly than $B(y)$ as shown in Fig.2.1. Consequently, the orbit of the particle becomes flatter and flatter with decreasing elevation y until the vertical motion is almost zero and the particle near the bed moves back and forth in purely horizontal oscillatory motion, in which the horizontal displacement of the water particle can be estimated by taking $y \rightarrow -h$ in Eq.(2.6)

$$A = \frac{H}{2\sinh kd} \tag{2.8}$$

and the horizontal velocity is

$$U(x,t)|_{y\rightarrow -h} = A\omega\cos(\omega t - kx) \tag{2.9}$$

Assuming that a bottom boundary layer exists and that its thickness is much less than water depth, the horizontal velocity at the upper edge of the boundary layer is given by

$$U_\infty(t) \approx A\omega\cos\omega t \tag{2.10}$$

Here, ∞ denotes the outer edge of a layer as shown in Fig.2.1. Inside this layer, Airy wave theory derived under the assumption of an inviscid fluid can not be applied to calculate local fluid velocities and accelerations due to the effects of bottom friction. Therefore, a different theory is required to describe the velocity distribution and shear stress in the boundary layer.

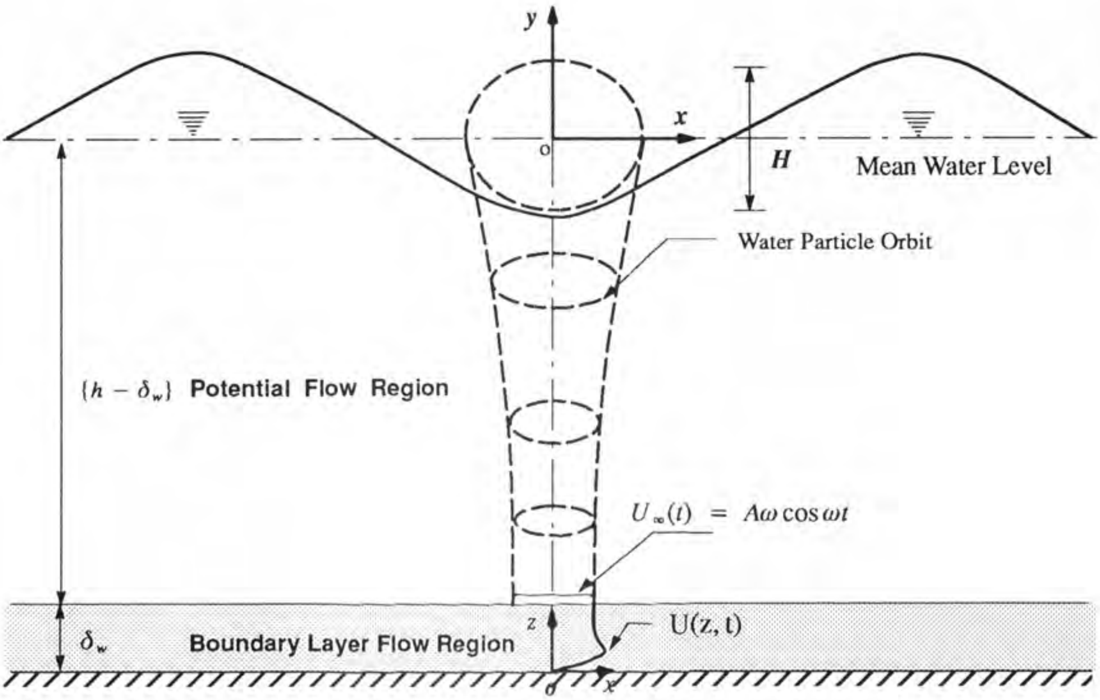

Fig.2.1 Sketch of an oscillatory boundary layer generated by progressive waves

Although the thickness of the boundary layer δ_w is generally very small, the boundary layer has a significant effect on sediment transport which takes place mainly within this layer. Therefore, it is of interest to investigate the following features of the boundary layer.

1. The flow regimes of oscillatory boundary layers.
2. The boundary layer thickness δ_w.
3. The velocity field $U(z, t)$ in the boundary layer.
4. The wave friction factor f_w and bed shear stress $\hat{\tau}_b$.

§2.1.2 OSCILLATORY BOUNDARY LAYERS IN THE LABORATORY

Laboratory experiments can give useful insight into the nature of wave boundary layers induced by progressive waves. There are three different kinds of the laboratory facilities which can be used to produce oscillatory boundary layers in the laboratory.

The first and most commonly used kind is wave flumes and wave basins in which most aspects of wave motion outside the wave boundary layer can be modelled in accordance with Froudes model law. However, it is very difficult to obtain sufficiently large Reynolds Numbers $A^2\omega/\nu$ for modelling boundary layer phenomena in the laboratory because the size of wave flumes and basins is limited. A general overview of a wave flume is shown in Fig.2.2.

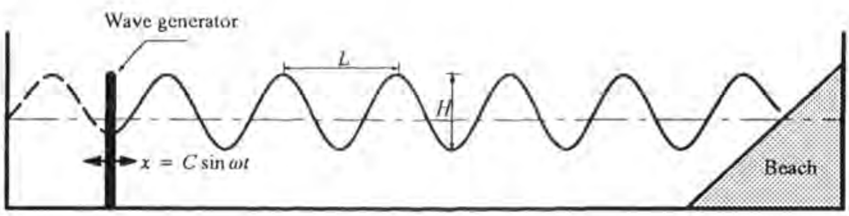

Fig.2.2 An oscillatory boundary layer simulated in a wave flume

The second and now most commonly used type of facility is oscillating water tunnels. The oscillating water tunnel has a large U−tube in which the flow can be driven by a piston in one of the vertical legs. The general layout of an oscillating water tunnel is shown in Fig.2.3. The horizontal displacement produced in the test section of an oscillating water tunnel can be up to several meters, so that Reynolds Numbers $A^2\omega/\nu$ in excess of 10^6 can be obtained. However, the orbital motion of a water particle produced by the wave flume differs from that made by the oscillating water tunnel in which there is no oscillatory component of vertical motion.

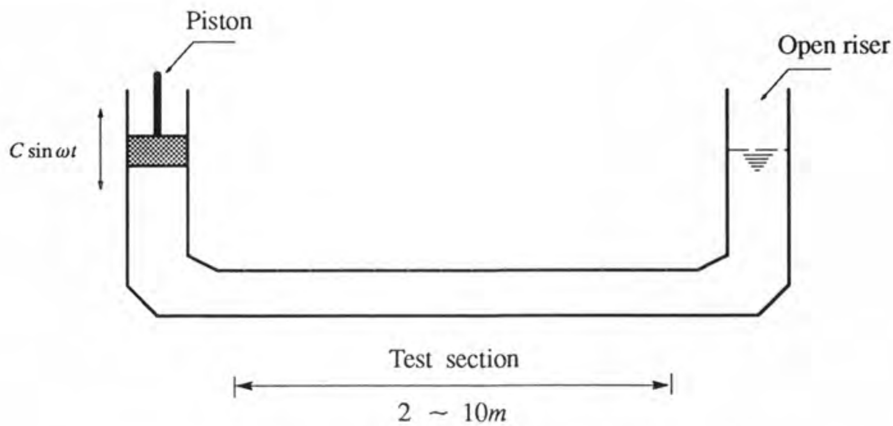

Fig.2.3 An oscillatory boundary layer simulated in an oscillating water tunnel

The third, but not often used kind is the oscillating flat plane in still water, which was suggested by Bagnold (1947). The oscillating flat plane in still water is similar to the oscillating water tunnel, but the velocity measured near a plate corresponds to the velocity defect in an oscillating water tunnel. The general structure of the apparatus is shown in Fig.2.4

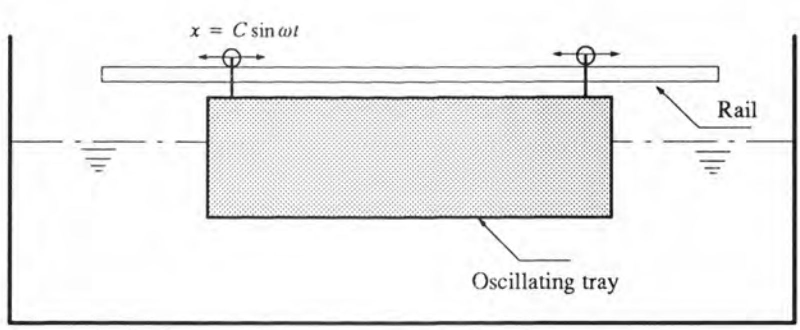

Fig.2.4 An oscillatory boundary layer simulated by an oscillating tray in still water

§2.1.3 FLOW REGIMES

The first step in discussing the characteristics of the oscillatory boundary layer flow is to determine the flow regimes. That is, determine if the flow in the boundary layer is laminar or turbulent. Oscillatory boundary layer flows, like steady flows, have very different characteristics depending on whether they are in laminar, transitional or turbulent regimes. The parameters which determine the flow regimes are the Reynolds Number $\mathbf{Re} = A^2\omega/\nu$ and the relative roughness K_N/A, where K_N is the Nikuradse roughness.

(1) For smooth beds, Jonsson (1980) suggested that the boundary layer is

$$\text{Turbulent :} \qquad \text{if } \mathbf{Re} \geq 3 \times 10^5$$

(2) For rough flat beds, the relative roughness K_N/A of the bed needs to be considered. For example, for flat beds of sand or gravel of diameter d, Sleath (1984) suggested using the criterion

$$\text{Laminar :} \qquad \text{if } \mathbf{Re} < \frac{104A}{d}$$

$$\text{Turbulent :} \qquad \text{if } \mathbf{Re} \geq \frac{1000A}{d}$$

(3) For rippled beds, Sleath (1984) defined the critical Reynolds number to be

$$\mathrm{Re} = 108.2(A/\lambda)/(\eta/\lambda)^{1.16} \qquad \text{for } A/\lambda > 0.38$$

where λ and η denote the length and height of the ripple.

§2.2 THE EQUATION OF MOTION

The horizontal motion of fluid in the turbulent oscillatory boundary layer flow is governed by the Navier–Stokes equation

$$\frac{\partial U}{\partial t} + U\frac{\partial U}{\partial x} + W\frac{\partial U}{\partial z} = -\frac{1}{\varrho}\frac{\partial P}{\partial x} + \nu\left\{\frac{\partial^2 U}{\partial x^2} + \frac{\partial^2 U}{\partial z^2}\right\} \tag{2.11}$$

The continuity equation

$$\frac{\partial U}{\partial x} + \frac{\partial W}{\partial z} = 0 \tag{2.12}$$

and the boundary conditions

$$U(z,t) = 0 \qquad \text{for} \quad z = 0 \tag{2.13}$$

$$U(z,t) = U_\infty(t) \qquad \text{for} \quad z \to \infty \tag{2.14}$$

In Eq.(2.11) U and W are the horizontal and vertical components of the instantaneous velocity, ϱ the fluid density, ν the kinematic viscosity of the fluid and P the pressure. Combining Eqs.(2.11) and (2.12) leads to

$$\frac{\partial U}{\partial t} + \frac{\partial U^2}{\partial x} + \frac{\partial (\, UW \,)}{\partial z} = -\frac{1}{\varrho}\frac{\partial P}{\partial x} + \nu\left\{\frac{\partial^2 U}{\partial x^2} + \frac{\partial^2 U}{\partial z^2}\right\} \tag{2.15}$$

If we assume that the vertical velocity gradient is much greater than the horizontal velocity gradient, i.e. $\partial U/\partial x \approx 0$ in Eq.(2.15), we obtain

$$\frac{\partial U}{\partial t} + \frac{\partial (\, UW \,)}{\partial z} = -\frac{1}{\varrho}\frac{\partial P}{\partial x} + \nu\frac{\partial^2 U}{\partial z^2} \tag{2.16}$$

Furthermore, we assume that there is no net drift velocity inside the boundary layer, i.e. $\overline{U} = \overline{W} = 0$, and decompose the velocities U and W, and the pressure variable P into two parts, each namely, the periodic and random components, which are expressed by

$$U = \tilde{U} + u' \qquad W = \tilde{W} + w' \qquad P = \tilde{P} + p' \tag{2.17}$$

where the periodic component or phase average of the variable $\tilde{X}$ is defined as

$$\tilde{X}(z,t) = \frac{1}{N}\sum_{n=1}^{N} X(z, \quad t + nT) \tag{2.18}$$

Moreover, in the derivation the following relationships will be used

$$\tilde{X'} = \widetilde{\tilde{X}Y'} = \widetilde{\tilde{Y}X'} = 0 \qquad \widetilde{\tilde{X}\tilde{Y}} = \tilde{X}\tilde{Y} - \overline{\tilde{X}\tilde{Y}} \qquad \tilde{\tilde{X}} = \tilde{X} \tag{2.19}$$

Substitution of Eq.(2.17) into Eq.(2.16) gives

$$\frac{\partial(\tilde{U} + u')}{\partial t} + \frac{\partial(\tilde{U} + u')(\tilde{W} + w')}{\partial z} = -\frac{1}{\varrho}\frac{\partial(\tilde{P} + p')}{\partial x} + \nu\frac{\partial^2(\tilde{U} + u')}{\partial z^2} \qquad (2.20)$$

Applying the phase average definition Eq.(2.18) and relationships Eq.(2.19) into Eq.(2.20), we obtain

$$\frac{\partial \tilde{U}}{\partial t} + \frac{\partial(\widetilde{u'w'} + \tilde{U}\tilde{W})}{\partial z} = -\frac{1}{\varrho}\frac{\partial \tilde{P}}{\partial x} + \nu\frac{\partial^2 \tilde{U}}{\partial z^2} \qquad (2.21)$$

Eq.(2.21) can be rewritten as

$$\frac{\partial \tilde{U}}{\partial t} = -\frac{1}{\varrho}\frac{\partial \tilde{P}}{\partial x} + \frac{1}{\varrho}\frac{\partial \tilde{\tau}}{\partial z} \qquad (2.22)$$

where the shear stress $\tilde{\tau}$ is given by

$$\frac{\tilde{\tau}}{\varrho} = \left\{ -\widetilde{u'w'} - \tilde{U}\tilde{W} \right\} + \nu\frac{\partial \tilde{U}}{\partial z} \qquad (2.23)$$

It is assumed that outside the boundary layer the shear stress $\tilde{\tau}$ vanishes, so that Eq.(2.22) can be further simplified as

$$\frac{\partial U_\infty(t)}{\partial t} = -\frac{1}{\varrho}\frac{\partial \tilde{P}}{\partial x} \qquad (2.24)$$

Furthermore, we assume that the pressure gradient $\partial\tilde{P}/\partial x$ in the oscillatory boundary layer flow is hydrostatic which implies that the identity described by Eq.(2.24) also applies inside the boundary layer. Therefore, by substituting Eq.(2.24) into Eq.(2.22), it leads to

$$\frac{\partial}{\partial t}\left\{\tilde{U} - U_\infty(t)\right\} = \frac{1}{\varrho}\frac{\partial \tilde{\tau}}{\partial z} \qquad (2.25)$$

Eq.(2.25) is a governing equation of motion for a horizontally uniform oscillatory boundary layer flow, which will be often used in the following analysis. For simplicity in the following sections where only $\tilde{U}$ is considered, the "$\sim$" will be omitted.

§2.3 LAMINAR OSCILLATORY BOUNDARY LAYER FLOWS

§2.3.1 INTRODUCTION

Before discussing turbulent oscillatory boundary layers, it is useful to review the laminar boundary layer briefly since although some characteristics of the laminar boundary layer are quite different from those of the turbulent oscillatory boundary layer, the methods and some phenomena, which have been used and discovered in the laminar boundary layer, may be applied to study turbulent boundary layers. For example, the velocity distribution in the laminar boundary layer may provide hints to the study of turbulent oscillatory boundary layers. This will be seen in the review of the laminar–like models in Section §2.4.2.

§2.3.2 THE EQUATION OF MOTION

In order to simplify the mathematical treatment, the velocity in the boundary layer is assumed to be simply harmonic and is written in the form of the complex exponential

$$U(z,t) \;=\; U(z)\; e^{i\omega t} \qquad\qquad U_\infty(t) \;=\; A\omega\; e^{i\omega t} \tag{2.26}$$

of which the real part represents the physical velocity. For laminar flow the shear stress given by Eq.(2.23) can be simplified to

$$\frac{\tau(z,t)}{\varrho} \;=\; \nu \frac{\partial U(z,t)}{\partial z} \tag{2.27}$$

By substituting Eq.(2.27) into the equation of motion Eq.(2.25), it leads to

$$\frac{\partial}{\partial t}\Big\{U(z,t) \;-\; U_\infty(t)\Big\} \;=\; \nu \frac{\partial^2 U(z,t)}{\partial z^2} \tag{2.28}$$

We define a nondimensional velocity defect $D(z)$ as

$$D(z) \;=\; 1 \;-\; \frac{U(z,t)}{U_\infty(t)} \tag{2.29}$$

and substitute Eqs.(2.26) and (2.29) into Eq.(2.28), we get

$$i\omega D(z) \;=\; \nu \frac{\partial^2 D(z)}{\partial z^2} \tag{2.30}$$

with the boundary conditions corresponding to Eqs.(2.26) and (2.29)

$$U(z,t) = 0 \quad => \quad D(z) = 1 \qquad \text{for } z = 0 \tag{2.31}$$

$$U(z,t) = U_\infty(t) \quad => \quad D(z) \rightarrow 0 \qquad \text{for } z \rightarrow \infty \tag{2.32}$$

§2.3.3 THE VELOCITY DISTRIBUTION

The nondimensional velocity defect $D(z)$ defined in Eq.(2.29) can be determined by solving the ordinary differential equation of the second order Eq.(2.30) with the boundary conditions expressed in Eqs.(2.31) and (2.32).

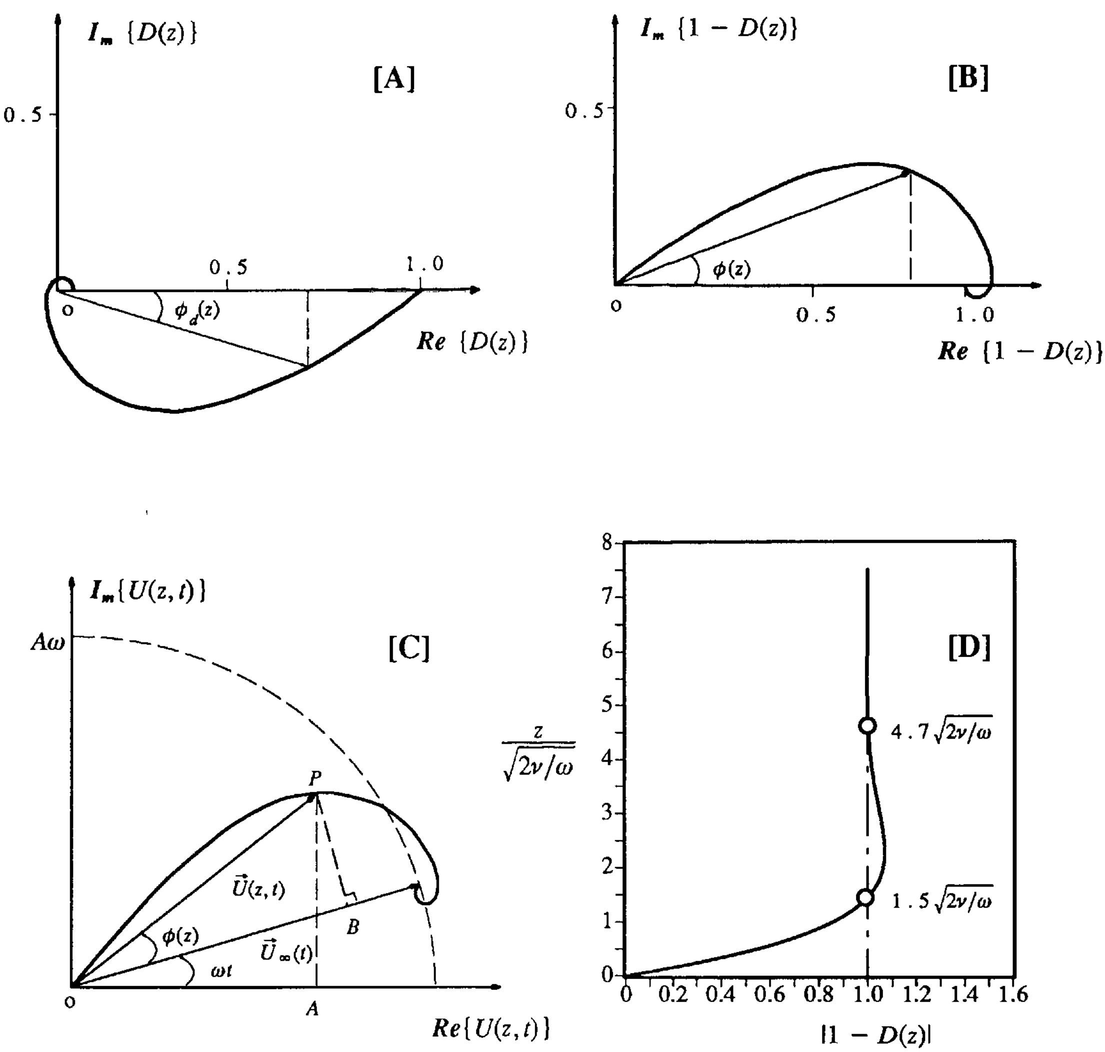

Fig.2.5 The relationship between $D(z)$ and $U(z,t)$ in a simple harmonic laminar boundary layer

The solution of Eq.(2.30) is given in the complex form by

$$D(z) \;=\; e^{-(1+i)\frac{z}{\sqrt{2\nu/\omega}}} \tag{2.33}$$

The locus of the complex number $D(z)$ in the complex plane is a logarithmic spiral starting at $D(z) = 1$ and approaching $D(z) = 0$ as the elevation z increases. The profile of variation of $D(z)$ is shown schematically in Fig.2.5 [B]. Fig.2.5 [C] shows the relationship between $\{1 - D(z)\}$ and $U(z,t)$, which can be constructed geometrically by rotating the logarithmic spiral $\{1 - D(z)\}$ at an angular speed ω around O. The variation of the velocity amplitude $|1 - D(z)|$ with elevation in the laminar flow is shown in Fig.2.5 [D].

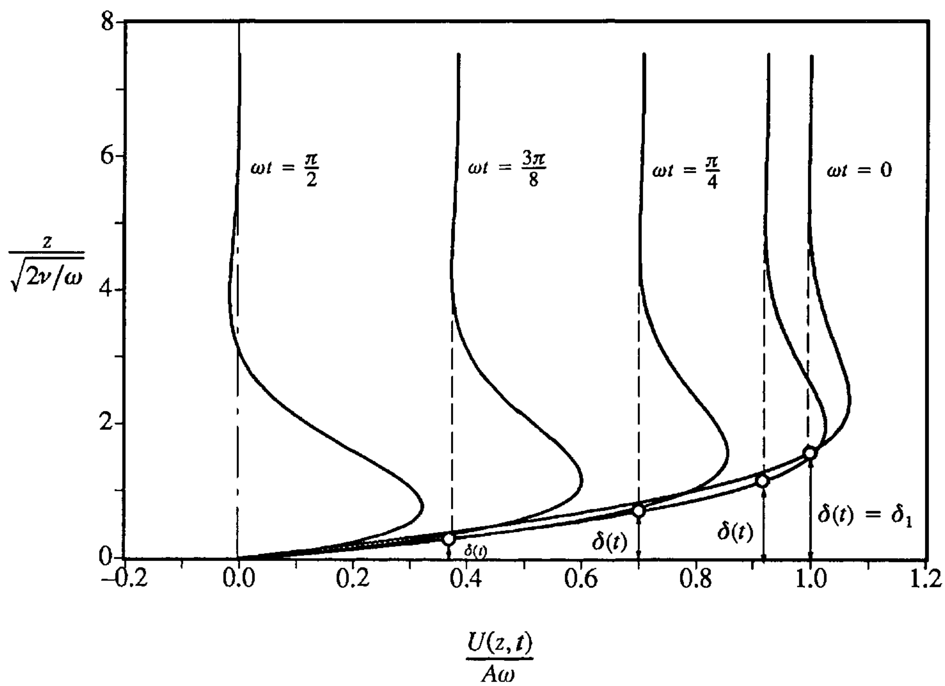

Fig.2.6 The variation of the velocity $U(z,t)$ with time and elevation in a laminar flow

Substituting the nondimensional velocity defect $D(z)$ Eq.(2.33) into Eq.(2.29), we obtain the velocity distribution in the laminar flow

$$U(z,t) \;=\; A\omega\ \{1 - D(z)\}\ e^{i\omega t} \;=\; A\omega \left\{ 1 - e^{-(1+i)\beta z} \right\} e^{i\omega t} \tag{2.34}$$

of which the physical velocity in the laminar flow is represented by the real part

$$U(z,t) \quad = \quad A\omega\Big\{ \cos\omega t \quad - \quad e^{-\beta z}\cos\{\omega t - \beta z\}\Big\} \tag{2.35}$$

in which $\beta = \sqrt{\frac{\omega}{2\nu}}$. The variation of $U(z,t)$ in Eq.(2.35) with elevation and time $[0 \le \omega t \le \frac{\pi}{2}]$ is shown in Fig.2.6.

§2.3.4 THE VELOCITY PHASE SHIFT $\phi(z)$

The velocity phase shift inside the boundary layer is defined as the difference between the local velocity phase and the free stream velocity phase. The velocity phase shift in the oscillatory boundary layer is one of the characteristics which make the oscillatory boundary layers different from the steady boundary layers.

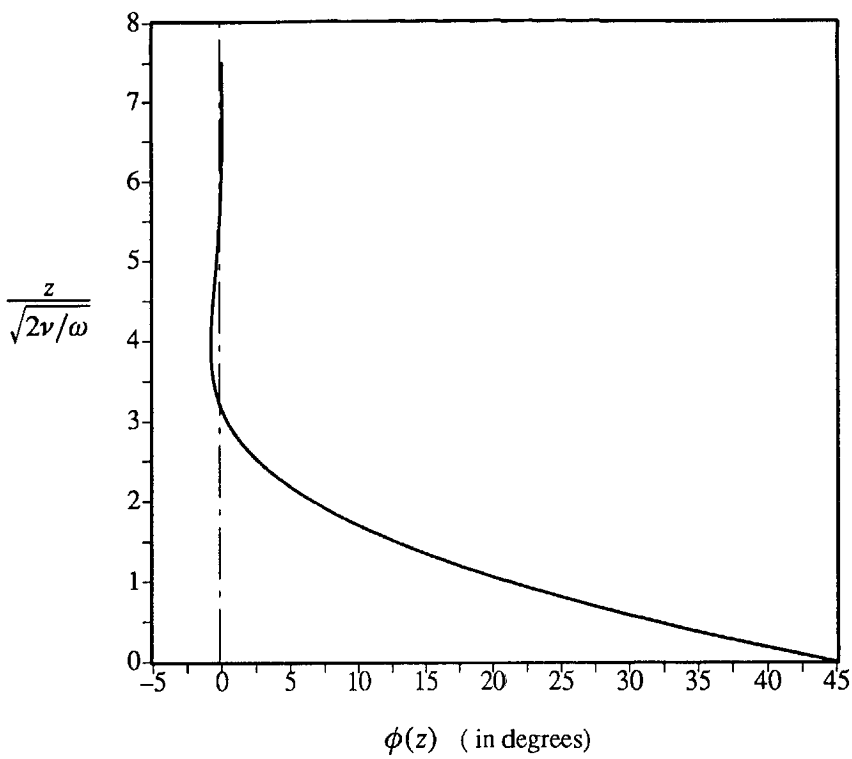

Fig.2.7 The variation of the velocity phase shift $\phi(z)$ with elevation in a laminar boundary layer

We rewrite Eq.(2.29) as

$$\frac{U(z,t)}{U_{\infty}(t)} = 1 - D(z) \tag{2.36}$$

of which the velocity phase shift $\phi(z)$ between $U(z,t)$ and $U_{\infty}(t)$ in the complex plane, see Fig.2.5 [C], is

$$\phi(z) = \mathrm{Arg}\{1 - D(z)\} \tag{2.37}$$

Fig.2.7 quantitatively demonstrates the variation of the velocity phase shift $\phi(z)$ with elevation in the laminar boundary layer.

§2.3.5 THE VELOCITY OVERSHOOT

It is shown in Fig.2.5 [D] that the local velocity amplitudes $|U(z,t)|$ at certain levels are greater than the free stream velocity amplitude $A\omega$. This phenomenon $|U(z,t)| - A\omega > 0$ is called the velocity overshoot. This is another character which makes oscillatory boundary layers different from steady boundary layers.

Now, we try to determine the range over which $|U(z,t)| > A\omega$ based on the velocity amplitude profile, see Fig.2.5 [D]. Now when

$$|U(z,t)| - A\omega > 0 \tag{2.38}$$

it follows that

$$|1 - D(z)| > 1.0 \tag{2.39}$$

Substituting the nondimensional defect velocity Eq.(2.33) into Eq.(2.39), we obtain

$$e^{-\beta z} > 2\cos\beta z \tag{2.40}$$

which yields

$$1.4550 \leq \beta z \leq 4.7165 \tag{2.41}$$

This means that at the range of $1.4550 \leq \beta z \leq 4.716$, the velocity amplitude $|U(z,t)|$ is larger than the free stream velocity amplitude $A\omega$. The maximum velocity amplitude is $1.069A\omega$ and occurs at $z = 2.284\sqrt{2\nu/\omega}$ as shown in Fig.2.5 [D].

§2.3.6 THE BOUNDARY LAYER THICKNESS

The boundary layer thickness of the oscillatory boundary layer, like the steady boundary layer, is defined from the velocity profile. However, one thing we should keep in mind is that there are three different ways to describe the velocity profiles in the oscillatory boundary layer. On the basis of Eq.(2.34)

$$U(z,t) \;=\; A\omega\ \{1 - D(z)\}\ e^{i\omega t} \tag{2.42}$$

we have :

(1) The instantaneous or time-dependent velocity profile $U(z,t)$

$$U(z,t) \;=\; A\omega\ \{1 - D(z)\}\ e^{i\omega t} \tag{2.43}$$

of which the physical velocity is given by the real part, that is

$$U(z,t) \;=\; A\omega\left\{\cos\omega t \;-\; e^{-\beta z}\cos(\omega t \;-\; \beta z)\right\} \tag{2.44}$$

The instantaneous velocity profiles $U(z,t)$ described by Eq.(2.44) are shown in Fig.2.6.

(2) The time-independent velocity profile $U(z)$

$$U(z) \;=\; A\omega\ \{1 - D(z)\} \tag{2.45}$$

of which the physical velocity is given by the real part

$$U(z) \;=\; A\omega\left\{1 \;-\; e^{-\beta z}\cos\beta z\right\} \tag{2.46}$$

The time-independent velocity profile $U(z)$ given by Eq.(2.46) is shown in Fig.2.8.

(3) The velocity amplitude profile $|U(z)|$

$$|U(z)| \;=\; A\omega|1 \;-\; D(z)| \tag{2.47}$$

$$\;=\; A\omega\left\{1 \;-\; 2e^{-\beta z}\cos\beta z \;+\; e^{-2\beta z}\cos^2\beta z\right\}$$

It is shown in Fig.2.8 that the difference between $U(z)$ and $|U(z)|$ is generally small, especially when $z/\sqrt{2\nu/\omega} \geq 2$, the time-independent velocity $U(z)$ is equal to the velocity amplitude $|U(z)|$.

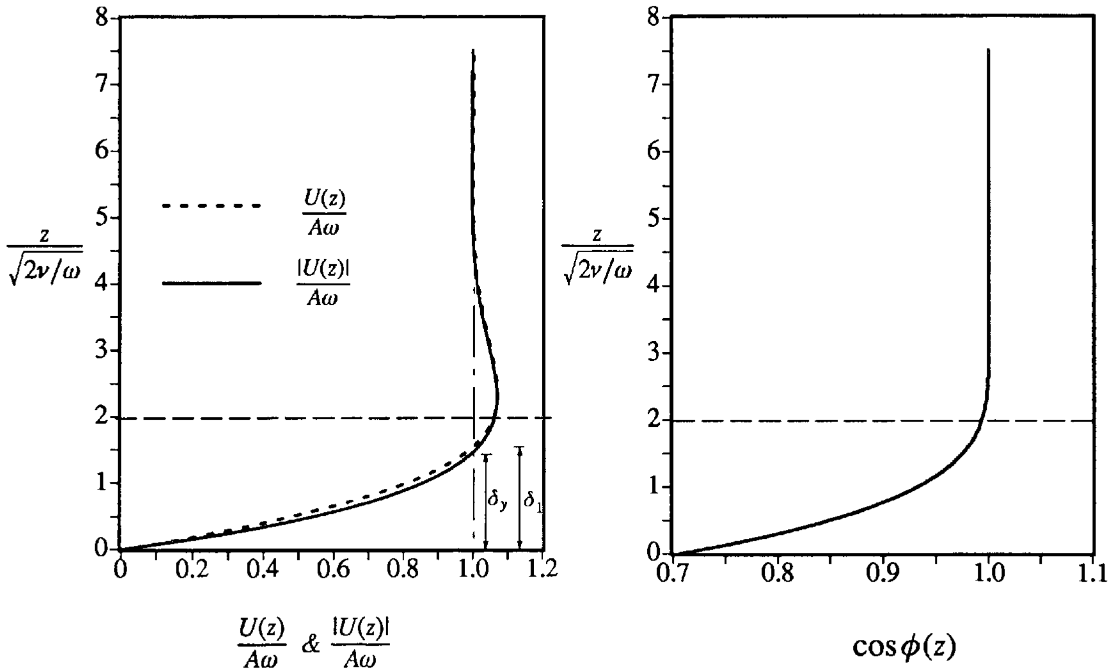

Fig.2.8 The variations of $U(z)$, $|U(z)|$ and $\cos\phi(z)$ with elevation in a laminar flow

Based on the velocity profiles listed above, there are different definitions of the boundary layer thickness. For example,

Fredsoe (1984) defined a time-dependent boundary layer thickness $\delta(t)$ as a minimum distance between the bed and a level at which the instantaneous velocity is equal to the free stream velocity $U_\infty(t)$, which can be expressed as

$$U(z,t) \quad = \quad U_\infty(t) \tag{2.48}$$

The time-dependent boundary layer thickness $\delta(t)$ determined from Eq.(2.48) can be simply described by a general expression

$$\delta(t) \quad = \quad \sqrt{2\nu/\omega}\; F\left\{\omega t,\ \frac{z}{\sqrt{2\nu/\omega}}\right\} \tag{2.49}$$

which is shown in Fig.2.6.

Jonsson & Carlsen (1976) defined the boundary layer thickness as a minimum distance δ_1 between the bed and a level at which the local velocity is equal to the free steam velocity when the latter is maximum, which can be expressed as

$$U(z,t) \quad = \quad U_\infty(t) \qquad \text{and} \qquad \omega t = 0 \tag{2.50}$$

which gives

$$\delta_1 \approx 1.6\sqrt{2\nu/\omega} \tag{2.51}$$

Sleath (1987) applied an intuitive definition of the boundary layer thickness, which is defined as a distance between the bed and a level at which the amplitude of the velocity defect is 5% of the free stream velocity amplitude, which can be expressed by the form

$$|D(z)| = 0.05A\omega \tag{2.52}$$

which gives

$$\delta_s \approx 3.0\sqrt{2\nu/\omega} \tag{2.53}$$

Kajiura (1968) worked with the displacement thickness δ_d defined as

$$\delta_d = \frac{1}{A\omega}\left\{\int_0^\infty \{U_\infty(t) - U(z,t)\}dz\right\}_{Max} \tag{2.54}$$

The boundary layer thickness defined by Eq.(2.54) is fairly thin [$\delta_d < \delta_1$]. In the laminar case, the displacement thickness can be simplified as

$$\delta_d = \frac{1}{2}f_w A \approx \frac{\sqrt{2}}{2}\sqrt{2\nu/\omega} \tag{2.55}$$

The definition of the displacement thickness given in Eq.(2.55) provides a connection between δ_d and the other important boundary layer parameter, the friction factor. However, δ_d can not be determined directly from the velocity profiles.

Here, we will not discuss the time-dependent oscillatory boundary layer thickness $\delta(t)$ since the equation of motion for the oscillatory boundary layer flow can be finally simplified as a time-independent equation in terms of $U(z)$ when a simple harmonic solution is required. Therefore, the study of the boundary layer thickness defined through the time-independent velocity profile $U(z)$ may be more useful.

§2.3.7 BED SHEAR STRESS AND FRICTION FACTOR

In a two–dimensional laminar boundary layer, the shear stress is given by Eq.(2.27)

$$\frac{\tau(z,t)}{\varrho} = \nu\frac{\partial U(z,t)}{\partial z} \tag{2.27}$$

Therefore, by combining the velocity distribution $U(z,t)$ Eq.(2.35) with Eq.(2.27), the shear stress in the laminar oscillatory flow can be deduced as

$$\frac{\tau(z,t)}{\varrho} = \frac{\{A\omega\}^2}{\sqrt{\mathrm{Re}}}e^{-\beta z}\sin(\ \omega t - \beta z + \frac{\pi}{4}\ ) \tag{2.56}$$

where Re is the Reynolds number $\mathrm{Re} = A^2\omega/\nu$. Since the bed shear stress is of special interest in the study of sediment transport, it can be derived by inserting $z = 0$ in Eq.(2.56), as

$$\frac{\tau_b(t)}{\varrho} = \frac{\{A\omega\}^2}{\sqrt{\mathrm{Re}}}\sin(\ \omega t + \frac{\pi}{4}\ ) \tag{2.57}$$

and the maximum bed shear stress $\hat{\tau}_b$ is given by

$$\frac{\hat{\tau}_b}{\varrho} = \frac{\{A\omega\}^2}{\sqrt{\mathrm{Re}}} \tag{2.58}$$

On the other hand, the wave friction factor is commonly defined by an expression of the form

$$\frac{\hat{\tau}_b}{\varrho} = \frac{1}{2}f_w\{A\omega\}^2 \tag{2.59}$$

So that, the wave friction factor f_w in the laminar case is given by

$$f_w = \frac{2}{\sqrt{\mathrm{Re}}} \tag{2.60}$$

§2.4 MODELS OF TURBULENT BOUNDARY LAYERS

§2.4.1 CLASSIFICATION OF EXISTING MODELS

Before developing a new model for turbulent oscillatory boundary layers, a brief survey will be given of existing models. In general, all the existing models can be classified into five major kinds, namely, *Laminar–Like Models*, e.g. Kalkanis (1968), *Quasi Steady Models*, e.g. Jonsson & Carlsen (1976), *Eddy Viscosity Models*, e.g. Kajiura (1968), *Mixing Length Models*, e.g. Bakker (1974), and *$\varkappa - \varepsilon$ Models*, e.g. Justesen (1988). All these five major kinds of models will be discussed briefly in the following sections.

§2.4.2 LAMINAR–LIKE MODELS

The laminar–like models are the models which use the solution of the laminar boundary layer, and then extend these results in a modified form to describe the phenomena of turbulent boundary layers. In this section, the models of Kalkanis (1966), Sleath (1982) and Nielsen (1985) will be briefly reviewed.

§2.4.2.1 The Model of Kalkanis (1966)

Kalkanis (1966) made use of the solution of the velocity distribution for the laminar oscillatory boundary layer

$$U(z,t) \;=\; A\omega\Big\{\; \cos\omega t - e^{-\beta z}\cos(\omega t - \beta z) \;\Big\}$$

and then suggested that the velocity distribution in the turbulent oscillatory boundary layer could be

$$U(z,t) \;=\; A\omega\Big\{\; \cos\omega t - f_1(z)\cos\big[\omega t - f_2(z)\;\big]\;\Big\} \tag{2.61}$$

where $f_1(z)$ and $f_2(z)$ should be determined from experiments. Kalkanis (1966) analysed his experimental data, which were taken over a plate oscillating in still water, and found that over two–dimensional roughness elements, $f_1(z)$ and $f_2(z)$ were given by

$$f_1(z) = \exp\left\{-\frac{10^3 z}{A\beta d}\right\} \qquad \text{and} \qquad f_2(z) = 1.55(\beta z)^{1/3}$$

and over three–dimensional roughness elements, $f_1(z)$ and $f_2(z)$ were determined as

$$f_1(z) = 0.5\exp\left\{-\frac{133\ z}{A\beta d}\right\} \qquad \text{and} \qquad f_2(z) = 0.5(\beta z)^{2/3}$$

where d is the diameter of the roughness element and $\beta = \sqrt{\omega/2\nu}$. As Kalkanis (1966) discussed, the expressions of $f_1(z)$ and $f_2(z)$ above are purely empirical and obtained by curve fitting to the actual measurements, so that the true distributions of $f_1(z)$ and $f_2(z)$ may follow some other law which conceivably would be described by an equation derived by a more rigorous analytical process.

§2.4.2.2 The Model of Sleath (1982)

Sleath (1982) carried out more experiments with flat sand and gravel beds oscillating in still water, and proposed the following revised relationship

$$U(z,t) = A\omega\left\{\cos\omega t - \hat{U}\, e^{-\frac{\beta z}{X_1}}\cos\left\{\omega t - \frac{\beta z}{X_2} - \phi\right\}\right\} \tag{2.62}$$

in which X_1, X_2, $\hat{U}$ and ϕ are constants for given test conditions. For example, $\{A\omega\ d\}/\nu > 700$ and $A/d > 70$, the parameters were evaluated to be

$$X_1 = 0.2\left\{\frac{A\omega\ d}{\nu}\right\}^{\frac{1}{2}} \qquad \text{and} \qquad X_2 = 5.0$$

$$\hat{U} = 0.48 \qquad \text{and} \qquad \phi = 22.5^o$$

Eq.(2.62) is the velocity distribution from the bed. Very close to the bed, i.e. within a grain diameter or so of the bed, the velocities follow a different distribution, and therefore, there is no satisfactory empirical relationship although Sleath (1982) suggested that the laminar relationship might be used as a rough approximation.

§2.4.2.3 The Model of Nielsen (1985)

Nielsen (1985) also made use of the laminar solution expressed in complex form

$$U(z,t) = A\omega\left\{ 1 - D(z) \right\}\exp(i\omega t) \tag{2.63}$$

where the nondimensional velocity defect $D(z)$ is given by

$$D(z) = \exp\left\{ -(1+i)\frac{z}{\sqrt{2\nu/\omega}} \right\} \tag{2.64}$$

Hence, the following identity can be derived as

$$\ln|D(z)| \equiv \mathrm{Arg}\{D(z)\} = -\frac{z}{\sqrt{2\nu/\omega}} \tag{2.65}$$

Analysing experimental data for turbulent boundary layers such as Josson & Carlsen (1976) Test No.1 and Test No.2, van Doorn (1980) V00RA, and van Doorn (1982) S00RAL and M00RAL, Nielsen found an empirical distribution for the nondimensional velocity deficit

$$D(z) = \exp\left\{ -(1+i)\left\{\frac{z}{z_k}\right\}^{p} \right\} \tag{2.66}$$

where z_k and p are given by

$$p = 0.59\exp\left\{ 0.59\frac{1-\left(\frac{A}{38K_N}\right)^{1.8}}{1+\left(\frac{A}{38K_N}\right)^{1.8}} \right\} \qquad \text{and} \qquad z_k = 0.09\sqrt{K_N A}$$

Nielsen's model (1985) is compared with experimental data from Jonsson & Carlsen (1976) Test No.2 in Fig.2.9. From presently available experimental data, it appears that the quantitative description of z_k and p describes $U(z,t)$ well for turbulent and transitional oscillatory boundary layers with relative roughness K_N/A greater than about 0.01. However, for turbulent boundary layers with small relative roughness like those investigated by Jensen (1989) Test−12 and Test−13, there is no longer identity between $Arg\ D$ and $\ln\ |D|$, see Fig.2.10. Nielsen's model (1985) is simple and revealed an interesting analogy between laminar and fully turbulent oscillatory boundary layers. On the other hand, improvements of Nielsen's model are still needed so as to give a good prediction for small relative roughness.

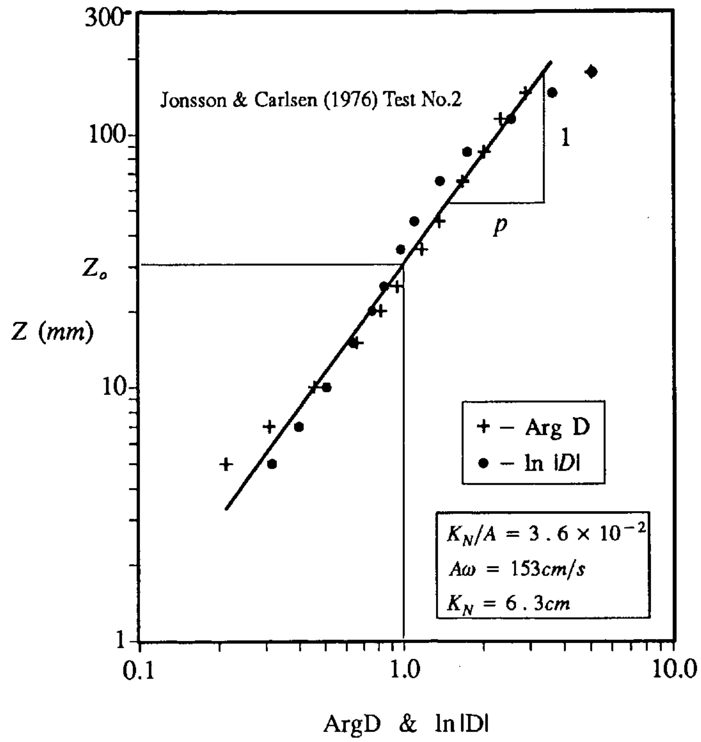

Fig.2.9 Variations of ln|D| and Arg(D)in the turbulent boundary layer with large relative roughness

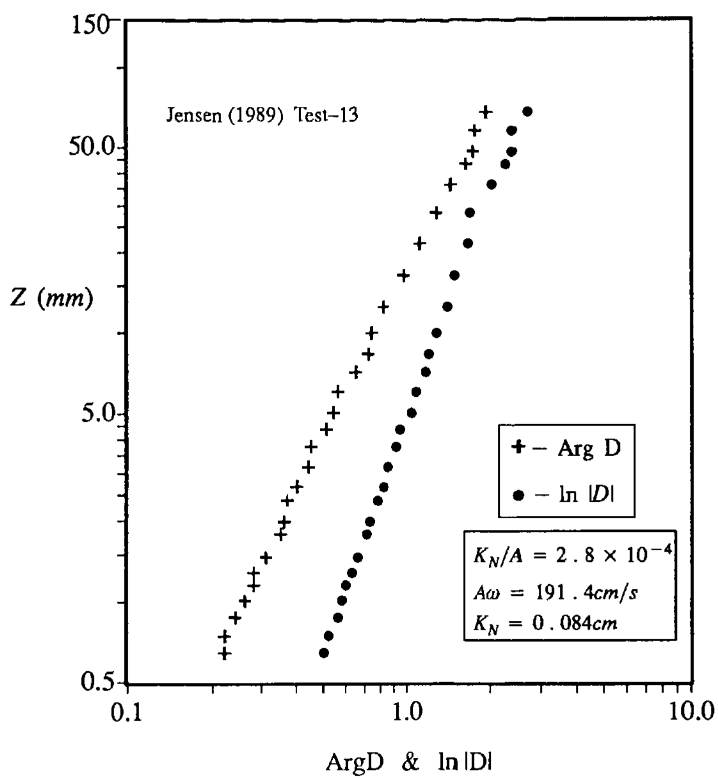

Fig.2.10 Variations of ln|D| and Arg(D)in the turbulent boundary layer with small relative roughness

§2.4.3 QUASI STEADY MODELS

§2.4.3.1 The Model of Jonsson & Carlsen (1976)

Based on the steady boundary layer solution, Jonsson & Carlsen (1976) assumed that the lower part of the velocity profile in a turbulent oscillatory boundary layer is logarithmic as shown in Fig.2.11,

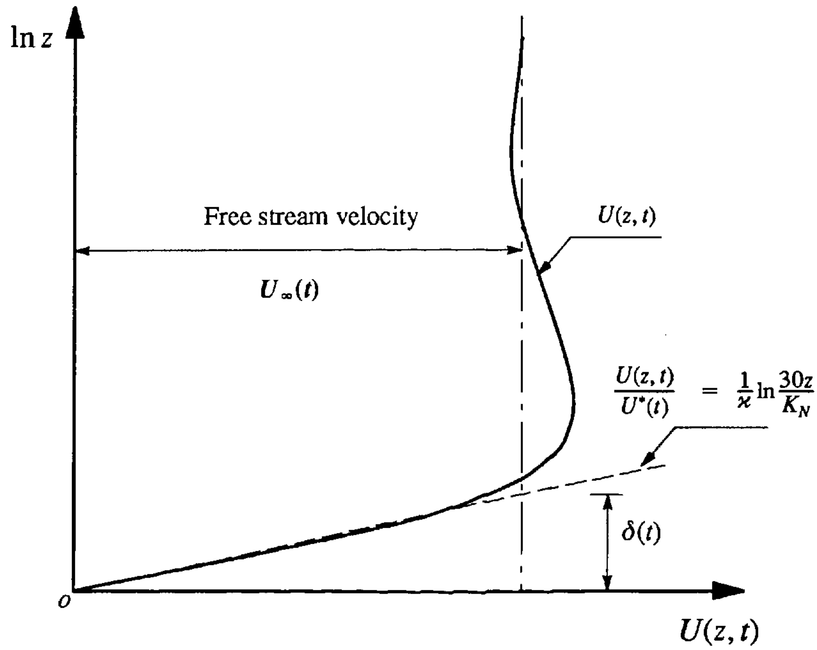

Fig.2.11 The velocity profile assumed by the quasi steady model after Jonsson & Carlsen (1976)

so that

$$\frac{U(z,t)}{U^*(t)} = \frac{1}{\varkappa}\ln\frac{30z}{K_N} \qquad \frac{K_N}{30} \le z \le \delta(t) \tag{2.67}$$

where $U^*(t)$ is the instantaneous bed friction velocity defined as

$$U^*(t) = \sqrt{|\tau_b(t)|/\varrho} \tag{2.68}$$

in which the bed shear stress $\tau_b(t)$ is evaluated from

$$\frac{\tau_b(t)}{\varrho} = \int_{K_N/30}^{\delta(t)} \frac{\partial}{\partial t}\Big\{ U_\infty(t) - U(z,t) \Big\} dz \tag{2.69}$$

where $\delta(t)$ is the instantaneous boundary layer thickness determined from

$$\frac{U_\infty(t)}{U^*(t)} = \frac{1}{\varkappa}\ln\frac{30\delta(t)}{K_N} \tag{2.70}$$

Based on the logarithmic velocity profile Eq.(2.67), Jonsson & Carlsen (1976) derived an implicit semi–empirical formula for the wave friction factor f_w

$$\frac{1}{4\sqrt{f_w}} + \log_{10}\frac{1}{4\sqrt{f_w}} = m_f + \log_{10}\frac{A}{K_N} \tag{2.71}$$

which was translated by Swart (1974) into an explicit formula

$$f_w = \exp\left\{5.213\left\{\frac{2.5d}{A}\right\}^{0.194} - 5.977\right\} \tag{2.72}$$

which gives a good prediction of the wave friction factor f_w as Myrhaug (1989) recently indicated.

Although Jonsson & Carlsen's model (1976) is simple and gives a good prediction of the wave friction factor f_w, the logarithmic velocity profile assumed inside the turbulent oscillatory boundary layer can not hold for all wave phases. As Jensen (1989) indicated, the logarithmic layer in the oscillatory boundary layer comes into existence at $\omega t \geq 15^o$, and is maintained up to $\omega t \leq 160^o$ which is very close to the near bed flow reversal, or in other words, the logarithmic distribution of the velocity $U(z,t)$ can not exist when the flow is at these phases, $0 \leq \omega t \leq 15^o$ and $160^o \leq \omega t \leq 180^o$ because the boundary layer is not thick enough to house the logarithmic layer in itself.

In addition, the quasi steady model can not model the nature of the velocity overshoot in the oscillatory boundary layer as Fig.2.11 shows, and it ignores the velocity phase shift in the boundary layer. However, the characteristics of the velocity overshoot and phase shift in the boundary layers make the oscillatory boundary layers quite different from the steady boundary layers. Therefore, the Quasi Steady Model of Jonsson & Carlsen (1976) has a limited ability of modelling the velocity distribution itself while related aspects like f_w are surprisingly well modelled.

§2.4.4 EDDY VISCOSITY MODELS

Eddy viscosity models are the models in which the relationship between the velocity $U(z,t)$ and shear stress $\tau(z,t)$ in the boundary layer is assumed to be of the form

$$\frac{\tau(z,t)}{\varrho} = \varepsilon\frac{\partial U(z,t)}{\partial z} \tag{2.73}$$

and in which the velocity $U(z,t)$ and shear stress $\tau(z,t)$ in the boundary layer are then found on the basis of the governing equation

$$\frac{\partial}{\partial t}\{U(z,t) - U_\infty(t)\} = \frac{1}{\varrho}\frac{\partial \tau(z,t)}{\partial z} \tag{2.25}$$

with the assumed distribution of ε and the boundary conditions.

§2.4.4.1 The Model of Kajiura (1968)

Kajiura (1968) divided the turbulent oscillatory boundary layer into three layers, namely, the inner, overlap and outer layers. For small relative roughness, the eddy viscosity was assumed to have the distribution

$$\varepsilon(z) = 0.185\varkappa\hat{U}^* K_N \qquad z_o \le z \le D_1 \tag{2.74}$$

$$\varepsilon(z) = \varkappa\hat{U}^* z \qquad D_1 \le z \le D_2 \tag{2.75}$$

$$\varepsilon(z) = \varkappa\hat{U}^* D_2 \qquad D_2 \le z \le \delta_w \tag{2.76}$$

where $\hat{U}^*$ is the maximum friction velocity at the bed, D_1 is the level of the upper edge of the inner layer and D_2 is the level of the upper edge of the overlap layer, which are defined by

$$D_1 = 0.5K_N \qquad D_2 = \frac{0.05\hat{U}^*}{\omega}$$

The sketch of the eddy viscosity distribution in the boundary layer with small relative roughness described by Eqs.(2.74) to (2.76) is shown in Fig.2.12 [A].

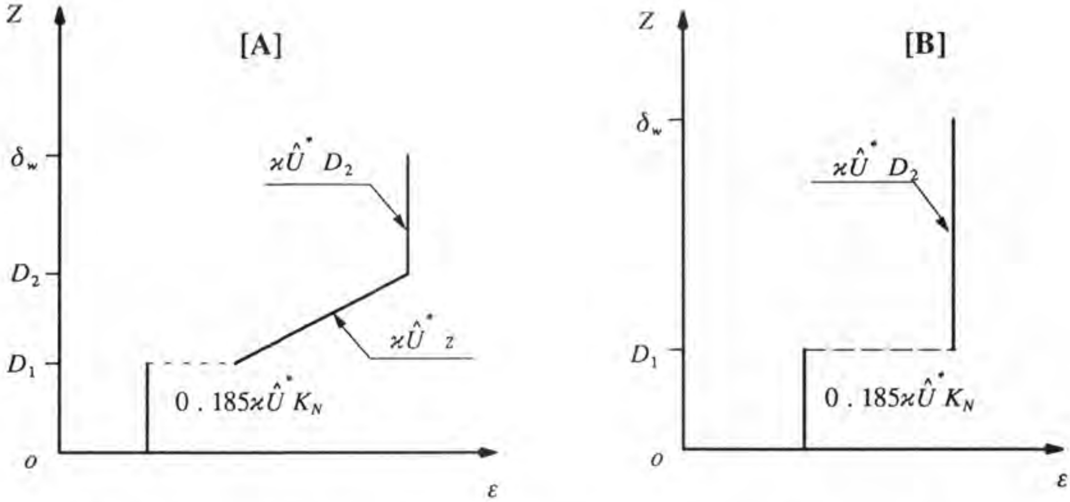

Fig.2.12 The eddy viscosity model for turbulent oscillatory boundary layer flows after Kajiura (1968)

On the other hand, for turbulent oscillatory boundary layers with large relative roughness Kajiura (1968) suggested that when $D_2 < D_1$, the overlap layer would disappear, so that the eddy viscosity distribution would be

$$\varepsilon(z) = 0.185\varkappa\hat{U}^* K_N \qquad z_o \leq z \leq D_1 \tag{2.77}$$

$$\varepsilon(z) = \varkappa\hat{U}^* D_2 \qquad D_1 \leq z < \delta_w \tag{2.78}$$

The eddy viscosity distribution in the boundary layer with large relative bed roughness described by Eqs.(2.77) and (2.78) is schematically shown in Fig.2.12 [B].

Christoffersen & Jonsson (1985) indicated that Kajiura's model overestimated the thickness of the inner layer while the thickness of the overlap layer was underestimated. You *et al.* (1991c) also pointed out that the assumption of a constant eddy viscosity in the inner layer by Kajiura (1968) failed to accurately predict the velocity distribution in the boundary layer. Fig.2.13 shows that Kajiura's (1968) model, in which the variation of eddy viscosity is shown in Fig.2.12 [A], overestimates the velocity in the inner layer measured in Jensen (1989) Test−12 with small relative roughness $K_N/A = 5.7 \times 10^{-4}$, and Fig.2.14 demonstrates that Kajiura's model, in which the variation of eddy viscosity is shown in Fig.2.12 [B], fails to give a good prediction of the velocity measured in Jonsson & Carlsen (1976) Test No.2 with large relative roughness $K_N/A = 3.6 \times 10^{-2}$.

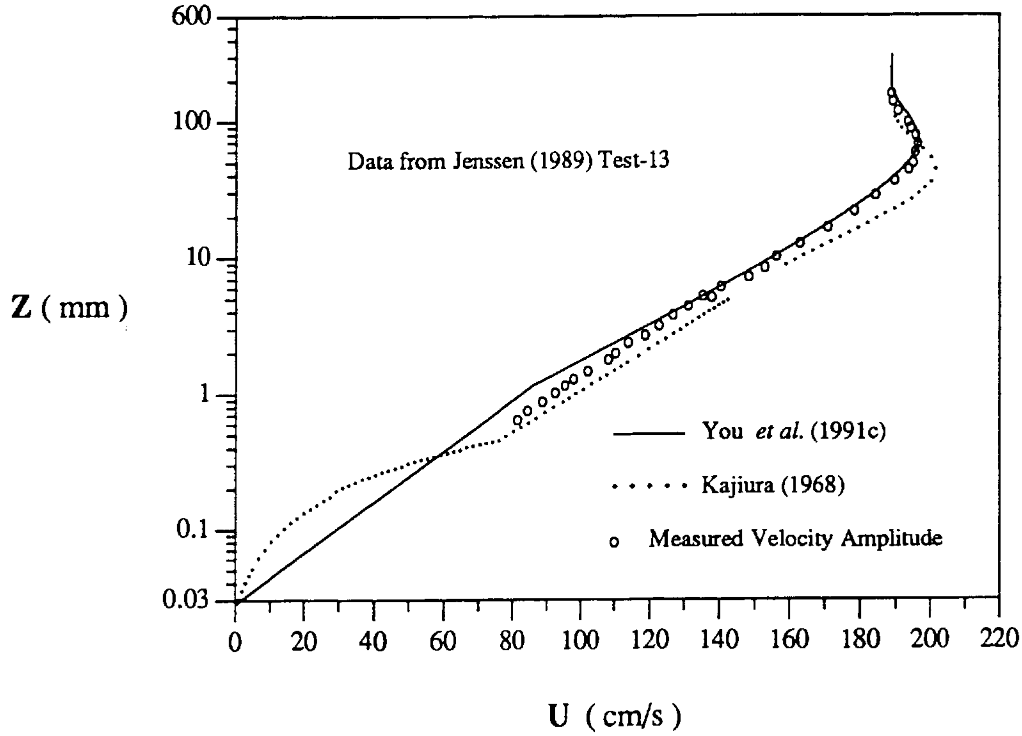

Fig.2.13 The comparison of Kajiura's model with Jensen (1989) Test–13 with small relative roughness

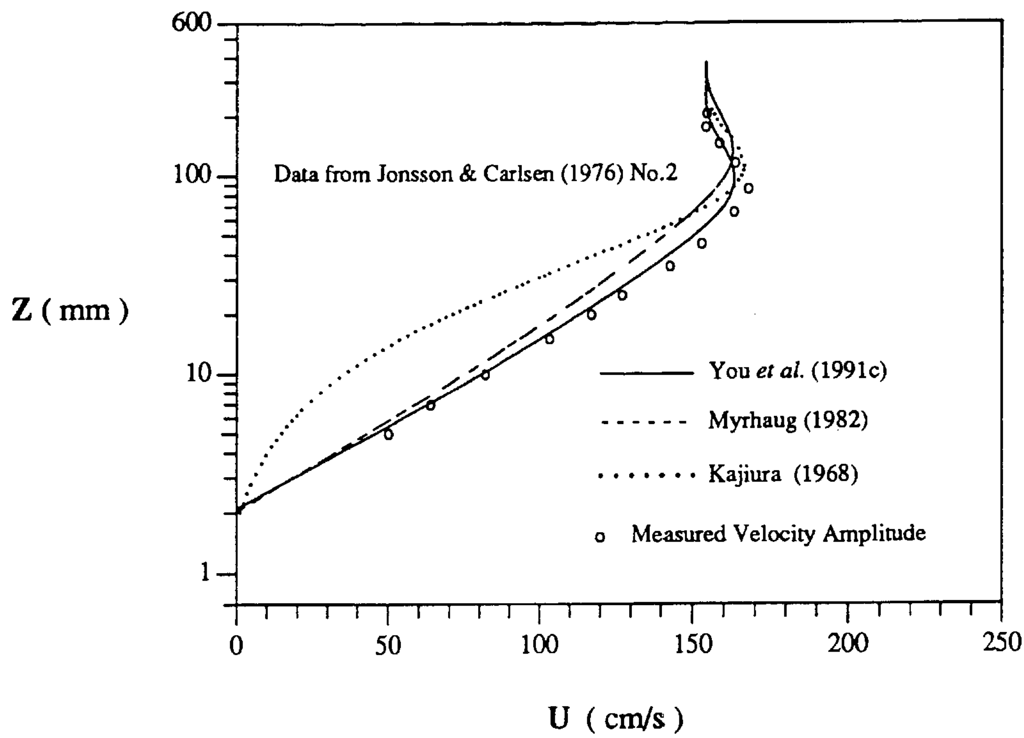

Fig.2.14 The comparison of Kajiura's model with Test No.2 with large relative roughness

§2.4.4.2 The Model of Brevik (1981)

Brevik (1981) modified Kajiura's model (1968) and simplified it into a two-layer eddy viscosity model, in which the eddy viscosity was assumed to have the distribution

$$\varepsilon(z) = \varkappa \hat{U}^{*} z \qquad z_o \leq z < \delta \tag{2.79}$$

$$\varepsilon(z) = \varkappa \hat{U}^{*} \delta \qquad \delta \leq z \leq \delta_w \tag{2.80}$$

in which δ is the thickness of the inner layer, see Fig.2.15 and whose value is unknown.

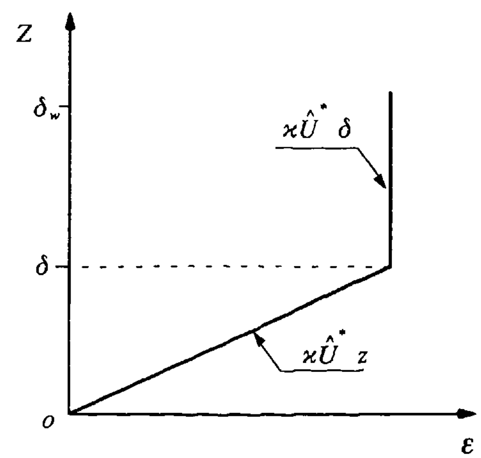

Fig.2.15 The eddy viscosity model for turbulent oscillatory boundary layer flows after Brevik (1981)

After solving Eq.(2.25) with Eqs.(2.79) and (2.80) and the relevant boundary conditions, Brevik compared his model with Jonsson & Carlsen (1976) Test No.1 and Test No.2 choosing an undetermined parameter δ in Eq.(2.80) as

$$\delta = 0.5\delta_1 \qquad \text{and} \qquad \delta = \frac{0.05\hat{U}^{*}}{\omega} \tag{2.81}$$

and found that the inner thickness $\delta = 0.5\delta_1$ gave a better prediction of Jonsson & Carlsen's (1976) Test No.1. As Sleath (1984) discussed, Brevik's model (1981) had not been compared with a wide range of experimental data yet to show how well it works.

§2.4.4.3 The Model of Myrhaug (1982)

In a similar way, Myrhaug (1982) developed an eddy viscosity model, in which the eddy viscosity was assumed to be

$$\varepsilon(z) = \frac{1}{2}\kappa\hat{U}^{*}\delta\left\{1 - \left(1 - z/\delta\right)^{2}\right\} \qquad z_o \leq z \leq \delta \tag{2.82}$$

$$\varepsilon(z) = \frac{1}{2}\kappa\hat{U}^{*}\delta \qquad \delta \leq z < \delta_w \tag{2.83}$$

in which δ is an unknown parameter, but Myrhaug (1982) used $\delta = 0.5\delta_1$ and $\delta = \delta_1$ respectively to compare his model with Jonsson & Carlsen Test No.1 and No.2. The variation of eddy viscosity described by Eqs.(2.82) and (2.83) is shown in Fig.2.16.

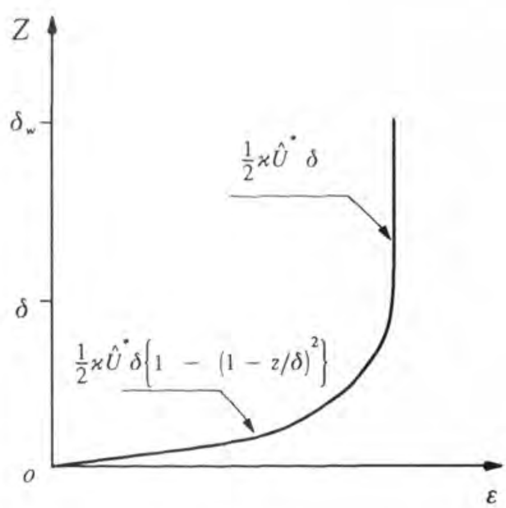

Fig.2.16 The eddy viscosity model for turbulent oscillatory boundary layers after Myrhaug (1982)

The comparison of the model of Myrhaug (1982) with the model of You *et al.* (1991c) and experimental data from Jonsson & Carlsen (1976) Test No.2 is shown in Fig.2.14. It is seen that the model of Myrhaug (1982) overestimates the boundary layer thickness. The further discussion of the difference between the models of Myrhaug (1982) and You *et al.* (1991c) will be given in the section §2.4.4.5.

§2.4.4.4 The Model of Trowbridge & Madsen (1984)

Trowbridge & Madsen (1984) presented a time–dependent eddy viscosity model, in which the eddy viscosity was assumed to have the form

$$\varepsilon(z,t) \;=\; \varkappa \overline{U^*} z \;\mathbf{Re}\left\{1 + A_2 e^{i2\theta}\right\} \qquad 0 \le z \le \delta \tag{2.84}$$

$$\varepsilon(z,t) \;=\; \varkappa \overline{U^*} \delta \;\mathbf{Re}\left\{1 + A_2 e^{i2\theta}\right\} \qquad \delta \le z < \delta_w \tag{2.85}$$

in which

$$\overline{U^*} \;=\; \overline{\left\{ |\tau_b(t)|/\varrho \right\}^{1/2}} \qquad\qquad \theta \;=\; \omega t - kx$$

$$A_2 \;=\; \overline{2e^{-i2\theta}\left\{|\tau_b(t)|/\varrho\right\}^{1/2}} \qquad\qquad \delta \;=\; \left\{0.167\varkappa\overline{U^*}\right\}/\omega$$

where an overbar denotes a time average over one wave period. After comparing their model with Jonsson & Carlsen (1976) Test No.1 & No.2 and van Doorn (1981) V00RA, Trowbridge & Madsen (1984) concluded that the temporal variation of eddy viscosity with time did not provide a better prediction of the first harmonic velocity component in comparison with existing time–invariant eddy viscosity models, e.g. Kajiura (1968), Grant (1977), Brevik (1981) and Myrhaug (1982), and that on the other hand this model was only applied to predict velocity measurements of turbulent boundary layers with small relative roughness $K_N/A < 0.1$. The model fails to predict the measurements of van Doorn's (1981) V00RA & S00RAL in which $K_N/A > 0.1$.

In the following section §2.4.4.5, it will be explained by You *et al.* (1991c) that the eddy viscosity should be time–independent when only the first harmonic component is considered. In other words, it is not necessary to assume a time dependent eddy viscosity as suggested by Trowbridge & Madsen (1984).

§2.4.4.5 The Model of You *et al.* (1991c)

You *et al.* (1991c) based the analysis of eddy viscosity on the equation of motion Eq.(2.25) and derived an expression of the eddy viscosity given by

$$\varepsilon(z) = \frac{i\omega \int_z^\infty \left\{A\omega - |U(z)|e^{i\phi(z)}\right\}dz}{\frac{\partial}{\partial z}\left\{A\omega - |U(z)|e^{i\phi(z)}\right\}} \tag{2.86}$$

where $A\omega$ is the free stream velocity amplitude, $|U(z)|$ the local velocity amplitude and $\phi(z)$ the phase shift of the local velocity relative to the free stream velocity. Based on Eq.(2.86), it was concluded that the eddy viscosity should be time independent when only the first harmonic component was considered.

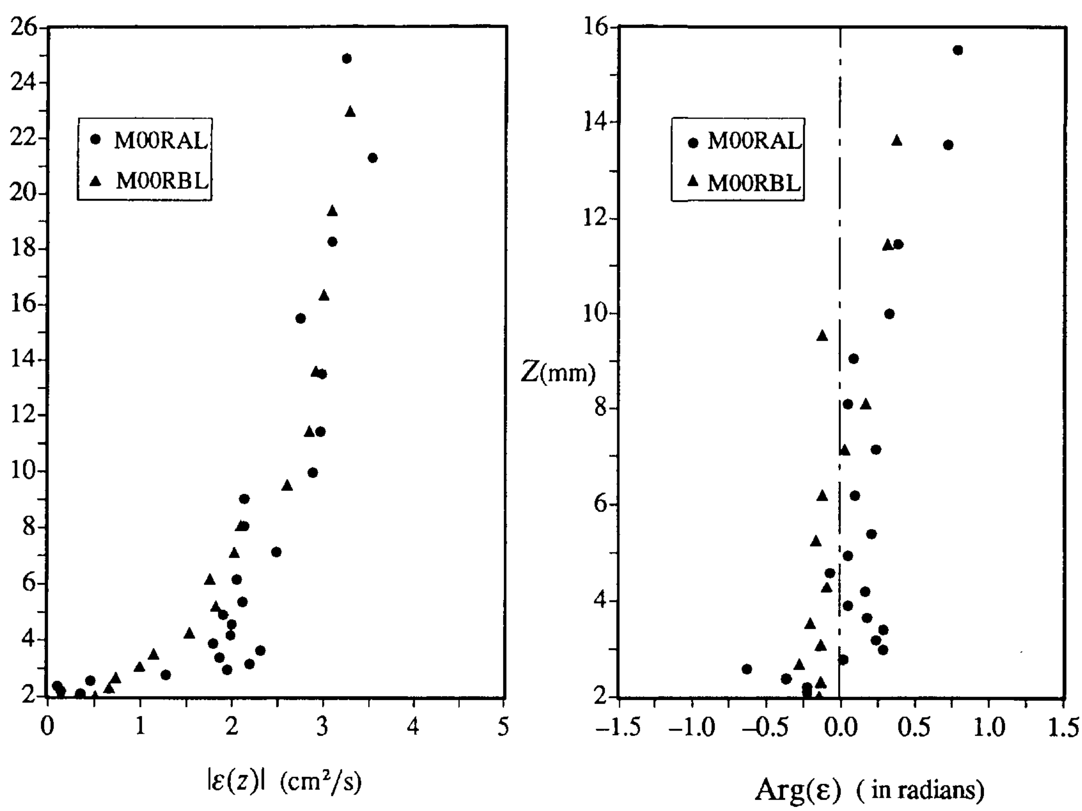

Fig.2.17 The eddy viscosity evaluated from van Doorn (1982) M0ORAL & M0ORBL via Eq.(2.86)

Furthermore, after analysing the eddy viscosity data calculated from van Doorn (1982) experimental data M00RAL and M00RBL via Eq.(2.86). You *et al.* (1991c) suggested that the complex eddy viscosity could be treated as a real-valued variable because the argument of the complex eddy viscosity is small as shown in Fig.2.17. Consequently, the distribution of eddy viscosity in turbulent oscillatory boundary layer flows was suggested to be of the form

$$\varepsilon = \varkappa \hat{U}^* \delta_o \left\{1 - (1 - z/\delta_1)^2\right\} \qquad z_o \le z \le \delta_1 \tag{2.87}$$

$$\varepsilon = \varkappa \hat{U}^* \delta_o \qquad \delta_1 \le z < \delta_w \tag{2.88}$$

which are shown in Fig.2.18

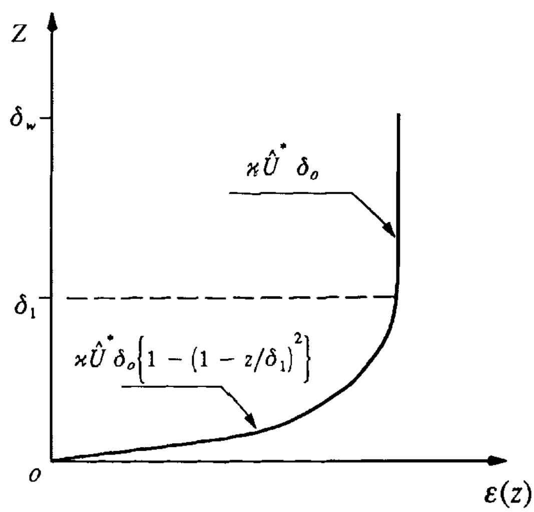

Fig.2.18 The eddy viscosity model for turbulent oscillatory boundary layer flows after You *et al.* (1991c)

where δ_1 is the boundary layer thickness defined by Jonsson & Carlsen (1976) and approximated by

$$\delta_1 = \frac{0.5 \varkappa \hat{U}^*}{\omega} \tag{2.89}$$

and δ_o was evaluated from a wide range of experimental data and chosen as

$$\delta_o = 0.4 \delta_1 \tag{2.90}$$

The comparison of the model of You *et al.* (1991c) with experimental data from Jonsson & Carlsen (1976) and Jensen (1989) is shown in Fig.2.13 and Fig.2.14. It is found that the model of You *et al.* (1991c) gives a better prediction of the velocity distribution than the models of Kajiura (1968) and Myrhaug (1982). In addition, Fig.2.19 shows that the model of You *et al.* (1991c) gives a good prediction of both the velocity distribution and the phase shift as well.

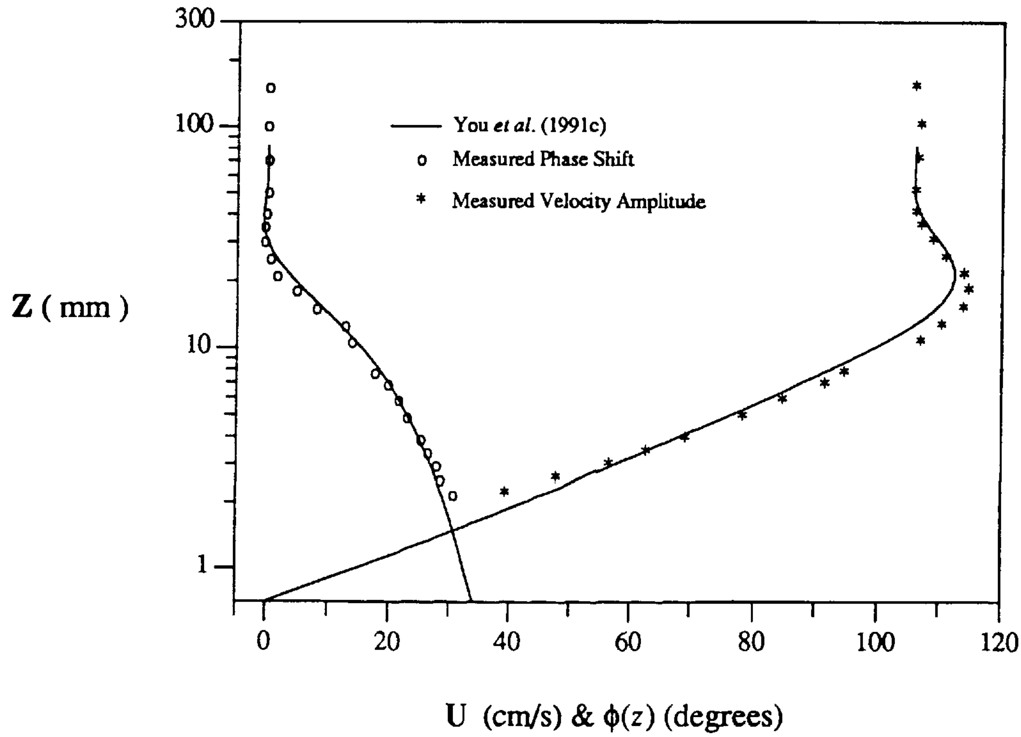

Fig.2.19 Comparison of the model of You *et al.* (1991c) with experimental data MOORAL

It is worthwhile to note here that the major differences between the models of Myrhaug (1982) and You *et al.* (1991c) have been made in the following aspects :

(1) In the model of You *et al.* (1991c), it was qualitatively proved that the eddy viscosity should be time–independent rather than time–dependent. In addition, an Eq.(2.86) was derived to calculate time–independent eddy viscosities from experimental data. These aspects are an advance on the model of Myrhaug (1982).

(2) The procedure for formulating the eddy viscosity model in the two models is quite different. In the model of You *et al.* (1991c), the distribution of eddy viscosity described by Eqs.(2.87) and (2.88) was formulated on the basis of the time independent and real−valued eddy viscosity data calculated from experimental data via Eq.(2.86). It is shown in Fig.2.20 [A] that the eddy viscosity model of You *et al.* (1991c) fits eddy viscosity data quite well.

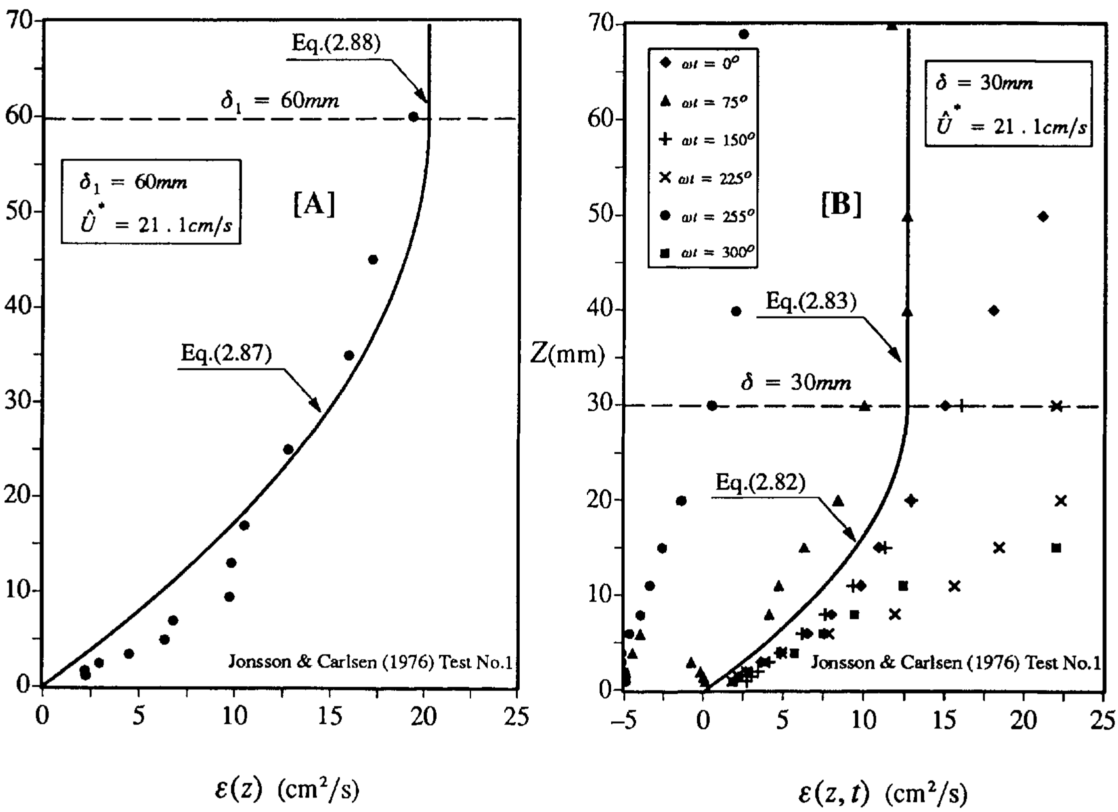

Fig.2.20 Different procedures for formulating time–independent eddy viscosity models

However, in the model of Myrhaug (1982), the eddy viscosity distribution was assumed on the basis of the time−dependent eddy viscosity data calculated by Jonsson & Carlsen (1976) according to the eddy viscosity definition in the real formalism, see Fig.2.20 [B]. It is evident that at a fixed level [δ = 30*mm*] the dependency of eddy viscosity with time [ωt] is so strong that the time–independent eddy viscosity model suggested by Myrhaug (1982) could not fit data at all. On the other hand, it would be meaningless to compare the time–independent eddy viscosity model with the time–dependent eddy viscosity data in such a way as shown in Fig.2.20 [B].

(3) The parameters and the formulas used to evaluate these parameters in the two models are quite different. In the model of You *et al.* (1991c), the two parameters δ_1 and δ_o were used and based on a wide range of experimental data the formulas Eqs.(2.89) and (2.90) were provided to calculate δ_1 and δ_o, respectively. However, in the model of Myrhaug (1982), only one undetermined parameter δ was used and in the model of Myrhaug & Slaattelid (1989), a formula used to calculate δ was adopted from Jonsson (1980), which is valid only for the range of $10^{-3} \le K_N/A \le 0.1$. It means that the model of Myrhaug & Slaattelid (1989) can not be applied for Jensen (1989) test–12 and Test–13 in which $K_N/A < 10^{-3}$ and van Doorn (1981 & 1982) V00RA and S00RAL in which $K_N/A > 0.1$.

§2.4.5 MIXING LENGTH MODELS

The mixing length models are the models which use Prandtl's (1931) assumption

$$l = \varkappa z \tag{2.91}$$

to connect the shear stress with the velocity gradient, that is

$$\frac{\tau(z,t)}{\varrho} = l^2 \frac{\partial U(z,t)}{\partial z} \left| \frac{\partial U(z,t)}{\partial z} \right| \tag{2.92}$$

and then solve the equation of motion Eq.(2.25) with the relevant boundary conditions. We will see in the following section that the mixing length models may be classified as time–dependent eddy viscosity models.

§2.4.5.1 The Model of Bakker (1974)

Bakker (1974) also started with the equation of motion Eq.(2.25)

$$\frac{\partial}{\partial t}\{U(z,t) \; - \; U_\infty(t)\} \;\; = \;\; \frac{1}{\varrho}\frac{\partial \tau(z,t)}{\partial z} \tag{2.25}$$

but instead of using the eddy viscosity concept, he made use of Prandtl's (1931) assumption Eq.(2.91) to rewrite the equation of motion Eq.(2.25) as

$$\frac{\partial U^*(z,t)}{\partial t} \;\; = \;\; \varkappa z \frac{\partial^2\{U^*(z,t)\; U^*(z,t)\}}{\partial z^2} \tag{2.93}$$

in which $U^*(z,t)$ is the instantaneous internal friction velocity

$$U^*(z,t) \;\; = \;\; \varkappa z \left| \frac{\partial U(z,t)}{\partial z} \right| \tag{2.94}$$

The differential equation Eq.(2.93) for the instantaneous friction velocity was solved numerically by Bakker (1974). The numerical method was further refined and, in some respects, revised by Bakker & van Doorn (1978). They used an implicit method in their mathematical model to calculate the velocity field. Furthermore, van Doorn (1981) used a more effective implicit method to calculate the velocity. It can be seen from Fig.2.21 that the mixing length model tends to overestimate the boundary layer thickness.

It is worthwhile to mention here that the mixing length models may be classified as the time–dependent eddy viscosity models. We rewrite Eq.(2.92) as

$$\frac{\tau(z,t)}{\varrho} \;\; = \;\; \varkappa z U^*(z,t) \, \frac{\partial U(z,t)}{\partial z} \tag{2.95}$$

If we define

$$\varepsilon(z,t) \;\; = \;\; \varkappa z U^*(z,t) \tag{2.96}$$

Eq.(2.95) can be rewritten as

$$\frac{\tau(z,t)}{\varrho} \;\; = \;\; \varepsilon(z,t) \, \frac{\partial U(z,t)}{\partial z} \tag{2.97}$$

Therefore, it is seen from Eq.(2.96) that the eddy viscosity increases linearly with elevation z, but changes with time as $U^*(z,t)$ varies in time.

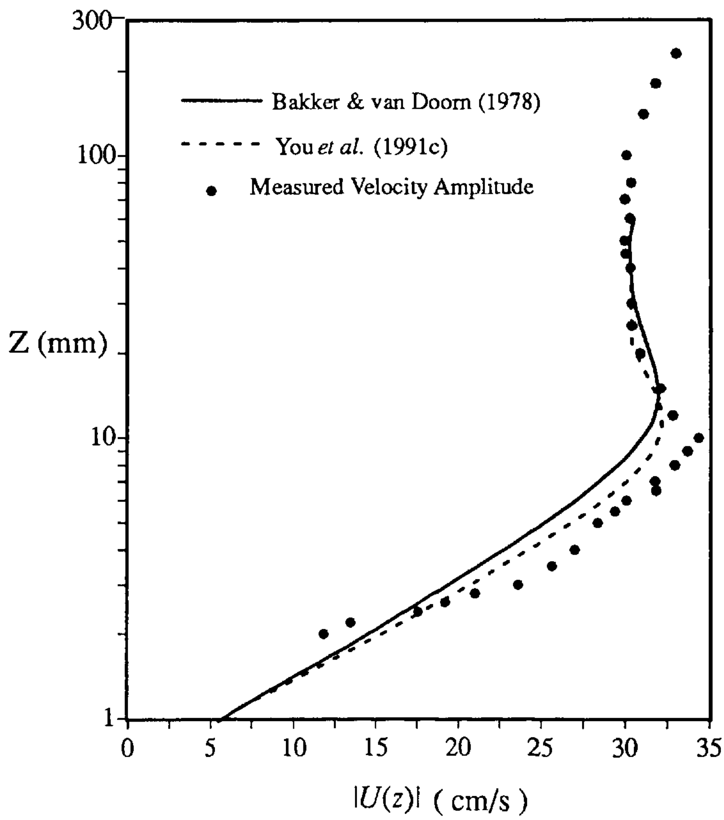

Fig.2.21 The prediction of models on experimental data RA from van Doorn & Godefroy (1978)

§2.4.6 $\varkappa - \varepsilon$ MODELS

$\varkappa - \varepsilon$ models are the models which combine Prandtl's (1931) assumption with the transport equation for the turbulent kinetic energy and dissipation equations for the energy dissipation to obtain an eddy viscosity distribution, and then solve the equation of motion Eq.(2.25) with appropriate boundary conditions to obtain distributions of velocity and shear stress across the flow field.

§2.4.6.1 The Model of Justesen (1988)

Based on Prandtl's assumption, the transport and dissipation equations, Justesen (1988) developed a $\varkappa - \varepsilon$ model. The basic approach is as follows. The equation of motion was still used to describe the velocity field

$$\frac{\partial U(z,t)}{\partial t} = -\frac{1}{\varrho}\frac{\partial P(x,z,t)}{\partial x} + \frac{\partial}{\partial z}\left\{\varepsilon\frac{\partial U(z,t)}{\partial z}\right\} \tag{2.98}$$

in which the eddy viscosity ε was defined as

$$\varepsilon = \sqrt{k}\ l \tag{2.99}$$

where k is the turbulent kinetic energy defined as

$$k = \frac{1}{2}(u'^2 + v'^2 + w'^2) \tag{2.100}$$

here u', v' and w' are the velocity random components. Then, the transport equation for the turbulent kinetic energy

$$\frac{\partial k}{\partial t} = \frac{\partial}{\partial z}\left\{\frac{\varepsilon}{\sigma_k}\frac{\partial k}{\partial z}\right\} + \varepsilon\left\{\frac{\partial U(z,t)}{\partial z}\right\}^2 - C_1\frac{k^{2/3}}{l} \tag{2.101}$$

was used to connect the turbulent kinetic energy k with the eddy viscosity ε. Here the constant factors were chosen in accordance with Launder & Spalding (1972), as

$$\sigma_k = 1.0 \qquad C_1 = 0.08 \tag{2.102}$$

In $\varkappa - \varepsilon$ models, the new feature is that the length−scale l is allowed to vary with time and space instead of being given by a linear relation $l = \varkappa z$ as the mixing length model requires. However, the introduction of a new variable requires an extra equation as well. An extra variable, which Justesen (1988) used, is the dissipation

$$D = \frac{k^{3/2}}{l} \tag{2.103}$$

in which the dissipation D was determined from the transport equation

$$\frac{\partial D}{\partial t} = \frac{\partial}{\partial z}\left\{\frac{\varepsilon}{\sigma_D}\frac{\partial D}{\partial z}\right\} + C_{D1}\frac{D}{k}\varepsilon\left\{\frac{\partial U(z,t)}{\partial z}\right\}^2 - C_1 C_{D2}\frac{D^2}{k} \tag{2.104}$$

in which three constant factors were taken from steady boundary layer flows in accordance with Launder & Spalding (1972), as

$$C_{D1} = 1.44 \qquad C_{D2} = 1.92 \qquad \sigma_D = 1.3 \tag{2.105}$$

Justesen (1988) compared his model with the mixing length model of Bakker & van Doorn (1978) and experimental data V10RA and V20RA of van Doorn (1981). The results from the comparison with V10RA is shown in Fig.2.22. It is seen that the model of Justesen (1988) did not give any better prediction of the velocity distribution than either the mixing length model or the eddy viscosity model. The reason for this may be that all constant factors in the transport equation for the turbulent kinetic energy k and in the dissipation equation for the dissipation D are taken from the steady case, so it is unclear if $\varkappa - \varepsilon$ models can give a better prediction of the velocity field than does the eddy viscosity model.

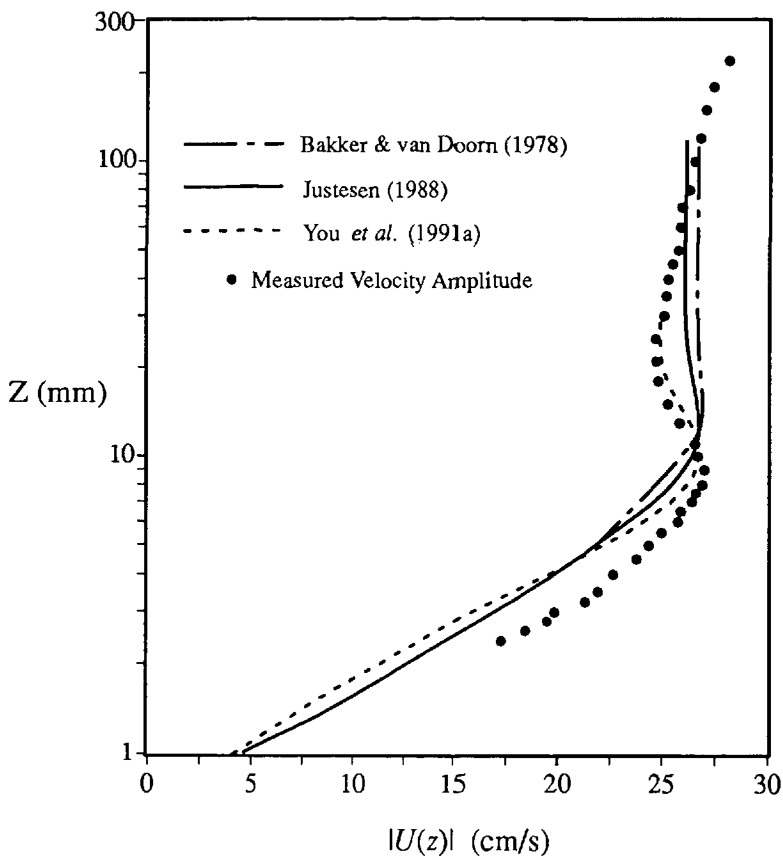

Fig.2.22 The comparison of the $\varkappa - \varepsilon$ model with van Doorn (1981) V10RA after Justesen (1988)

§2.4.7 CONCLUSIONS ON FORMER MODELS

The general features of the eddy viscosity model, the mixing length model and the $k - \varepsilon$ model to model an oscillatory boundary layer are shown as follows

A basic equation of motion

$$\frac{\partial U}{\partial t} = -\frac{1}{\varrho}\frac{\partial P}{\partial x} + \frac{1}{\varrho}\frac{\partial}{\partial z}\left\{\varepsilon\frac{\partial U}{\partial z}\right\}$$

Eddy Viscosity Model : Assume ε

Mixing Length Model : Use Prandtl's assumption to obtain ε

$k - \varepsilon$ Model : Use Prandtl's assumption, the transport and dissipation equations to obtain ε

To obtain

1. velocity field $U(z,t)$
2. shear stress $\tau_w(z,t)$
3. friction factor f_w
4. phase shift $\phi(z)$

Therefore, the model used to describe the eddy viscosity will determine the possibility, complexity and difficulty of solving the equation of motion Eq.(2.25). However, the difficulty and complexity of a model does not automatically mean a good performance of that model. For example, the $k - \varepsilon$ model requires considerable computing effort and complicated mathematical treatment compared with the time−independent eddy viscosity model, but the prediction of the $k - \varepsilon$ model on experimental data such as V10RA is not as good as the time−independent eddy viscosity model [see Fig.2.22]. In most cases, if only the first−order solution for a two−dimensional oscillatory boundary layer flow is considered, a time−independent eddy viscosity model can describe the turbulent boundary layer more precisely and simply since the nature of the periodic boundary layer flow will reduce the equation of motion Eq.(2.25) into a time−independent equation.

§2.5 DEVELOPMENT OF AN ANALYTICAL MODEL

§2.5.1 INTRODUCTION

In the section, based on the equation of motion Eq.(2.25) we are going to derive a formula to qualitatively discuss the nature of eddy viscosity in turbulent oscillatory boundary layer flows. Then, based on the formula provided and a wide range of experimental data, we will calculate the values of eddy viscosity and quantitatively study the eddy viscosity. Finally, we will develop an analytical model and give a comparison of the present model with the former models and experimental data.

§2.5.2 THE EDDY VISCOSITY CONCEPT

The equation of motion as expressed in the form of Eq.(2.25) involves two variables, the shear stress $\tau(z,t)$ and the velocity $U(z,t)$. Therefore, a further relationship between $\tau(z,t)$ and $U(z,t)$ is needed so as to solve the equation of motion. The relation for laminar flows is well understood and is given by Newton's formula Eq.(2.27), but not well understood for turbulent flows. Nevertheless, in turbulent boundary layer flows, the relationship between the shear stress and the velocity can be assumed to be of the form

$$\frac{\tau}{\varrho} = \varepsilon \frac{\partial U}{\partial z} \qquad \Leftrightarrow \qquad \varepsilon = \frac{\tau}{\varrho \partial U/\partial z} \tag{2.106}$$

in which ε is called turbulent eddy viscosity. For example, in the steady flow the shear stress $\tau/\varrho = \overline{u'w'} + \nu\ \partial \overline{U}/\partial z$, so that the eddy viscosity can be expressed by

$$\varepsilon = -\frac{\overline{u'w'}}{\partial \overline{U}/\partial z} + \nu \tag{2.107}$$

Similarly, for a horizontally uniform oscillatory boundary flow with zero net flow $[\overline{U} = 0]$, the analogous expression for the eddy viscosity becomes

$$\varepsilon = \frac{-\widetilde{\tilde{U}\tilde{W}} - \widetilde{u'w'}}{\partial \tilde{U}/\partial z} + \nu \tag{2.108}$$

in which $\tau/\varrho = -\tilde{U}\tilde{W} - \widetilde{u'w'}$ is in accordance with Eq.(2.23). It seems that the eddy viscosity in an oscillatory boundary layer defined by Eq.(2.108) may be time−dependent. However, if we use different formalisms, either the real formalism or the complex formalism, to analyse the eddy viscosity, we may arrive at different expressions as pointed out by Nielsen (1985).

§2.5.2.1 A Real Formalism Definition

In the section, we use the real formalism to analyse the eddy viscosity defined in Eq.(2.106) assuming

$$U(z,t) = |U(z)| \cos\omega t \tag{2.109}$$

$$\tau(z,t) = |\tau(z)| \cos\{ \omega t + \theta(z) \} \tag{2.110}$$

where $\theta(z)$ is the phase lead of $\tau(z,t)$ relative to $U(z,t)$ at an arbitrary level. Therefore,

$$\frac{\partial U(z,t)}{\partial z} = \frac{\partial |U(z)|}{\partial z} \cos\omega t \tag{2.111}$$

so that

$$\varepsilon = \frac{\tau(z,t)}{\varrho\ \partial U(z,t)/\partial z} = \frac{|\tau(z)| \cos\{ \omega t + \theta(z) \}}{\varrho\ \partial |U(z)|/\partial z\ \cos\omega t} \tag{2.112}$$

$$= \frac{|\tau(z)|}{\varrho\ \partial |U(z)|/\partial z} \left\{ \cos\theta(z) - \sin\theta(z) \tan\omega t \right\}$$

which indicates that the eddy viscosity defined in the real formalism may be a function of elevation and time.

Horikawa & Watanabe (1968) used their experimental data and Eq.(2.106) to evaluate the spatial and temporal variation of eddy viscosity in the real formalism and found that the eddy viscosity was time−dependent. The variation of eddy viscosity with time calculated by Horikawa & Watanabe (1968) is shown in Fig.2.23.

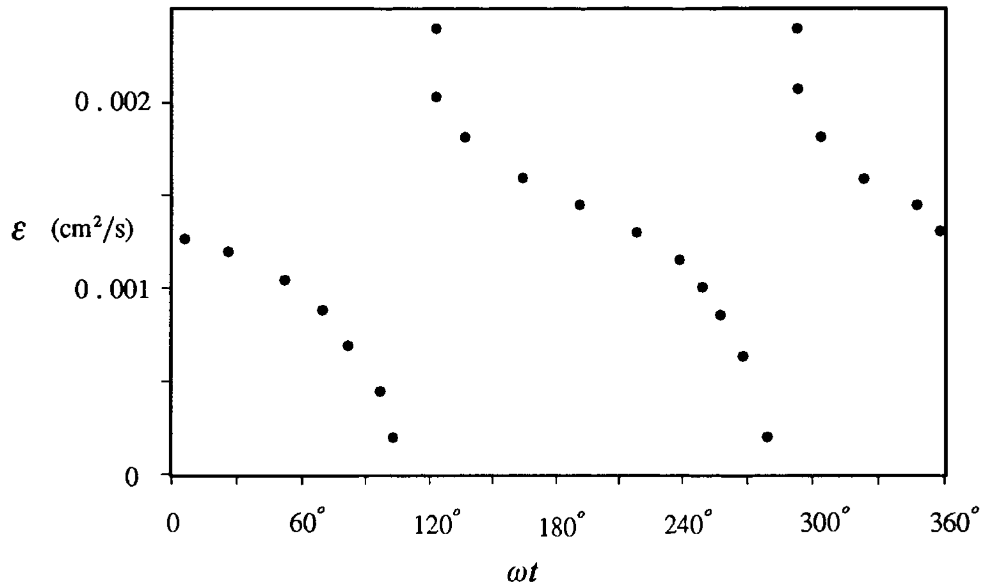

Fig.2.23 The variation of the time–dependent eddy viscosity at $z = 19.1mm$ above smooth bed

§2.5.2.2 A Complex Formalism Definition

Now, we apply the complex formalism to analyse Eq.(2.106) writing the velocity and shear stress in the form of complex exponential

$$U(z,t) = |U(z)|\ e^{i\omega t} \tag{2.113}$$

$$\tau(z,t) = |\tau(z)|\ e^{i\omega t + i\,\theta(z)} \tag{2.114}$$

Hence

$$\varepsilon(z) = \frac{\tau(z,t)}{\varrho \partial U(z,t)/\partial z} = \frac{|\tau(z)|}{\varrho |\partial U(z)|/\partial z} e^{i\theta(z)} \tag{2.115}$$

which indicates that the eddy viscosity is time–independent, but may be complex. You *et al.* (1991c) studied the dependency of eddy viscosity with time in the complex formalism. It was concluded from Eq.(2.86) that the eddy viscosity should be time–independent when only the first harmonic component was considered. The variation of eddy viscosity derived from experimental data M00RAL & M00RBL of van Doorn (1982) via Eq.(2.86) is shown in Fig.2.17.

§2.5.2.3 Eddy Viscosities from the Two Formalisms

Through the simple mathematical derivation of eddy viscosity above, it is evident that the two forms of eddy viscosity derived in the real formalism and in the complex formalism are both correct, but quite different. Therefore, the following questions remain to be answered

(1) What formalism should be chosen for studying the eddy viscosity ?

(2) What is the relationship between the eddy viscosity defined in the real formalism and the one defined in the complex formalism ?

The choice of the eddy viscosity definition in the complex formalism or in the real formalism depends on which formalism is used to solve the equation of motion Eq.(2.25). Normally, for the eddy viscosity models, the equation of motion Eq.(2.25) is solved analytically in the complex formalism, so that the eddy viscosity should be defined in the complex formalism. This is also the approach which is used in the present study.

The eddy viscosity defined in the complex formalism is time independent and may be considered as a real–valued finite parameter as You *et al.* (1991c) discussed, see Fig.2.17. However, the eddy viscosity defined in the real formalism is time–dependent and goes infinite at a certain phase as shown in Fig.2.23. Therefore, the values of eddy viscosity calculated from the real formalism definition are quite different from those from the complex formalism definition.

§2.5.3 DERIVATION OF A FORMULA FOR EDDY VISCOSITY

In this section, we are going to derive an eddy viscosity based on the equation of motion Eq.(2.25) and the definition of the eddy viscosity Eq.(2.106) in the complex formalism. Combining Eq.(2.25) with Eq.(2.106) leads to

$$\frac{\partial U(z,t)}{\partial t} = \frac{\partial U_{\infty}(t)}{\partial t} + \frac{\partial}{\partial z}\left\{\varepsilon \frac{\partial U(z,t)}{\partial z}\right\} \tag{2.116}$$

which can be rewritten as

$$\frac{\partial}{\partial t}\{\ U_\infty(t) - U(z,t)\ \} = \frac{\partial}{\partial z}\left\{\varepsilon \frac{\partial}{\partial z}\{\ U_\infty(t) - U(z,t)\ \}\right\} \tag{2.117}$$

Now, writing a simple harmonic velocity component in the form of complex exponential

$$U_\infty(t) = A\omega\ e^{i\omega t} \tag{2.118}$$

$$U(z,t) = |U(z)|\ e^{i\phi(z)}\ e^{i\omega t} \tag{2.119}$$

where $\phi(z)$ is the phase lead of $U(z,t)$ relative to $U_\infty(t)$, $A\omega$ is the amplitude of the free stream velocity $U_\infty(t)$ and $|U(z)|$ the local velocity amplitude.

Therefore,

$$U_\infty(t) - U(z,t) = \left\{\ A\omega - |U(z)|\ e^{i\phi}\ \right\}\ e^{i\omega t} \tag{2.120}$$

and

$$\frac{\partial}{\partial t}\{\ U_\infty(t) - U(z,t)\ \} = i\omega\left\{\ A\omega - |U(z)|\ e^{i\phi(z)}\ \right\}\ e^{i\omega t} \tag{2.121}$$

$$\frac{\partial}{\partial z}\{\ U_\infty(t) - U(z,t)\ \} = \frac{\partial}{\partial z}\left\{\ A\omega - |U(z)|\ e^{i\phi(z)}\ \right\}\ e^{i\omega t} \tag{2.122}$$

Substituting (2.121) and (2.122) into (2.117) and simplifying it, we obtain

$$i\omega\left\{\ A\omega - |U(z)|e^{i\phi(z)}\ \right\} = \frac{\partial}{\partial z}\left\{\varepsilon \frac{\partial}{\partial z}\left\{A\omega - |U(z)|e^{i\phi(z)}\right\}\right\} \tag{2.123}$$

Hence

$$\varepsilon = \frac{i\omega \displaystyle\int_z^\infty \left\{\ A\omega - |U(z)|\ e^{i\phi(z)}\ \right\}dz}{\dfrac{\partial}{\partial z}\left\{\ A\omega - |U(z)|\ e^{i\phi(z)}\ \right\}} \tag{2.124}$$

It is shown in Eq.(2.124) that the eddy viscosity must be time−independent, but may be complex when the first harmonic component is considered.

§2.5.4 EDDY VISCOSITY VALUES EVALUATED FROM EXPERIMENTS

§2.5.4.1 Introduction to Experimental Measurements

Before calculating the values of eddy viscosity from Eq.(2.124), we briefly introduce experimental measurements in Table.2.1.

Jonsson & Carlsen (1976)		van Doorn (1981) & (1982)			Sleath (1987)					Jensen (1989)	
No.1	No2	VRA	SRAL	MRAL	Test3	Test4	Test5	Test9	Test10	Test12	Test13

TESTS	Experimental Parameters						Estimation
	$A\omega$ (cm/s)	T (s)	K_N (mm)	K_N/A	$\hat{U}^*$ (cm/s)	δ_1 (mm)	$\frac{0.5\kappa\hat{U}^*}{\omega}$ (mm)
No.1	211.0	8.39	21.0	7.4×10^{-3}	21.1	60.0	56.4
No.2	153.0	7.20	63.0	3.6×10^{-2}	21.5	57.0	49.3
V00RA	26.7	2.00	21.0	2.5×10^{-1}	4.3	5.0	2.7
S00RAL	32.3	2.00	21.0	2.0×10^{-1}	5.7	5.3	3.6
M00RAL	106.0	2.00	21.0	6.2×10^{-2}	15.3	10.0	9.8
Test3	68.6	4.54	3.3	6.9×10^{-3}	7.6	9.0	11.0
Test4	61.7	4.58	3.3	7.3×10^{-3}	5.6	8.0	8.1
Test5	49.0	4.48	3.3	9.4×10^{-3}	4.6	6.5	6.6
Test9	62.1	4.55	16.2	3.6×10^{-2}	7.6	11.5	11.2
Test10	48.7	4.50	16.2	4.8×10^{-2}	6.9	10.0	9.9
Test−12	95.5	9.72	0.8	5.7×10^{-4}	6.2	20.0	19.2
Test−13	191.4	9.72	0.8	2.8×10^{-4}	11.0	36.0	34.1

Table.2.1 Basic parameters measured in turbulent oscillatory boundary layer flows

In Table.2.1, the friction velocity $\hat{U}^*$ is obtained by fitting a logarithmic profile to the experimentally determined velocity distribution as demonstrated in Fig.2.24 using van Doorn (1981) experimental data V00RA, and the boundary layer thickness δ_1 defined by Jonsson & Carlsen (1976) is approximated by δ_y defined in Fig.2.24.

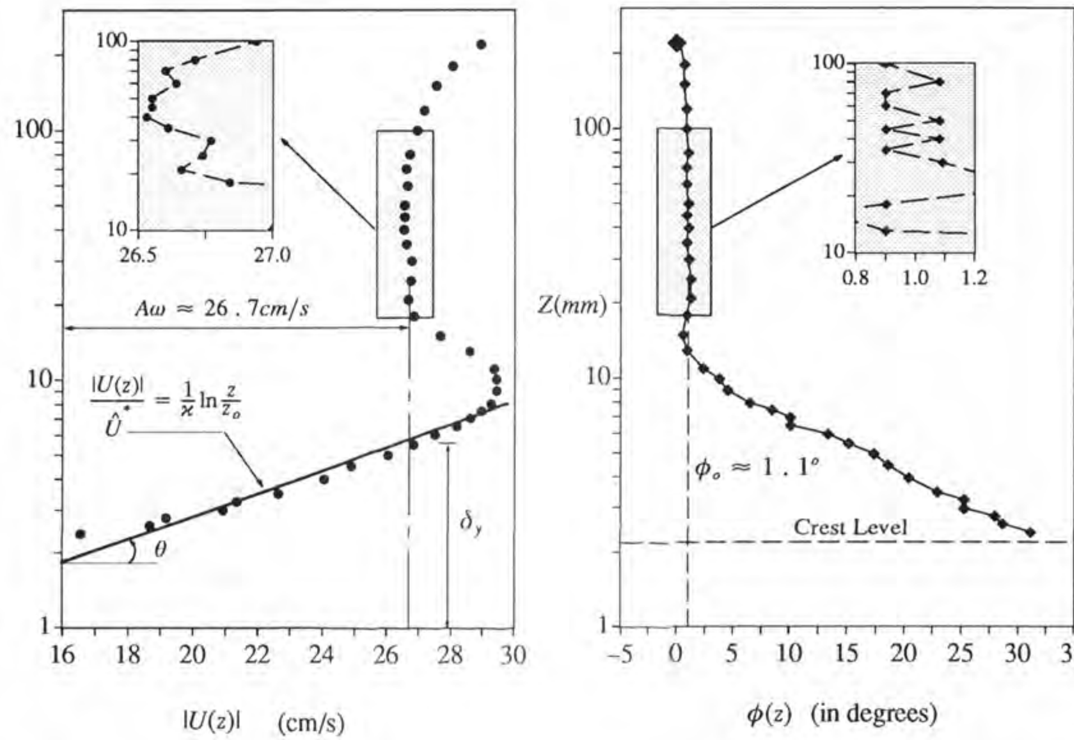

Fig.2.24 Determination of experimental parameters $A\omega$, δ_y, $\phi_o(z)$ and $\hat{U}^*$ in turbulent boundary layers

As we discussed in the smooth laminar flow, it is acceptable to have $\delta_1 \approx \delta_y$ since $\delta_1 = 1.6\sqrt{2\nu/\omega}$ and $\delta_y = 1.5\sqrt{2\nu/\omega}$ as shown in Fig.2.8. For turbulent oscillatory boundary layer flows, it is still reasonable to have $\delta_1 \approx \delta_y$ because as $z \geq \delta_1$, the velocity phase shift relative to the free stream velocity in the turbulent boundary layer is small, and therefore $U(z)/|U(z)| \rightarrow 1.0$ as shown in Fig.2.25. This implies that δ_1 defined from the velocity profile $U(z)$ is approximately equal to δ_y defined from the velocity amplitude profile $|U(z)|$.

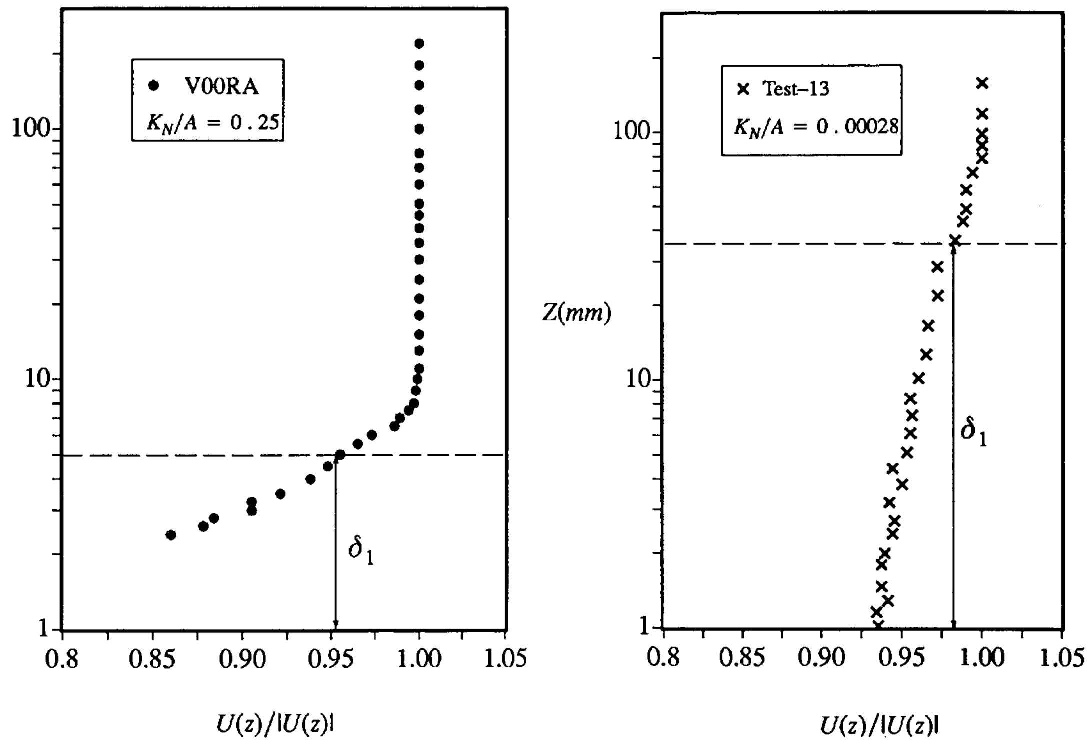

Fig.2.25 Variation of $U(z)/|U(z)|$ with elevation and relative roughness in turbulent boundary layers

The reason for this approximation is that most of measurements in Table.2.1 directly give the velocity amplitude profiles $|U(z)|$ instead of the time independent velocity profiles $U(z)$, so that it is convenient to measure δ_1 directly from the velocity amplitude profile $|U(z)|$.

§2.5.4.2 Evaluation of the Eddy Viscosity from Data

Values of the eddy viscosity in a turbulent boundary layer can be calculated from Eq.(2.124), which for discrete data can be approximated by

$$\varepsilon(z_N) = \frac{i\omega \sum_{j=N}^{\infty} \left\{A\omega - |U_j(z)|e^{i\phi_j(z)}\right\}\left\{z_{j+1} - z_{j-1}\right\}}{\dfrac{\left\{|U_{N+1}(z)|e^{i\phi_{N+1}(z)} - |U_{N-1}(z)|e^{i\phi_{N-1}(z)}\right\}}{\left\{z_{N+1} - z_{N-1}\right\}}} \qquad N = 2,\ 3,\ 4,\ 5\ \ldots\ldots \qquad (2.125)$$

It is worthwhile to mention here that the eddy viscosity calculated from Eq.(2.125) will be affected by the following aspects :

(A) The elevation increments $\{z_{N+1} - z_{N-1}\}$. The velocity gradient $\partial U(z)/\partial z$ can be approximated by

$$\frac{\partial U(z)}{\partial z}\bigg|_{z=z_N} \approx \frac{U_{N+1}(z) - U_{N-1}(z)}{z_{N+1} - z_{N-1}} \tag{2.126}$$

only when $\{z_{N+1} - z_{N-1}\}$ is relative small.

(B) The defect velocity $\{A\omega - U(z)\}$. The defect velocity is the difference between the two quantities of the free stream velocity $A\omega$ and the local velocity $U(z)$ Therefore, beyond a certain height [e.g. $z > 13mm$ in Fig.2.24] the calculated defect velocities are not reliable because the local velocities are so close to the free stream velocity and show erratic behaviours.

In general, the eddy viscosity values determined from Eq.(2.125) in the region of $z < \delta_1$ are reliable since the defect velocity $\{A\omega - U(z)\}$ is a substantial fraction of $A\omega$, see Fig.2.24, and the elevation increments are small. However, when $z > 2\delta_1$ the eddy viscosity evaluated from Eq.(2.125) may be not reliable since the the local velocity $U(z)$ is so close to the free stream velocity $A\omega$ and shows erratic behaviours as shown in Fig.2.24. The eddy viscosity values estimated in the region of $\delta_1 < z < 2\delta_1$ may be suspected in some tests, e.g. Jonsson & Carlsen Test No.1 and Jensen (1989) Test−12 & Test−13. The reason for this may be that the elevation increments $\{z_{N+1} - z_{N-1}\}$ are too large to give true velocity gradients.

Therefore, estimated eddy viscosity values will not be given for the range of $z \geq 2\delta_1$ in Fig.2.26 to Fig.2.31, and in the range of $\delta_1 < z < 2\delta_1$ caution should be taken when the eddy viscosity data are studied.

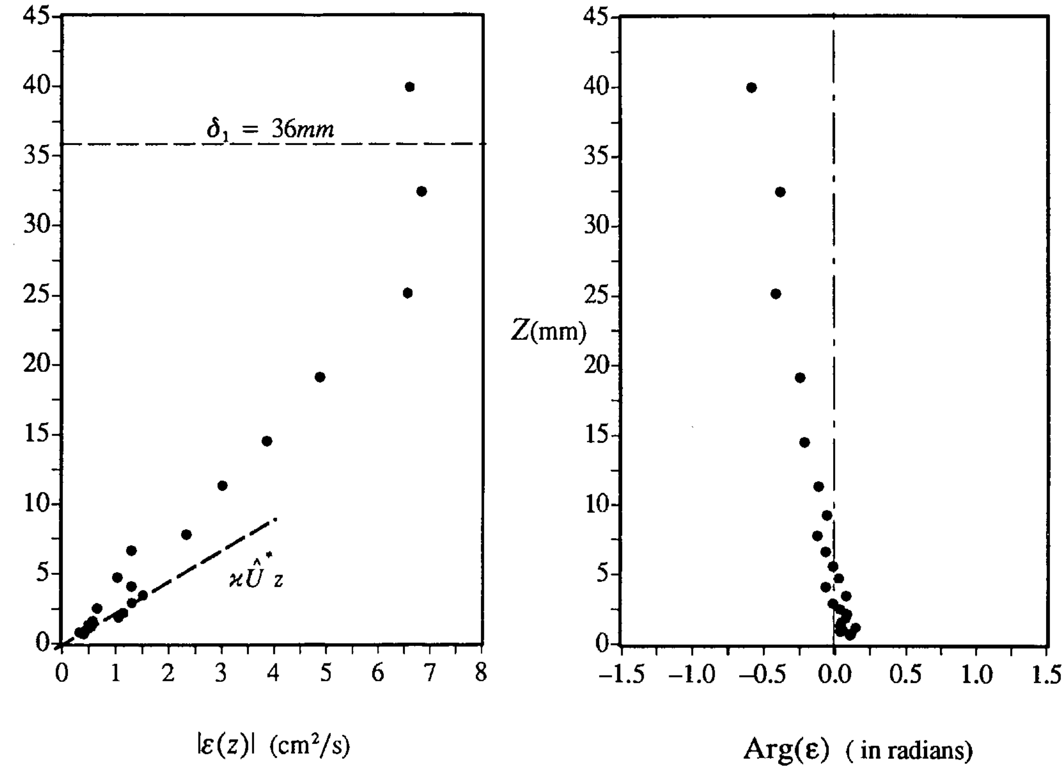

Fig.2.26 The eddy viscosity evaluated from Jensen (1989) Test–13 via Eq.(2.125)

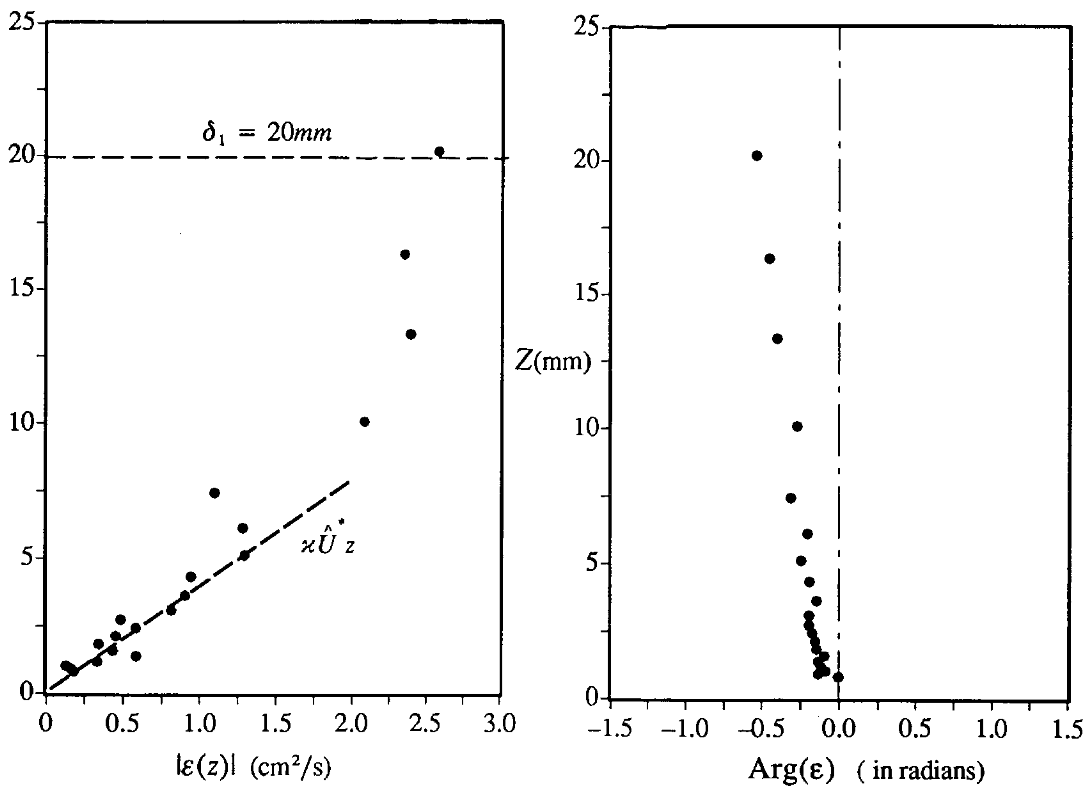

Fig.2.27 The eddy viscosity evaluated from Jensen (1989) Test–12 via Eq.(2.125)

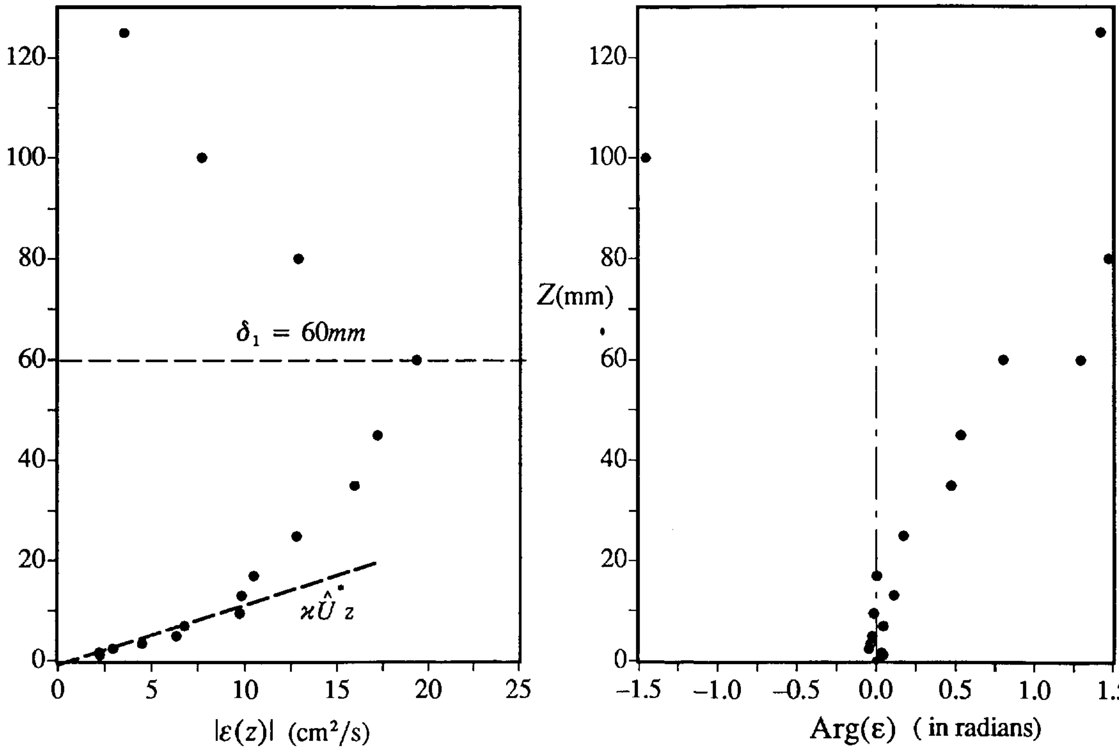

Fig.2.28 The eddy viscosity estimated from Jonsson & Carlsen (1976) test No.1 via Eq.(2.125)

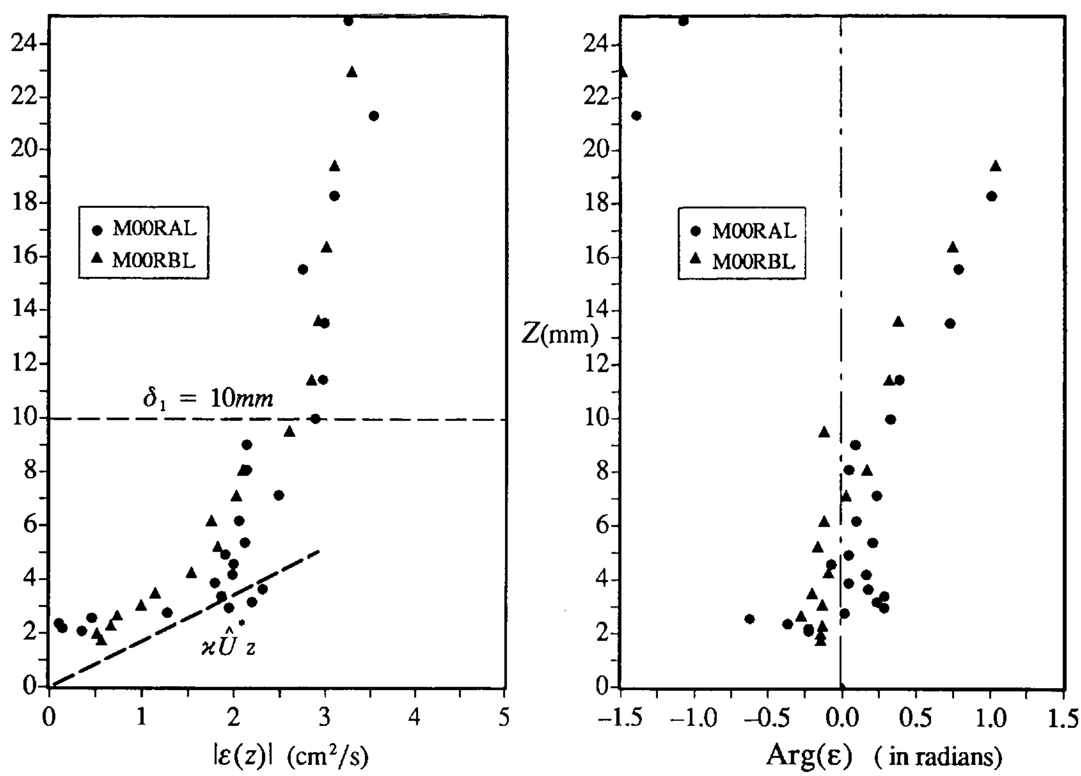

Fig.2.29 The eddy viscosity evaluated from van Doorn (1982) M00RAL & M00RBL via Eq.(2.125)

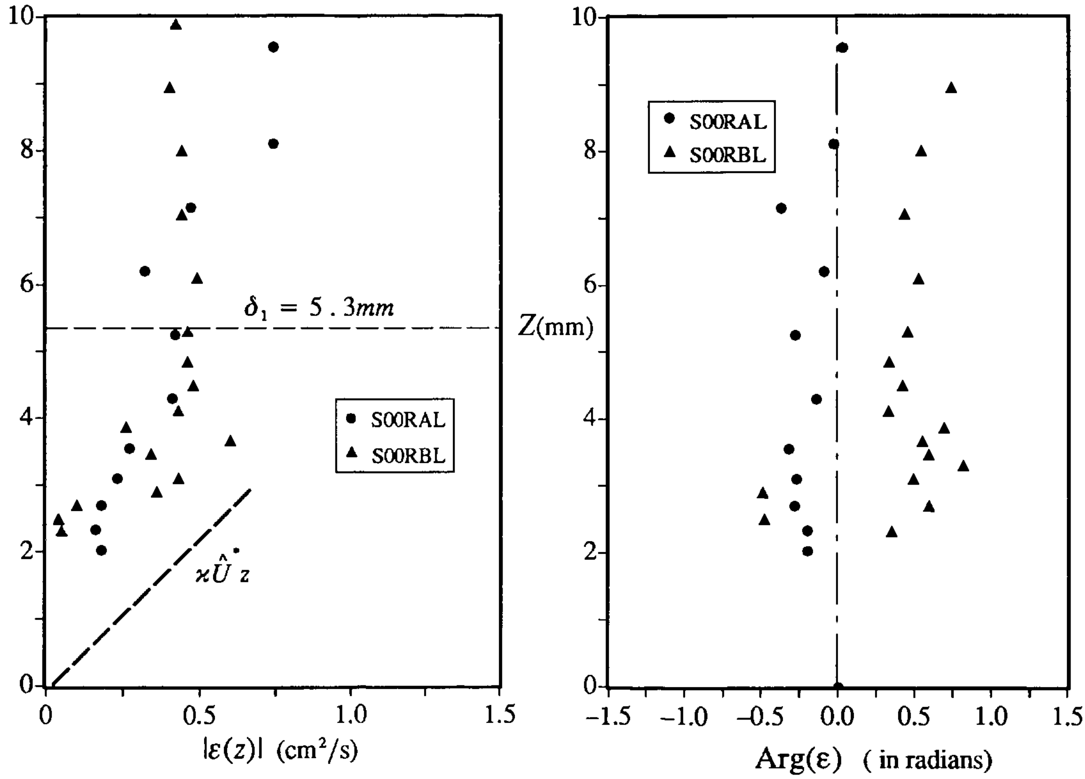

Fig.2.30 The eddy viscosity evaluated from van Doorn (1982) S00RAL & S00RBL via Eq.(2.125)

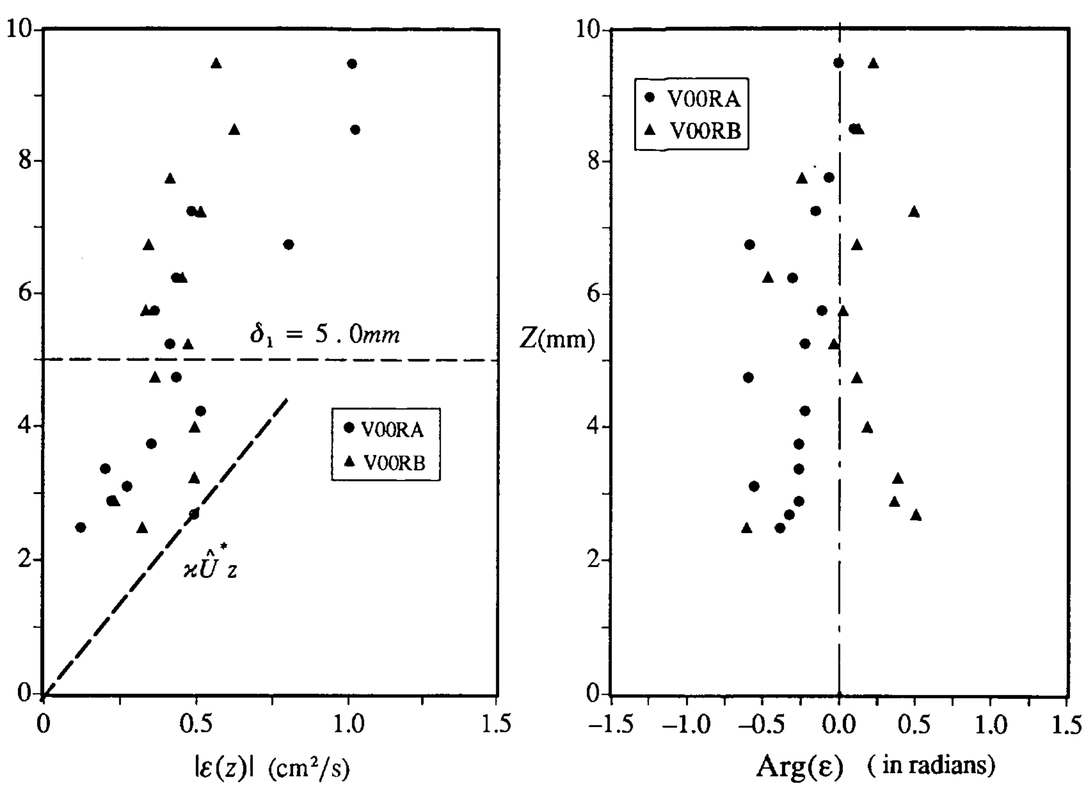

Fig.2.31 The eddy viscosity evaluated from van Doorn (1981) V00RA & V00RB via Eq.(2.125)

§2.5.5 THE EDDY VISCOSITY MODEL

Fig.2.26 through Fig.2.31 show the variation of the complex eddy viscosity with elevation. It is seen that the argument of the complex eddy viscosity Arg(ε) is generally small in the region of $z < \delta_1$, and in the region of $\delta_1 < z < 2\delta_1$ the argument Arg(ε) is considerable for some tests, e.g. Jonsson & Carlsen Test No.1, but we shall still assume that Arg(ε) is small because the increase of Arg(ε) in this region may be caused by too large elevation increments $\{z_N - z_{N-1}\}$. Consequently, as a first approximation, the imaginary part of the eddy viscosity will be neglected in the following and the eddy viscosity is assumed to be a real−valued function of elevation z only

Based on the analysis of the eddy viscosity in Fig.2.26 to Fig.2.31, the eddy viscosity distribution in the turbulent oscillatory boundary layer is described by the following functional form as suggested by You *et al.* (1991c) [see Fig.2.18]

$$\varepsilon(z) = \kappa \hat{U}^* \delta_o \left\{1 - (1 - z/\delta_1)^2 \right\} \qquad 0 \le z \le \delta_1 \qquad (2.127)$$

$$\varepsilon(z) = \kappa \hat{U}^* \delta_o \qquad \delta_1 \le z < \delta_w \qquad (2.128)$$

where

$$\delta_o = C\delta_1$$

where C is constant which should be determined from the experiments. Based on all of the available experimental data from Jonsson & Carlsen (1976) Test No.1 & No.2, van Doorn (1981 & 1982) V00RA, S00RAL & M00RAL, Sleath (1987) Test−3, Test−4, Test−5, Test−9 & Test−10, and Jensen (1989) Test−12 & Test−13, it has been found that $C \approx 0.4$. The eddy viscosity model described by Eqs.(2.127) and (2.128), in which the values of δ_1 and $\hat{U}^*$ are taken from Table.2.1, is plotted against the eddy viscosities evaluated from the above experiments in Fig.2.32 to Fig.2.34.

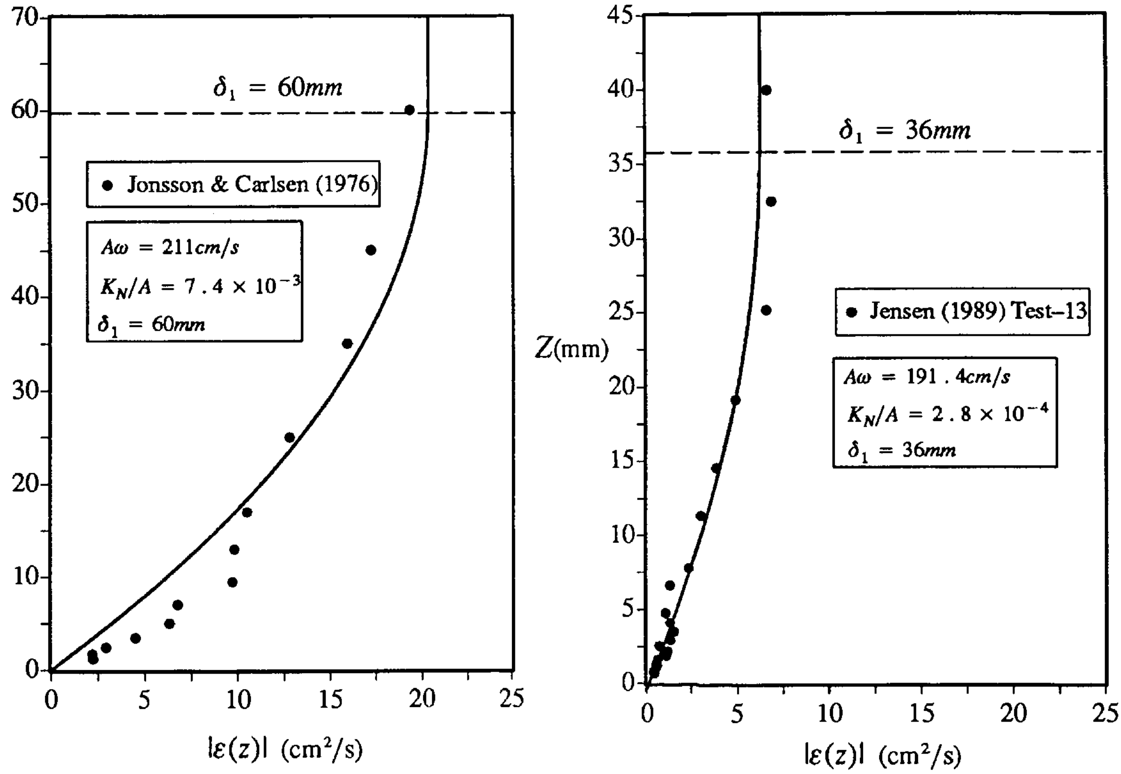

Fig.2.32 The comparison of the present eddy viscosity model with eddy viscosity data evaluated

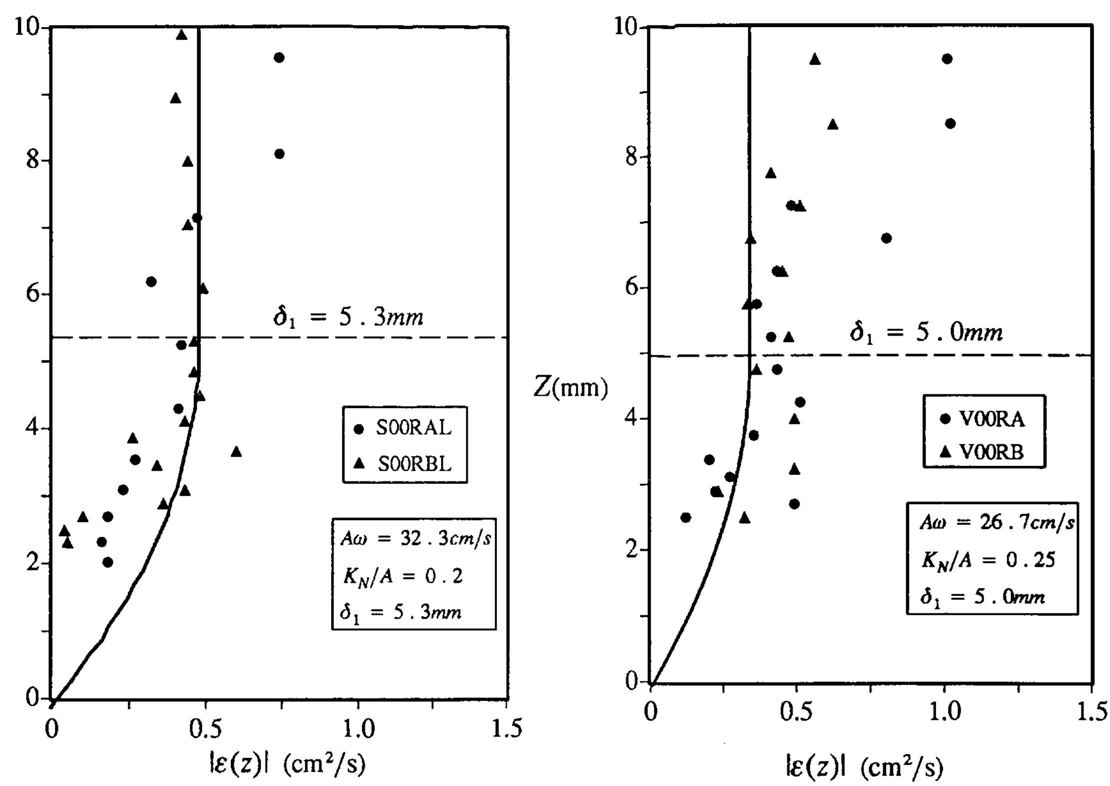

Fig.2.33 The comparison of the present eddy viscosity model with eddy viscosity data evaluated

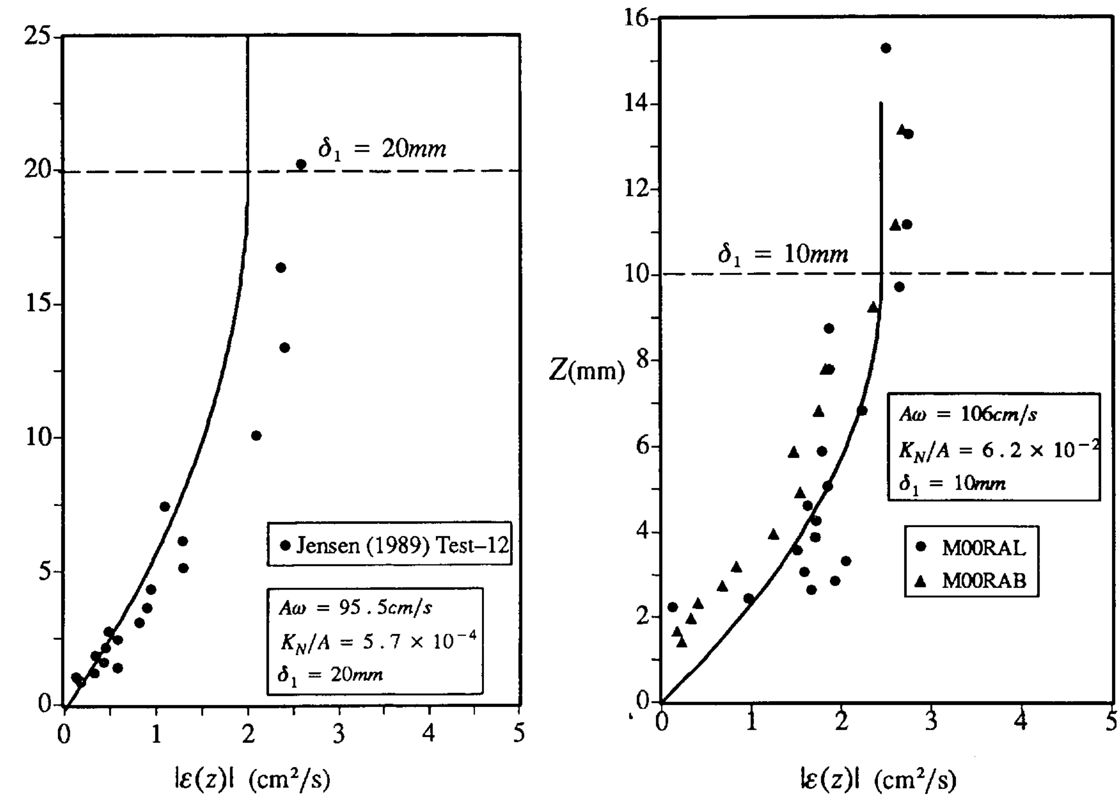

Fig.2.34 The comparison of the present eddy viscosity model with eddy viscosity data evaluated

It can be seen from Fig.2.32 to Fig.2.34 that the present eddy viscosity model is in reasonable agreement with the experimental data over a wide range of relative roughness $[2.8 \times 10^{-4} \le K_N/A \le 0.25]$.

However, application of the eddy viscosity model requires knowledge of the unknown parameter δ_1 in Eqs.(2.127) and (2.128). In other words, a further relationship between δ_1 and $\hat{U}^*$ is needed. In Fig.2.35, values of δ_1 taken from Table.2.1 are plotted against predicted values. It is seen that the data from the oscillating water tunnel experiments are fitted quite well by the formula

$$\delta_1 = \frac{0.5\kappa\hat{U}^*}{\omega} \tag{2.129}$$

but the V00RA data from from a wave flume experiment is not so well predicted by Eq(2.129). The reasons for this are not clear and therefore further experimental data would be required to resolve this. Nevertheless, we assume that δ_1 measured in wave flume experiments may be twice that predicted by Eq.(2.129). This relationship should be confirmed by more experimental data in future.

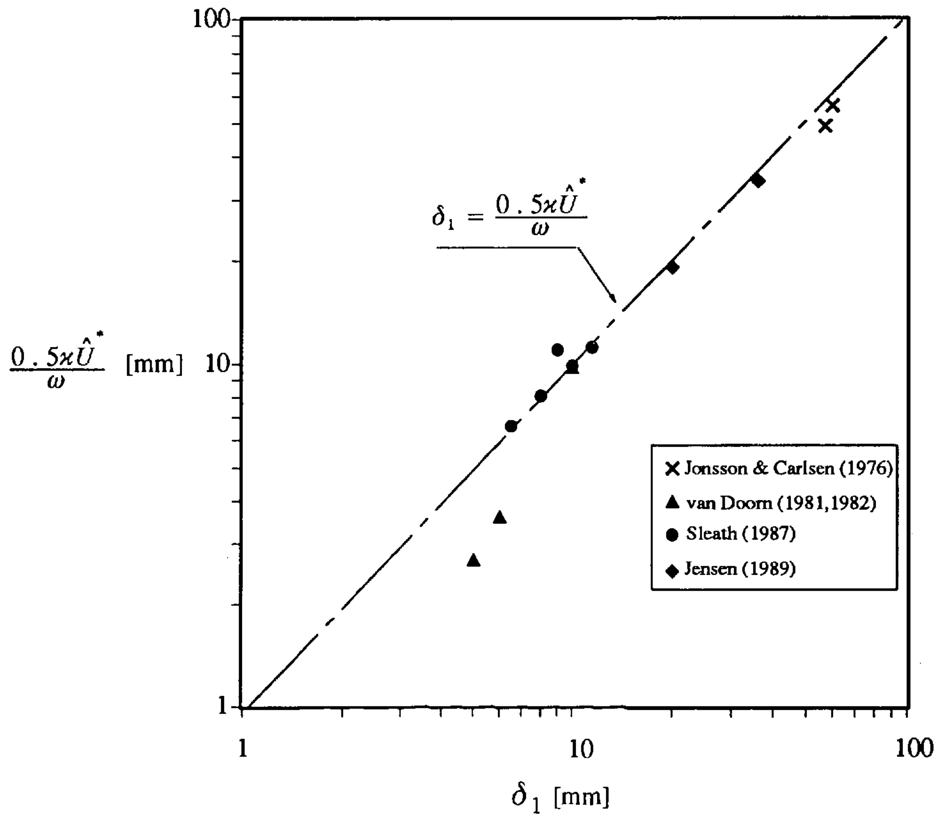

Fig.2.35 The comparison between measured δ_1 and that predicted in oscillatory boundary layers

§2.5.6 SOLUTION OF THE EQUATION OF MOTION

The formalism used for solving the equation of motion is the complex notation since when only the first−order solution is required, the use of the complex formalism deletes the time dependency and simplifies the solution procedure. Expressing the velocities in complex form, we have

$$U_\infty(t) \quad = \quad A\omega\ e^{i\omega t} \tag{2.130}$$

$$U(z,t) \quad = \quad U(z)\ e^{i\omega t} \quad = \quad |U(z)|\ e^{i\phi(z)}\ e^{i\omega t} \tag{2.131}$$

Similarly, the defect velocity $U_d(z,t)$ is assumed to have the form

$$U_d(z,t) = U_d(z)\ e^{i\omega t} = |U_d(z)|\ e^{i\phi_d(z)}\ e^{i\omega t} \tag{2.132}$$

By substituting Eq.(2.132) into Eq.(2−25), the equation of motion can be written in terms of $U_d(z)$ as

$$\varepsilon(z)\frac{\partial^2 U_d(z)}{\partial^2 z} + \frac{\partial \varepsilon(z)}{\partial z}\frac{\partial U_d(z)}{\partial z} - i\omega U_d(z) = 0 \tag{2.133}$$

The physical interpretation of the velocities and phase shifts in the complex plane are indicated in Fig.2.36.

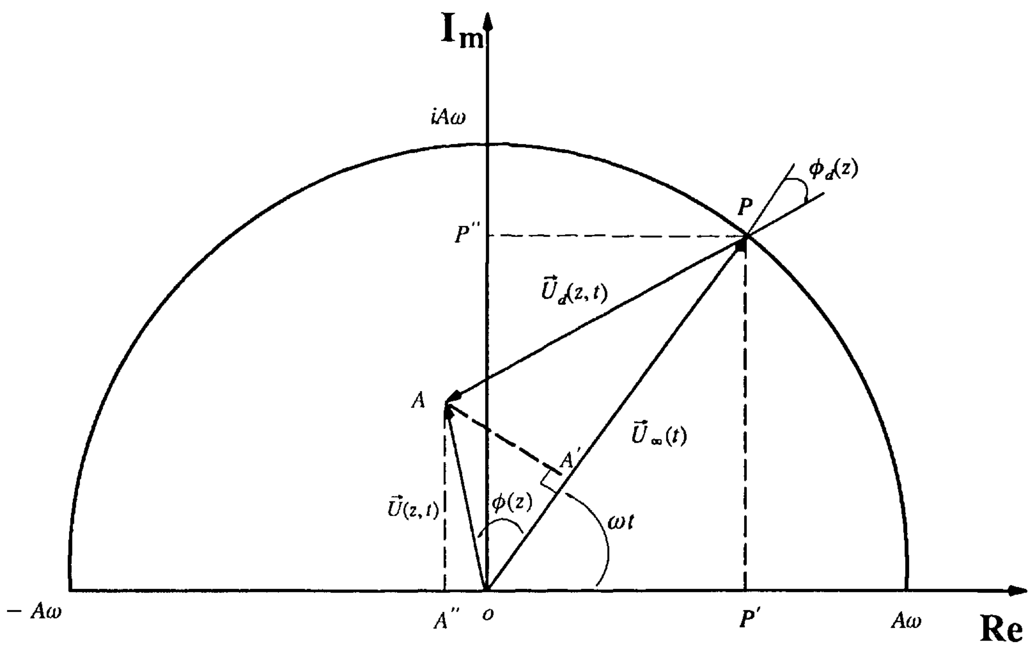

Fig.2.36 The definitions of the velocities and phase shifts in a complex plane

Here, it would be better, we think, to explain the physical meaning of the velocity phase shift $\phi(z)$ in the real plane. As mentioned previously, the velocity phase shift $\phi(z)$ is defined as the difference between the phase of the free stream velocity and that of the local velocity, which is physically shown in Fig.2.37.

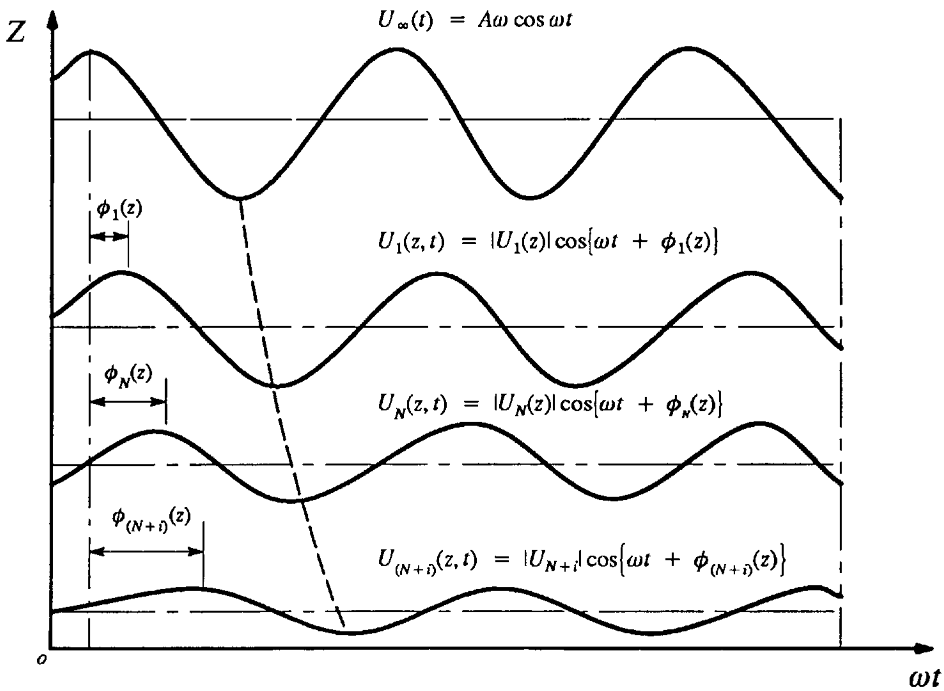

Fig.2.37 The definition of local velocity phase shift relative to free stream velocity in a real plane

§2.5.6.1 Wave Motion in the Inner Layer

The defect velocity $U_d(z)$ in Eq.(2.133) may be solved out analytically after appropriate substitutions are made for the vertical distribution of the eddy viscosity and boundary conditions. Substituting the previously determined distribution of the eddy viscosity $\varepsilon(z)$ in the inner layer

$$\varepsilon(z) = \varkappa \hat{U}^* \delta_o \left\{ 1 - \left\{ 1 - z/\delta_1 \right\}^2 \right\} \tag{2.127}$$

into the equation of motion Eq.(2.133) and introducing the nondimensional variable

$$\xi = \frac{z}{\delta_1} - 1$$

we obtain

$$(1 - \xi^2)\frac{\partial^2 U_d(z)}{\partial \xi} - 2\xi\frac{\partial U_d(z)}{\partial \xi} + \lambda(\lambda + 1)U_d(z) = 0 \tag{2.134}$$

where

$$\lambda\,(\lambda\,+\,1) \;=\; -\,i\beta \qquad\qquad \beta \;=\; \frac{\delta_1^2\omega}{\varkappa\hat{U}^*\delta_o} \tag{2.135}$$

Eq.(2.134) is known as Legendre's differential equation. The general solution of Legendre's equation was discussed by Gradshteyn & Ryzhik (1980), and given by

$$U_d(\xi) \;=\; C_1 P_\lambda(\xi) \;+\; C_2 Q_\lambda(\xi) \tag{2.136}$$

where C_1 and C_2 are unknown constants to be determined from the boundary conditions. The functions $P_\lambda(\xi)$ and $Q_\lambda(\xi)$, called Legendre's function of the first and second orders respectively, are given by

$$P_\lambda(\xi) = F\left\{-\lambda, 1+\lambda, 1, \frac{1-\xi}{2}\right\} \qquad |1-\xi| < 2 \tag{2.137}$$

$$Q_\lambda(\xi) = \frac{\pi}{2\sin(\lambda\pi)}\left\{\cos(\lambda\pi)\;P_\lambda(\xi) \;-\; P_\lambda(-\xi)\right\} \qquad |1-\xi| < 2 \tag{2.138}$$

where the first order Legendre's function is defined by

$$F(a,b;c;z) \;=\; \frac{\Gamma(c)}{\Gamma(a)\,\Gamma(b)}\sum_{n=0}^{\infty}\frac{\Gamma(a+n)\,\Gamma(b+n)}{\Gamma(c+n)}\,\frac{z^n}{n!}$$

§2.5.6.2 Wave Motion in the Outer Layer

In a similar way, by substituting the suggested eddy viscosity distribution in the outer layer

$$\varepsilon(z) \;=\; \varkappa\hat{U}^*\delta_o \tag{2.128}$$

into Eq.(2.133), it leads to

$$\frac{\partial^2 U_d(z)}{\partial z^2} \;-\; \frac{i\omega}{\varkappa\hat{U}^*\delta_o}U_d(z) \;=\; 0 \tag{2.139}$$

Eq.(2.139) is an ordinary differential equation of the second order, and has the particular solution

$$U_d(z) = C_3 \exp\{ -\eta(1+i)z \} \tag{2.140}$$

after applying the boundary condition

$$U_d(z) = 0 \qquad \text{for} \quad z \to \infty \tag{2.141}$$

where η is defined as

$$\eta = \left\{ \frac{\omega}{2\varkappa \hat{U}^* \delta_o} \right\}^{0.5} \tag{2.142}$$

and C_3 is an unknown constant, whose value is determined by the boundary conditions.

§2.5.6.3 The Boundary Conditions

In order to determine the unknown constants C_1, C_2 and C_3 in Eqs.(2.136) and (2.140), the boundary conditions must be given properly and completely. The boundary conditions in the inner and outer layers are given as

i. The velocity $U(z,t)$at the bed should be equal to zero, that is

$$C_1\, P_\lambda(\xi_o) + C_2 \frac{\pi}{2\sin\lambda\pi}\{ \cos\lambda\pi\, P_\lambda(\xi_o) - P_\lambda(-\xi_o) \} = -A\omega \tag{2.143}$$

ii. The velocity calculated by Eq.(2.136) at $z = \delta_1$ in the inner layer should be equal to that calculated by Eq.(2.140) at $z = \delta_1$ just outside the inner layer, that is

$$C_1\, P_\lambda(0) + C_2 \frac{\pi}{2\sin\lambda\pi}\{ \cos\lambda\pi - 1 \} P_\lambda(0) = C_3\, e^{-\eta(1+i)\delta_1} \tag{2.144}$$

iii. The continuity of the shear stress at $z = \delta_1$, which implies the continuity of the velocity gradient $U_d(z)/\partial z$ at $z = \delta_1$, that is

$$C_1\, P'_\lambda(0) + C_2 \frac{\pi}{2\sin\lambda\pi}\{ \cos\lambda\pi + 1 \} P'_\lambda(0) = -C_3 \eta(1+i)\delta_1\, e^{-\eta(1+i)\delta_1} \tag{2.145}$$

§2.5.6.4 Solution of the Equation of Motion

We now have got the velocity distributions in the inner layer and the outer layer, and the boundary conditions. Therefore, the unknown constants C_1, C_2 and C_3 can be determined by combining Eqs.(2.143), (2.144) and (2.145) as

$$C_1 = -A\omega \frac{\pi \left\{\eta(1+i)\delta_1(\cos\lambda\pi - 1)P_\lambda(0) + (\cos\lambda\pi + 1)P'_\lambda(0)\right\}}{2\sin\lambda\pi \; D \; e^{\eta(1+i)\delta_1}} \tag{2.146}$$

$$C_2 = A\omega \frac{\eta(1+i)\,\delta_1\, P_\lambda(0) + P'_\lambda(0)}{D\; e^{\eta(1+i)\delta_1}} \tag{2.147}$$

$$C_3 = -A\omega \frac{\pi\, P_\lambda(0)\, P'_\lambda(0)}{2\sin\lambda\pi\; D} \tag{2.148}$$

where D is the determinant of the matrix

$$\begin{bmatrix} P_\lambda(\xi_o) & \frac{\pi}{2\sin\lambda\pi}\left\{\cos\lambda\pi\; P_\lambda(\xi_o) - P_\lambda(-\xi_o)\right\} & 0 \\ P_\lambda(0) & \frac{\pi}{2\sin\lambda\pi}\{\cos\lambda\pi - 1\}P_\lambda(0) & -e^{-\eta(1+i)\delta_1} \\ P'_\lambda(0) & \frac{\pi}{2\sin\lambda\pi}\{\cos\lambda\pi + 1\}P'_\lambda(0) & \eta(1+i)\delta_1\, e^{-\eta(1+i)\delta_1} \end{bmatrix}$$

By introducing C_1, C_2 and D in Eq. (2.136) and rearranging, the final expression of $U(\xi, t)$ in the inner layer is given by

$$U(\xi,t) = \left\{ 1 - \frac{(p - \cos\lambda\pi)\, P_\lambda(\xi) + P_\lambda(-\xi)}{(p - \cos\lambda\pi)\, P_\lambda(\xi_o) + P_\lambda(-\xi_o)} \right\} U_\infty(t) \tag{2.149}$$

where p is given by

$$p = \frac{\eta(1+i)\delta_1(\cos\lambda\pi - 1) + (\cos\lambda\pi + 1)q}{\eta(1+i)\delta_1 + q}$$

and q is given by

$$q = \frac{P'_\lambda(0)}{P_\lambda(0)} = \frac{1}{4\pi^2}\lambda^2 \sin\lambda\pi \ \left\{ \Gamma\,(\lambda/2)\ \Gamma\,(1/2 - \lambda/2) \right\}^2$$

In a similar way, by substituting C_3 and D into Eq.(2.140) and rearranging, the final expression of $U(z, t)$ in the outer layer is given by

$$U(z,t) = \left\{ 1 - \frac{(\ p - \cos\lambda\pi + 1\ )\ P_\lambda(0)}{(\ p - \cos\lambda\pi\ )\ P_\lambda(\xi_o) + P_\lambda(-\ \xi_o)} e^{\{-\eta(1+i)(z-\delta_1)\}} \right\} \qquad (2.150)$$

where λ is given by

$$\lambda = -\frac{1}{2}(1 - a) - i\frac{\beta}{a} \qquad \text{where} \qquad a = \left\{ \frac{1}{2}\left\{ 1 + (1 + 16\beta^2)^{\frac{1}{2}} \right\} \right\}^{\frac{1}{2}}$$

§2.5.7 BED SHEAR STRESS AND FRICTION FACTOR

Although the forms of the velocity distribution in the inner and outer layers are given in Eqs.(2.149) and (2.150), we can not directly calculate the velocities unless the bottom shear stress, or alternatively wave friction factor are known. From Eq.(2.106), the maximum shear stress at the bed can be expressed as

$$\frac{\hat{\tau}_b(z_o)}{\varrho} = \left\{ \varepsilon(z) \frac{\partial U(\xi, t)}{\partial z} \right\}_{Max} \qquad (2.151)$$

On the other hand, the maximum bed shear stress $\hat{\tau}_b(z_o)$ is given by

$$\frac{\hat{\tau}_b(z_o)}{\varrho} = \frac{1}{2}\ f_w\ \{A\omega\}^2 \qquad (2.152)$$

By combining Eqs.(2.149), (2.151) and (2.152), wave friction factor f_w can be written as

$$f_w = 0\,.\,0512\left\{ 1 - \xi_o^2 \right\}^2\ Z(\xi_o)\ \hat{Z}(\xi_o) \qquad (2.153)$$

where $\hat{Z}(\xi_o)$ denotes the complex conjugate of $Z(\xi_o)$, which is given by

$$Z(\xi_o) = \frac{(p - \cos\lambda\pi)\,P'_\lambda(\xi_o) - P'_\lambda(-\xi_o)}{(p - \cos\lambda\pi)\,P_\lambda(\xi_o) + P_\lambda(-\xi_o)} \tag{2.154}$$

In the calculation of f_w, we have used

$$\frac{\partial P_\lambda(x)}{\partial x} = \frac{\lambda + 1}{x^2 - 1}\left\{ P_{(\lambda+1)}(x) - xP_\lambda(x) \right\} \tag{2.155}$$

However, wave friction factor f_w can not be obtained explicitly from Eq.(2.153) because f_w is the function of ξ and p, however ξ and p are also functions of f_w. Therefore, f_w can be obtained by iterating Eq.(2.153).

The definition of wave friction factor f_w given by Eq.(2.153), or defined by Kajiura (1968) and Jonsson & Carlsen (1976), corresponds to the level $z = K_N/30$, at which the velocity is assumed to be zero. Therefore, the friction factor $f_w(z_A)$ at $z = z_A$, which as shown in Fig.2.38, would be significantly different from that at $z = K_N/30$ if the relative roughness $K_N/A \geq 1$.

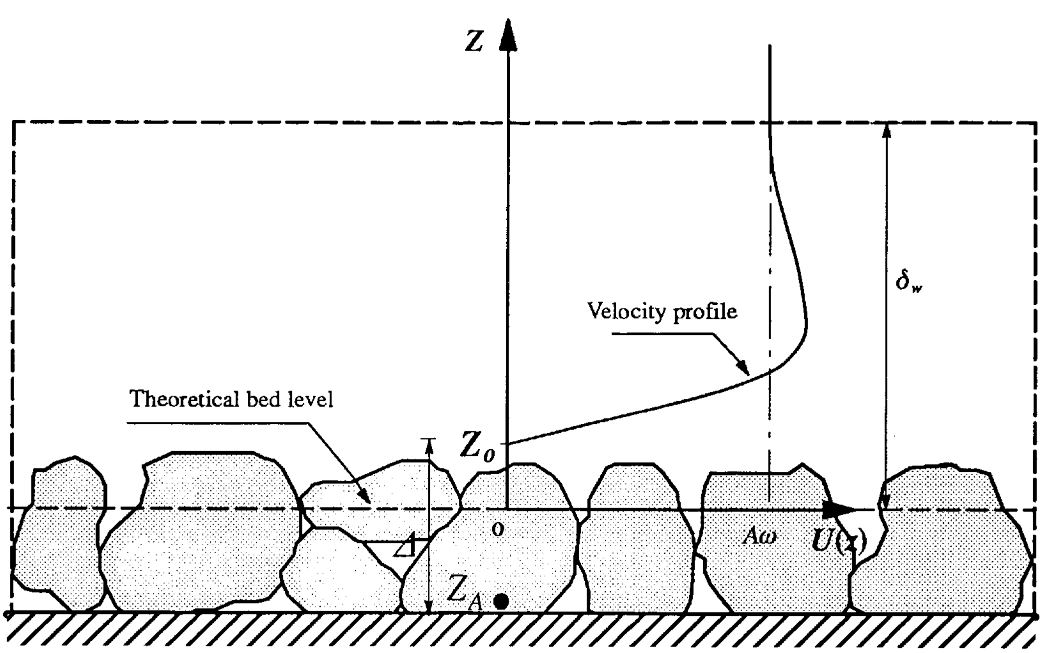

Fig.2.38 Sketch of a sand layer attached to a flat plate

The reason for this can be explained as follows. We use the simplified equation of motion which has been given in Eq.(2.25)

$$\frac{\partial U}{\partial t} = \frac{\partial U_\infty}{\partial t} + \frac{1}{\varrho}\frac{\partial \tau}{\partial z} \tag{2.25}$$

Hence, the shear stress at $z = z_A$ is obtained by integration of the above equation with respect to z between z_A and ∞, so that

$$\frac{\tau(z_A)}{\varrho} = \int_{z_A}^{\infty} \frac{\partial}{\partial t}\{ U - U_\infty \} \, dz \tag{2.156}$$

$$= \int_{z_A}^{z_o} \frac{\partial}{\partial t}\{ U - U_\infty \} \, dz + \int_{z_o}^{\infty} \frac{\partial}{\partial t}\{ U - U_\infty \} \, dz$$

$$= \int_{z_A}^{z_o} \frac{\partial}{\partial t}\{ - U_\infty \} \, dz + \int_{z_o}^{\infty} \frac{\partial}{\partial t}\{ U - U_\infty \} \, dz$$

$$= \int_{z_A}^{z_o} \frac{\partial}{\partial t}\{ - U_\infty \} \, dz + \frac{\tau(z_o)}{\varrho}$$

so that

$$\frac{\tau(z_A)}{\varrho} = \int_{z_A}^{z_o} \frac{\partial}{\partial t}\{ - U_\infty \} \, dz + \frac{\tau(z_o)}{\varrho} \tag{2.157}$$

Moreover, if we assume that

$$U_\infty(t) = A\omega \cos \omega t \tag{2.158}$$

and consider the maximum bed shear stress $\hat{\tau}_b(z_o)$, and then apply the definition of the bed friction factor

$$\frac{\hat{\tau}_b(z_o)}{\varrho} = \frac{1}{2} f_w(z_o) \{A\omega\}^2 \qquad (2.159)$$

it follows that

$$\frac{1}{2} f_w(z_A) \{A\omega\}^2 = \int_{z_A}^{z_o} A\omega^2 \, dz + \frac{1}{2} f_w(z_o) \{A\omega\}^2 \qquad (2.160)$$

which can be rewritten as

$$f_w(z_A) = f_w(z_o) + \frac{2(z_o - z_A)}{A} \qquad (2.161)$$

$$= f_w(z_o) + \frac{2\Delta}{A}$$

As we see from Eq.(2.161), when the bed is made of coarse sands or covered with sand ripples, i.e. Δ is increased, the friction factor $f_w(z_o)$ at z_o will be quite different from the friction factor $f_w(z_A)$ at z_A. On the other hand, from Eq.(2.161), we realize that the friction factor measured by Kamphuis(1975) corresponds to the level z_A rather than the level z_o. Therefore, when one compares the measured friction factor $f_w(z_A)$ with a theoretical prediction, e.g. by Kajiura (1968) or Jonsson & Carlsen (1976) one thing he should keep in mind that there is difference $2\Delta/A$ between the measured friction factor $f_w(z_A)$ and the predicted friction factor $f_w(z_o)$.

§2.5.8 THE PROCEDURES OF CALCULATION

Calculation of velocity amplitude $|U(z)|$, bed friction factor f_w and maximum shear stress $\hat{\tau}_b(z_o)$ can be easily performed by a short computer program. The input parameters of the program are $A\omega$, T, K_N, where $A\omega$ is the free stream velocity amplitude, T the wave period, K_N the Nikuradse roughness. The order of calculation is shown in Fig.2.39.

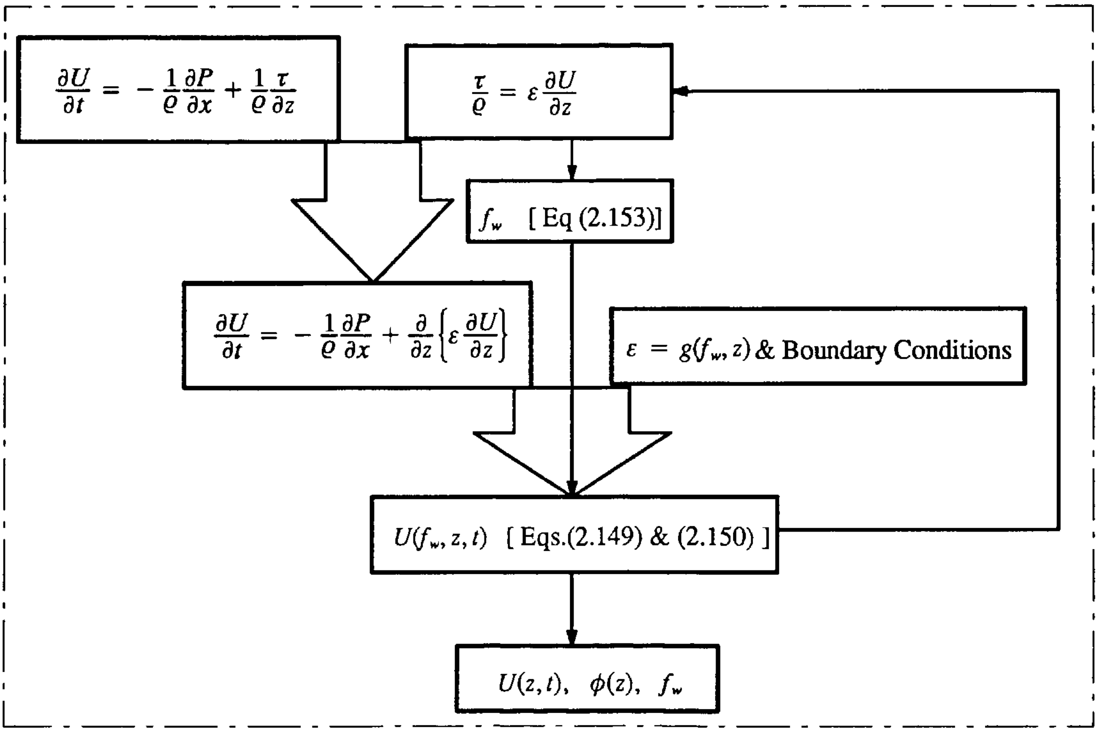

Fig.2.39 The procedures of calculating the velocity field and shear stress in the boundary layers

§2.5.9 COMPARISON WITH EXPERIMENTS

The present model has been compared with laboratory data such as Jonsson & Carlsen (1976) Test No.1 and Test No.2, van Doorn (1981) V00RA, van Doorn (1982) S00RAL and M00RAL, Sleath (1987) Test−3, Test−4, Test−5, Test−9 and Test−10, and Jensen (1989) Test−12 and Test−13. The regimes of the boundary layer flows in all these experiments above are turbulent. The relative roughness K_N/A in these experiments are at the range of $2.8 \times 10^{-4} \sim 2.5 \times 10^{-1}$. The eddy viscosity models of Kajiura (1968) and Myrhaug (1982) have also been compared with the experimental data. The results from the comparison show that the present model gives a better prediction of the velocity measured in the above mentioned experiments than the models of Kajiura (1968) and Myrhaug (1982).

§2.5.9.1 Comparison with Jonsson & Carlsen (1976) Test No.1

The experimental data from Test No.1 of Jonsson & Carlsen (1976) has been widely used to compare with the former models, e.g. by Brevik (1981), Myrhaug (1982) and You *et al.* (1991a). Data from Test No.1 is compared with the present model and the models of Kajiura (1968) and Myrhaug (1982) to examine how well the present model performs. The input parameters in the present model are $A\omega = 211cm/s$, $T = 8.39s$ and $K_N = 2.3cm$. It is evident from Fig.2.40 that Kajiura's model underestimates the velocity in the inner layer and overestimates the value of the velocity overshoot. Myrhaug's model overestimates the boundary layer thickness. In contrast, the present model gives a better prediction of the velocity distribution in Test No.1 than the models of Kajiura (1968) and Myrhaug (1982).

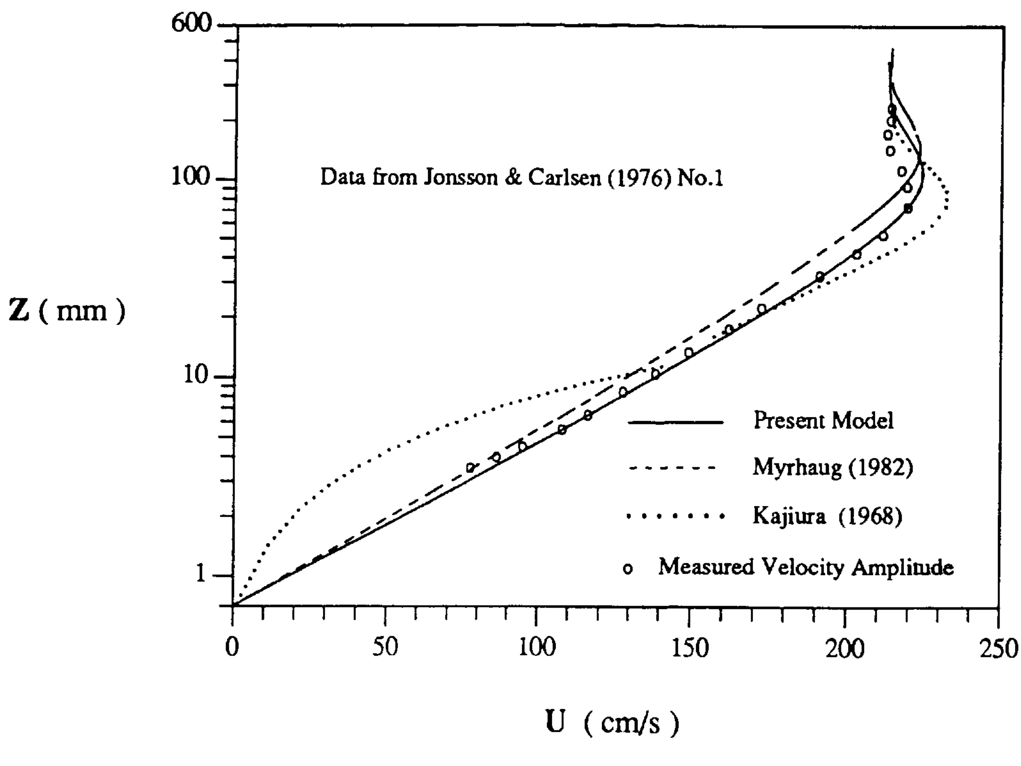

Fig.2.40 The comparison of the present model with the models of Kajiura and Myrhaug and Test No.1

§2.5.9.2 Comparison with Jensen (1989) Test−12

Jensen (1989) undertook experiments to investigate the turbulent oscillatory layer in an oscillating water tunnel. The instantaneous velocity $U(z,t)$ near the sand bed was measured with a laser doppler anemometer. Here, we use the harmonic analysis on $U(z,t)$ to obtain the first and higher harmonic components, but only the first harmonic component will be used to compare with the eddy viscosity models since the higher harmonic components are small in comparison with the first component. The input parameters in the present model are $A\omega = 95.5 cm/s$, $T = 9.2s$ and $K_N = 0.0084 cm$. The comparison of the present model with the model of Kajiura (1968) and Jensen Test−12 has been shown in Fig.2.41. It can been seen that Kajiura's model still overestimates the velocity in the inner layer and underestimates the boundary layer thickness. In contrast, the present model really gives a better prediction of the velocity distribution in Jensen's (1989) Test−12.

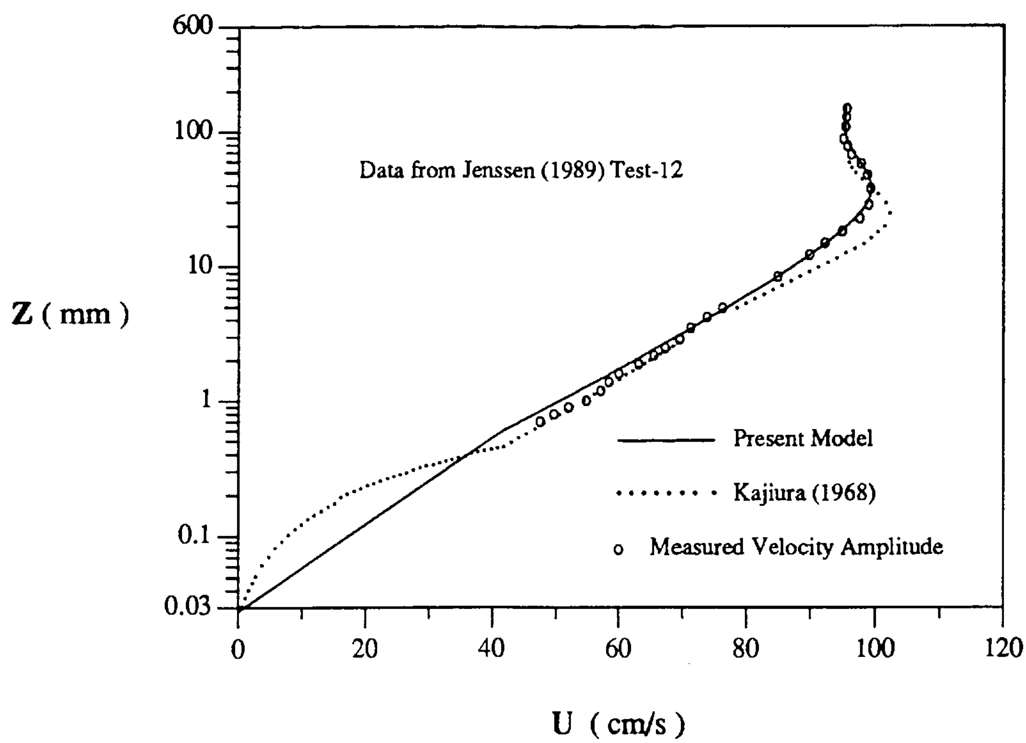

Fig.2.41 The comparison of the present model with Kajiura's model and Jensen (1989) Test−12

§2.5.9.3 Comparison with van Doorn (1981) V00RA

van Doorn (1981) did experimental work to investigate the turbulent oscillatory boundary layer over the artificially roughened bed in a wave flume. The bed roughness consisted of $2mm \times 2mm$ cubes spaced $18mm$ apart. The instantaneous velocity was measured over the trough between two elements with a laser doppler anemometer. The harmonic analysis was used to obtain the first, the second and higher components, and the phase shift. The input parameters in the present model are $A\omega = 26.5\,cm/s$, $T = 2\ s$ and $K_N = 2,1\ cm$. The comparison of the present model with experimental data from van Doorn (1981) V00RA is shown in Fig.2.42, and it can be seen that the present model give an accurate prediction of both the velocity amplitude and the phase shift in this experiment.

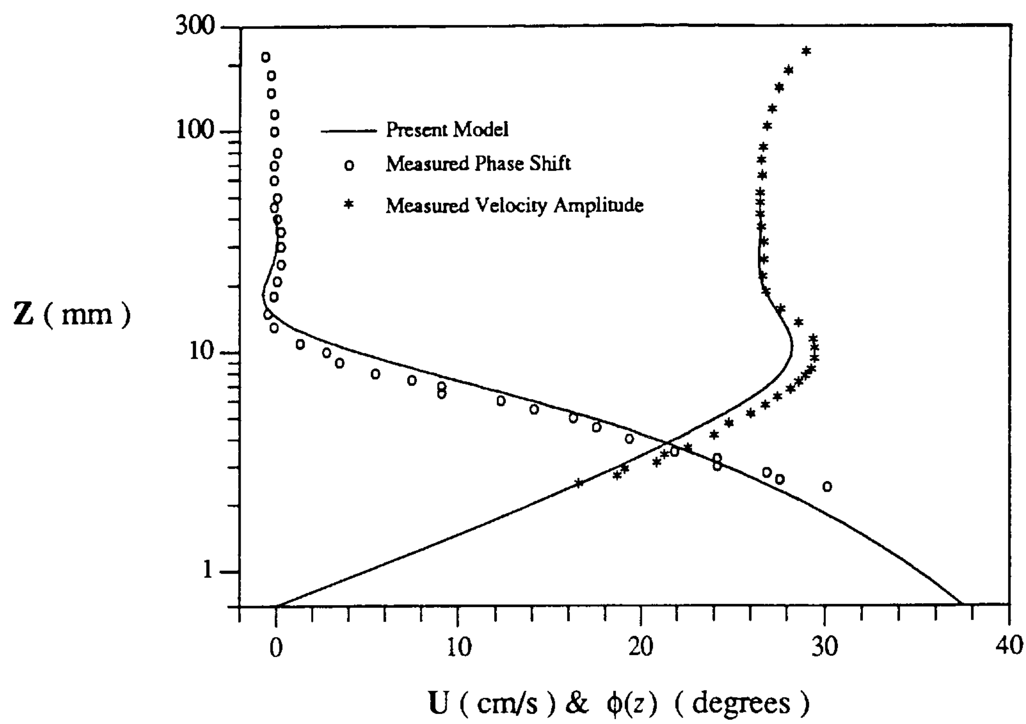

Fig.2.42 The comparison of the present eddy viscosity model with van Doorn (1981) V00RA

§2.5.9.4 Comparison with van Doorn (1982) S00RAL

van Doorn (1982) extended his previous work to continue investigating the turbulent oscillatory boundary layer over the artificially roughened bed in an oscillating water tunnel. The bed roughness was similar to that of V00RA. The instantaneous velocity was measured over the trough between two elements with a laser doppler anemometer, and again harmonic analysis was used to determine the first, the second and higher components, and the phase shift. The input parameters are $A\omega = 32.2cm/s$, $T = 2s$ and $K_N = 2.1cm$. The comparison of the present model with experimental data S00RAL is shown in Fig.2.43, and it is found that the present model again gives an accurate prediction of both the velocity amplitude and the phase shift of S00RAL.

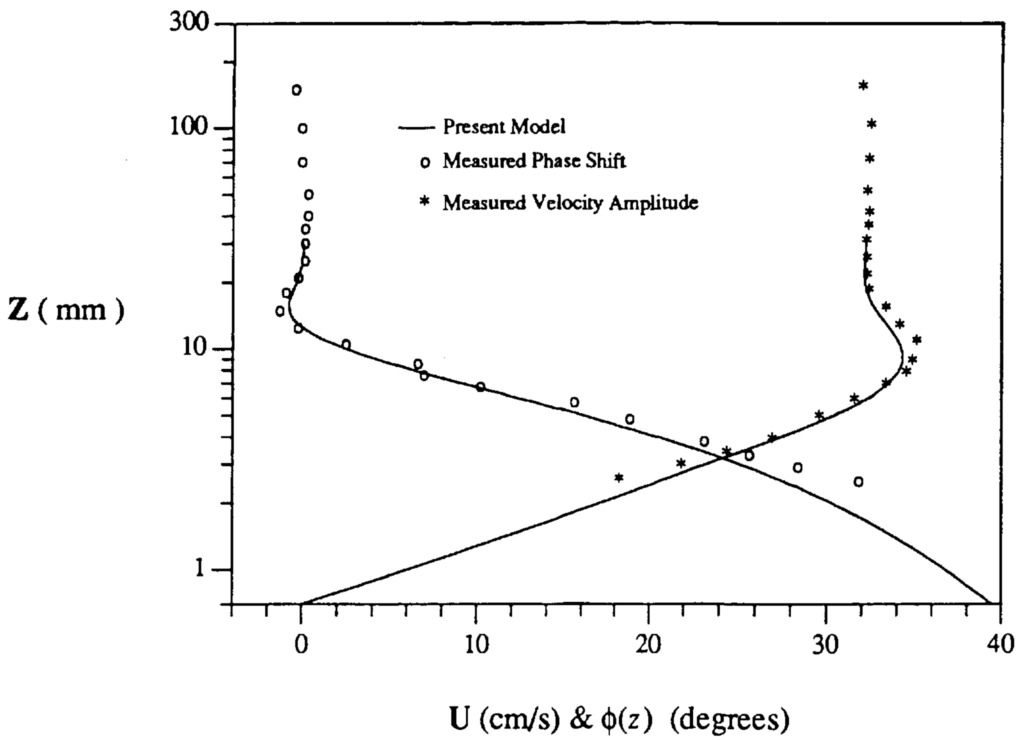

Fig.2.43 The comparison of the present eddy viscosity model with van Doorn (1982) S00RAL

§2.5.9.5 Comparison with Sleath (1987) Test−3

Sleath (1987) carried out an experimental investigation on the turbulent oscillatory boundary layer over a roughened sand bed in an oscillating water tunnel. The bed roughness in Test−3 consisted of a single layer of 1 . 6 *mm* sand glued to the flat bottom surface. The horizontal and the vertical velocity components and the phase shift were measured vertically up from the mean sand surface with a laser doppler anemometer. The input parameters are $A\omega = 68.6 cm/s$, $T = 4.54 s$ and $K_N = 2.0 d = 0.33 cm$. The theoretical bed level was located $0.15d$ below the mean sand surface. A comparison of the present model with the experimental data is shown in Fig.2.44. In addition, Test−4, Test−5, Test−9 and Test−9 are also compared with the presented model in Fig.2.45 to Fig.2.48. The input parameters for each test are shown in Table.2.1 [see, pp. 49].

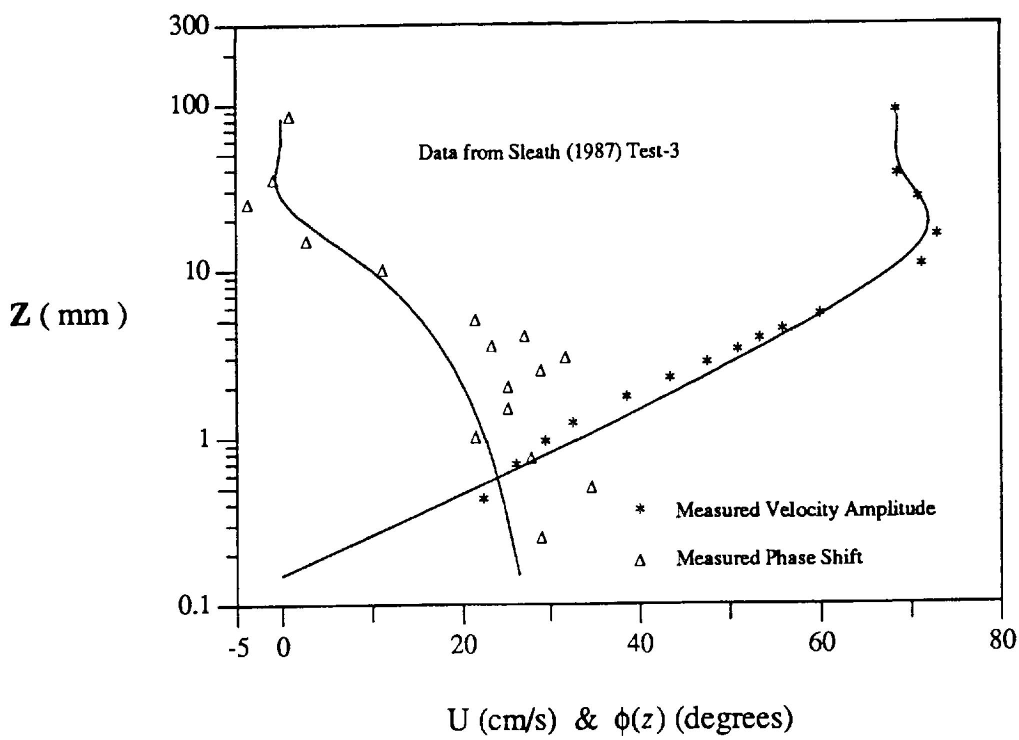

Fig.2.44 The comparison of the present eddy viscosity model with Sleath (1987) Test−3

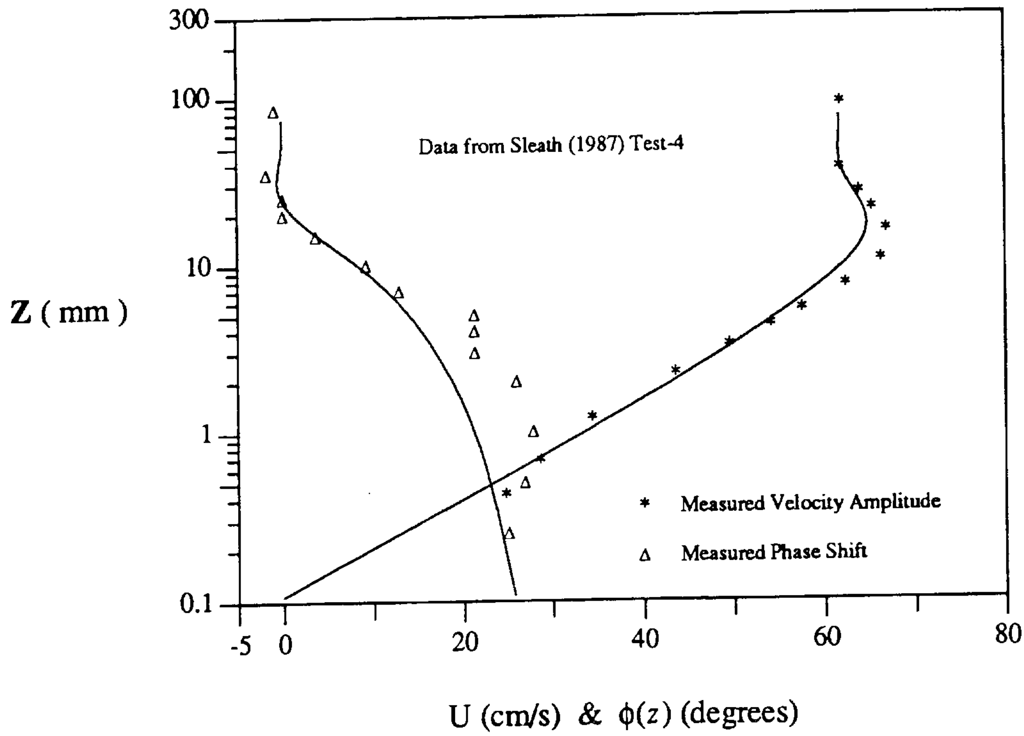

Fig.2.45 The comparison of the present eddy viscosity model with Sleath (1987) Test-4

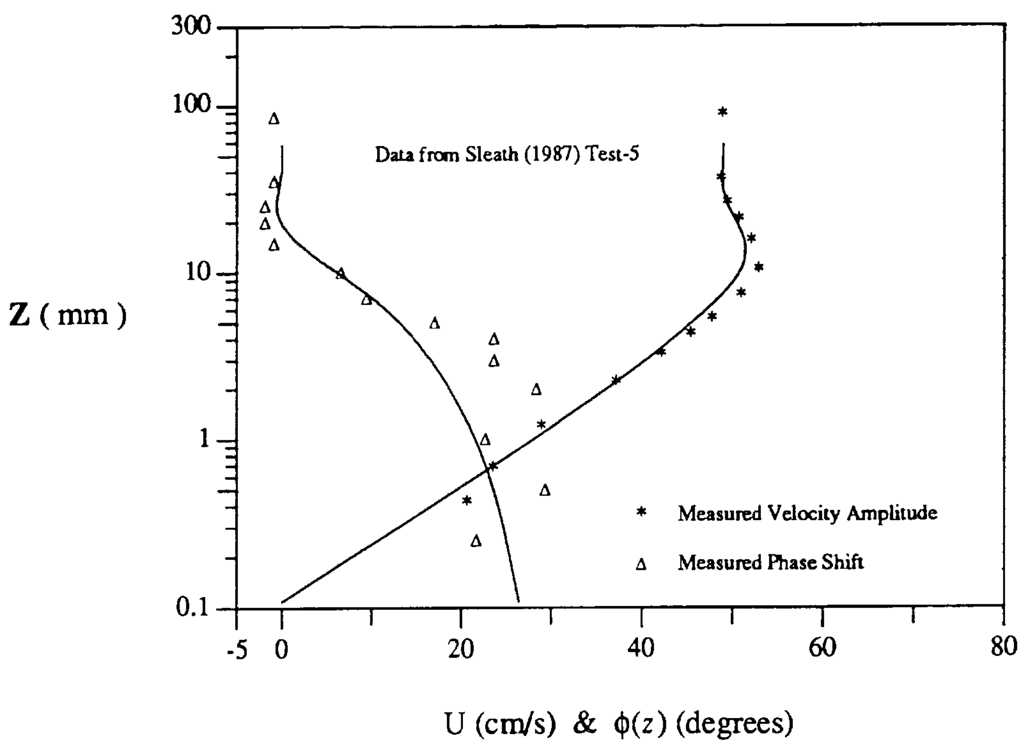

Fig.2.46 The comparison of the present eddy viscosity model with Sleath (1987) Test-5

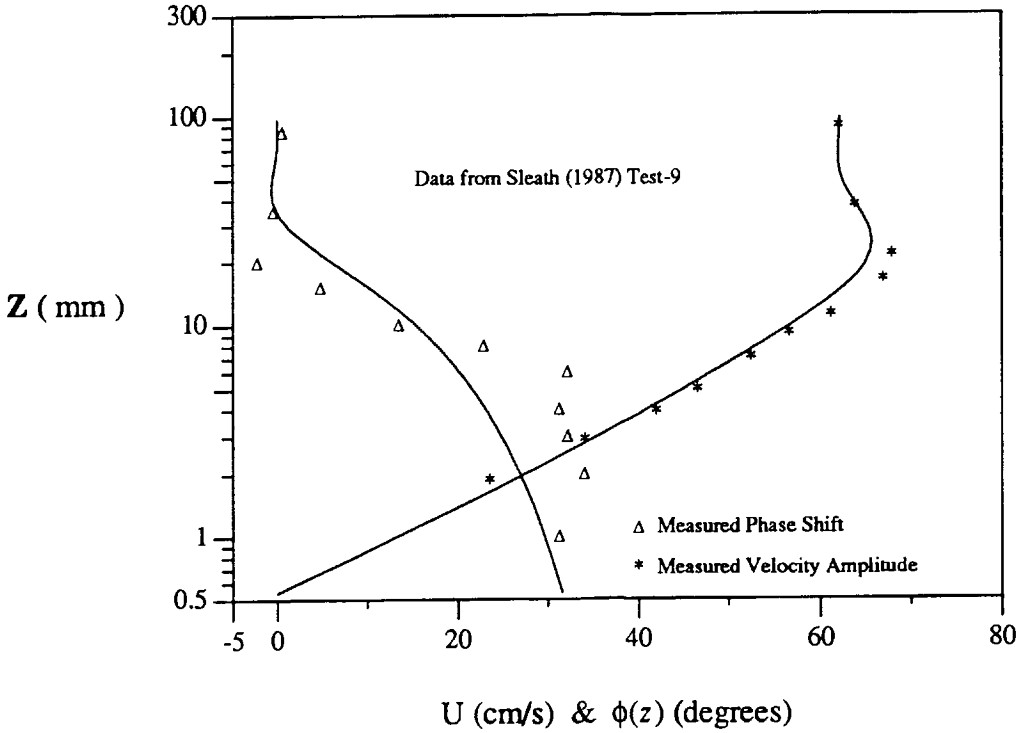

Fig.2.47 The comparison of the present eddy viscosity model with Sleath (1987) Test–9

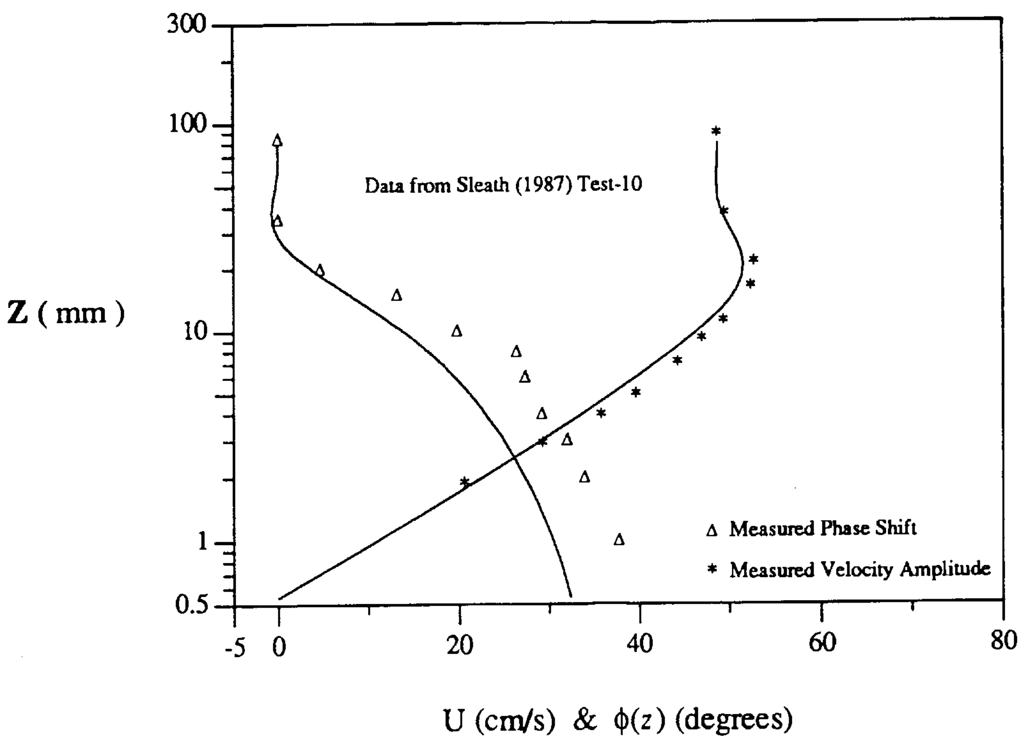

Fig.2.48 The comparison of the present eddy viscosity model with Sleath (1987) Test–10

§2.5.10 CONCLUSIONS

(1) Examination of experimental data on the eddy viscosity ε indicates that ε can be considered as a time-independent and real-valued parameter in turbulent oscillatory boundary layer flows.

(2) The shape of $\varepsilon(z)$ is reasonably described by the functional form

$$\varepsilon(z) = \varkappa \hat{U}^{*} \delta_o \left\{ 1 - \left\{ 1 - z/\delta_1 \right\}^2 \right\} \qquad z_o < z < \delta_1$$

$$\varepsilon(z) = \varkappa \hat{U}^{*} \delta_o \qquad \delta_1 < z < \delta_w$$

with the vertical length scaling parameters

$$\delta_1 = \frac{0.5 \varkappa \hat{U}^{*}}{\omega} \qquad \text{and} \qquad \delta_o = 0.4 \delta_1$$

(3) The present model gives better prediction of the velocity distribution and bed shear stress than former models.

CHAPTER 3

MASS TRANSPORT VELOCITY UNDER PROGRESSIVE WAVES

§3.1. INTRODUCTION TO MASS TRANSPORT

§3.1.1. THE CONCEPT OF MASS TRANSPORT

In chapter 2, we have studied in detail the velocity distribution, local velocity phase shift, bed shear stress and friction factor in a turbulent oscillatory boundary layer. If we look for a time-averaged velocity, we will find it to be zero. This is not surprising since when we discussed the characteristics of the turbulent oscillatory boundary layer, we have already assumed that the flow was purely periodic or sinusoidal. However, in nearly all practical cases, the time-averaged velocity induced by progressive waves is not zero. This comes obvious if we inject dye tracer into the water beneath gravity waves. The dye streak, which is originally straight and vertical, will become curved after a period of time, see Fig.3.1 . Similarly, if we watch a neutrally buoyant particle moving under waves, we will typically find that the particle has not a closed orbital path and experiences a net movement after one wave period as shown in Fig.3.1 . The phenomena demonstrated by the dye tracer and neutrally buoyant particle indicate that there is a net drift or mass transport induced under progressive waves.

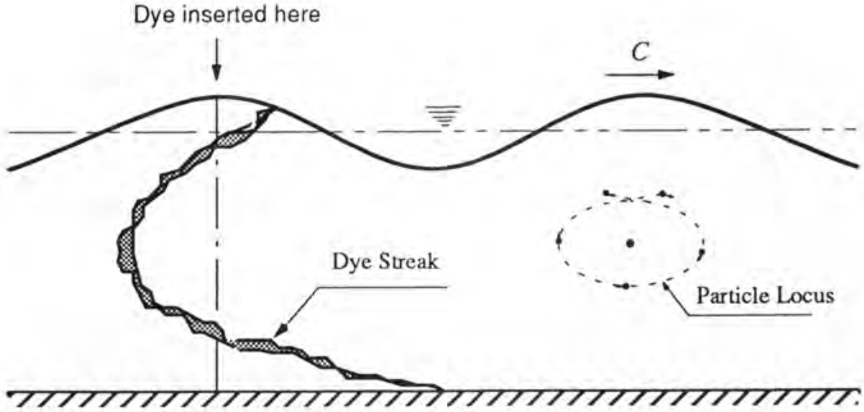

Fig.3.1 Mass transport velocity induced by gravity waves

Although the mass transport velocity is generally small in comparison with the wave–induced orbital velocity, its effect on sediment transport is often of great importance since sediments swept into suspension by the relatively large wave induced orbital velocity are subsequently transported by the mean flow. Thus, it is important to study the mass transport induced by progressive waves in order to understand the mechanism of wave–induced sediment transport.

§3.1.2. METHODS USED TO STUDY MASS TRANSPORT

§3.1.2.1. Lagrangian Velocity Measurements

Before going further, we shall examine the concept of mass transport velocity. The motion of a fluid can be studied either by the method of Lagrange or the method of Euler. The Lagrangian method addresses the question of what occurs to a certain fluid particle while it is moving along its own path. This method involves following the fluid particle during the course of time, and giving the path, velocity and pressure in terms of its original position and the time elapsed since the particle occupied its original position. Accordingly, the Lagrangian mass transport velocity $\overline{U}$ is obtained experimentally by tracking a given particle and measuring the net distance ΔS after a few wave periods, $\Delta t = nT$. Therefore, the Lagrangian mass transport velocity is determined as

$$\overline{U} = \frac{\Delta S}{\Delta t} \tag{3.1}$$

§3.1.2.2. Eulerian Velocity Measurements

In contrast, the Eulerian method addresses the question of what occurs at a fixed point. This is the most frequently adopted approach, partly because most of the available measuring equipments can only measure " Eulerian velocities ". The Eulerian mean velocity $\overline{u}$ is thus obtained experimentally by measuring the velocity at a fixed point and taking a time average over several wave periods

$$\overline{u} = \frac{1}{nT}\int_0^{nT} u \, dt \tag{3.2}$$

§3.1.2.3. Difference Between Lagrangian and Eulerian Velocities

The difference between the Lagrangian mass transport velocity $\overline{U}$ and the Eulerian mean velocity $\overline{u}$ is quantified by means of the following derivation.

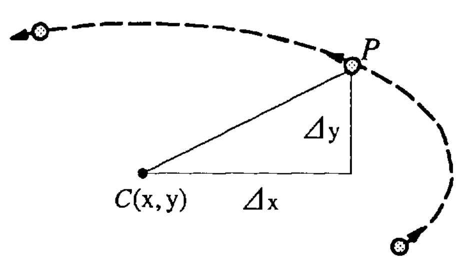

Fig.3.2 A particle P moving around its own path from its original position $C(x, y)$

Analytically, assuming that P in Fig.3.2 is at an arbitrary position on its orbit, the instantaneous velocity U of a particle at $P(x + \Delta x, y + \Delta y)$ will, to the second approximation, differ from u at $C(x, y)$ by an amount

$$U - u = \frac{\partial u}{\partial x}\Delta x + \frac{\partial u}{\partial y}\Delta y \tag{3.3}$$

where Δx, Δy are the horizontal and vertical displacements of P from $C(x, y)$ as shown in Fig.3.2 . These displacements are approximately given by

$$\Delta x = \int u dt \qquad \Delta y = \int w dt$$

Hence, Eq.(3.3) can be rewritten as

$$U - u = \frac{\partial u}{\partial x}\int u dt + \frac{\partial u}{\partial y}\int w dt \tag{3.4}$$

Therefore, the difference between the Lagrangian mass transport velocity of the particle at $P(x + \Delta x, y + \Delta y)$ and the Eulerian mean velocity at $C(x, y)$ is given, to the second approximation, by time averaging Eq.(3.4) over one wave period

$$\overline{U} = \overline{u} + \overline{\frac{\partial u}{\partial x}\int u dt} + \overline{\frac{\partial u}{\partial y}\int w dt} \tag{3.5}$$

This shows that there may still be a Lagrangian mass transport velocity even if the Eulerian mean velocity $\overline{u} = 0$, and thus in general, $\overline{U} \neq \overline{u}$

§3.2. LITERATURE REVIEW

§3.2.1. INTRODUCTION

The present section is a brief review of previous theoretical and experimental work on mass transport induced by progressive waves. The purpose is to give a general overview of how much work has been done theoretically and experimentally, and which problems are still unsolved. On the theoretical side, we will review a few basic theories which are of importance for explaining the mechanism of the mass transport induced by progressive waves and providing formulas to quantitatively calculate the mass transport velocity. On the experimental side, we will review some typical experiments which have revealed some new aspects, which are not accounted for by the existing theories.

§3.2.2. REVIEW OF PREVIOUS THEORETICAL WORK

§3.2.2.1. Stokes (1847)

Stokes' (1847) inviscid wave theory indicated that the individual fluid particles do not have closed orbital paths. The particles have a second–order Lagrangian mean velocity, the mass transport velocity, in the direction of wave propagation. It can be explained physically by the fact that the horizontal orbital velocity increases with elevation. Consequently, a particle at a top of the orbit moves faster in the forward direction than the particle at the bottom of the orbit does in the backward direction. As a result, there is a net drift in the direction of wave propagation.

According to Stokes's theory, the mass transport under progressive waves can be determined by examining the horizontal and vertical displacements of a fluid particle from its original position.

$$\zeta_x = a\frac{\cosh k(y+h)}{\cosh kh}\sin(kx-\omega t) + \frac{a^2k}{4}\frac{1}{\sinh^2 kh}\left\{1-\frac{3}{2}\frac{\cosh 2k(y+h)}{\sinh^2 kh}\right\}$$

$$\times \sin 2(kx-\omega t) + \frac{a^2k}{2}\frac{\cosh 2k(y+h)}{\sinh^2 kh}\omega t \tag{3.6}$$

$$\zeta_y = a\frac{\sinh k(y+h)}{\sinh kh}\cos(kx-\omega t) + \frac{3}{8}a^2k\frac{\sinh 2k(y+h)}{\sinh^2 kh}\cos 2(kx-\omega t) \tag{3.7}$$

In the right side of Eq.(3.6), the first two terms are periodic whereas the third term is not periodic but a linear function of time. Consequently, after one wave period T, the fluid particle has travelled a net distance in the horizontal direction

$$\Delta\zeta_x = a^2\omega k\frac{\cosh 2k(y+h)}{2\sinh^2 kh}T \tag{3.8}$$

and a nil drift in the vertical direction

$$\Delta\zeta_y = 0 \tag{3.9}$$

Hence, the horizontal mass transport velocity can is given by

$$\overline{U} = \frac{\Delta\zeta_x}{T} = a^2\omega k\frac{\cosh 2k(y + h)}{2\sinh^2 kh} \tag{3.10}$$

According to Eq.(3.10), the mass transport velocity at the mean surface level can be obtained simply by substituting $y = 0$ in Eq.(3.10) to give

$$\overline{U}_s = a^2\omega k\frac{\cosh 2kh}{2\sinh^2 kh} \tag{3.11}$$

and the mass transport velocity very close to the bed can be derived by substituting $y \rightarrow -h$ in Eq.(3.10)

$$\overline{U}_b = \frac{a^2\omega k}{2\sinh^2 kh} \tag{3.12}$$

Since a volume of fluid is continuously carried in the direction of wave propagation due to the positive second–order Lagrangian mean velocity over the depth as shown in Eq.(3.10), a net flow is produced. However, if the co–ordinate system is shifted at a certain speed, the condition of no net flow across a section such as in a laboratory wave tank can be satisfied. This leads to

$$\overline{U} = a^2\omega k\frac{\cosh 2k(y + h)}{2\sinh^2 kh} - \frac{a^2\omega}{2h}\coth kh \tag{3.13}$$

which is shown in Fig.3.3 , and it is found that the mass transport velocity near the free water surface is always in the direction of wave propagation while the mass transport near the bed is always in the opposite direction of wave propagation and the vertical gradient of the mass transport velocity is always equal zero.

The mass transport velocity distributions close to the bed as shown in Fig.3.3 differ markedly from those observed in laboratory experiments, especially in water of moderate depth. For example, Vincent (1958), Russell & Osorio (1958), Brebner *et al.* (1966), Bijker, *et al.* (1974) and You *et al.* (1991b) all found that the drift velocity near the bottom was in the direction of wave propagation. However, apart from these discrepancies between Stokes' theory and laboratory experiments close to the bed, Stokes's drift theory gives a good prediction of the mass transport velocity near the free water surface as shown Fig.3.6 , and can be applied to predict the mass transport velocity in the interior flow when $kh > 3.0$ as suggested by Russell & Osorio (1958).

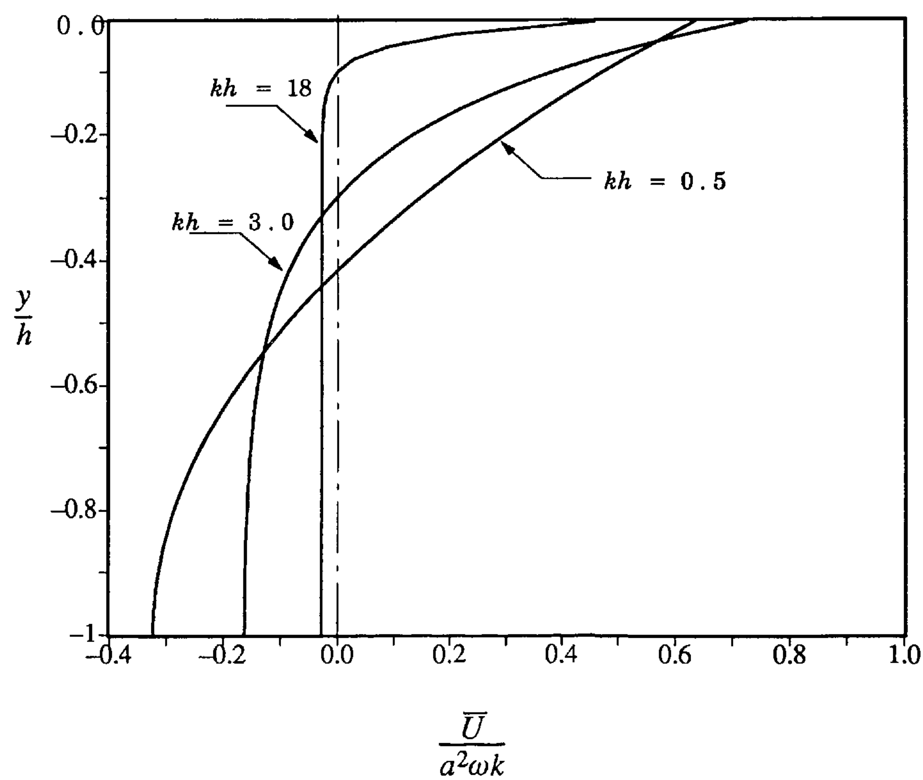

Fig.3.3 Variation of mass transport velocity with depth under progressive waves after Stokes (1847)

§3.2.2.2. Longuet–Higgins (1953)

Longuet–Higgins (1953) realized that the irrotational flow assumed by Stokes (1847) was not valid close to the bed where there is strong vorticity due to the large velocity gradient.

Longuet–Higgins produced a new theory starting with the equation of motion for a viscous, incompressible interior fluid, which in component form is given by

$$\frac{\partial u}{\partial t} + u\frac{\partial u}{\partial x} + w\frac{\partial u}{\partial y} = -\frac{1}{\varrho}\frac{\partial p}{\partial x} + \nu\left\{\frac{\partial^2 u}{\partial x^2} + \frac{\partial^2 u}{\partial y^2}\right\} \tag{3.14}$$

$$\frac{\partial w}{\partial t} + u\frac{\partial w}{\partial x} + w\frac{\partial w}{\partial y} = -\frac{1}{\varrho}\frac{\partial p}{\partial y} - g + \nu\left\{\frac{\partial^2 w}{\partial x^2} + \frac{\partial^2 w}{\partial y^2}\right\} \tag{3.15}$$

Differentiating Eq.(3.14) with respect to y and Eq.(3.15) with respect to x and then subtracting each other, we obtain

$$\left\{\frac{\partial}{\partial t} + u\frac{\partial}{\partial x} + w\frac{\partial}{\partial y} - \nu\nabla^2\right\}\nabla^2\psi = 0 \tag{3.16}$$

in which ψ is the stream function defined by

$$u = \frac{\partial\psi}{\partial y} \qquad w = -\frac{\partial\psi}{\partial x} \tag{3.17}$$

and the operator ∇^2 is defined as

$$\nabla^2 = \frac{\partial^2}{\partial x^2} + \frac{\partial^2}{\partial y^2}$$

The mean value of Eq.(3.16) with respect to time over a complete period is given by

$$\overline{\left\{u\frac{\partial}{\partial x} + w\frac{\partial}{\partial y} - \nu\nabla^2\right\}\nabla^2\psi} = 0 \tag{3.18}$$

The first two terms in the left side of Eq.(3.18) represent the rate of change of the vorticity at a fixed point due to convection $[u\frac{\partial}{\partial x} + w\frac{\partial}{\partial y}]$. The last term, which is similar to a term in the equation of heat conduction, represents the rate of change of the vorticity due to viscous diffusion $[\nu\nabla^2]$.

§3.2.2.2.1. The conduction solution

Longuet–Higgins considered the case $[a^2 \ll \delta^2]$ in which the conduction term $(\nu\nabla^2)$ in Eq.(3.18) is dominant and gave the conduction solution

$$\begin{aligned}\overline{U} = \frac{a^2\omega k}{4\sinh^2 kh}\Big\{&2\cosh 2kh(-y/h-1) + 3 + kh\sinh 2kh\left[3(-y/h)^2 - 4(-y/h) + 1\right] \\ &+ 3\left\{\frac{\sinh 2kh}{2kh} + \frac{3}{2}\right\}\left\{(-y/h)^2 - 1\right\}\Big\}\end{aligned} \tag{3.19}$$

where a is the wave amplitude $[H = 2a]$ and δ the Stokes length $\sqrt{2\nu/\omega}$. The variation of the mass transport velocity with the normalised depth y/h outside the wave boundary layer described by Eq.(3.19) is shown in Fig.3.4 .

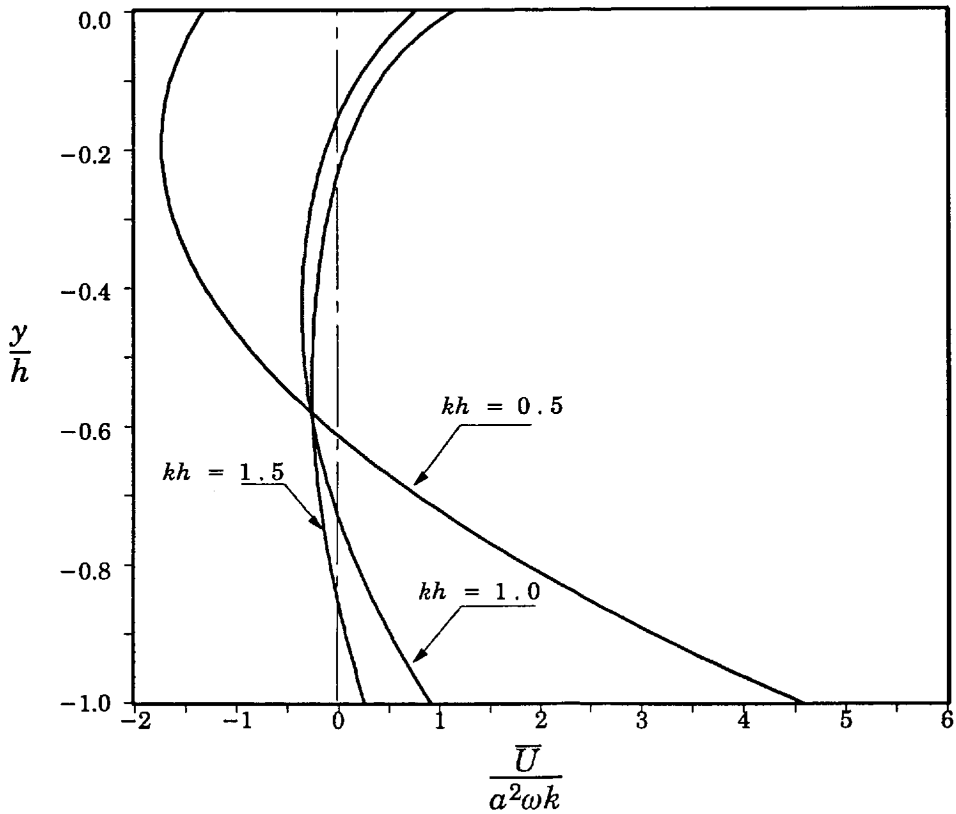

Fig.3.4 Variation of mass transport velocity outside the boundary layer after Longuet–Higgins (1953)

Based on Eq.(3.19), the mass transport velocity near the free wave surface can be deduced by taking $y = 0$

$$\overline{U}_s = \frac{a^2\omega k}{4\sinh^2 kh}\left\{2\cosh 2kh + 3 + kh\sinh 2kh - 3\left\{\frac{\sinh 2kh}{2kh} + \frac{3}{2}\right\}\right\} \qquad (3.20)$$

and the mass transport velocity just outside the water boundary layer is given by substituting $y \rightarrow -h$ in Eq.(3.19)

$$\overline{U}_b = \frac{5}{4}\frac{a^2\omega k}{\sinh^2 kh} = \frac{5}{4}\frac{\{A\omega\}^2}{C} \qquad (3.21)$$

in which

$$A\omega = \frac{a\omega}{\sinh kh} \qquad C = \frac{L}{T} = \frac{\omega}{k} \qquad (3.22)$$

Longuet–Higgins (1956) derived the distributions of the Lagrangian mass transport velocity and the Eulerian mean velocity inside a laminar wave boundary layer, given respectively by

$$\overline{U} = \frac{(A\omega)^2}{4C}\left\{ 5 - 8e^{-\beta z}\cos\beta z + 3e^{-2\beta z} \right\} \tag{3.23}$$

$$\overline{u} = \frac{(A\omega)^2}{4C}\left\{3 + e^{-\beta z}\left\{- 4\cos\beta z + 2\sin\beta z + e^{-\beta z} - 2\beta z\sin\beta z - 2\beta z\cos\beta z\right\}\right\} \tag{3.24}$$

in which $\beta = \sqrt{\omega/2\nu}$. The variations of $\overline{U}$ and $\overline{u}$ with βz inside the wave boundary layer are shown in Fig.3.5 .

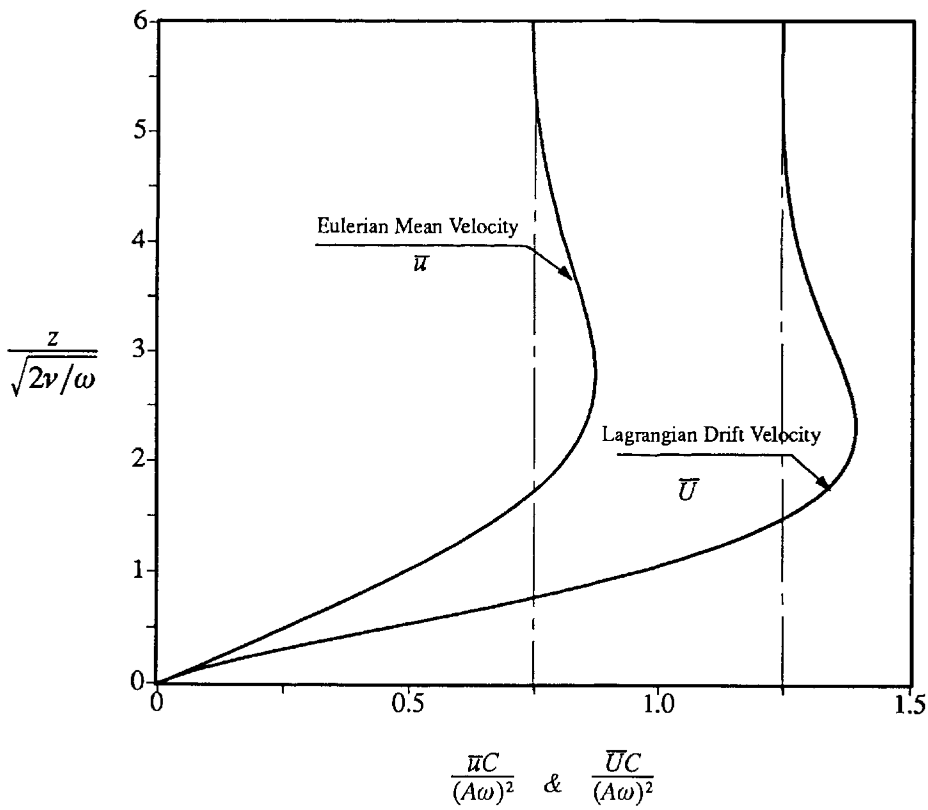

Fig.3.5 The Lagrangian and Eulerian mean velocities in the laminar boundary layer

The Lagrangian mass transport velocity $\overline{U}$ at the outer edge of the boundary layer is given by

$$\overline{U}_b = \frac{5}{4}\frac{(A\omega)^2}{C} \tag{3.25}$$

while the Eulerian mean velocity $\overline{u}$ is given by

$$\overline{u} = \frac{3}{4}\frac{(A\omega)^2}{C} \tag{3.26}$$

It is worthwhile to mention here that the mass transport velocity inside wave boundary layer given in Eq.(3.23) does not depend critically on the assumption that $a^2 \ll \delta^2$, which is required specially for the conduction solution in the interior flow.

§3.2.2.2.2. The convection solution

Under normal wave conditions one would expect that $a^2 \gg \delta^2$, so that the convective term $\left\{u\frac{\partial}{\partial x} + w\frac{\partial}{\partial y}\right\}$ in Eq.(3.18) is dominant. Longuet–Higgins (1953) gave the convection solution for the mass transport velocity induced by progressive waves as

$$\overline{U} = \frac{a^2\omega}{4\sinh^2 kh}\left\{\frac{Ck^2}{r^2} + \frac{4k^2}{4k^2 + r^2}\sinh 2k(-y-h) + F(z)\right\} \tag{3.27}$$

in which

$$F(z) = \frac{\{12k^2 + 5r^2\}k}{(4k^2 + r^2)r}\frac{\sin(-ry)}{\cos rh} + \frac{\{2k^2 + r^2\}8k^2}{(4k^2 + r^2)r^2}\sin 2kh\frac{\cos r(-y-h)}{\cos rh}$$

and

$$r^2 = 4k^2 + \frac{m^2\pi^2}{h^2}$$

in which C is the wave celerity and m is a positive integer. Eq.(3.27) has an infinite number of solutions, each corresponding to a different integer m, or in other words, the convection solution for progressive waves is not unique. It can be proven that the expression in big brackets in Eq.(3.27) can not vanish when $kh > 0$. Therefore, the convection solution given by Eq.(3.27) does not satisfy the condition of no net mean flow across a section. Until now, a complete convection solution has not been found.

Although Longuet–Higgins conduction solution is derived under the assumption of $a^2 \ll \delta^2$, it does give a good agreement with some experiments where $a^2 \gg \delta^2$, for example, Russell & Osorio (1958). However, the conduction solution fails to give a better prediction of the mass transport velocity near the free water surface than Stokes drift theory (1847). This is illustrated in Fig.3.6 .

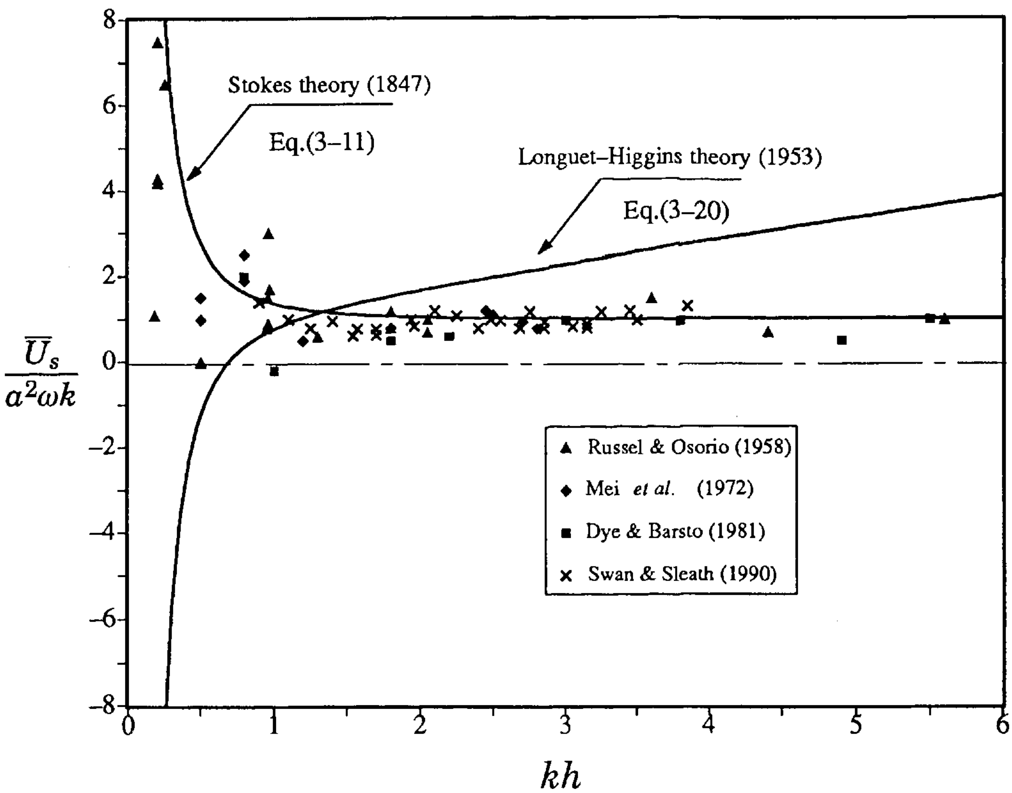

Fig.3.6 Comparison of theoretical predictions of surface mass transport velocity with experimental data

§3.2.2.3. Johns (1970)

Johns (1970) calculated the mass transport velocity in a turbulent wave boundary layer using the concept of eddy viscosity

$$\frac{\tau}{\varrho} = \nu\, K(z)\, \frac{\partial u}{\partial z} \tag{3.28}$$

and the equation of motion

$$\frac{\partial u}{\partial t} + u\frac{\partial u}{\partial x} + w\frac{\partial u}{\partial z} = -\frac{1}{\varrho}\frac{\partial p}{\partial x} + \frac{1}{\varrho}\frac{\partial \tau}{\partial z} \tag{3.29}$$

where $K(z)$ is a dimensionless function, which is analogous to the eddy viscosity. The distribution of $K(z)$ was assumed to have the form

$$K(z) = K_\infty + \{1 - K_\infty\}\, e^{-\beta z} \tag{3.30}$$

with $K_\infty = 1$ and $K_\infty = 100$ for the laminar and turbulent cases respectively, see Fig.3.7 .

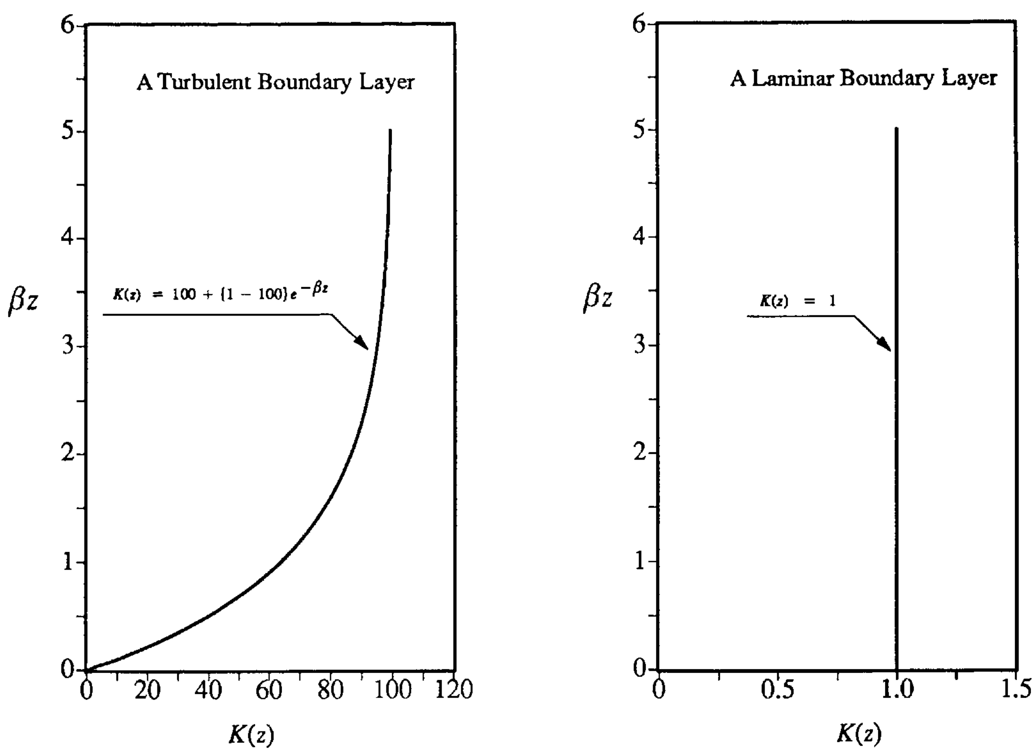

Fig.3.7 Variations of eddy viscosity in laminar and turbulent boundary layers after Johns (1970)

Eventually, Johns found that the mass transport velocities for both laminar and turbulent boundary layers were approximately equal, and the maximum mass transport velocity in the turbulent boundary layer was found to be

$$\overline{U} = \frac{a^2 \omega k}{\sinh^2 kh} I_m\{H(\beta z)\} \tag{3.31}$$

in which $H(\beta z)$ is a function of βz. The magnitude of the imaginary part $I_m\{H(\beta z)\}$ just outside the turbulent boundary layer was

$$I_m\{H(\beta z)\} \approx \frac{5}{4} \tag{3.32}$$

which is approximately equal to that in Eq.(3.21) predicted by the conduction solution of Longuet–Higgins (1953) .

Although Johns (1970) confirmed the conclusion of Longuet–Higgins (1956) that the mass transport velocity distribution derived from the laminar boundary layer could be used for the turbulent boundary layer provided that the eddy viscosity was a function of z only, he did not discuss the questions of how the mass transport velocity would vary if the eddy viscosity distribution was changed, and how the mass transport velocity would be affected if different specified values K_∞ were used. Therefore, the model of Johns (1970) is incomplete.

§3.2.2.4. Sleath (1973)

Sleath (1973) undertook a theoretical and experimental investigation of mass transport induced by very small waves [$H = 1mm$, $T = 1s$] in order to confirm the validity of the conduction solution of Longuet–Higgins (1953). Sleath applied the concept of a damping coefficient of wave propagation in the longitudinal direction, previously introduced by Hunt (1952) and obtained the following expression for the distribution of the mass transport velocity over the depth

$$\overline{U} = \overline{u} + a^2 \omega k \frac{\cosh 2kz}{2 \sinh^2 kh} \tag{3.33}$$

where $\bar{u}$ is the Eulerian mean velocity. There are three possible solutions of Eq.(3.33) for the Eulerian mean velocity $\bar{u}$ under very small waves. The solutions of the mean velocity $\bar{u}$ for a few values of kh are shown in Fig.3.8 .

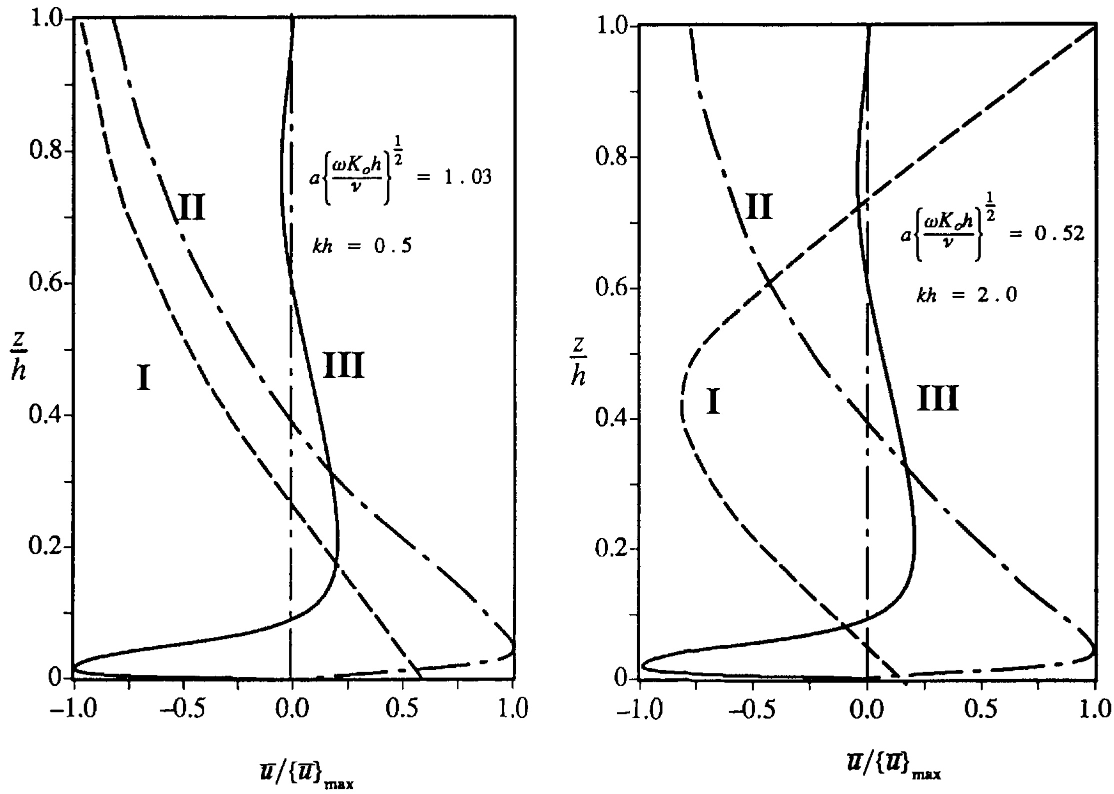

Fig.3.8 Three possible theoretical distributions of Eulerian mean velocity $\bar{u}$ after Sleath (1973)

The type **I** profiles in Fig.3.8 are similar to those given by the conduction solution of Longuet–Higgins (1953). However, on no occasion was a mass transport velocity profile of the type **I** observed in Sleath (1973) experiments in which the minimum amplitude was $1mm$ for both 1–second and 2–second waves.

The Types **II** and **III** in Fig.3.8 are quite different distributions from that predicted by Longuet–Higgins (1953) conduction solution as shown in Fig.3.4 . The most striking difference of the types **II** and **III** from the conduction solution of Longuet–Higgins (1953) is the strong peak in the mass transport velocity close to the bed. With the type **II**, the peak mass transport velocity is in the direction of wave propagation, while with the type **III**, it is in the opposite direction to that of wave propagation.

Sleath (1973) found in his experiments that for the first two or three hours after the wave generator was started, mass transport velocity profiles of the type **II** were usually observed whiles after four hours or more the profiles of mass transport velocity had invariably switched to the type **III**, and the mass transport velocity profile showed no further change.

§3.2.2.5. Wang & Liang (1975)

Wang & Liang (1975) derived a mass transport solution similar to the conduction solution of Longuet–Higgins (1953) except that an empirically determined turbulent boundary layer solution was used as a bottom matching condition. Their solution takes the form

$$\overline{U} = \frac{a^2\omega k}{4\sinh^2 kh}\left\{2\cosh 2kh\left\{\frac{y}{h}+1\right\} + \frac{3\sinh 2kh}{2kh}\left\{(y/h)^2 - 1\right\}\right\}$$

$$+ \frac{a^2\omega^2 k}{4\nu(E^2 + 0.09\beta^2)}\left\{\frac{1.2\beta E}{E^2+0.09\beta^2} - 0.075\frac{\beta}{E}\right\}\left\{\frac{3}{2}(y/h)^2 - \frac{1}{2}\right\} \qquad (3.34)$$

where

$$E = 133\sinh\left\{\frac{kh}{a\beta d}\right\} \qquad \beta = \sqrt{\frac{\omega}{2\nu}}$$

in which d is the diameter of the bed roughness. For the case of a smooth bottom, the mass transport velocity predicted by Wang & Liang can be written as

$$\overline{U} = \frac{a^2\omega k}{4\sinh^2 kh}\left\{2\cosh 2kh\left(\frac{y}{h}+1\right) + \frac{3\sinh 2kh}{2kh}\left((y/h)^2 - 1\right)\right\} \qquad (3.35)$$

The comparison of theoretical work by Stokes (1847), Longuet–Higgins (1953), Dean (1965), and Wang & Liang (1975) with experimental data from Wang & Liang (1982) is shown in Fig.3.9 . It is evident that the solutions of Longuet–Higgins and Wang & Liang are similar, but Wang & Liang 's solution is closer to experimental data. It may be reasonable to conclude here that the bed roughness does have effect on the mass transport velocity near the bed.

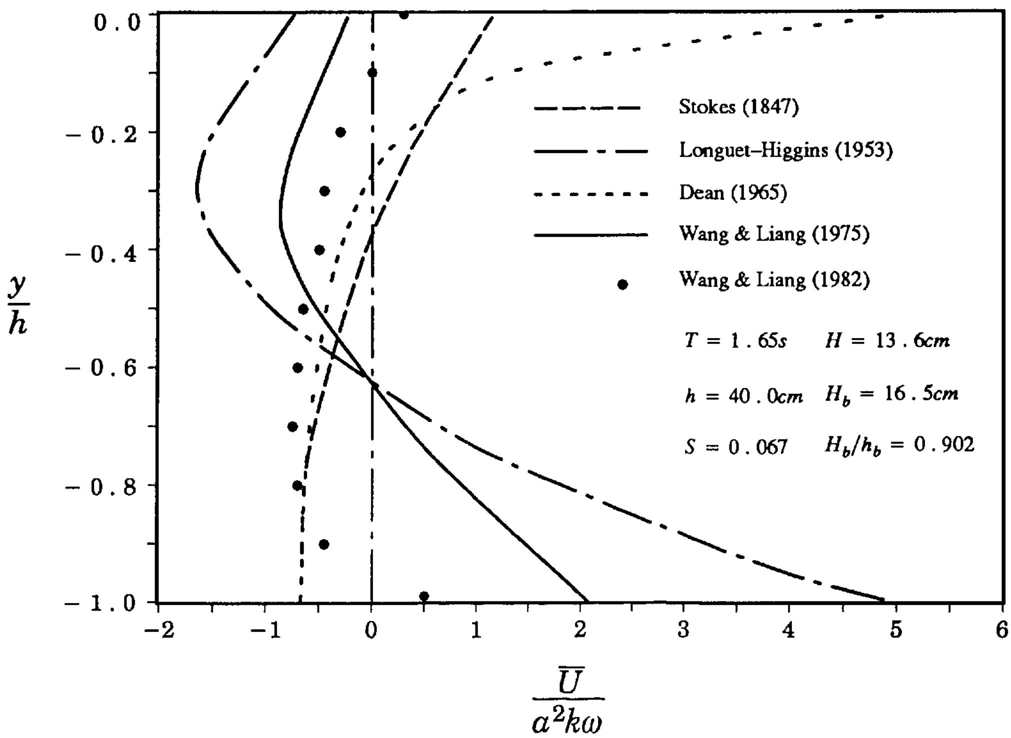

Fig.3.9 Comparison of theoretical predictions on mass transport velocity with experimental data

§3.2.2.6. Johns (1977)

As discussed in the section §3.2.2.3., Johns (1970) assumed the eddy viscosity inside the boundary layer to be function of elevation but independent of time Eq.(3.30) and derived that the mass transport velocity in the turbulent wave boundary layer was approximately equal to that in the laminar boundary layer as predicted by Longuet–Higgins (1953). However, as Johns (1977) indicated, the theoretical result given by Eq.(3.31) appeared to be contradicted by Collins (1963) experimental study which indicated that the mass transport velocity in a turbulent boundary layer was much less than that in a laminar boundary layer.

Johns (1977) adopted different approach from his previous one (1970). He started with the equation of motion

$$\frac{\partial u}{\partial t} + \frac{\partial}{\partial x}u^2 + \frac{\partial}{\partial z}uw = \frac{\partial U_\infty}{\partial t} + U_\infty\frac{\partial U_\infty}{\partial x} + \frac{\partial}{\partial z}\left\{K\frac{\partial u}{\partial z}\right\} \tag{3.36}$$

and the equation for turbulent kinetic energy density E

$$\frac{\partial E}{\partial t} + \frac{\partial}{\partial x}\{uE\} + \frac{\partial}{\partial z}\{wE\} = K\left\{\frac{\partial u}{\partial z}\right\}^2 + \frac{\partial}{\partial y}\left\{K\frac{\partial E}{\partial z}\right\} - D \tag{3.37}$$

in which

$$K = c^{\frac{1}{4}}\varkappa\, z\, E^{\frac{1}{2}} \qquad D = \frac{c^{\frac{3}{4}}E^{\frac{3}{2}}}{\varkappa\, z} \tag{3.38}$$

where $c = 0.08$ and $\varkappa = 0.4$. Johns (1977) solved Eqs.(3.36) and (3.37) numerically with the appropriate boundary conditions. Fig.3.10 shows the variation of $\overline{u}/\{A\omega\}$ with elevation for a few values of kA, where A is the semi−excursion of the orbit just outside the boundary layer, k the wave number and $K_N = 30z_o$.

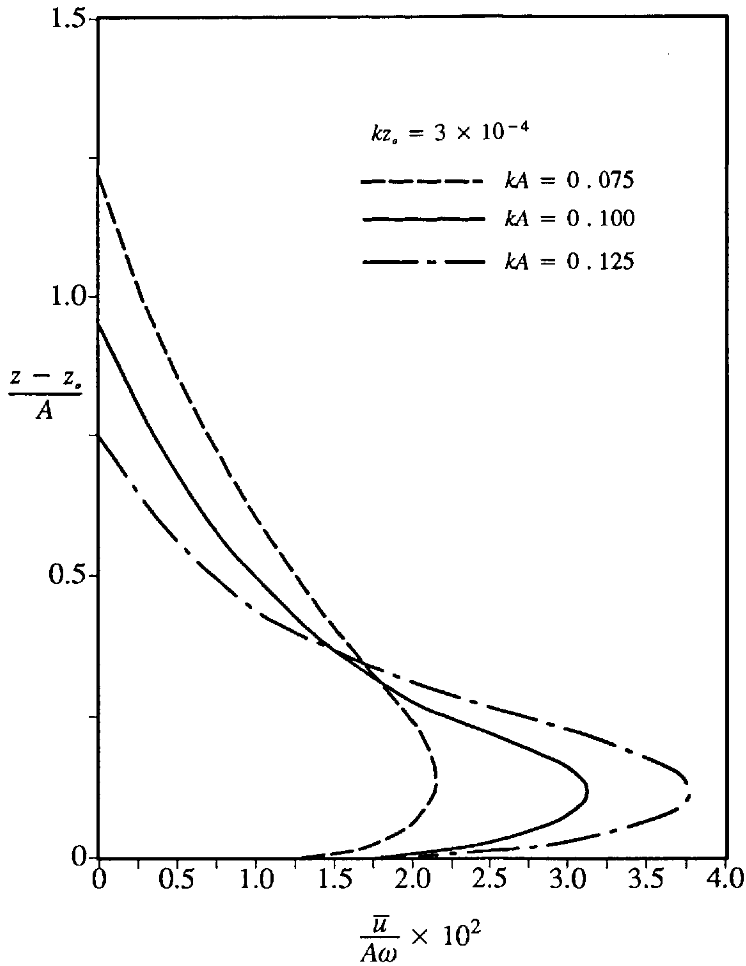

Fig.3.10 The mass transport velocities induced in a turbulent boundary layer after Johns (1977)

Johns (1977) found that the Eulerian mean velocity at the edge of the boundary layer was given by

$$\frac{\bar{u}}{\bar{u}_L} = \frac{0.30}{0.75} = \frac{1}{2.5} \tag{3.39}$$

where $\bar{u}_L$ is the Eulerian mean velocity given by Longuet–Higgins (1956) in the laminar boundary layer. Eq.(3.39) indicates that the Eulerian mean velocity derived by Johns (1977) in the turbulent boundary layer is appreciably less than that predicted by Longuet–Higgins (1956) conduction solution for the laminar boundary layer.

For the model of Johns (1977), several points should be noted here. Firstly, when Johns (1977) chose the boundary conditions near the bed, he adopted Jonsson & Carlsen's (1976) assumption that the instantaneous velocity profile near the bed in the turbulent boundary layer was logarithmic. However, as Jensen (1989) indicated in his test No.10, the assumption was valid only for a certain range of the wave phase, but not correct when $0^o < \omega t \leq 15^o$ and $165^o < \omega t \leq 180^o$. In addition, the assumption adopted from steady boundary layers did not take account of the phase shift between the velocity and the shear stress, which normally occurs in the wave boundary layer as Nielsen (1985) pointed out. Secondly, as Trowbridge & Madsen (1984) discussed, the boundary conditions just outside the wave boundary layer employed by Johns (1977) were not physically realistic and did not allow the Eulerian mean velocity to appear at the outer edge of the boundary layer as shown in Fig.3.10 . Thirdly, as Trowbridge & Madsen (1984) pointed out, the eddy viscosity used in the equation of motion should be a time dependent parameter if the second–order velocity components are taken into account. Fourthly, the diffusion coefficient, which is analogous to eddy viscosity, used in Eqs.(3.36) and (3.37) was assumed to be the same for both momentum and energy fluxes based on the hypotheses used for the steady flows by Launder & Spalding (1972). Finally, the relationship given by Eq.(3.38) is also adopted from the steady flows. Consequently, it is questionable whether the theoretical results given by Johns (1977) are realistic.

§3.2.2.7. Jacobs (1984)

Jacobs (1984) used the turbulence model of Saffman (1970 & 1974) to investigate the mass transport velocity in turbulent oscillatory boundary layers and obtained an expression for the mass transport velocity at the outer edge of the turbulent boundary layer

$$Q = \frac{4}{5}\left\{ c_1 + \frac{1}{2} \right\} \tag{3.40}$$

in which Q denotes a ratio of the mass transport velocity at the outer edge of the turbulent boundary layer predicted by Jacobs (1984) to that at the outer edge of the laminar boundary layer given by Longuet–Higgins (1953), and the parameter c_1 was approximately given by

$$c_1 = \frac{1}{3}\left\{ 1 - \frac{3}{4\sinh^2 kh} \right\} \tag{3.41}$$

by substituting Eq.(3.41) into Eq.(3.40), the ratio Q can be derived as

$$Q = \frac{2}{3} - \frac{1}{5\sinh^2 kh} \tag{3.42}$$

Jacobs (1984) compared his theoretical solution Eq.(3.42) with the experimental data from Bijker *et al.* (1974), and found that there was a good agreement between the calculated and observed values of Q as shown in Fig.3.11 .

Therefore, Jacobs (1984) concluded that Longuet–Higgins conduction solution (1953) would overestimate the mass transport velocity at the outer edge of a turbulent boundary layer by about a factor of two. However, this conclusion is only correct when $kh \geq 0.7$ because as $kh > 0.7$, the ratio $1/Q$ is approximately equal to 1.5 whereas when $kh < 0.7$, it is unlikely that Eq. (3.42) can be used to predict the mass transport velocity as shown in Fig.3.11 .

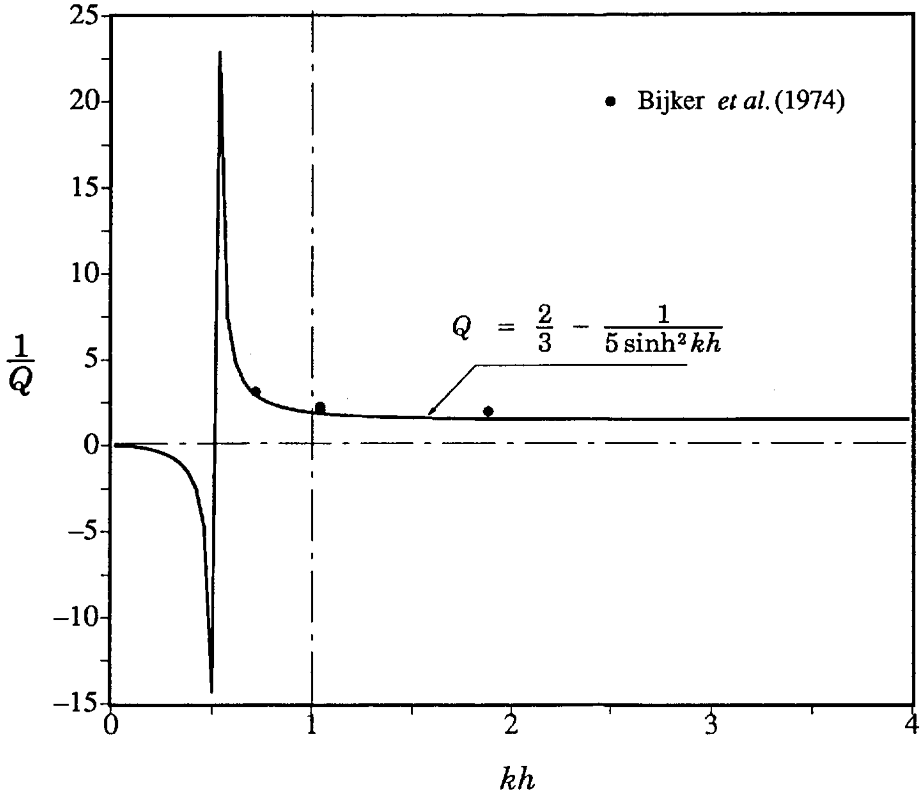

Fig.3.11 Variation of $1/Q$ with kh at the outer edge of the boundary layer after Jacobs (1984)

§3.2.2.8. Swan & Sleath (1990)

Swan & Sleath (1990) attempted to investigate the influence of the higher–order terms, which are neglected in Longuet–Higgins (1953) second–order solution for mass transport velocity under progressive waves. They derived a fourth–order solution for the mass transport velocity and found that the fourth–order conduction solution generally agreed better with available experimental data from Swan (1987) and Russell & Osorio (1958) than did the second order solution given by Longuet–Higgins (1953) as shown in Fig.3.12 .

Particularly, they showed that the fourth–order solution predicts the observed tendency of the surface mass transport velocity as shown in Fig.3.6 . Moreover, Swan & Sleath found that the agreement of the fourth–order solution with the measurements of mass transport velocity in the interior of the flow is inferior to those with the measurements of mass transport velocity near the free water surface. Therefore, Swan & Sleath (1990) suggested that the discrepancy between the fourth–order solution and the experimental data in the interior of flow might be eliminated if the solution was continued to still higher orders of approximation.

Although the fourth–order solution by Swan & Sleath (1990) gave a better prediction of the mass transport velocities near the water surface and in the interior of flow in comparison with Longuet–Higgins (1953) conduction solution, the theory is only a higher order version of Longuet–Higgins conduction solution, and thus still depending on the assumption that $a^2 \ll \delta^2$.

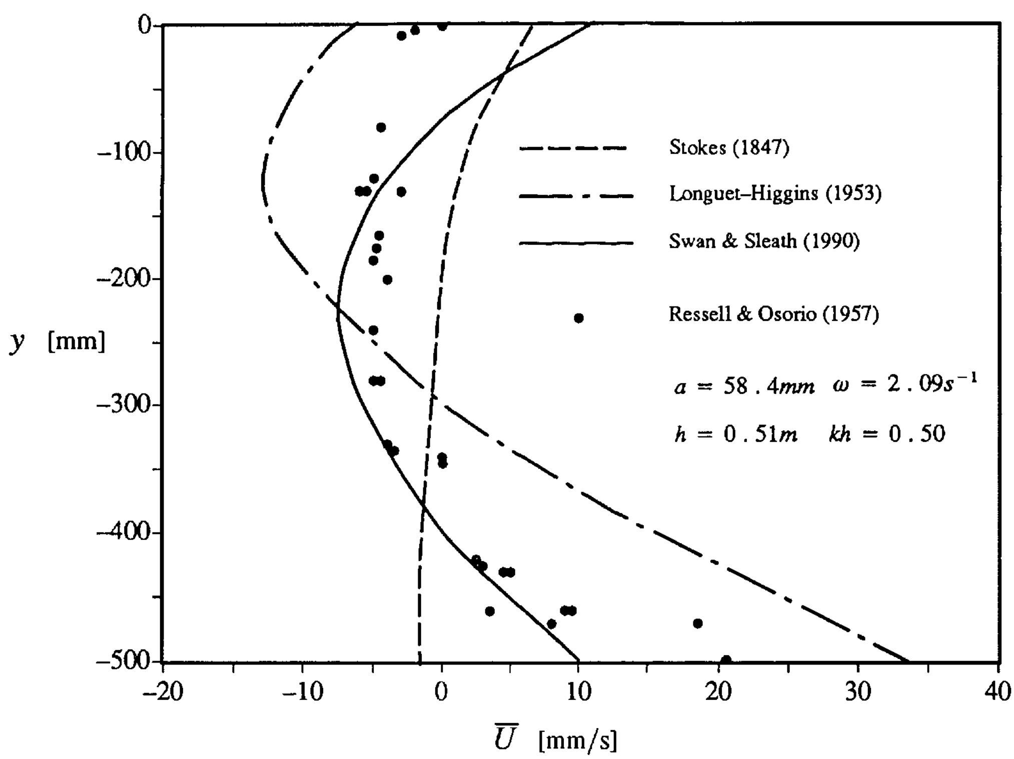

Fig.3.12 Comparison of theoretical predictions on mass transport velocity with experimental data

§3.2.3. REVIEW OF PREVIOUS EXPERIMENTAL WORK

§3.2.3.1. Bagnold (1947)

Bagnold (1947) first recognised that the mass transport could have an important effect on the sediment transport by progressive waves. Bagnold's experiments were made in a glass−sided wave flume, 11m long, 0 . 30m wide and 0 . 30m deep.

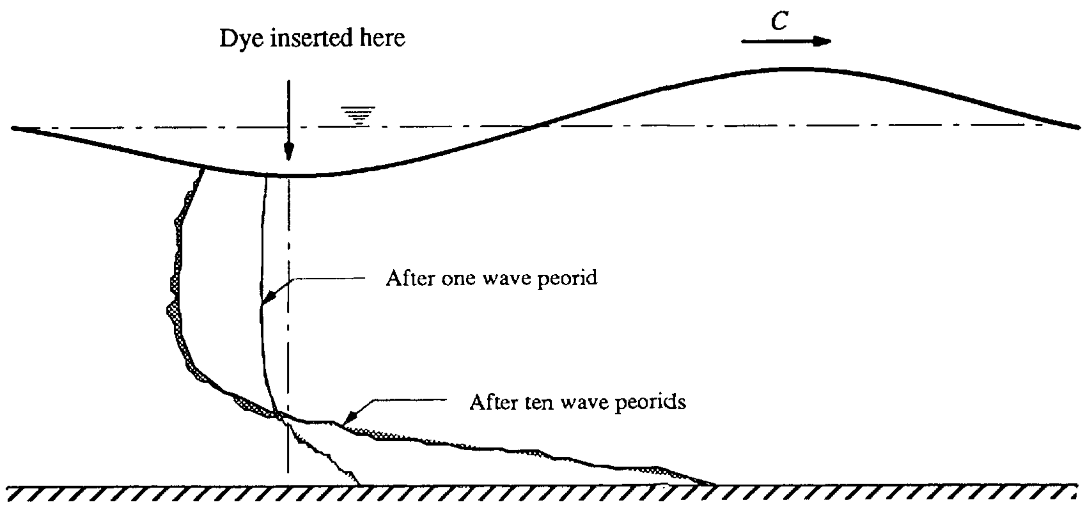

Fig.3.13 Existence of mass transport velocity observed by Bagnold (1947)

The observation of the mass transport for the smooth bed was made using hygroscopic particles impregnated with fluorescence. These particles were dropped into the wave field where they sank leaving a laminar dye streak which gradually deformed with time, giving a direct picture of the drift velocity profile. Fig.3.13 illustrates the successive drift profiles observed by Bagnold.

It was observed that in no case was a forward drift observed near the water surface. Moreover, motions in the upper part of the interior region were unsteady and inconsistent. Best results were observed when the channel was freshly filled with water, but after a few hours of exposure to the air, a film was found to form on the water surface, which was sufficiently strong to completely suppress the surface drift.

§3.2.3.2. Russell & Osorio (1958)

Russell & Osorio (1958) conducted a comprehensive set of experiments on mass transport in a wave flume, which was $56m$ long, $1.2m$ wide and $0.56m$ deep. A wave filter was installed in the front of the wave generator. In order to minimize wave reflection from the beach and keep the conditions steady, Russell & Osorio installed a flexible plastic curtain near the beach, which hung from a floating wooden bar at its upper edge and carried an iron bar at its lower edge. This instrument was moored by thin elastic threads. The device had no apparent effect on waves, but ensured that there was zero drift at the point where the plastic curtain was installed. In the experiment, Russell & Osorio used small particles to measure the mass transport velocity at different levels, and chose vertical dye tracers to observe the general profile of mass transport velocity across the test section. Through the experiments, Russell & Osorio found that

(1) The net drift near the free water surface was in the direction of wave propagation in all tests.

(2) The net drift near a horizontal bed was invariabably in the direction of wave propagation, and quantitatively in good agreement with that predicted by the conduction solution of Longuet–Higgins (1953).

(3) When $0.7 \leq kh \leq 1.5$, the conduction solution of Longuet–Higgins (1953) could be applied to predict the drift velocity in the interior flow whereas when $kh > 3.0$, the Stokes theory (1847) could be used.

§3.2.3.3. Brebner *et al.* (1966)

Brebner *et al.* (1966) carried out experiments to investigate the effect of the bed roughness on the mass transport velocity near the bed. The experimental bed consisted of sand grains and six different grain sizes in the range of $0.5 \sim 2.2mm$ were used in different experiments. Experiments were also conducted with a smooth bed. The general profile of the mass transport velocity across a test section was observed by using fluorescent tracer–sand, and the mass transport velocity near the bed was measured by using neutrally buoyant beads. Brebner *et al.* (1966) defined the Reynolds Number in the boundary layer as

$$R_\delta = \frac{A\omega\delta}{\nu} \tag{3.43}$$

where δ is the Stokes length $\sqrt{2\nu/\omega}$ and $A\omega$ is the free stream velocity amplitude just outside the boundary layer, which was calculated from the first order theory as

$$A\omega = \frac{H\omega}{2\sinh kh}$$

Brebner *et al.* (1966) experiments indicated that

(1) When $R_\delta < 160$, the boundary flow was laminar. The maximum mass transport velocity near the bed increased with increasing bed roughness.

(2) The boundary layer flow became quite turbulent over the smooth bed and the sand beds when $R_\delta > 160$. The maximum mass transport velocity near the bed decreased with increasing bed roughness, and was found to be proportional to $H^{1.2}$ rather than H^2 as predicted by Longuet–Higgins (1953).

§3.2.3.4. Mei *et al.* (1972)

Mei *et al.* (1972) carried out a detailed and comprehensive experiment to investigate the mass transport under progressive waves. The experiment was conducted in a wave flume of $12m$ long, $0.76m$ wide and $0.20m$ deep over a smooth horizontal bed. The wave absorber consisted of a piece of foam material of fairly high porosity with holes. From their experiments, Mei *et al.* (1972) found that in most cases a stable state was achieved after a period of about one hour. At that time it was found that the mass transport velocity profile measured at the center line of the flume agreed with Longuet–Higgins (1953) conduction solution for $0.9 \le kh \le 1.5$, but for larger kh, the mass transport velocity profile was close to Stokes' (1847) second order solution.

§3.2.3.5. Sleath (1973)

Sleath (1973) did an experiment to investigate the mass transport velocity under small waves [$H = 1mm$, $T = 1s$]. The experiment was conducted in a wave flume of $17.50m$ long and $0.56m$ wide. Waves were generated at one end by a simple hinged paddle, and absorbed at the other by a single beach of slope 1 : 20. A wave filter was placed $1.0m$ from the wave generator. The bed of the test section consisted of a glass sheet of $3.0m$ long. The minimum wave amplitude in this experiment was $1mm$ for wave periods of 1−second and 2−second, respectively. From the experiments, Sleath (1973) found that

(1) The mass transport velocity near the free water surface was predicted very well by Stokes (1847) solution, as shown in Fig.3.6 .

(2) On no occasion was a mass transport velocity profile predicted by Longuet Higgins (1953) conduction solution.

(3) There was a negative peak mass transport velocity near the bed.

§3.2.3.6. Bijker *et al.* (1974)

Bijker *et al.* (1974) investigated the effect of the bottom slope on the mass transport velocity under gravity waves. Their experiment was conducted in a wave flume of $30.0m$ long, $0.80m$ wide and $0.60m$ deep. Three different slopes of 1 : 10, 1 : 25 and 1 : 40 were used in the experiment. The slope surface was rigid, but its roughness was varied from a painted smooth concrete to glued sand grain and artificial ripple beds, respectively. The diameter of the sand grains was between $1.6 \sim 2.0mm$, and the length and height of the symmetrical ripples were $80mm$ and $18mm$. All waves broke on the beach. The reflection from the beach was always less than 6%. Curtains were installed at both ends of the wave flume to minimize the wave reflection from both the beach and wave generator. From the experiments, Bijker *et al.* (1974) found that

(1) The bottom mass transport velocity was primarily determined by wave height, wave period and local water depth while the slope of the bottom has no significant influence.

(2) The bottom mass transport velocity predicted by Longuet–Higgins (1953) conduction solution for a horizontal bottom was larger than the measured velocity. The discrepancy between Longuet–Higgins conduction solution and experimental data increased with decreasing depth and increasing relative wave length.

(3) The drift velocity changed slightly with increasing bottom roughness, but considerably with the presence of a ripple–like roughness.

§3.2.3.7. You *et al.* (1991b)

You *et al.* (1991b) studied experimentally the effect of bed roughness on the mass transport velocity near the bed under progressive waves. The experimental set–up is shown in Fig.3.16. The maximum mass transport velocity near the bed was measured with neutrally buoyant liquid particles, consisting of oil–based white paint and two different kinds of hydrocarbon solvents, one lighter than water and the other denser than water. The distribution of the maximum mass transport velocities measured near different bed configurations are shown in Fig.3.19 . It was concluded that

(1) The maximum mass transport velocity measured near the bed decreased with increasing the bed roughness when $R_\delta < 160$, which is at variance with Brebner *et al.* (1966). The reasons for this difference are unclear.

(2) The direction of the mass transport velocity near the bed was always observed to be in the direction of wave propagation rather than in the opposite direction as Sleath (1973) observed.

(3) The mass transport velocity measured over the smooth bed was approximately proportional to the wave height instead of the square of the wave height as predicted by Longuet–Higgins (1953).

§3.3. EXPERIMENTAL STUDY

§3.3.1. OBJECTIVES OF THE PRESENT EXPERIMENT

The maximum mass transport velocity at the outer edge of the laminar boundary layer as determined by Longuet–Higgins (1953) is given by

$$\overline{U}_b = \frac{5a^2 k\omega}{4\sinh^2 kh} \tag{3.44}$$

and later [Longuet–Higgins (1956)] showed that Eq.(3.44) could be used to predict the maximum mass transport velocity at the edge of the turbulent boundary layer if the eddy viscosity was assumed to be a function of elevation only. This implies that the bed roughness has no effect on the mass transport velocity near the bed. However, Brebner *et al.* (1966) found from his experimental study that when $R_\delta < 160$ increasing bed roughness would increase the mass transport velocity while for $R_\delta > 160$ the mass transport velocity decreased with increasing bed roughness. On the other hand, Sleath (1973) found in his experiments that the direction of the maximum mass transport velocity near the smooth bed was opposite to that of the wave propagation rather than in the direction of wave propagation as Longuet–Higgins (1953) predicted and Brebner *et al.* (1966), Russell & Osorio (1958) and Bijker *et al.* (1974) observed. Therefore, in order to settle these disparities the present study was undertaken with the specific aims

(1) To examine the validity of the conduction solution of Longuet–Higgins (1953) under the condition of $a^2 \ll \delta^2$.

(2) To review the effect of bed roughness on the mass transport reported by Brebner *et al.* (1966) when $R_\delta < 160$.

(3) To investigate Sleath's (1973) finding that the mass transport velocity near a smooth bed was in the opposite direction of wave propagation.

§3.3.2. EXPERIMENTAL APPARATUS

§3.3.2.1. Wave Flume

The measurements were carried out in a wave flume at Water Research Laboratory of The University of New South Wales. The length of the wave flume is about 35 . 0*m*, the width 0 . 9*m*, the total depth 1 . 5*m*, and the slope of the beach 1 : 14. The walls are made of rendered brick except for a glass panelled section covering over half of the front. This working section is used for observations, photography and video. The bed is horizontal for 20*m*, and then has a fixed slope of about 1 : 14 for 6*m*, and finally has a horizontal section 4*m* long and 0 . 65*m* above the bed level. Re−circulation of water from the beach end to the wave maker end of the flume is possible via Pipes fitted underneath the bed. The pipes can be closed if not required. The flume is fitted with a 40kw hydraulically powered, piston type wave generator that can be fed with either a sine wave signal to produce simple harmonic waves or with a recorded or synthesized signal to generate random or spectrally defined waves. The signal generators used normally allow both the amplitude and period of wave to be changed while the wave generator is operating. Wave periods are generally in the range 0 . 5*s*−3 . 0*s*. The range of wave height that can be generated depends on the water depth and wave period used.

§3.3.2.2. Bed Configurations

[1] A smooth false bottom was made of perspex of 8 . 0*m* long, 0 . 89*m* wide and 5 . 0*mm* thick. The perspex bed was raised up to 7 . 5*cm* from previous bed level so as to clearly observe the motion of particles and to make it more convenient to take photos. One end of the perspex bed was located in the front of the beach toe. The other end of the perspex was slightly bent into a curve to join the concrete bed smoothly. In order to protect the perspex from bending along the wave flume direction, a frame was used to ensure that the smooth bed was always horizontal during testing. The construction of the smooth bed is shown in Fig.3.14 .

[2] A rough bed consisted of a layer sand grains of 2*mm* diameters glued to the perspex surface. In order to ensure that the thickness of the sand layer was equal

everywhere, a piece of wood with a horizontal surface was used to level the surface of the sand layer. Sand grains on the bed were painted black to reduce the light reflection and assisting with the tracking of white neutrally buoyant oil droplets which were used as flow markers.

[3] In a further series of experiments a very rough bed was made using $2.5cm$ average diameter gravel. A layer of gravel was put on the surface of sand bed, and then a piece of straight wood was used to level the gravel surface to ensure that the thickness of the gravel layer was uniform. The weight of the gravel was pretty heavy that it was not necessary to glue it to the sand bottom.

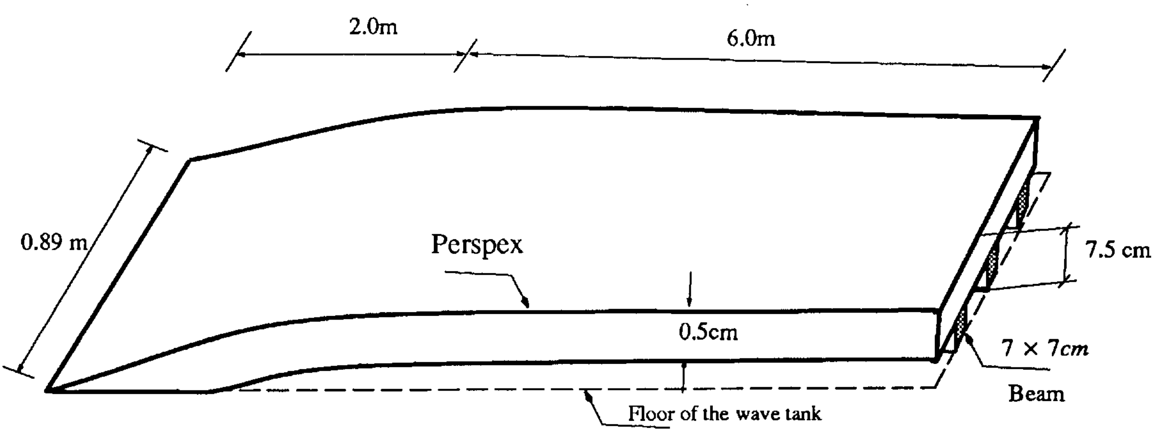

Fig.3.14 Configuration of the smooth bed for measurement of mass transport velocity

§3.3.2.3. A Plastic Curtain

Following Russell & Osorio (1958) and Bijker *et al.* (1974), a plastic curtain was used to isolate the test section from the turbulence generated at the beach and this was found to keep mass transport velocity in a stable condition during tests.

Recently, Swan & Sleath (1990) also demonstrated that the installation of a curtain in the front of the beach was of great effect helping mass transport velocity reach a stable condition. Otherwise the mass transport velocity tends to be unstable. The curtain used in the present experiment consisted of a floating foam bar, a thin plastic sheet and an iron bar, see Fig.3.15 .

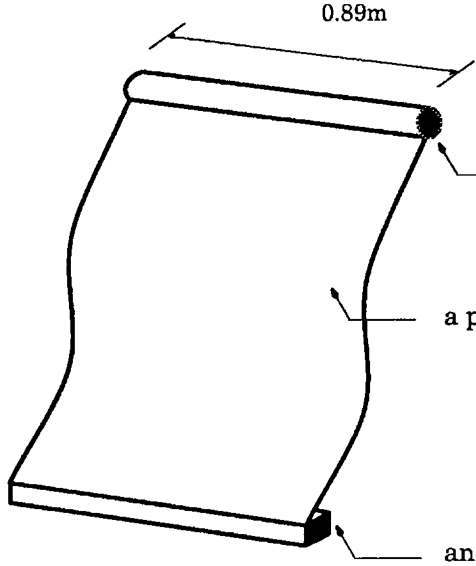

Fig.3.15 Construction of the plastic curtain used in the present study

§3.3.2.4. Tracking Particles

Measurement of the Lagrangian mean velocity induced by progressive waves was accomplished using neutrally buoyant oil droplets. Previous investigators used neutrally buoyant plastic beads as tracking particles. However, these small solid beads tend not to be neutral under waves. For example, Russell & Osorio (1958) found that small particles rose and fell more than $2.0cm$ during measuring period. In the present experiments, liquid droplets were used as tracers. The advantages of this are that the density of liquid particles can be easily adjusted to account for temperature effects on water density by a method of trial and error, and the diameter of liquid particles can be made as small as required by simply changing the diameter of the injector. The liquid particles were made of a mixture of xylene [$\varrho = 0.80$] and carbon tetrachloride [$\varrho = 1.15$]. A white oil based paint was used to pigmentation. In order to produce a few droplets near the bed, a syringe was used to inject the mixed white hydrocarbon solvent into water. The syringe needle was extended to reach the bed and produced a few fine droplets near the bed.

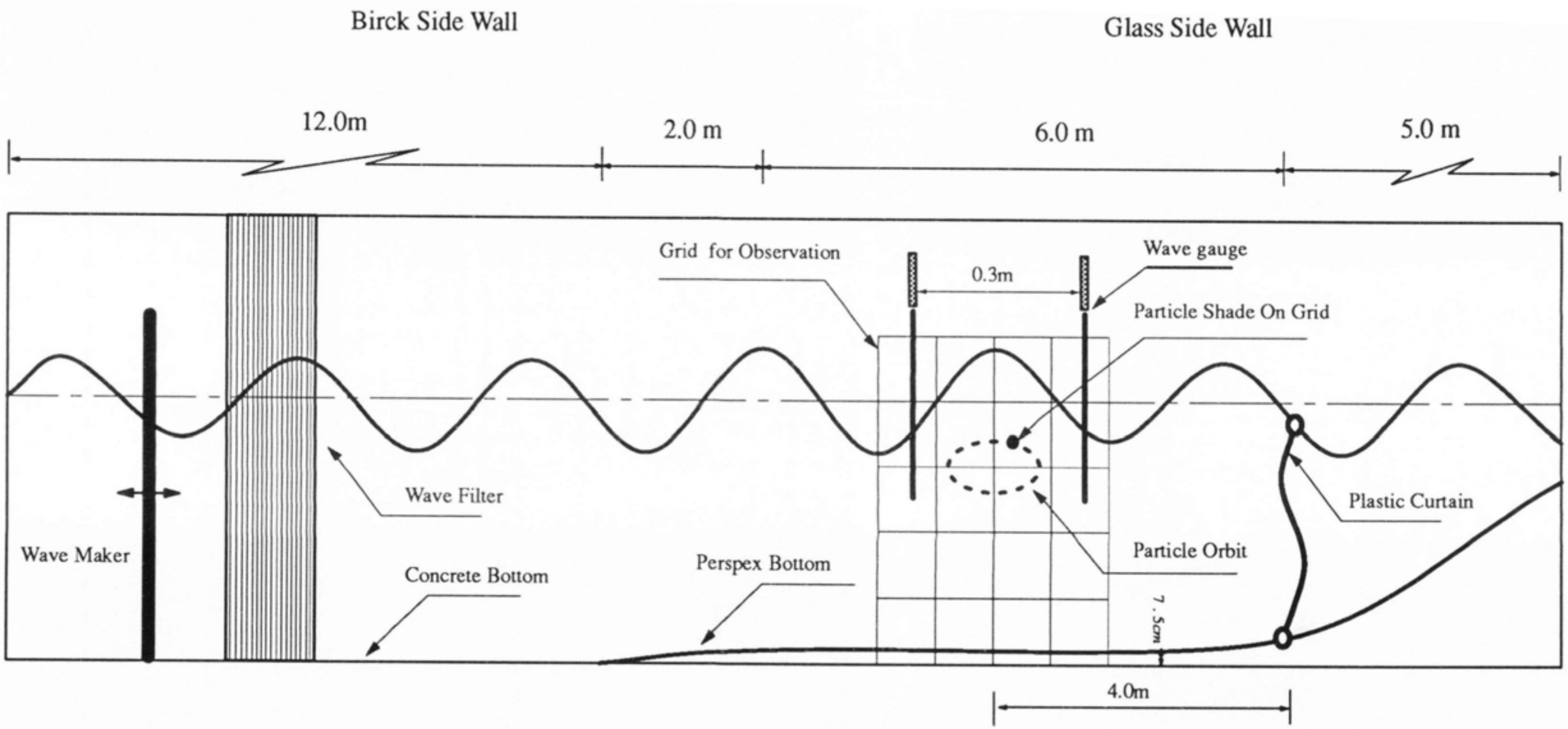

Fig.3.16. Sketch of wave flume for measurement of mass transport velocity near the bed

§3.3.2.5. Other Equipments

In order to watch such small white droplets moving under waves in the experiments, a video camera and monitor screen were used to enlarge the droplets and show their locus on the monitor screen. The video camera was set $0.5m$ from the glass wall in the front of the test section. The wave height was recorded by using two wave gauges located in the middle of the test section $0.3m$ apart, see Fig.3.16 .

§3.3.3. METHOD OF MEASUREMENT

§3.3.3.1. The Level of Velocity Measured

The velocity measured near the bed is a maximum mass transport velocity in a laminar boundary $[R_\delta < 160]$ according to the criterion defined by Brebner *et al.* (1966). In a laminar boundary layer the mass transport velocity distribution is given by

$$\overline{U} = \frac{(A\omega)^2}{4C}\left\{ 5 - 8e^{-\beta z}\cos\beta z + 3e^{-2\beta z} \right\}$$

in which the maximum mass transport velocity inside the laminar boundary layer is

$$\overline{U} = \frac{1.376A^2}{C}$$

corresponding to the elevation

$$z_j \approx 2.34\sqrt{\frac{2\nu}{\omega}} \tag{3.45}$$

as shown in Fig.3.5 . Eq.(3.45) shows that the level z_j corresponding to the maximum mass transport velocity is a function of wave period only. However, it was found in the present experiment that the level z_j also depended on wave height as shown in Fig.3.18 . Therefore, how to determine the level of the maximum velocity is a practical subject in the present study. A more readily distinguishable point of maximum mass transport velocity in the present experiment was chosen as the level at which the velocity of a given particle was moving faster than others near the bed, which is shown in Fig.3.17 .

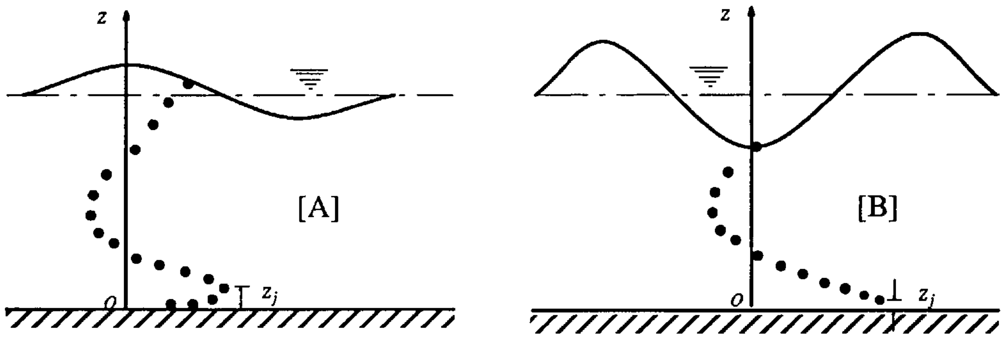

Fig.3.17 Determination of the level z_j of maximum mass transport velocity in the present study

§3.3.3.2. Determination of Mass Transport Velocity

The mass transport velocity is defined as a time averaged velocity of a given particle averaged over several wave periods, which is

$$\overline{U} = \frac{\Delta S}{\Delta t} \tag{3.1}$$

where ΔS is a net displacement which a droplet travels in the period of time Δt. Therefore, the measurement of mass transport velocity involved measuring a net displacement ΔS during a time period Δt. The procedure adopted for measurements of the drift velocity was to inject a few droplets near the bed with a syringe after the waves had been running for about an hour. At the same time, the video camera was set to record the locus of the small droplets moving under waves. Then, watching a chosen particle on the monitor screen, which was moving faster than others near the bed, passing a certain distance ΔS, e.g. $5cm$ or $10cm$, i.e. one grid or two grids marked on the glass wall and recording the time period Δt with a stop watch. The measurement of the drift velocity for each wave condition was repeated at least ten times to get an averaged value of the maximum drift velocity near the bed. During the experiment, the mean water depth was $0.3m$, and the wave period $T = 1.0s$. The measurements of maximum mass transport velocity over different bed configurations are shown in Appendix I.

§3.3.4. EXPERIMENT RESULTS AND ANALYSIS

§3.3.4.1. The Vertical Distribution

The vertical distribution of mass transport velocity was observed by using a vertical dye streak. Fig.3.18 shows the vertical profiles of the mass transport velocity measured in the two tests in which the boundary layers were laminar (A) with $R_\delta \approx 2.3$ and (B) with $R_\delta \approx 44.6$ according to the criterion defined by Brebner *et al.* (1966).

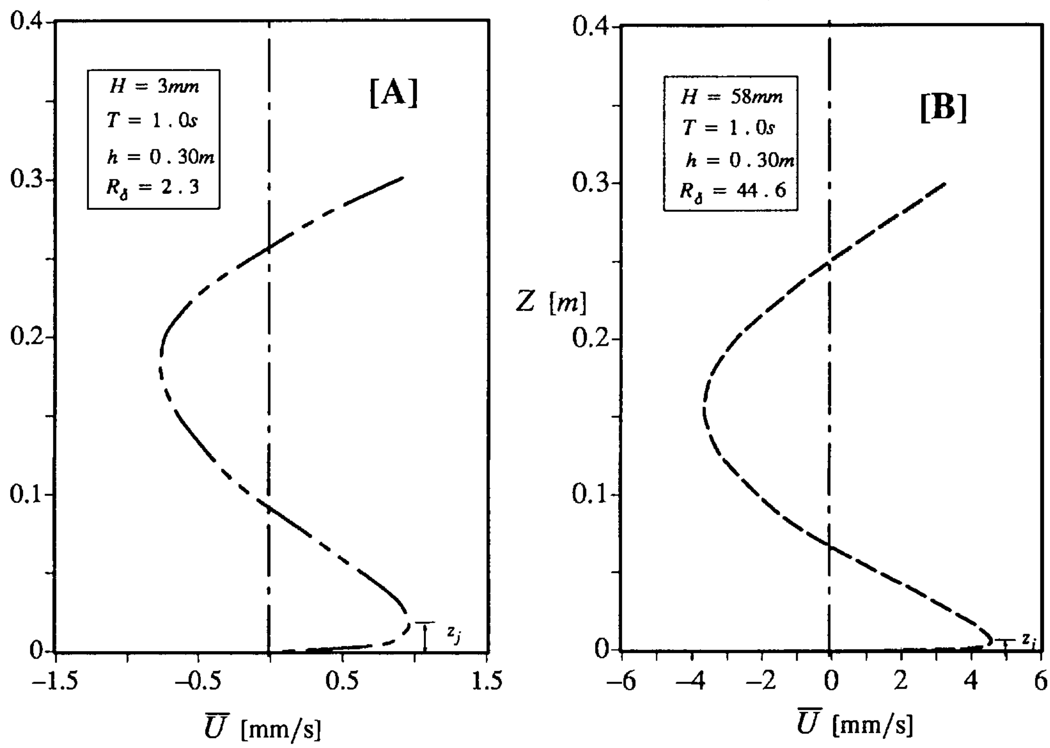

Fig.3.18 Observed vertical variation of mass transport velocity along the depth over smooth bed

The general profiles of the mass transport velocity over the depth in the two tests are similar, however the level of the maximum mass transport velocity with a small wave steepness $[H/L]$ is much higher than that with a large wave steepness. The general distribution of the mass transport velocity outside the boundary layer in both experiments [A] and [B] is quite similar to that predicted by Longuet−Higgins (1953) conduction solution, see Fig.3.4. It should be noted here that the profile of the mass transport velocity induced by small waves as shown Fig.3.18 [A], is different from that observed in Sleath (1973) experiments and the type III of Sleath (1973) three possible solutions [Fig.3.8], and that the maximum mass transport velocity is in the direction of wave propagation rather than the opposite direction observed by Sleath (1973). The reason for this is unclear.

§3.3.4.2. Variation of Drift Velocity with Bed Roughness

The effect of bed roughness on maximum mass transport velocity near the bed was investigated using a water depth $h = 0.30m$ and wave period $T = 1.0s$, and systematically changing the wave height in the range of $2mm < H < 60mm$. The boundary layer regimes generated in the present experiments were laminar according to the criterion defined by Brebner *et al.* (1966).

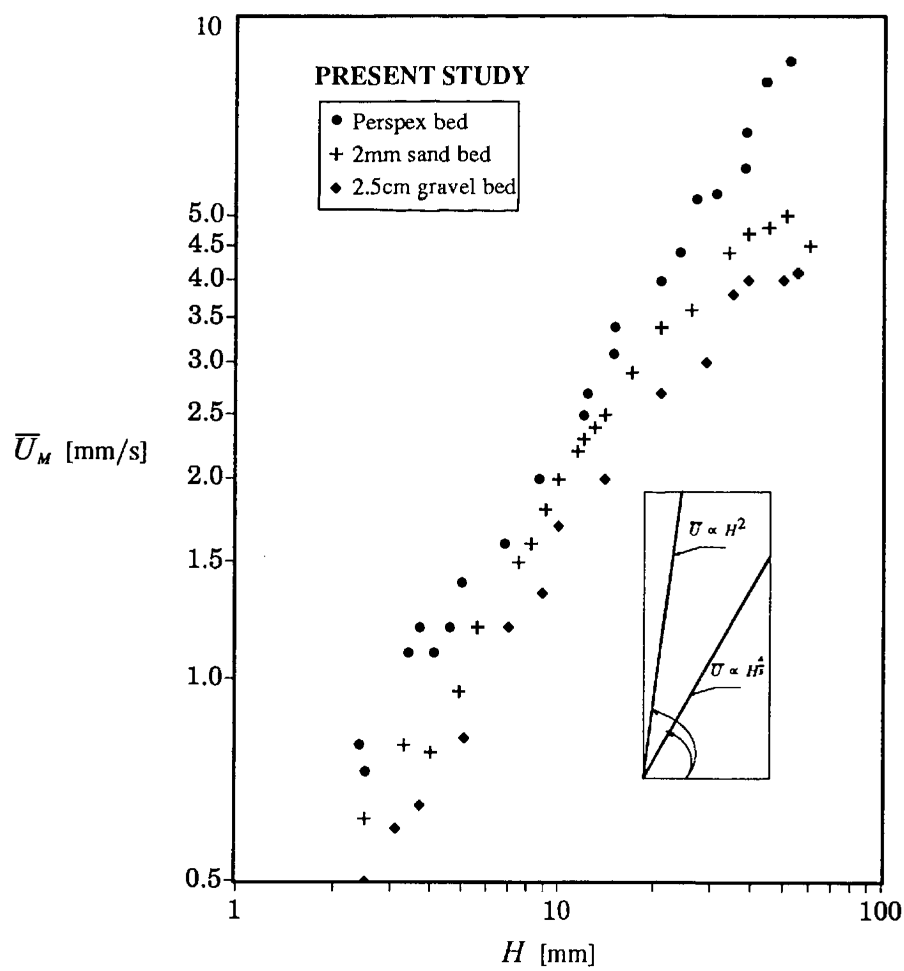

Fig.3.19 The variation of maximum mass transport velocity near the bed with bed roughness

The variation of maximum mass transport velocity near the bed with wave height and bed roughness is shown in Fig.3.19 . It can be seen that the maximum mass transport velocity near the smooth bed is only slightly greater than that near the rough bed when the wave height is not so large, e.g. $H \le 20mm$. However, if the wave height is increased, the maximum mass transport velocity near the smooth bed is much greater than those near the rough beds. On the other hand, the maximum mass transport velocities near the beds with different roughness are approximately proportional to $H^{\frac{4}{5}}$ rather than the square of the wave height H^2 as shown in Fig.3.19 .

§3.3.4.3. Comparison with Longuet–Higgins (1953) Solution

Longuet–Higgins (1953) conduction solution for the mass transport velocity at the outer edge of the laminar boundary layer yields

$$\overline{U}_L = \frac{5a^2\omega k}{4\sinh^2 kh} \tag{3.46}$$

Fig.3.20 shows the variation of the ratio $\overline{U}_M/\overline{U}_L$ of the measured maximum mass transport velocity to that estimated from Eq.(3.46) with the Reynolds number $R_\delta = A\omega\delta/\nu$. It can be seen in Fig.3.20 [A] that the ratio $\overline{U}_M/\overline{U}_L$ decreases with increasing R_δ. When $R_\delta < 25$ Longuet–Higgins (1953) conduction solution fails to agree with the experimental data. However, when $R_\delta > 25$ the ratio $\overline{U}_M/\overline{U}_L$ is close to 1, which indicates that Longuet–Higgins (1953) conduction solution may give a rough estimation of the mass transport velocity at large Renolds numbers. This conclusion is also supported by Brebner *et al.* (1966) experimental data as shown in Fig.3.20 [B].

Therefore, doubt is cast on the adequacy of Longuet–Higgins (1953) conduction solution since it was derived under the assumption of $a^2 \ll \delta^2$, which corresponds to a small R_δ.

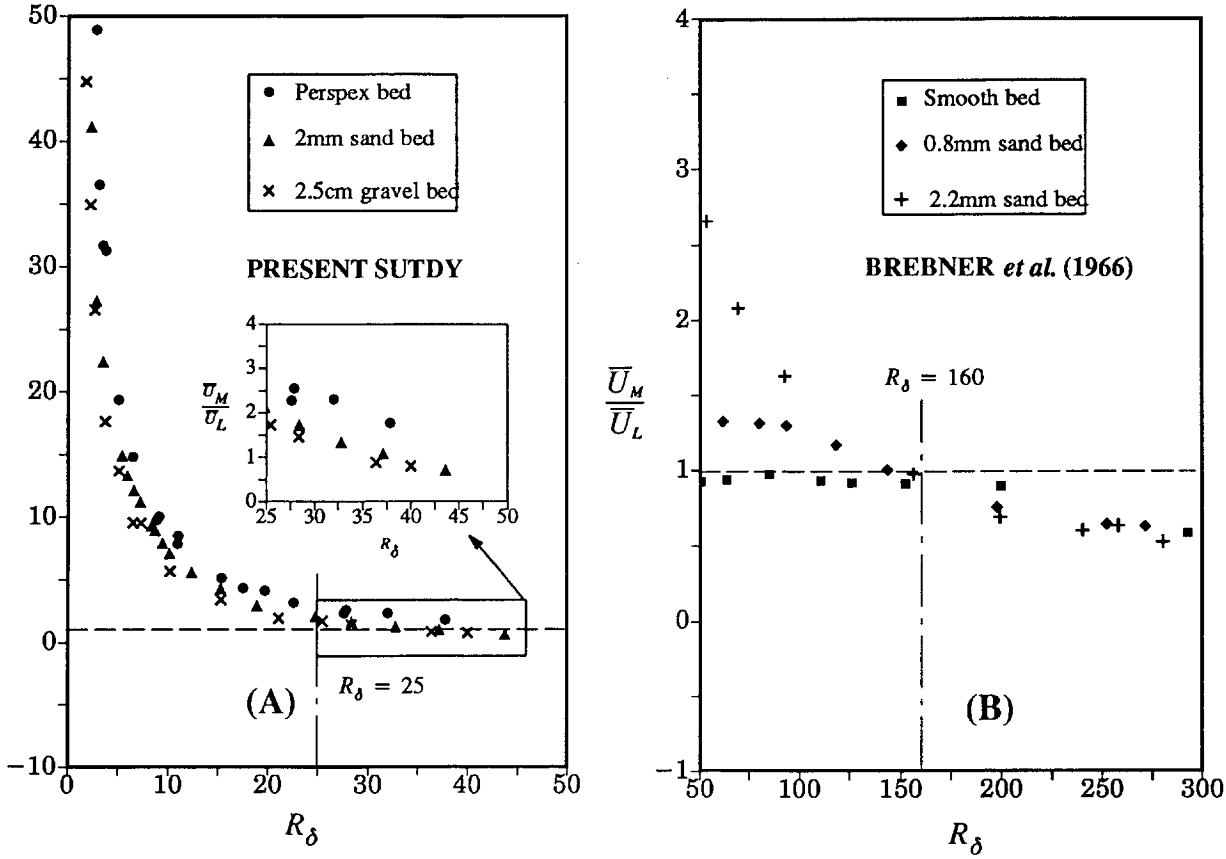

Fig.3.20 Comparison of Longuet–Higgins (1953) conduction solution with experimental data

§3.3.4.4. Discussions

The relationship between the maximum mass transport velocity $\overline{U}_M$ measured near the bed and the free stream velocity amplitude $A\omega$ is investigated in Fig.3.21 which shows the ratio $\overline{U}_M/\{A\omega\}$ plotted as a function of the Renolds Number R_δ. However, as Fig.3.21 shows, the ratio $\overline{U}_M/\{A\omega\}$ indicates no systematical sensitivity to the Renolds Number R_δ. For example, for the present experiments, the ratio $\overline{U}_M/\{A\omega\}$ decreases with increasing the Renolds number whereas for Brebner *et al.* (1966) study the ratio $\overline{U}_M/\{A\omega\}$ increases with increasing the Renolds number. On the other hand, as Brebner & Collins (1961) concluded in their experiments [$H > 30mm$], the maximum mass transport velocity measured near the smooth bed was quite well predicted by Longuet–Higgins (1953) conduction solution Eq.(3.46).

However, in the present study [$2.5mm < H < 60mm$] the maximum mass transport velocity measured near the smooth bed is not well predicted by Eq.(3.46) when the wave height is very small, but getting better when the wave height increases as shown in Fig.3.20 [A]. Therefore, it is still unclear whether the conclusion made by Brebner & Collins (1961) is correct or not if the maximum mass transport velocities near the smooth bed were measured under very small waves [$H < 30mm$].

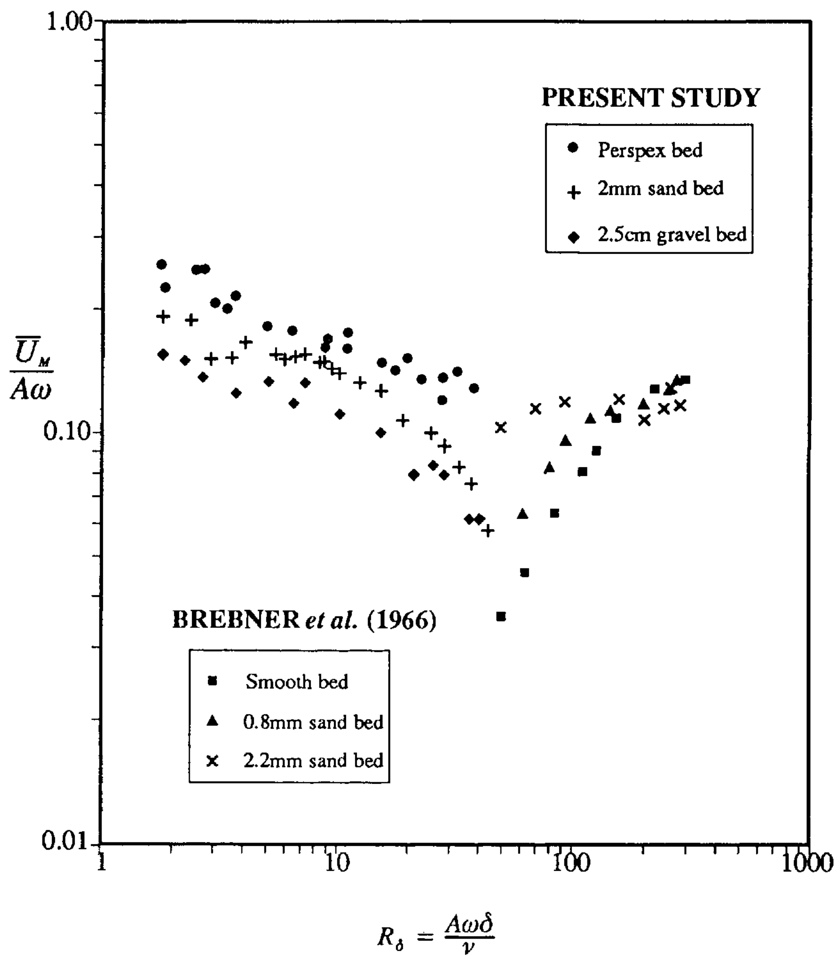

Fig.3.21 Variation of $\overline{U}_M/\{A\omega\}$ with the Renolds Number and bed roughness

§3.3.5. CONCLUSIONS

(1) Maximum mass transport velocity near the bed decreases with increasing bed roughness. The conclusion that increasing bed roughness would increase the mass transport velocity for $R_\delta < 160$ made by Brebner *et al.* (1966) is not supported by the present study.

(2) The effect of the bed roughness on the maximum mass transport velocity near the bed is getting more significant as wave steepness increases.

(3) The conduction solution of Longuet–Higgins (1953) fails to give a good prediction of the maximum mass transport velocity measured near the bed in the present experiments when the wave height is very small [$R_\delta < 20$].

(4) The maximum mass transport velocity near a smooth bed measured under waves of very low steepness was found to be in the direction of wave propagation rather than in the opposite direction as reported by Sleath (1973).

(5) The mass transport velocity was found to be proportional to $H^{\frac{4}{5}}$ instead of H^2 as Longuet–Higgins (1953) conduction solution predicts.

CHAPTER 4

OSCILLATORY BOUNDARY LAYERS WITH CURRENTS

§4.1 INTRODUCTION TO COMBINED FLOWS

§4.1.1 THE COMBINED WAVE–CURRENT FLOWS

In former chapters, we have studied the velocity distribution, bed shear stress, friction factor, and mass transport velocity in the wave boundary layer in the absence of currents. However, the water motion in coastal and estuarine areas is generally a combination of waves and currents instead of a pure wave motion.

It is worthwhile to consider, from a qualitative view, the different roles of waves and currents in the sediment transport process. Often, the near bed orbital velocities due to waves are of the same magnitude as the stronger coastal currents. However, the boundary shear stress associated with the wave motion may be an order of magnitude larger than the shear stress related to the current of comparable magnitude. This is due to the small vertical scale of the wave boundary layer in comparison with that of the current boundary layer. Thus, waves are capable of entraining significant amounts of sediment from the sea bed when the current of comparable magnitude may be unable to even initiate sediment motion. On the other hand, waves are an inefficient transporter of sediment. Therefore, it is important to study the combined wave–current flow in order to understand the mechanism of sediment transport and quantitatively determine the rate of sediment transport.

§4.1.2 THE STUDY OF COMBINED FLOWS IN THE LABORATORY

Detailed studies of the combined wave–current flows have been conducted in the laboratory by many investigators. For example, van Doorn (1981) & (1982) conducted comprehensive experimental study of the combined wave–current flow in wave flumes and oscillating water tunnels in the laboratory, see Fig.4.1.

TESTS	Facility	$A\omega$ [cm/s]	T [s]	K_N [cm]	$<\overline{U}>$ [cm/s]	$\hat{U}^*$ [cm/s]	$\overline{U}^*$ [cm/s]
V00RA	Flume	26.7	2.0	2.1	0.0	4.3	0.00
V10RA	Flume	25.3	2.0	2.1	10.0	5.6	1.70
V20RA	Flume	24.3	2.0	2.1	20.0	5.2	2.60
S00RAL	Tunnel	32.3	2.0	2.1	0.0	5.7	0.00
S10RAL	Tunnel	32.3	2.0	2.1	10.0	5.7	2.03
S20RAL	Tunnel	32.3	2.0	2.1	20.0	5.7	3.18
M00RAL	Tunnel	106.0	2.0	2.1	0.0	15.3	0.00
M10RAL	Tunnel	106.0	2.0	2.1	10.0	15.3	2.36
M20RAL	Tunnel	106.0	2.0	2.1	20.0	15.3	3.30

Table.4.1 Measurements of combined wave–current flows conducted by van Doorn (1981 & 1982)

The instantaneous velocities were measured with a laser doppler anemometer, and the steady velocity component and the periodic component were obtained by using a harmonic analysis on $U(z, t)$. Table.4.1 shows the series tests carried out by van Doorn (1981) and (1982)

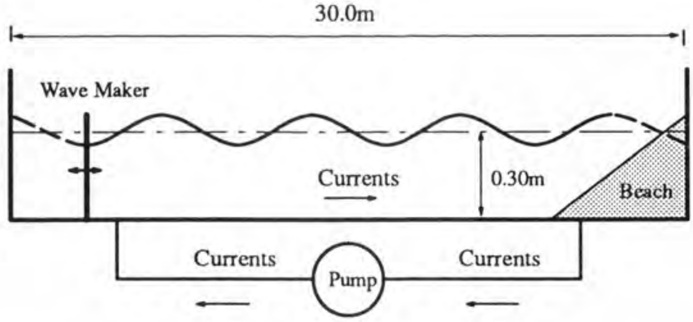

Fig.4.1 The study of the combined wave–current flow in a wave flume by van Doorn (1981)

§4.1.3 THE SCOPE OF THE PRESENT STUDY

(1) To calculate the current velocity in the presence of waves ;

(2) To calculate the wave–induced orbital velocity in the presence of currents ;

(3) To evaluate the bed shear stresses of combined wave–current flow.

§4.2 THE EQUATION OF MOTION

The horizontal motion of fluid in a combined wave–current flow is governed by the Navier–Stokes equation

$$\frac{\partial U}{\partial t} + U\frac{\partial U}{\partial x} + W\frac{\partial U}{\partial z} = -\frac{1}{\varrho}\frac{\partial P}{\partial x} + \nu\left\{\frac{\partial^2 U}{\partial x^2} + \frac{\partial^2 U}{\partial z^2}\right\} \tag{4.1}$$

and the continuity equation

$$\frac{\partial U}{\partial x} + \frac{\partial W}{\partial z} = 0 \tag{4.2}$$

By combining Eqs.(4.1) and (4.2), the momentum equation can be expressed as

$$\frac{\partial U}{\partial t} + \frac{\partial (UU)}{\partial x} + \frac{\partial (UW)}{\partial z} = -\frac{1}{\varrho}\frac{\partial P}{\partial x} + \nu\left\{\frac{\partial^2 U}{\partial x^2} + \frac{\partial^2 U}{\partial z^2}\right\} \tag{4.3}$$

In Eq.(4.3), If the combined flow is assumed to be horizontally uniform, the terms $\partial(UU)/\partial x$ and $\nu\ \partial^2 U/\partial x^2$ can be omitted. Therefore, Eq.(4.3) can be rewritten as

$$\frac{\partial U}{\partial t} + \frac{\partial (UW)}{\partial z} = -\frac{1}{\varrho}\frac{\partial P}{\partial x} + \nu \frac{\partial^2 U}{\partial z^2} \tag{4.4}$$

On the other hand, the velocity components U and W, and the pressure component P in Eq.(4.4) can be decomposed into three components, namely, the steady, the periodic and the random turbulent components

$$U = \overline{U} + \tilde{U} + u' \tag{4.5}$$

$$W = \overline{W} + \tilde{W} + w' \tag{4.6}$$

$$P = \overline{P} + \tilde{P} + p' \tag{4.7}$$

in which the steady and the periodic components are defined respectively as

$$\overline{X}(z) = \frac{1}{N}\sum_{i=1}^{N} X_i(z,t) \tag{4.8}$$

$$\tilde{X}(z,t) = \frac{1}{N}\sum_{i=1}^{N} X_i(z, t + iT) - \overline{X}(z) \tag{4.9}$$

where T is the wave period, t the time variable and N the number of waves. Based on the definitions above, it can be readily shown that

$$\overline{X'} = \overline{\tilde{X}} = \overline{\overline{X}\tilde{Y}} = \overline{\overline{X}Y'} = \overline{\tilde{X}Y'} = 0 \qquad \overline{\overline{X}} = \overline{X} \tag{4.10}$$

$$\tilde{X'} = \tilde{\overline{X}} = \widetilde{\overline{X}Y'} = \widetilde{\tilde{X}Y'} = 0 \qquad \tilde{\tilde{X}} = \tilde{X} \tag{4.11}$$

$$\widetilde{\tilde{X}\tilde{Y}} = \tilde{X}\tilde{Y} - \overline{\tilde{X}\tilde{Y}} \qquad \widetilde{\overline{X}\tilde{Y}} = \overline{X}\tilde{Y} \tag{4.12}$$

Substituting Eqs.(4.5), (4.6) and (4.7) into Eq.(4.4) leads to

$$\frac{\partial}{\partial t}(\overline{U} + \tilde{U} + u') + \frac{\partial}{\partial z}\left\{(\overline{U} + \tilde{U} + u')(\overline{W} + \tilde{W} + w')\right\} \tag{4.13}$$

$$= -\frac{1}{\varrho}\frac{\partial}{\partial x}(\overline{P} + \tilde{P} + P') + \nu\frac{\partial^2}{\partial z^2}(\overline{U} + \tilde{U} + U')$$

§4.2.1 THE GOVERNING EQUATION FOR $\overline{U}$

Using the time−average definition Eq.(4.8) and considering the identities given by Eq.(4.10), we obtain from Eq.(4.13)

$$\frac{\partial}{\partial z}\left\{\overline{U}\;\overline{W} + \overline{\tilde{U}\tilde{W}} + \overline{u'w'}\right\} = -\frac{1}{\varrho}\frac{\partial \overline{P}}{\partial x} + \nu\frac{\partial^2 \overline{U}}{\partial z^2} \tag{4.14}$$

which can be rewritten as

$$\frac{\partial}{\partial z}\left\{\nu\frac{\partial \overline{U}}{\partial z} - \overline{U}\;\overline{W} - \overline{\tilde{U}\tilde{W}} - \overline{u'w'}\right\} = \frac{1}{\varrho}\frac{\partial \overline{P}}{\partial x} \tag{4.15}$$

where all the terms in the bracket represent the vertical transfer of momentum in the horizontal direction, it is therefore reasonable to define them as the shear stress

$$\frac{\overline{\tau}}{\varrho} = \nu\frac{\partial \overline{U}}{\partial z} - \overline{U}\;\overline{W} - \overline{\tilde{U}\tilde{W}} - \overline{u'w'} \tag{4.16}$$

Hence, combining Eqs.(4.15) and (4.16), we obtain a governing equation for the steady component of the combined flow

$$\frac{\partial \overline{\tau}}{\partial z} = \frac{\partial \overline{P}}{\partial x} \tag{4.17}$$

The governing equation Eq.(4.17) for the steady component of the combined flow is similar to that for a pure steady flow.

§4.2.2 THE GOVERNING EQUATION FOR $\tilde{U}$

Using the phase average definition Eq.(4.9) and taking Eqs.(4.11) and (4.12) into account, we obtain

$$\frac{\partial \tilde{U}}{\partial t} + \frac{\partial}{\partial z}\left\{\overline{U}\tilde{W} + \tilde{U}\overline{W} + \tilde{U}\tilde{W} - \overline{\tilde{U}\tilde{W}} + \widetilde{u'w'}\right\} = -\frac{1}{\varrho}\frac{\partial \tilde{P}}{\partial x} + \nu\frac{\partial^2 \tilde{U}}{\partial z^2} \tag{4.18}$$

which can be rewritten as

$$\frac{\partial \tilde{U}}{\partial t} = -\frac{1}{\varrho}\frac{\partial \tilde{P}}{\partial x} + \frac{\partial}{\partial z}\left\{\nu\frac{\partial \tilde{U}}{\partial z} - \overline{U}\tilde{W} - \tilde{U}\overline{W} - \widetilde{\tilde{U}\tilde{W}} - \widetilde{u'w'}\right\} \tag{4.19}$$

in which all terms in the bracket stand for the vertical transfer of momentum in the horizontal direction, it is therefore reasonable to define them as the shear stress

$$\frac{\tilde{\tau}}{\varrho} = \nu \frac{\partial^2 \tilde{U}}{\partial z^2} - \overline{U}\tilde{W} - \tilde{U}\overline{W} - \widetilde{\tilde{U}\tilde{W}} - \widetilde{u'w'} \tag{4.20}$$

Hence, Eq.(4.18) can be rewritten as

$$\frac{\partial \tilde{U}}{\partial t} = -\frac{1}{\varrho}\frac{\partial \tilde{P}}{\partial x} + \frac{1}{\varrho}\frac{\partial \tilde{\tau}}{\partial z} \tag{4.21}$$

Outside the boundary layer where $U = U_\infty$ and $\tilde{\tau} = 0$, Eq.(4.21) can be simply written as

$$\frac{\partial \tilde{U}_\infty}{\partial t} = -\frac{1}{\varrho}\frac{\partial \tilde{P}}{\partial x} \tag{4.22}$$

Furthermore, if we assume that the distribution of the pressure gradient $\partial \tilde{P}/\partial x$ in Eq.(4.21) is hydrostatic, or in other words $\partial \tilde{P}/\partial x$ is constant with elevation, Eq.(4.22) will be valid inside the boundary layer. Therefore, The governing equation for the wave motion in the boundary layer can be written as

$$\frac{\partial \tilde{U}}{\partial t} = \frac{\partial U_\infty}{\partial t} + \frac{1}{\varrho}\frac{\partial \tilde{\tau}}{\partial z} \tag{4.23}$$

Eq.(4.23) is the governing equation for the wave motion in the combined flow.

§4.3 STEADY FLOW

§4.3.1 THE VELOCITY DISTRIBUTION

Prandtl (1927) found empirically that the current velocity distributions for turbulent steady flows are logarithmic

$$\frac{\overline{U}(z)}{\overline{U}^*} = \frac{1}{\varkappa}\ln z + C \tag{4.24}$$

where $\overline{U}^*$ is the current friction velocity and $\varkappa$ von Karman's constant (≈ 0.4). Normally, Equation(4.24) is written in the form

$$\frac{\overline{U}(z)}{\overline{U}^*} = \frac{1}{\varkappa}\ln\frac{z}{z_o} \tag{4.25}$$

in which $K_N = 30z_o$ and K_N is the equivalent sand grain roughness or the Nikuradse roughness.

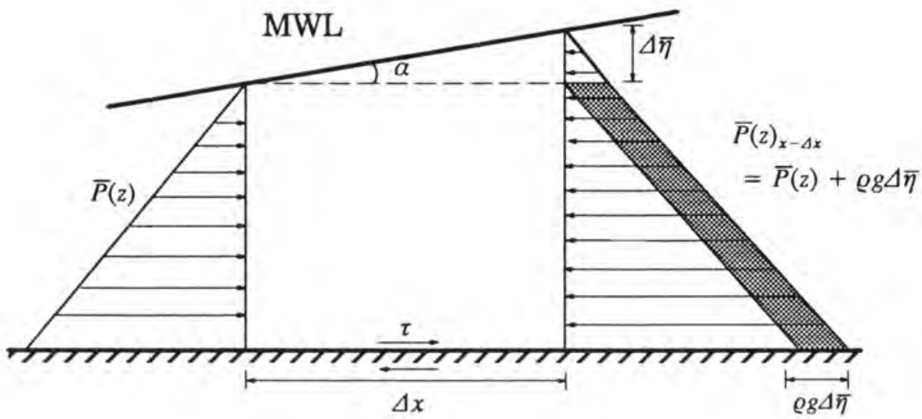

Fig.4.2 Variation of the pressure in a steady flow with horizontal and vertical directions

§4.3.2 SHEAR STRESS AND FRICTION FACTOR

The governing equation for steady flow is

$$\frac{\partial\overline{\tau}(z)}{\partial z} = \frac{\partial\overline{P}(x,z)}{\partial x} \tag{4.26}$$

The physical meaning of Eq.(4.26) is that the shear stress gradient in the vertical direction is balanced by the pressure gradient in the horizontal direction. For a uniform steady flow, the pressure gradient in the horizontal direction must come from a slope of the mean water surface, see Fig.4.2. Therefore,

$$\frac{\partial\overline{P}(x,z)}{\partial x} = \varrho\ g\ \tan\alpha \tag{4.27}$$

where α is the slope of the mean water level. Hence, combining Eq.(4.26) with (4.27) leads to

$$\frac{\partial \overline{\tau}(z)}{\partial z} = \varrho\ g\ \tan\alpha \tag{4.28}$$

Therefore, the distribution of the shear stress with elevation can be obtained from Eq.(4.28) as

$$\overline{\tau}(z) = \overline{\tau}_b \left\{1 - \frac{z}{h}\right\} \tag{4.29}$$

where $\overline{\tau}_b$ is the bed shear stress given by

$$\overline{\tau}_b = \varrho\ gh \tan\alpha \tag{4.30}$$

If a current friction factor f_c is defined by

$$\frac{\overline{\tau}_b}{\varrho} = \frac{1}{2} f_c < \overline{U} > \ < \overline{U} > \qquad \frac{\overline{\tau}_b}{\varrho} = \overline{U}^* \overline{U}^* \tag{4.31}$$

where $\overline{U}^*$ is the current friction velocity, and $< \overline{U} >$ is a depth−averaged mean current velocity given by

$$< \overline{U} > = \frac{1}{h} \int_{z_o}^{h} \overline{U}(z) dz = \frac{\overline{U}^*}{\varkappa} \ln \frac{11h}{K_N} \tag{4.32}$$

and then the bed friction factor f_c can be determined from Eqs.(4.31) and (4.32) as

$$f_c = 2.0 \left\{ \frac{1}{\varkappa} \ln \left\{ \frac{11h}{K_N} \right\} \right\}^{-2} \tag{4.33}$$

§4.3.3 THE EDDY VISCOSITY DISTRIBUTION

The eddy viscosity in turbulent steady flows is defined as

$$\frac{\overline{\tau}(z)}{\varrho} = \varepsilon_c \frac{\partial \overline{U}(z)}{\partial z} \tag{4.34}$$

Then, substituting the shear stress distribution Eq.(4.29) into Eq.(4.34) we will obtain the well−known eddy viscosity profile of the steady flow as shown in Fig.4.3.

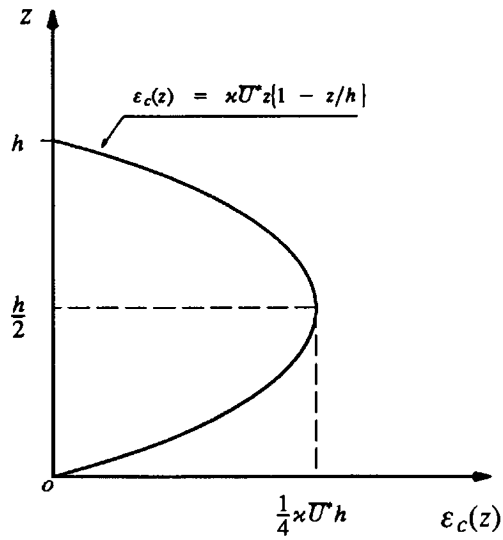

Fig.4.3 Variation of the eddy viscosity with elevation in a steady turbulent flow

§4.4 MODELS OF COMBINED WAVE–CURRENT FLOWS

§4.4.1 THE MODEL OF BIJKER (1967)

Bijker (1967) was the first to present a model for a combined wave–current boundary layer flow. The model was developed before many theoretical insights into oscillatory boundary layers were available. Therefore, the model of Bijker (1967) relies very much on the concepts derived from steady flows.

Bijker (1967) assumed that the current velocity profile was not affected by the presence of waves, see Fig.4.4, and then based on Prandtl's mixing length hypothesis, Bijker (1967) derived the time–averaged resultant bed shear stress $\overline{\tau}(z,t)$ at $z = ez_o$ as

$$\frac{\overline{\tau}(z,t)}{\varrho \overline{U}^* \overline{U}^*}\Big|_{z=ez_o} = \left\{1 + 0.5\left\{0.16\, A\omega/\overline{U}^*\right\}^2\right\} \tag{4.35}$$

Eq.(4.35) implies that the time–averaged bed shear stress with the presence of waves is larger than that in a pure steady flow. For general combined wave–current flows, Eq.(4.35) was suggested to be

$$\frac{\overline{\tau}(z,t)}{\varrho \overline{U}^* \overline{U}^*}\Big|_{z=ez_o} = f\left\{A\omega/\overline{U}^*,\ \Phi\right\} \tag{4.36}$$

where Φ is an angle between the current and the direction of wave propagation.

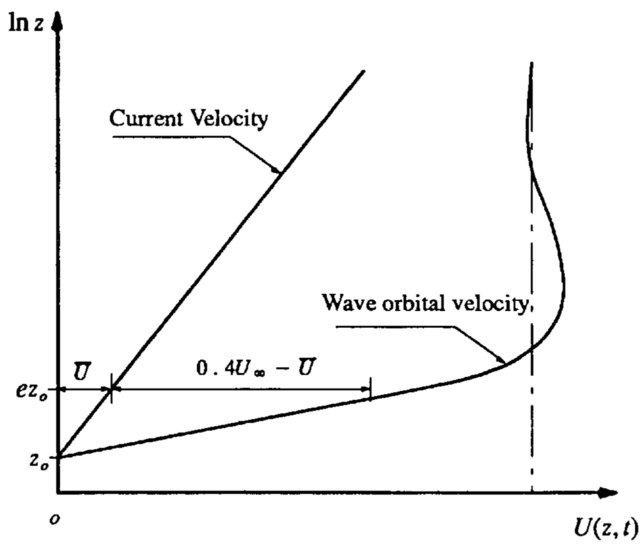

Fig.4.4 Assumptions of velocity profiles of currents and waves in a combined flow after Bijker (1967)

§4.4.2 THE MODEL OF LUNDGREN (1972)

Lundgren (1972) presented a detailed model to examine the influence of waves on the current profile. He divided the combined flow into the four regions as shown in Fig.4.5 and discussed qualitatively how the current eddy viscosity would be affected in each zone by the presence of waves.

It was assumed that in Z_1 zone the presence of waves had no influence on the current eddy viscosity while in Z_2 zone the presence of waves had a slight influence on the current eddy viscosity. Therefore, the current eddy viscosity $\varepsilon_{co,c}$ induced in a combined wave−current flow was suggested to be the same as that in a steady flow

$$\varepsilon_{co,c} = \varkappa \overline{U}^* z\left\{1 - \frac{z}{h}\right\} \tag{4.37}$$

but the current velocity was reduced by the presence of waves

$$\frac{\overline{U}(z)}{\overline{U}^*} = \frac{1}{\varkappa}\ln\frac{z}{z_1} = \frac{1}{\varkappa}\ln\frac{z}{z_o} - \frac{1}{\varkappa}\ln\frac{z_1}{z_o} \tag{4.38}$$

in comparison with that in a pure steady flow as shown in Fig.4.6. In Eq.(4.38), z_1 was described by an expression of the form

$$\frac{z_1}{z_o} = F\left\{\frac{A}{K_N}, \frac{A\omega}{\overline{U}^*}, \Phi\right\} \tag{4.39}$$

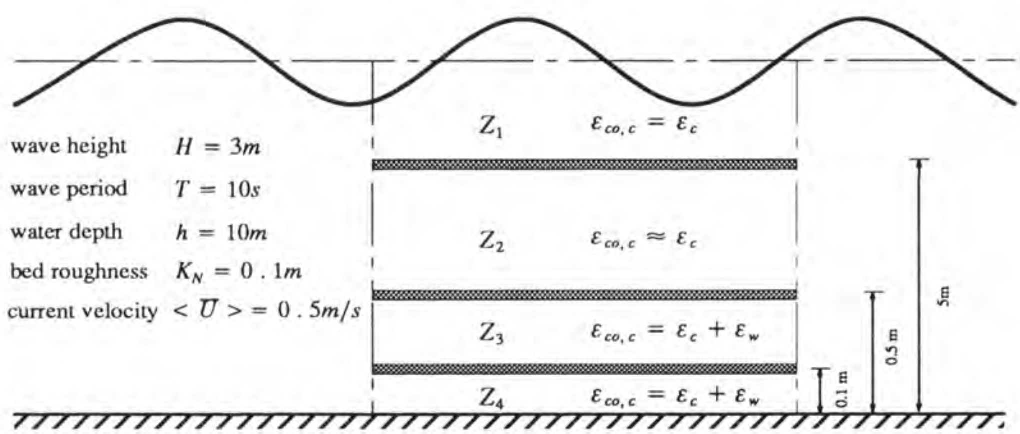

Fig.4.5 Influence of the presence of waves on the current eddy viscosity in a combined flow

In Z_3 and Z_4 zones, it was assumed that the current eddy viscosity was determined by the waves and currents together. The wave–produced eddy viscosity was of the same order of magnitude as the current–produced eddy viscosity. In the current–dominated flows, the Z_4 zone may vanish, and the Z_3 zone extends all ways to the bed. Lundgren (1972) suggested that the current eddy viscosity would be calculated by the means of the formula

$$\varepsilon_{co,c} = \varepsilon_c + \varepsilon_w \tag{4.40}$$

and then the current velocity in Z_3 and Z_4 zones could be derived from the equation

$$\overline{U}(z) = \int_{z_o}^{z} \frac{\overline{U}^*\overline{U}^*}{\varepsilon_c + \varepsilon_w} dz \tag{4.41}$$

where ε_c is the current eddy viscosity for the steady flow alone and ε_w the wave produced eddy viscosity for the wave motion alone.

§4.4.3 THE MODEL OF BAKKER & VAN DOORN (1978)

Based on the mixing length theory of Prandtl (1934) and the equation of motion Bakker & van Doorn (1978) presented a model to study the current velocity profile with the presence of waves. It was suggested that the current velocity profile consisted of two logarithmic parts with a transition zone between as shown in Fig.4.6.

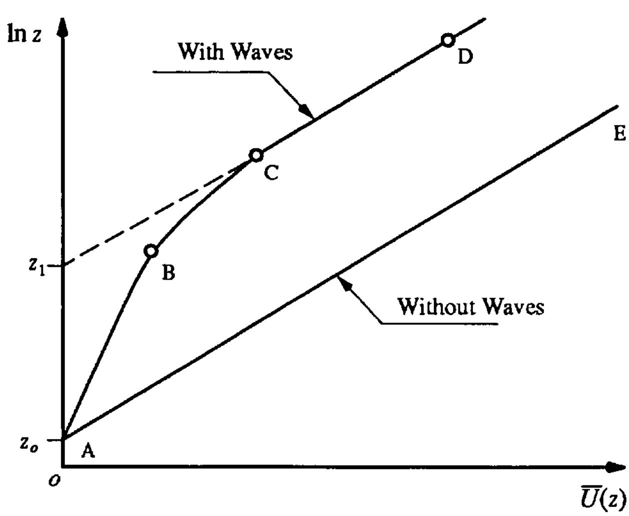

Fig.4.6 The influence of waves on the current profile after Bakker & van Doorn (1978)

$\overline{AB}$ $\quad \overline{U}(z) = \frac{\overline{p}_b}{\varkappa} \ln \frac{z}{z_o}$ (4.42)

$\hat{BC}$ $\quad \overline{U}(z) = \frac{\overline{p}_b}{\varkappa} \left\{ F(z^*) - F(z_o^*) \right\}$ (4.43)

$\overline{CD}$ $\quad \overline{U}(z) = \frac{\overline{U}^*}{\varkappa} \ln \frac{z}{z_1}$ (4.44)

In Eq.(4.43)

$$z^* = \frac{z}{\varkappa \tilde{p}_b T} \qquad z_o^* = \frac{z_o}{\varkappa \tilde{p}_b T}$$

where $\overline{p}_b$ is the time–averaged resultant shear stress velocity at the bed and $\tilde{p}_b$ is the amplitude of the periodic shear stress velocity at the bed. $\overline{p}_b$ and $\tilde{p}_b$ were determined numerically from the differential equation

$$\frac{\partial p}{\partial t} = \varkappa z \frac{\partial^2 \{ p \; |p| \}}{\partial z^2} \tag{4.45}$$

Fig.4.7 schematically shows the variation of the time–averaged resultant shear stress $\overline{\tau}(z,t)$ calculated by van Kesteren & Bakker (1986).

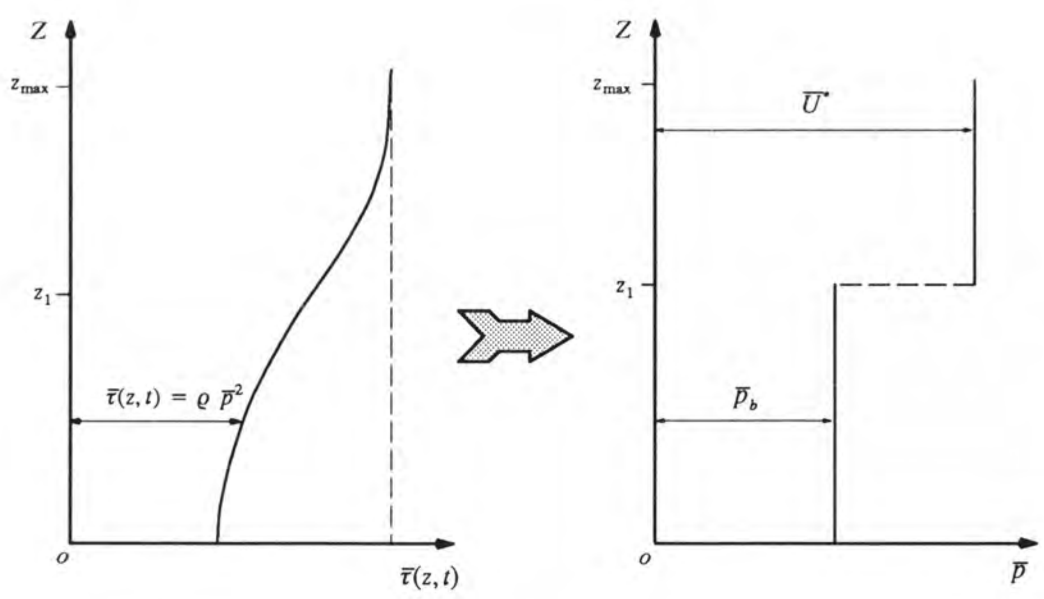

Fig.4.7 Variation of computed $\overline{\tau}(z,t)$ schematically after Kesteren & Bakker (1986)

§4.4.4 THE MODEL OF GRANT & MADSEN (1979)

Grant & Madsen (1979) presented an analytical model to study the velocity profiles of waves and currents in the combined flow based on the concept of eddy viscosity. The model of Grant & Madsen (1979) was developed before detailed measurements of combined flows were available. The model was developed on the basis of the assumed distributions of the current eddy viscosity ε_c and the wave eddy viscosity ε_w in the combined wave–current flow. The wave–induced orbital velocity $\tilde{U}(z,t)$ was obtained by solving the equation of wave motion

$$\frac{\partial \tilde{U}(z,t)}{\partial t} = \frac{\partial U_\infty(t)}{\partial t} + \frac{\partial}{\partial z}\left\{\varepsilon_w \frac{\partial \tilde{U}(z,t)}{\partial z}\right\} \tag{4.46}$$

and the current velocity $\overline{U}(z)$ was then obtained from the equation

$$\overline{U}(z) = \int \frac{\overline{U^*}\,\overline{U^*}}{\varepsilon_c} dz \tag{4.47}$$

§4.4.4.1 The Eddy Viscosity Model

Grant & Madsen (1979) assumed that the distribution of eddy viscosity for the steady component of the combined flow was given by

$$\varepsilon_c(z) = \varkappa \hat{U}^*_{cw}\, z \qquad z_o \leq z \leq \delta \tag{4.48}$$

$$\varepsilon_c(z) = \varkappa \overline{U^*}\, z \qquad \delta \leq z < h \tag{4.49}$$

and the distribution of eddy viscosity for the wave motion in the combined flow was

$$\varepsilon_w(z) = \varkappa \hat{U}^*_{cw}\, z \qquad z_o \leq z \tag{4.50}$$

where $\hat{U}^*_{cw}$ is the friction velocity associated with waves and currents and δ was defined as

$$\delta = \frac{2\varkappa \hat{U}^*_{cw}}{\omega} \tag{4.51}$$

The vertical distributions of eddy viscosity for waves and currents according to Eqs.(4.48), (4.49) and (4.50) are shown in Fig.4.8.

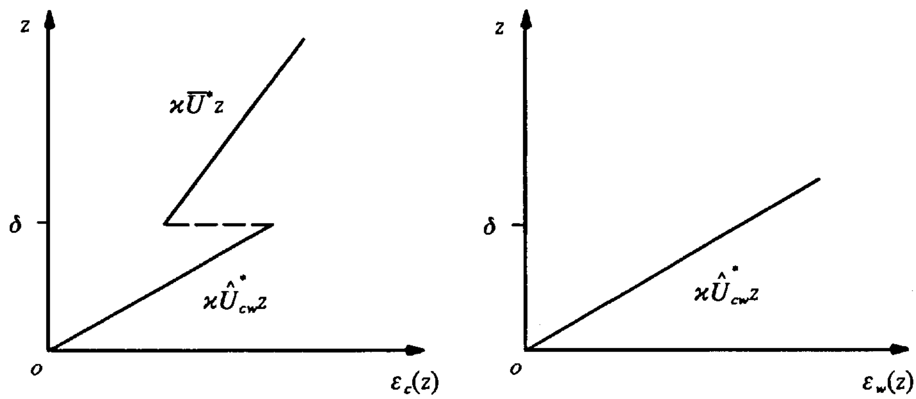

Fig.4.8 Variations of $\varepsilon_c(z)$ and $\varepsilon_w(z)$ in a combined wave–current flow after Grant & Madsen (1979)

§4.4.4.2 The Bed Shear Stresses

In order to establish the relationship between the shear stress and the velocity field, the instantaneous bed shear stress was defined as

$$\frac{\tau_b(t)}{\varrho} = \frac{1}{2} f_{cw}\left\{ U^2_{\infty}(t) + 2U_{\infty}(t)\overline{U}(a)\cos\Phi + \overline{U}^2(a) \right\} \tag{4.52}$$

where f_{cw} is a friction factor associated with the waves and currents, $\overline{U}(a)$ is an undetermined reference current velocity at $z = a$ from the bed, and Φ an angle between the current and the direction of wave propagation. The time–averaged bed shear stress was derived from Eq.(4.52) as

$$\frac{\overline{\tau}_b(t)}{\varrho} = \frac{1}{2} f_{cw} \frac{1}{2\pi} \int_0^{2\pi} \tau_b(t)\, dt \quad \text{and} \quad \frac{\overline{\tau}_b(t)}{\varrho} = \overline{U}^*\overline{U}^* \tag{4.53}$$

The maximum bed shear stress due to the combined waves and currents was found from Eq.(4.52) as

$$\frac{\hat{\tau}_b}{\varrho} = \frac{1}{2} f_{cw} \left\{ (A\omega)^2 + 2A\omega\ \overline{U}(a) \cos \Phi + \overline{U}^2(a) \right\} \quad \text{and} \quad \frac{\hat{\tau}_b}{\varrho} = \hat{U}^*_{cw} \hat{U}^*_{cw} \tag{4.54}$$

in which $A\omega$ is the amplitude of the free stream velocity $U_\infty(t)$.

§4.4.4.3 The Velocity Distributions

By substituting the current eddy viscosity given in Eqs.(4.48) and (4.49) into Eq.(4.47), the current velocity profile was derived as

$$\frac{\overline{U}(z)}{\overline{U}^*} = \frac{1}{\varkappa} \left\{ \frac{\overline{U}^*}{\hat{U}^*_{cw}} \right\} \ln \frac{z}{z_o} \qquad z_o \le z \le \delta \tag{4.55}$$

$$\frac{\overline{U}(z)}{\overline{U}^*} = \frac{1}{\varkappa} \ln \frac{z}{z_1} \qquad \delta \le z < h \tag{4.56}$$

in which

$$\frac{z_1}{z_o} = \left\{ \frac{\delta}{z_o} \right\}^{1 - \frac{\overline{U}^*}{\hat{U}^*_{cw}}} \tag{4.57}$$

In a similar way, by substituting the wave eddy viscosity given in Eq.(4.50) into Eq.(4.46) the wave–induced orbital velocity was given by

$$\tilde{U}(z,t) = \left\{ 1 - \frac{Ker\ 2\xi^{1/2} + i\ Kei\ 2\xi^{1/2}}{Ker\ 2\xi_o^{1/2} + i\ Kei\ 2\xi_o^{1/2}} \right\} U_\infty(t) \tag{4.58}$$

in which $Ker\xi$ and $Kei\xi$ are Kelvin functions of zeroth order and $\xi = \{2z\}/\delta$. In Fig.4.9, the model of Grant & Madsen (1979) is compared with van Doorn (1981) experimental data V20RA and with the model of You *et al.* (1991a). It can be seen that the model of Grant & Madsen (1979) can not accurately predict the wave–induced velocity in the boundary layer in comparison with the model of You *et al.* (1991a).

§4.4.4.4 Summary

The model of Grant & Madsen (1979) has some weaknesses as followings :

(1) Because of a somewhat awkward definition of friction factor f_{cw} in Eq.(4.52), the model has to introduce a reference velocity $U_c(a)$ at an unknown level $z = a$, which greatly increases the complexity of the model.

(2) The thickness δ of the boundary interaction zone was estimated too thick as was pointed out by Christoffersen & Jonsson (1985) and as indicated in Fig.4.9.

(3) The assumption that $\varepsilon_w \propto z$ in Eq.(4.50) is only valid for the immediate vicinity of the bed, not throughout the boundary layer, see Figs.2.26 to 2.31 in Chapter2.

(4) It may not be correct to assume that the same eddy viscosity is felt by the waves and currents in the boundary interaction zone. The reason for this was explained partly by You *et al.* (1991a) and will be explained quantitatively in Section §4.5.4.

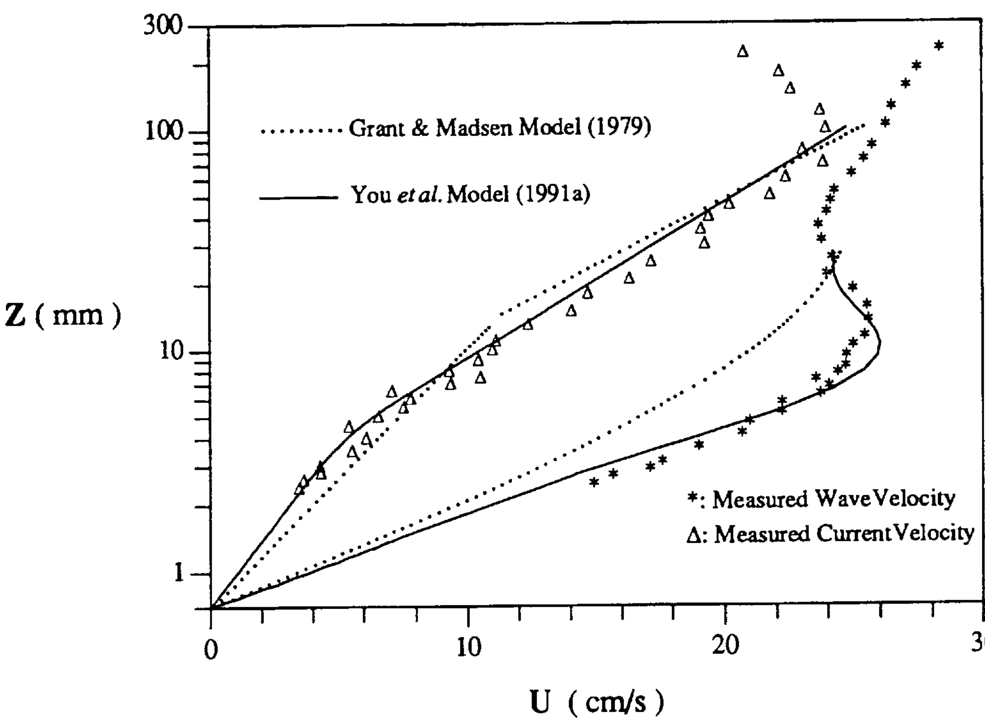

Fig.4.9 Comparison of the model of Grant & Madsen (1979) with experimental data V20RA

§4.4.5 THE MODEL OF CHRISTOFFERSEN & JONSSON (1985)

Christoffersen & Jonsson (1985) modified and in some respects refined the model of Grant & Madsen (1979). The following aspects are different from those of Grant & Madsen's (1979) model.

§4.4.5.1 The Eddy Viscosity Model

Christoffersen & Jonsson (1985) suggested that the distributions of eddy viscosity were determined by the relative roughness K_N/A of the boundary layer.

For large relative roughness $0.02 < K_N/A < 0.78$ the current eddy viscosity could be assumed as

$$\varepsilon_c(z) = 0.0747\ K_N\ \hat{U}^*_{cw} \qquad z_o \leq z \leq \delta \tag{4.59}$$

$$\varepsilon_c(z) = \varkappa z\left\{1 - \frac{z}{h}\right\}\overline{U}^* \qquad \delta \leq z < h \tag{4.60}$$

as indicated in Fig.4.10, while the wave eddy viscosity was assumed as

$$\varepsilon_w(z) = 0.0747\ K_N\ \hat{U}^*_{cw} \qquad z_o < z < \delta_w \tag{4.61}$$

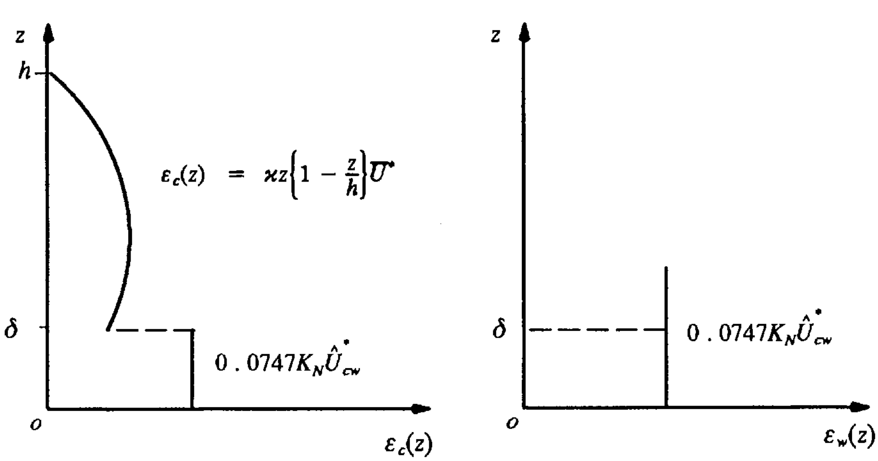

Fig.4.10 Eddy viscosity distributions of ε_c and ε_w in a combined flow with a large relative roughness

For small relative roughness $K_N/A < 0.02$, Christoffersen & Jonsson assumed that the current eddy viscosity was given by

$$\varepsilon_c(z) = \varkappa \, z \, \hat{U}^*_{cw} \qquad z_o \le z \le \delta \tag{4.62}$$

$$\varepsilon_c(z) = \varkappa z \left\{ 1 - \frac{z}{h} \right\} \overline{U}^* \qquad \delta \le z < h \tag{4.63}$$

while the wave eddy viscosity was

$$\varepsilon_w(z) = \varkappa z \hat{U}^*_{cw} \qquad z_o \le z < \delta_w \tag{4.64}$$

in which

$$\delta = \frac{0.367 \varkappa \hat{U}^*_{cw}}{\omega}$$

The assumed eddy viscosity distributions of ε_c and ε_w for a small relative roughness is very similar to that of Grant & Madsen (1979), see Fig.4.11.

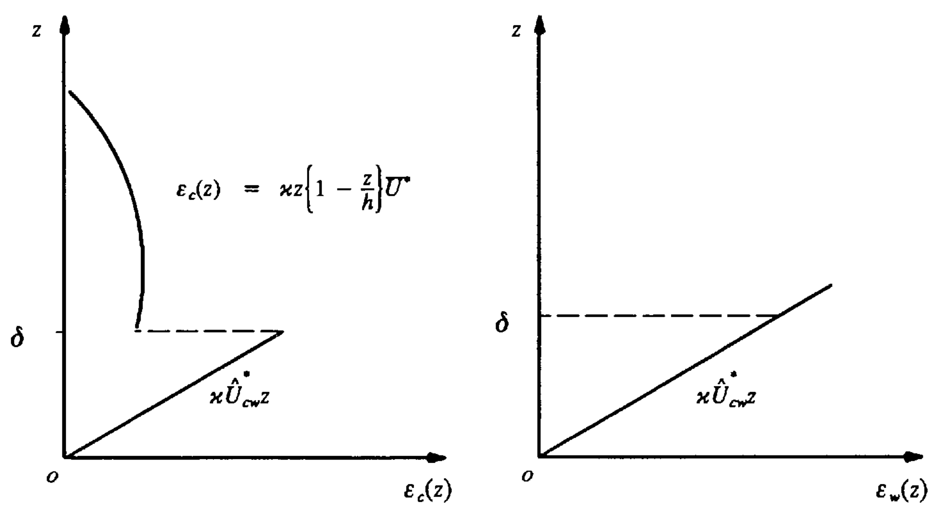

Fig.4.11 Eddy viscosity distributions of ε_c and ε_w in a combined flow with a small relative roughness

§4.4.5.2 The Bed Shear Stresses

In the model of Christoffersen & Jonsson (1985), the shear stresses due to waves and currents at the bed were given by, respectively

$$\frac{\overline{\tau}_{cb}}{\varrho} = \frac{1}{2} f_c < \overline{U} >< \overline{U} > \quad \text{and} \quad \frac{\overline{\tau}_b}{\varrho} = \overline{U}^* \overline{U}^* \tag{4.65}$$

$$\frac{\hat{\tau}_{wb}}{\varrho} = \frac{1}{2} f_w \{A\omega\}^2 \quad \text{and} \quad \frac{\hat{\tau}_{wb}}{\varrho} = \hat{U}^* \hat{U}^* \tag{4.66}$$

The total maximum bed shear stress was given by

$$\vec{\hat{\tau}}_b = \vec{\overline{\tau}}_{cb} + \vec{\hat{\tau}}_{wb} \quad \text{and} \quad \frac{\hat{\tau}_b}{\varrho} = \hat{U}^*_{cw} \hat{U}^*_{cw} \tag{4.67}$$

The definitions of the friction factors f_c and f_w in Eqs.(4.65) and (4.66) avoid the need to introduce an unknown reference velocity $\overline{U}(a)$ as used by Grant & Madsen (1979).

§4.4.5.3 The Zone of the Boundary Interaction Layer

Table.4.2 shows the effect of different values of δ on f_w, f_c, $\overline{U}^*$ and K_1. All the calculations are based on the model of Grant & Madsen (1979), and wave height $H = 2.0m$, wave period $T = 8.0s$, water depth $h = 10.0m$, the bed roughness $K_N = 0.032m$ and the depth−averaged current mean velocity $< \overline{U} > = 0.5m/s$.

$\delta = n\, \varkappa \hat{U}^*_{cw}/\omega$	f_w	f_c	$\overline{U}^*$ (cm/s)	K_1 (cm)	K_1/K_N
n=0.367	0.0343	0.00868	3.29	25.5	8.0
n = 2.00	0.0350	0.01230	3.90	67.2	21.0
$\frac{\lvert x_2 - x_1 \rvert}{x_2} \times 100\%$	2%	30%	16%	62%	62%

Table.4.2 The influence of different values of δ on f_w, f_c, $\overline{U}^*$ and K_1

Table.4.2 shows that although the choice of n has a slight influence on the wave friction factor f_w, the current friction factor f_c calculated with $n = 0.367$, which was chosen by Christoffersen & Jonsson (1985) is about 30% smaller than that estimated with $n = 2$, which was adopted by Grant & Madsen (1979), and the apparent roughness K_1 calculated with $n = 0.367$ is smaller than that calculated with $n = 2$ by a factor 3. This implies that the current profile is significantly affected by the vertical length scaling parameter δ.

§4.4.5.4 Summary

Christoffersen & Jonsson (1985) improved the model of Grant & Madsen (1979) in some aspects, but there are still some weaknesses

(1) The assumption that $\varepsilon_w \propto z$ for small relative roughness is only valid in the immediate vicinity of the bed, not throughout the boundary layer as shown Fig.2.32 to Fig.2.34 in Chapter 2.

(2) It may be not correct to assume the same eddy viscosity felt by waves and currents in the boundary layer. This point was examined by You *et al.* (1991a) and will be quantitatively studied in Section §4.5.4.

§4.4.6 THE MODEL OF COFFEY & NIELSEN (1986)

Coffey & Nielsen (1986) studied the reasons behind the reduction of the current velocity in the presence of waves. They suggested that this was due to the increase of current eddy viscosity near the bed, see Fig.4.12. Coffey & Nielsen suggested that the current eddy viscosity could be assumed as

$$\varepsilon_c(z) = \varkappa \overline{U}^* L \qquad z < L \tag{4.68}$$

$$\varepsilon_c(z) = \varkappa \overline{U}^* z \qquad z > L \tag{4.69}$$

in which L is a level above which the presence of waves has no effect on the current eddy viscosity, see Fig.4.12. Therefore, it was suggested as a first simple approximation that L/z_o was a function of the friction velocities only

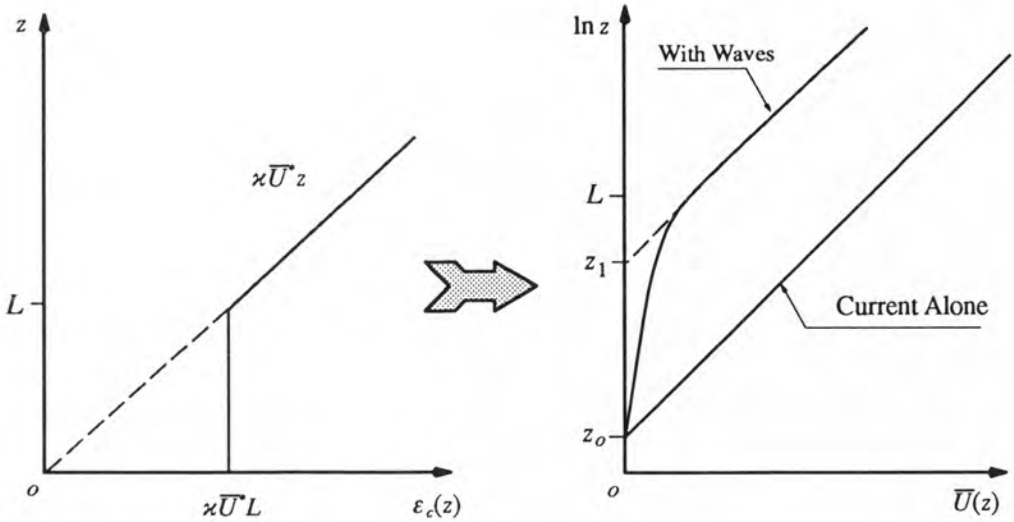

Fig.4.12 The influence of waves on the current velocity profile after Coffey & Nielsen (1986)

$$\frac{L}{z_o} = F\left\{\frac{\hat{U}_w^*}{\overline{U}^*}\right\} \tag{4.70}$$

Based on experimental data from van Doorn (1981) and Kemp & Simons (1982, 1983), $F(\hat{U}_w^*/\overline{U}^*)$ was suggested as

$$F = 1 + \frac{1}{6}\left\{\hat{U}_w^*/\overline{U}^*\right\}^3 \tag{4.71}$$

By assuming a constant shear stress near the bed, the current velocity was derived as

$$\overline{U}(z) = \frac{\overline{U}^*}{\varkappa F}\left\{\frac{z}{z_o} - 1\right\} \qquad z \le L \tag{4.72}$$

$$\overline{U}(z) = \frac{\overline{U}^*}{\varkappa} \ln\frac{z}{z_1} \qquad z \ge L \tag{4.73}$$

By equalling Eqs.(4.72) and (4.73) at $z = L$, z_1 was approximately simplified as

$$\frac{z_1}{z_o} = 1 + 0.06\left\{\hat{U}_w^*/\overline{U}^*\right\}^3 \tag{4.74}$$

The comparison of the model of Coffey & Nielsen (1986) with experimental data is shown in Fig.4.13. It is found that the model of Coffey & Nielsen (1986) can not generally predict z_1 very well, especially when $\hat{U}_w^*/\overline{U}^* > 5$.

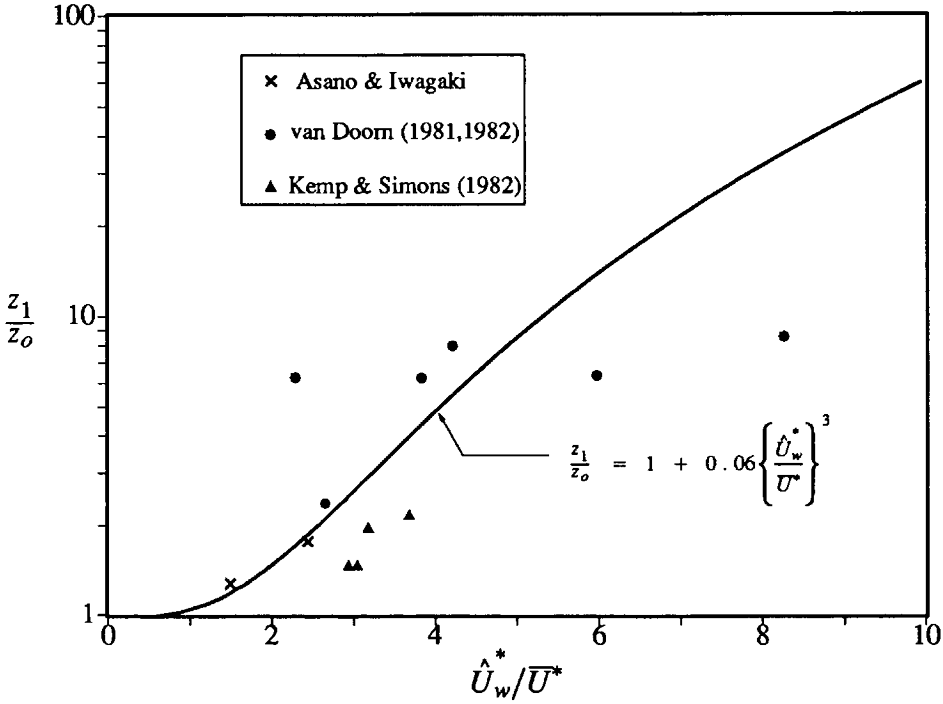

Fig.4.13 Comparison of the model of Coffey & Nielsen (1986) with experimental data

§4.4.7 THE MODEL OF MYRHAUG & SLAATTELID (1989)

Myrhaug & Slaattelid (1989) presented an analytical model describing the boundary interaction between waves and currents. Their approach was similar to that of Christoffersen & Jonsson (1985) except for the assumed distributions of eddy viscosity. In the model of Myrhaug & Slaattelid (1989), the current eddy viscosity was assumed as

$$\varepsilon_c(z) = \frac{1}{2}\varkappa\, \hat{U}_{cw}^*\delta_1 \left\{1 - \left\{z/\delta_1 - 1\right\}^2\right\} \qquad z_o < z < \delta_1 \tag{4.75}$$

$$\varepsilon_c(z) = \frac{1}{2}\varkappa\hat{U}_{cw}^*\delta_1 \qquad \delta_1 < z \leq \delta \tag{4.76}$$

$$\varepsilon_c(z) = \varkappa\overline{U}^* z \qquad \delta < z < h \tag{4.77}$$

which are shown schematically in Fig.4.14.

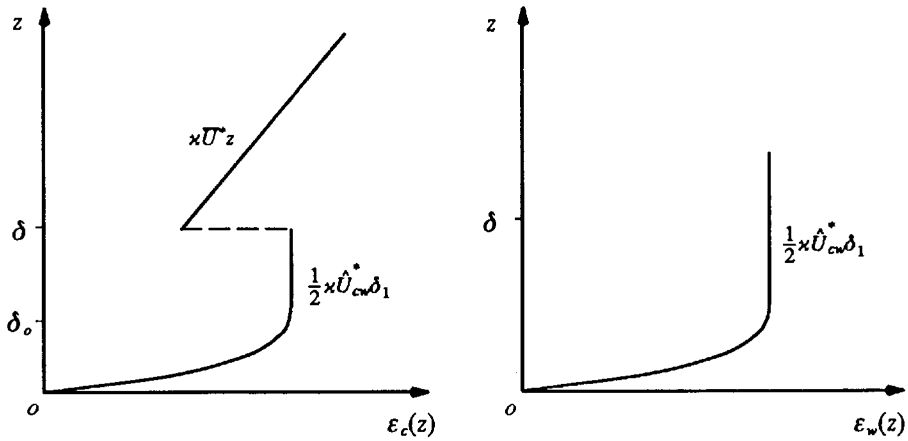

Fig.4.14 Eddy viscosity distributions of ε_c and ε_w after Myrhaug & Slaattelid (1989)

The wave eddy viscosity was given by

$$\varepsilon_w(z) = \frac{1}{2}\varkappa \; \hat{U}^*_{cw}\delta_1 \left\{1 - \{z/\delta_1 - 1\}^2\right\} \qquad z_o < z < \delta_1 \tag{4.78}$$

$$\varepsilon_w(z) = \frac{1}{2}\varkappa \hat{U}^*_{cw}\delta_1 \qquad z \geq \delta_1 \tag{4.79}$$

in which δ_1 was evaluated by Jonsson's (1980) formula

$$\delta_1 = 0.072 \; A\{K_N/A\}^{1/4} \tag{4.80}$$

and δ is the thickness of the boundary interaction zone as defined by Myrhaug & Slaattelid to be

$$\delta = \frac{\varkappa \hat{U}^*_{cw}}{\omega} \tag{4.81}$$

Equation (4.81) was used by Grant & Madsen (1979) except for a factor 2 that appears in their expression. Actually, the model of Myrhaug & Slaattelid (1989) is an extension of the model of Myrhaug (1982). The comparison of the model of Myrhaug & Slaattelid (1989) with experimental data was given in Fig.2.15, and it was shown that Myrhaug & Slaattelid (1989) model overestimates the boundary layer thickness.

§4.4.8 THE MODEL OF SLEATH (1991)

Sleath (1991) developed an analytical model which is in some respects similar to the model of Grant & Madsen (1979), but different with respect to the eddy viscosity distribution. It was assumed that the eddy viscosity induced in the combined wave–current flow could be estimated by means of the formula

$$\varepsilon \;=\; \varepsilon_c \;+\; \varepsilon_w \tag{4.82}$$

in which ε_c is the eddy viscosity for the steady current alone, defined as

$$\varepsilon_c \;=\; \varkappa \overline{U}^* z \tag{4.83}$$

and ε_w is the eddy viscosity for the wave motion alone, and was analyzed to be

$$\varepsilon_w \;=\; 0.0025\, A^2 \omega \sqrt{K_N/A} \tag{4.84}$$

Hence, the current velocity was derived from the equation

$$\overline{U}(z) \;=\; \int_{z_o}^{z} \frac{\overline{U}^* \overline{U}^*}{\varepsilon} dz \tag{4.85}$$

and the wave–induced orbital velocity in the boundary layer was obtained by solving the equation of motion

$$\frac{\partial \tilde{U}(z,t)}{\partial t} \;=\; \frac{\partial U_\infty(t)}{\partial t} \;+\; \frac{\partial}{\partial z}\left\{\varepsilon \frac{\partial \tilde{U}(z,t)}{\partial z}\right\} \tag{4.86}$$

In Eqs.(4.85) and (4.86), Sleath used the same eddy viscosity for the steady flow and the wave motion, see Fig.4.15.

§4.4.8.1 Summary

After reviewing the model of Sleath (1991), we find some weakness in the model :

(1) A constant eddy viscosity suggested by Eq.(4.84) may be valid only for boundary layers with very large relative roughness as Sleath acknowledged. Fig.2.32 to Fig.2.34 in Chapter 2 have shown that the eddy viscosity for the wave motion alone is not constant with elevation.

(2) The eddy viscosity for the steady flow should be different from that for the wave motion as You *et al.* (1991a) qualitatively discussed, and this will be studied quantitatively in Section §4.5.4.

(3) The eddy viscosity for the steady flow outside the boundary interaction zone may be affected little by the wave motion and the eddy viscosity for the wave motion may be dominated by the wave motion itself as experimental data shows in Section §4.5.4.

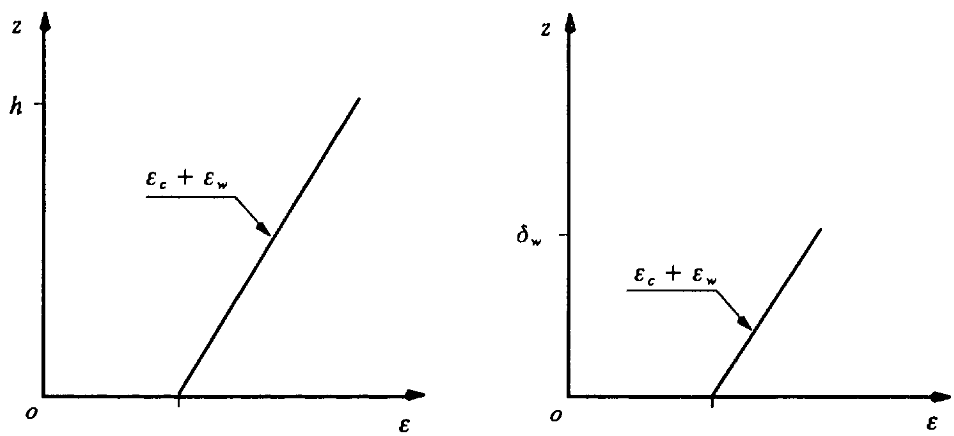

Fig.4.15 (A) Eddy viscosity for the steady flow (B) Eddy viscosity for the wave motion

§4.4.9 THE MODEL OF YOU *ET AL.* (1991a)

You *et al.* (1991a) qualitatively discussed the eddy viscosities of ε_c and ε_w in a combined wave−current flow based on the Navier−Stokes equation. The eddy viscosity for the steady component of combined wave−current flow was derived as

$$\bar{\varepsilon} = \nu + \frac{-\,\overline{U}\;\overline{W} - \overline{\tilde{U}\tilde{W}} - \overline{U'W'}}{\partial\overline{U}/\partial z} \tag{4.87}$$

and the eddy viscosity for the oscillatory component

$$\tilde{\varepsilon} = \nu + \frac{-\,\tilde{U}\overline{W} - \overline{U}\tilde{W} - \widetilde{\tilde{U}\tilde{W}} - \widetilde{U'W'}}{\partial\tilde{U}/\partial z} \tag{4.88}$$

Based on Eqs.(4.87) and (4.88), You *et al.* (1991a) concluded that the current eddy viscosity should be different from the wave eddy viscosity.

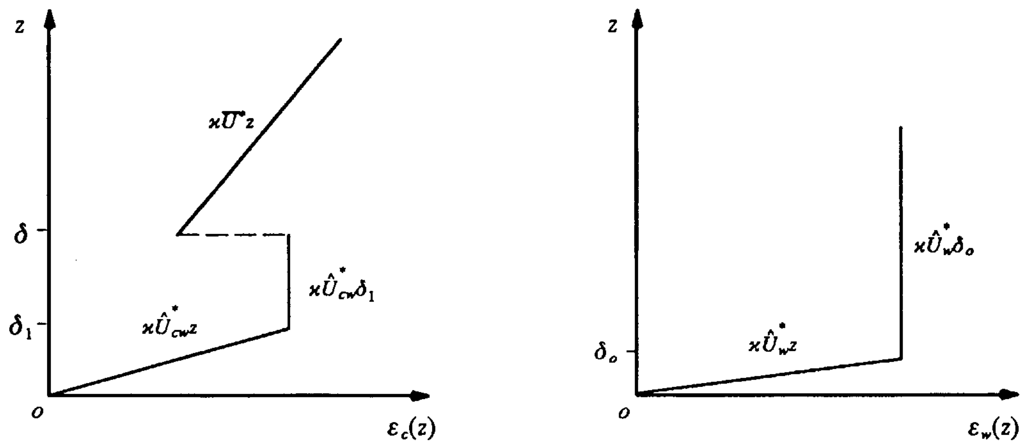

Fig.4.16 Eddy viscosity distributions of $\varepsilon_c(z)$ and $\varepsilon_w(z)$ after You *et al.* (1991a)

In the model of You *et al.* (1991a) [see Fig.4.16], the current eddy viscosity was assumed to have the following form

$$\varepsilon_c(z) = \varkappa \hat{U}^*_{cw} z \qquad z_o \le z \le \delta_1 \tag{4.89}$$

$$\varepsilon_c(z) = \varkappa \hat{U}^*_{cw} \delta_1 \qquad \delta_1 \le z \le \delta \tag{4.90}$$

$$\varepsilon_c(z) = \varkappa \overline{U}^* z \qquad \delta \le z < h \tag{4.91}$$

and the wave eddy viscosity was assumed to be dominated by the wave motion only so that

$$\varepsilon_w(z) = \varkappa \hat{U}^*_w z \qquad z_o \le z \le \delta_o \tag{4.92}$$

$$\varepsilon_w(z) = \varkappa \hat{U}^*_w \delta_o \qquad \delta_o \le z < \delta_w \tag{4.93}$$

in which δ_w, δ_1 and δ_o are given respectively as

$$\delta_w = \frac{4\varkappa \hat{U}^*_w}{\omega} \qquad \delta_1 = \frac{0.5\varkappa \hat{U}^*_w}{\omega} \qquad \delta_o = 0.5\delta_1 \tag{4.94}$$

Velocity profiles predicted by this model are compared with those from the model of Grant & Madsen (1979) in Fig.4.17.

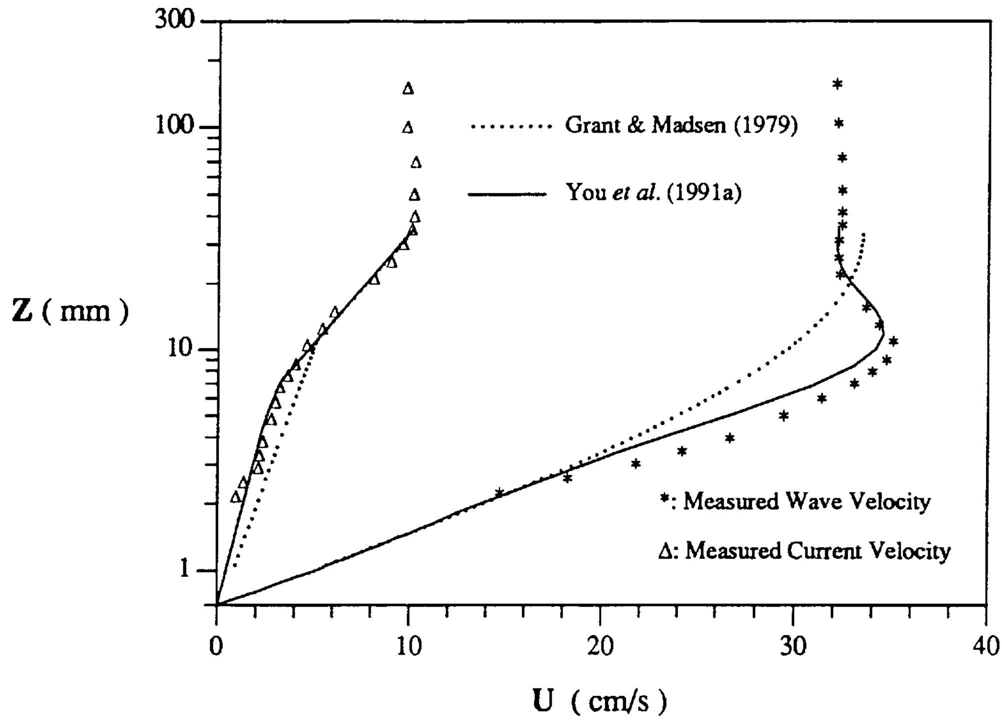

Fig.4.17 The prediction of You *et al.* (1991a) model on the experimental data S10RAL

§4.4.9.1 Summary

In comparison with the previous eddy viscosity models [Grant & Madsen (1979), Christoffersen & Jonsson (1985), Myrhaug & Slaattelid (1989) and Sleath (1991)], the model of You *et al.* (1991a) made following improvements on the former models.

(1) It was pointed out from Eqs.(4.87) and (4.88) that the eddy viscosities for the steady flow and for the wave motion should be different.

(2) The assumed distribution of ε_w [see Eqs.(4.92) and (4.93)] made it much simpler to calculate the velocities and bed shear stresses. In Section §4.5.3, the experimental data will support this assumption.

§4.5 DEVELOPMENT OF AN ANALYTICAL MODEL

§4.5.1 INTRODUCTION

In this section, we are going to quantitatively evaluate the eddy viscosities for the steady component and for the oscillatory component of combined wave−current flows from experimental data. Then, on the basis of the calculated eddy viscosity data, a new eddy viscosity model is developed. Finally, the new model will be compared with experimental data.

§4.5.2 THE EDDY VISCOSITY FOR THE STEADY FLOW

§4.5.2.1 Calculation of $\varepsilon_c(z)$ from Measurements

In analogy with the eddy viscosity definition for a pure steady flow, the eddy viscosity for the steady component of a combined wave−current flow is defined as

$$\frac{\overline{\tau}(z)}{\varrho} = \varepsilon_c(z)\frac{\partial \overline{U}(z)}{\partial z} \tag{4.95}$$

In Eq.(4.95), the steady component of a combined wave−current flow can be described by the equation

$$\frac{\partial \overline{\tau}(z)}{\partial z} = \frac{\partial \overline{P}}{\partial x} \tag{4.17}$$

If $\partial \overline{P}/\partial x$ is assumed to be constant like in a pure steady flow, the shear stress in Eq.(4.17) can be derived as

$$\overline{\tau}(z) = \overline{\tau}_b\left\{1 - \frac{z}{h}\right\} = \varrho \overline{U^*}^2\left\{1 - \frac{z}{h}\right\} \tag{4.96}$$

in which $\overline{U^*}$ can be determined from the velocity profile plotted in semi−log paper as shown in Fig.4.18.

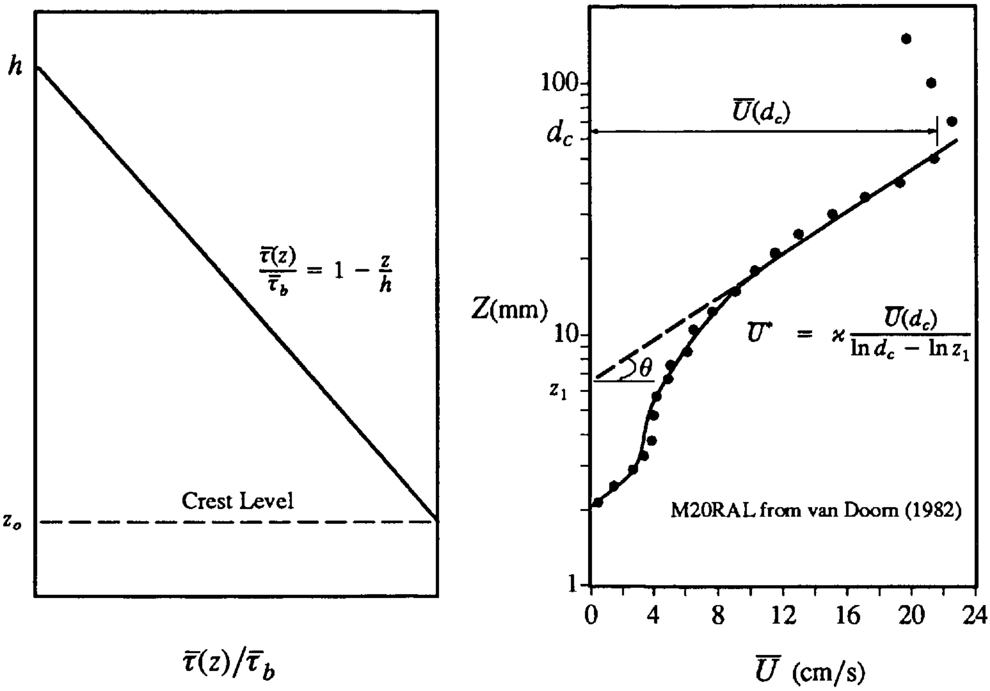

Fig.4.18 Estimation of the bed shear stress from the current velocity profile in a combined flow

Therefore,

$$\left\{\overline{\tau}_b/\varrho\right\}^{\frac{1}{2}} = \overline{U}^* = \frac{\varkappa\ \overline{U}(d_c)}{\ln d_c - \ln z_1} \tag{4.97}$$

On the other hand, the velocity gradient can be approximated by

$$\frac{\partial \overline{U}(z_i)}{\partial z} \approx \frac{\Delta \overline{U}}{\Delta z} = \frac{\overline{U}(z_{i+1}) - \overline{U}(z_{i-1})}{z_{i+1} - z_{i-1}} \tag{4.98}$$

Based on Eq.(4.95) the eddy viscosity $\varepsilon_c(z)$ for the steady flow in the combined wave–current flow can be estimated as

$$\varepsilon_c(z_i) = \frac{\left\{\overline{U}^{*2}\left\{1 - \frac{z_i}{h}\right\}\right\}}{\left\{\frac{\overline{U}(z_{i+1}) - \overline{U}(z_{i-1})}{z_{i+1} - z_{i-1}}\right\}} \tag{4.99}$$

Fig.4.19 to Fig.4.24 show the variations of $\varepsilon_c(z)$ calculated from smoothed velocity data via Eq.(4.99).

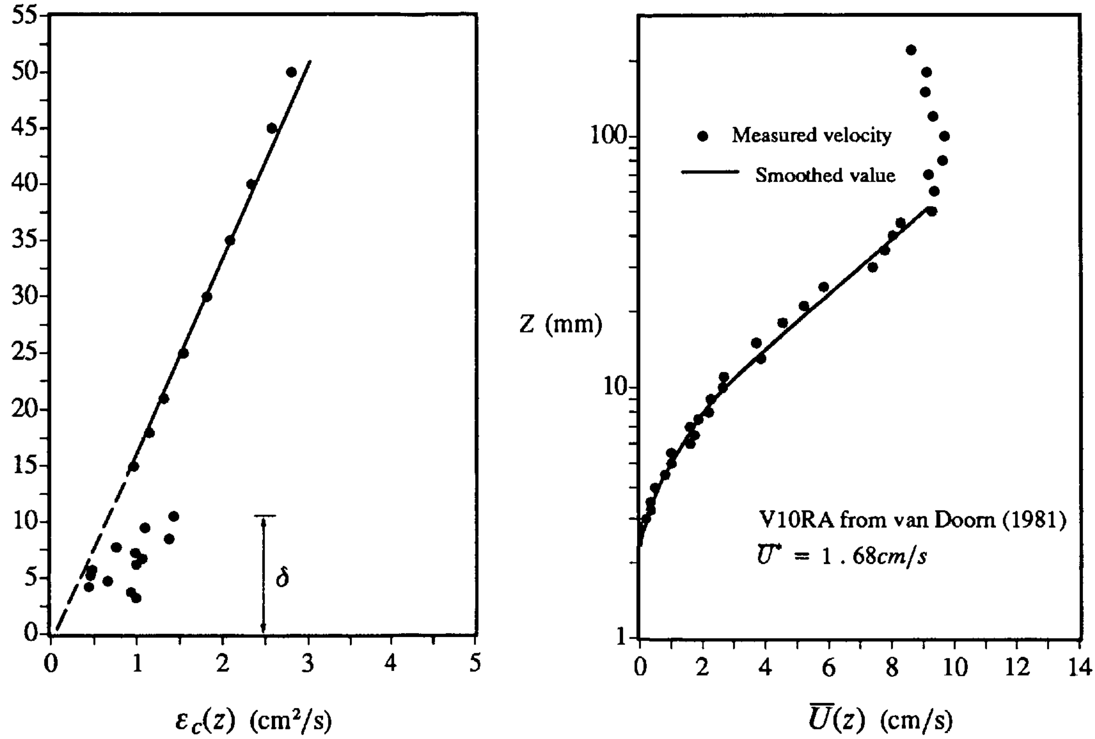

Fig.4.19 The current eddy viscosity calculated from van Doorn (1981) V10RA via Eq.(4.99)

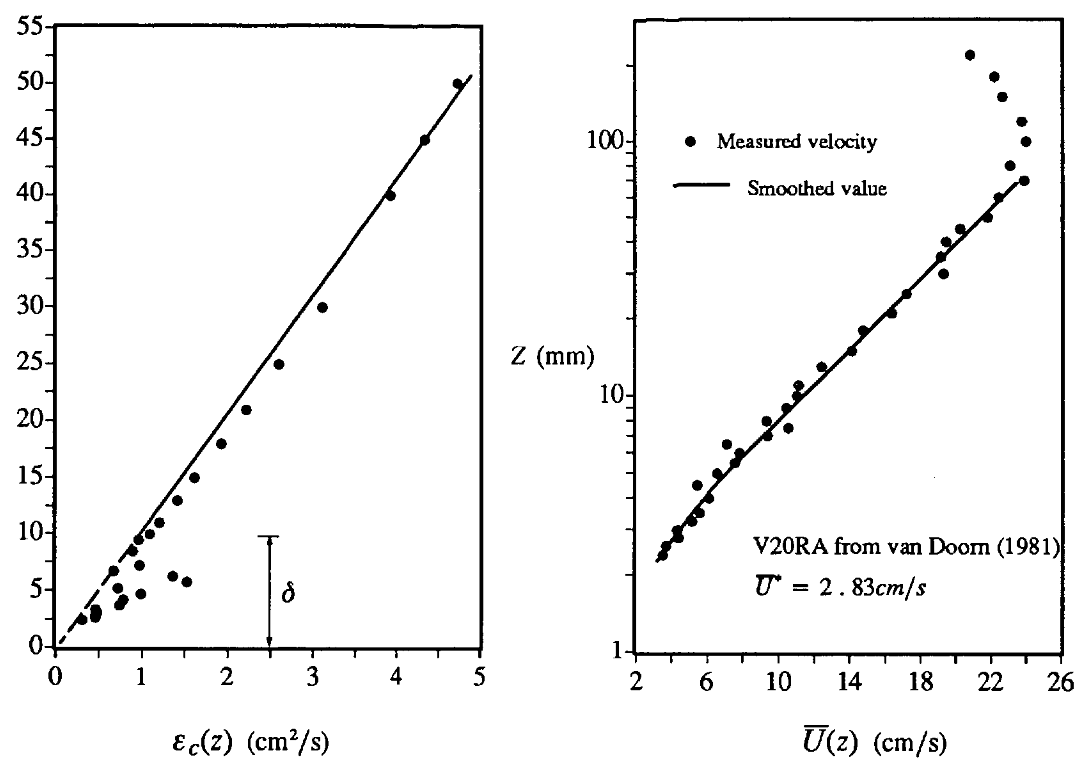

Fig.4.20 The current eddy viscosity calculated from van Doorn (1981) V20RA via Eq.(4.99)

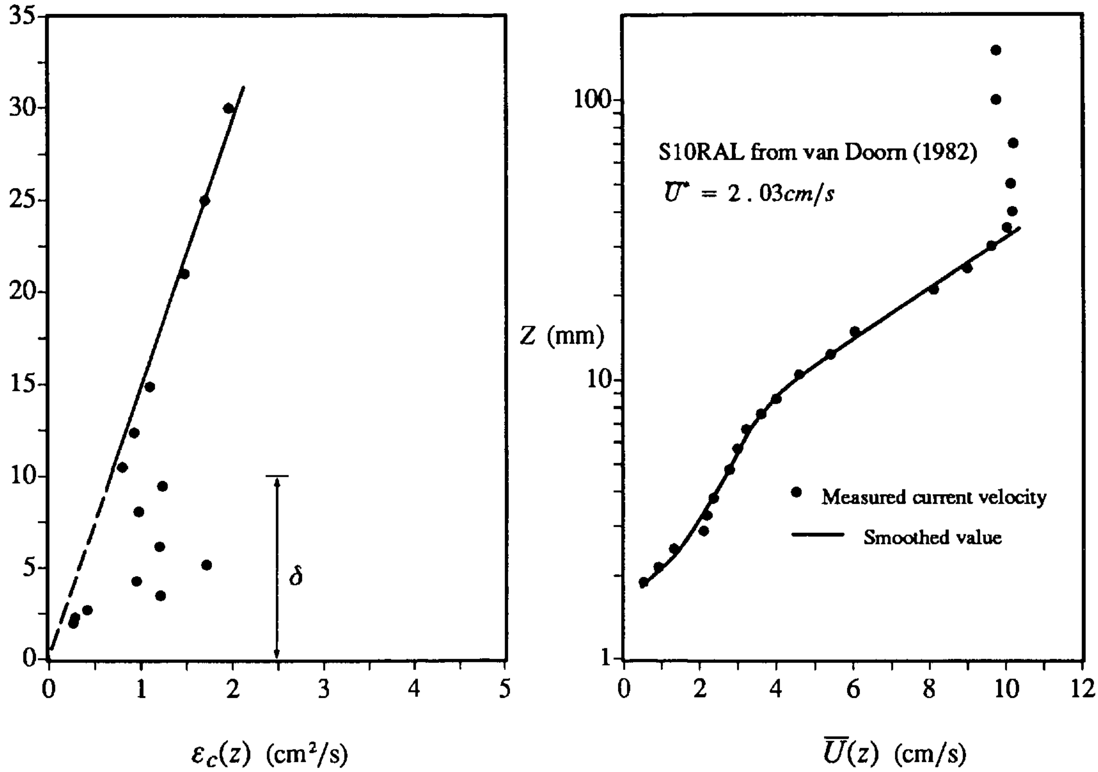

Fig.4.21 The current eddy viscosity calculated from van Doorn (1982) S10RAL via Eq.(4.99)

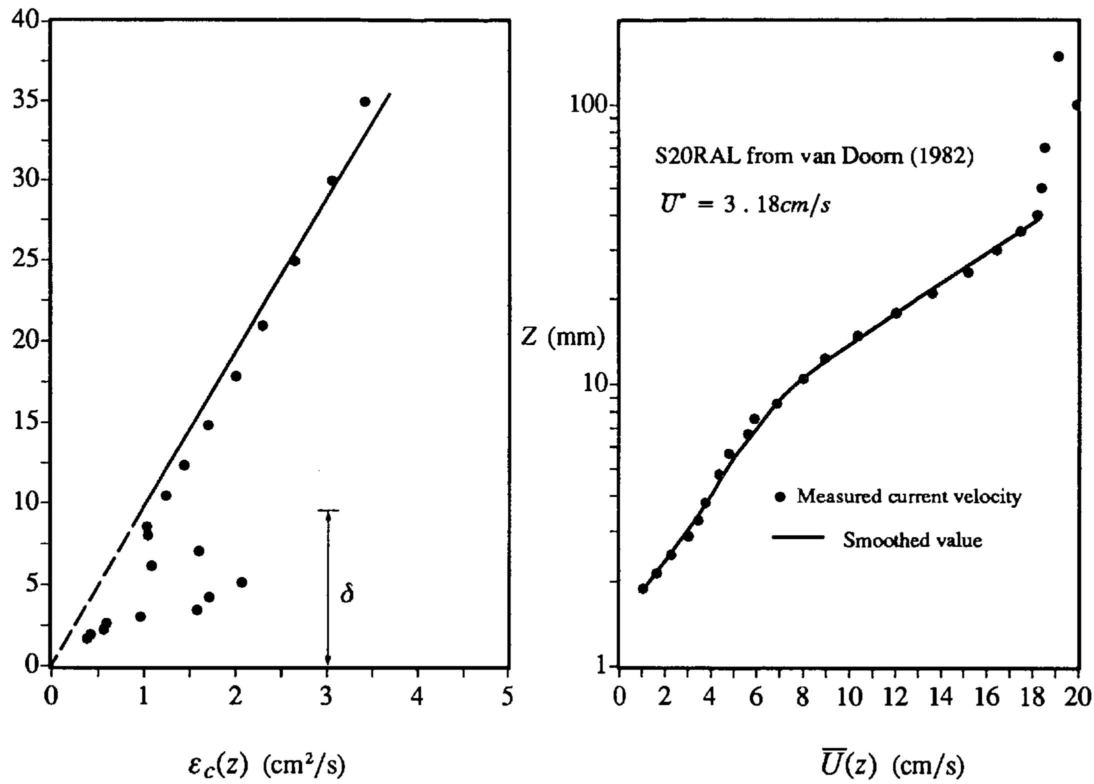

Fig.4.22 The current eddy viscosity calculated from van Doorn (1982) S20RAL via Eq.(4.99)

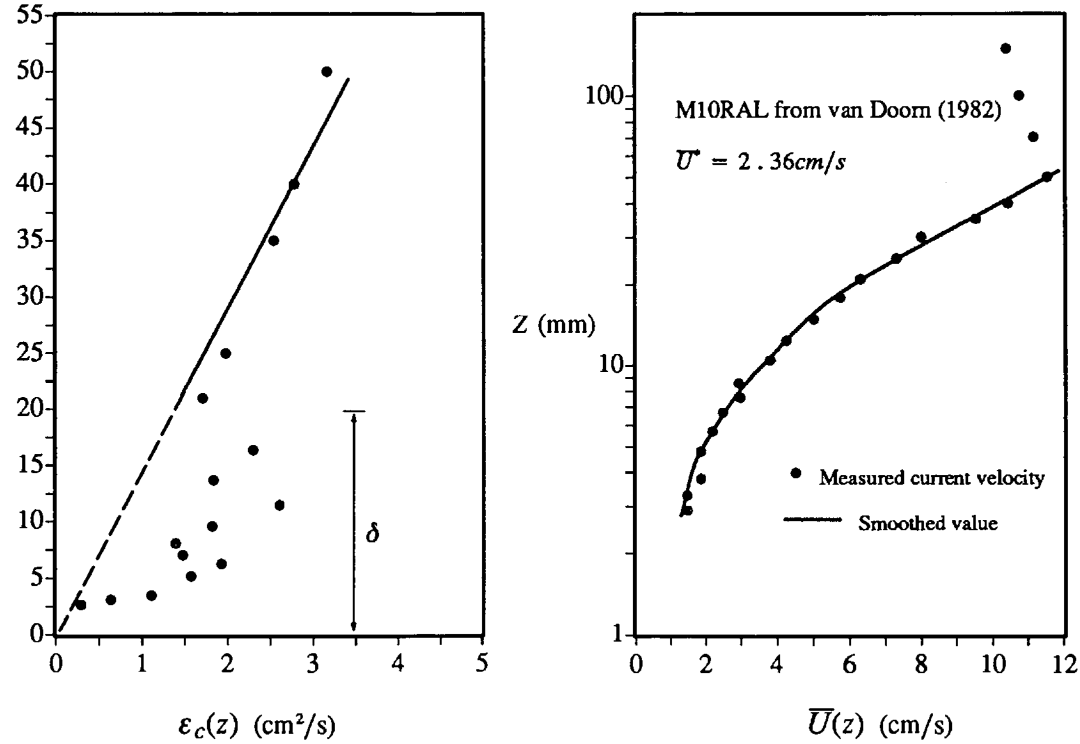

Fig.4.23 The current eddy viscosity calculated from van Doorn (1982) M10RAL via Eq.(4.99)

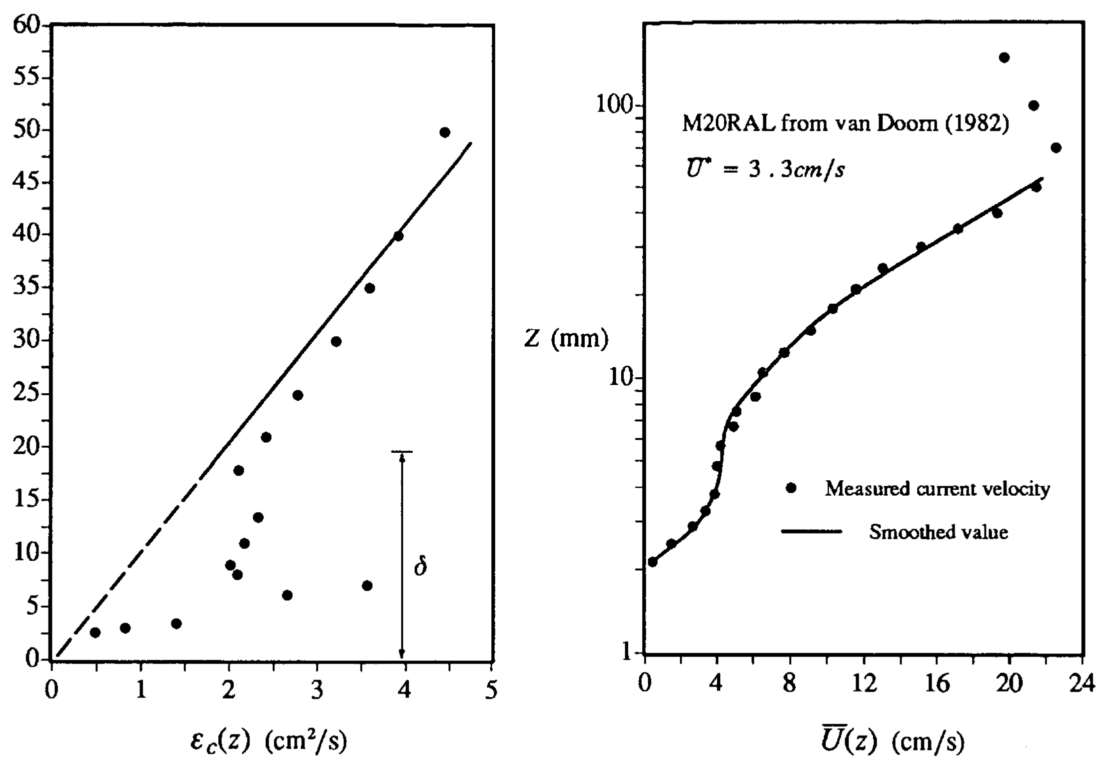

Fig.4.24 The current eddy viscosity calculated from van Doorn (1982) M20RAL via Eq.(4.99)

§4.5.2.2 Analysis of the Eddy Viscosity Data $\varepsilon_c(z)$

§4.5.2.2.1 The influence of current strength on $\varepsilon_c(z)$ and δ

Fig.4.25 [A], in which the wave conditions are fixed while the depth–averaged current velocity $< \overline{U} >$ is increased from $10cm/s$ to $20cm/s$, shows that $\varepsilon_c(z)$ inside the interaction zone $[z \leq \delta]$ varies little with increasing the current strength while outside the interaction zone $[z \geq \delta]$ $\varepsilon_c(z)$ increases apparently with the current strength. On the other hand, the thickness δ of the interaction zone changes little with current strength in the tests M10RAL and M20RAL. However, this should be examined later on because the effect of current strength on δ may be overshadowed by the wave motion due to $\hat{U}_w^*/\overline{U}^* = 4.6 \sim 6.5 \gg 1$ in the MRAL tests.

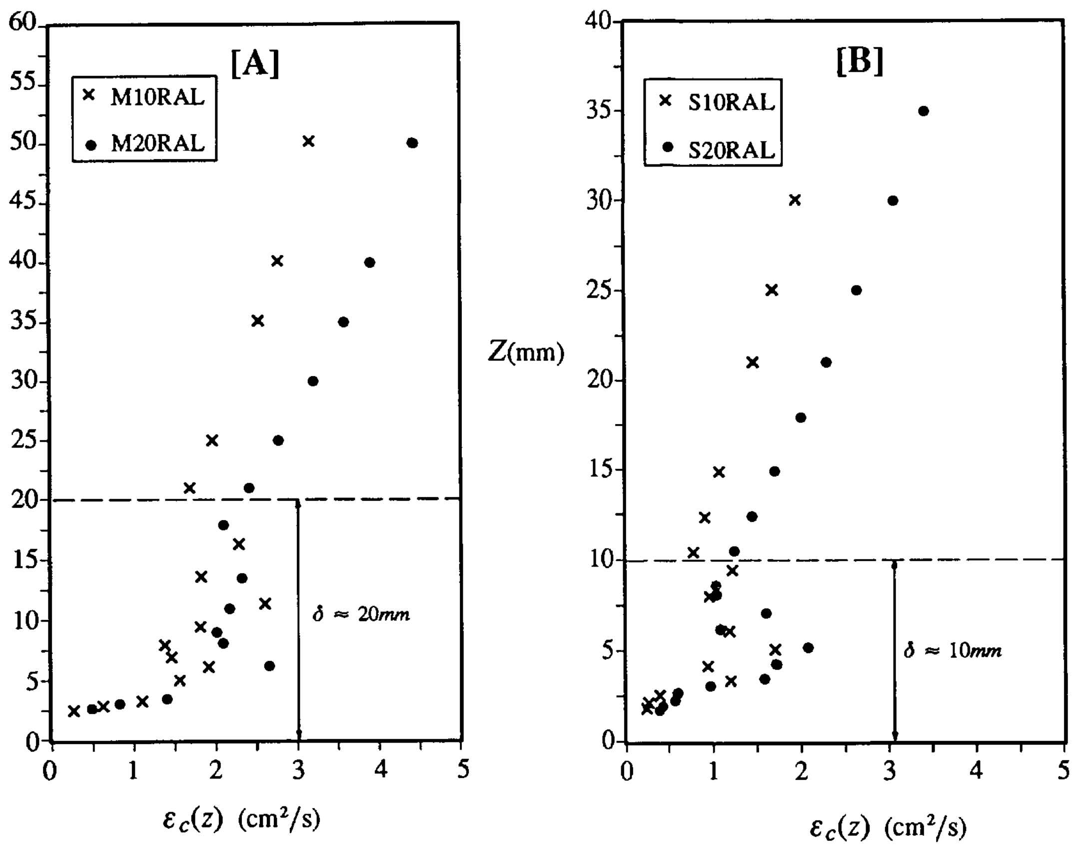

Fig.4.25 The influence of the current strength on the current eddy viscosity in the combined flow

Fig.4.25 [B], in which $\hat{U}_w^*/\overline{U}^* = 1.8 \sim 2.8$, also shows that $\varepsilon_c(z)$ outside the interaction zone increases with the current strength while the current strength has little effect on $\varepsilon_c(z)$ inside the interaction zone. On the other hand, Fig.4.25 [B] supports the hypothesis that the thickness δ of the interaction zone is independent of the current strength. The only difference between [A] and [B] in Fig.4.25 is that the thickness δ of the interaction zone in [A] is $\delta \approx 20mm$ while in [B] it is $\delta \approx 10mm$, and the magnitudes of $\varepsilon_c(z)$ near the bed in [A] is larger than those in [B].

§4.5.2.2.2 The influence of the wave motion on $\varepsilon_c(z)$ and δ

For the data shown in Fig.4.26 in which $< \overline{U} >$ is constant, it can can be seen that outside the interaction zone $[z > \delta]$ the current eddy viscosity ε_c is little affected by the wave motion even when $A\omega = 32.3cm/s$ in SRAL is increased to $A\omega = 106.0cm/s$ in MRAL.

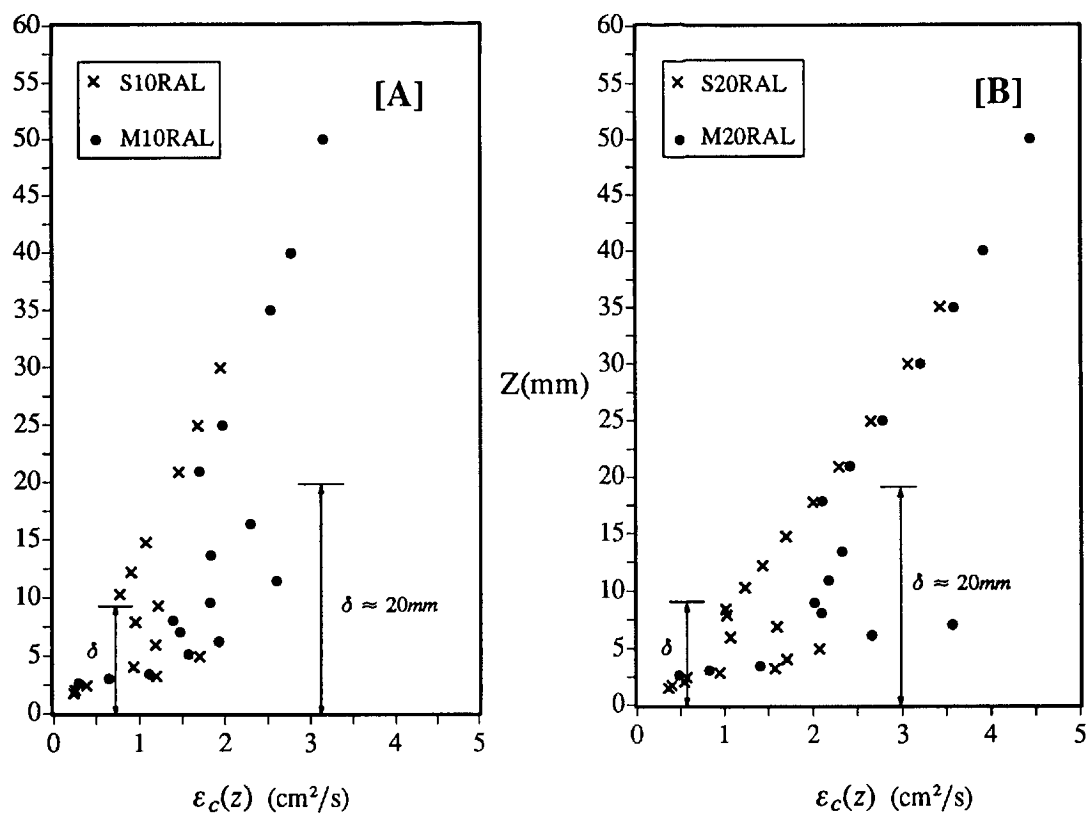

Fig.4.26 The influence of the wave motion on the current eddy viscosity in the combined flow

However inside the interaction zone [$z \le \delta$], $\varepsilon_c(z)$ increases with increasing $A\omega$. On the other hand, Fig.4.26 indicates that the thickness δ of the interaction zone is dominated by the wave motion because δ increases little with increasing current strength as was shown in Fig.4.25, but does increase with increasing the free stream velocity amplitude $A\omega$ as indicated in Fig.4.26.

§4.5.2.2.3 The influence of Φ on $\varepsilon_c(z)$

The general effects of the relative orientations of the current and the direction of wave propagation Φ on the current eddy viscosity have not been able to be studied in the present study. Kemp & Simons (1982–83) found experimentally that the apparent roughness $K_1 = 30z_1$ with the superposition of waves propagating on the current [$\Phi = 0^o$] is three times smaller than that with the superposition of waves propagating against the current [$\Phi = 180^o$], in other words, Φ may have a significant effect on the current profile. However, the effect of Φ on the current eddy viscosity can not be quantitatively discussed in the present study due to the lack of suitable experimental data.

§4.5.2.2.4 Conclusions on $\varepsilon_c(z)$

Combining the findings from Fig.4.19 to Fig.4.24, we may draw the conclusions on the behavior of the current eddy viscosity $\varepsilon_c(z)$ in the combined wave–current flows.

(1) $\varepsilon_c(z)$ outside the boundary interaction layer [$z \ge \delta$] is affected little by the wave motion, but dominated by current strength $\overline{U}^*$.

(2) $\varepsilon_c(z)$ inside the boundary interaction layer [$z \le \delta$] is increased by the presence of waves in comparison with that in a pure steady flow.

(3) The thickness δ of the boundary interaction layer is dominated by the wave motion.

§4.5.3 THE EDDY VISCOSITY FOR THE WAVE MOTION

§4.5.3.1 Calculation of ε_w from measurements

In analogy with the eddy viscosity definition for a pure wave motion, the eddy viscosity for the wave motion in the combined wave–current flow is defined by

$$\frac{\tilde{\tau}(z,t)}{\varrho} = \varepsilon_w \frac{\partial \tilde{U}(z,t)}{\partial z} \tag{4.100}$$

and then, using the equation of equation

$$\frac{\partial \tilde{U}(z,t)}{\partial t} = \frac{\partial U_\infty(t)}{\partial t} + \frac{1}{\varrho}\frac{\partial \tilde{\tau}(z,t)}{\partial z} \tag{4.23}$$

we obtain

$$\frac{\partial \tilde{U}(z,t)}{\partial t} = \frac{\partial U_\infty(t)}{\partial t} + \frac{1}{\varrho}\frac{\partial}{\partial z}\left\{\varepsilon_w \frac{\partial \tilde{U}(z,t)}{\partial z}\right\} \tag{4.101}$$

If we are interested in only the main harmonic component of $\tilde{U}(z,t)$ in Eq.(4.101), we may assume

$$\tilde{U}(z,t) = \hat{U}(z)\, e^{i\phi(z)}\, e^{i\omega t} \qquad\qquad U_\infty(t) = A\omega\, e^{i\omega t} \tag{4.102}$$

in which $A\omega$ is the amplitude of the free stream velocity, $\hat{U}(z)$ the amplitude of wave–induced local velocity and $\phi(z)$ the velocity phase shift between the free stream velocity $U_\infty(t)$ and the local velocity $\tilde{U}(z,t)$. All these parameters $A\omega$, $\hat{U}(z)$ and $\phi(z)$ can be obtain from presently available experimental data, e.g. V10RA & V20RA from van Doorn (1981) and S10RAL, S20RAL, M10RAL & M20RAL from van Doorn (1982). Hence, ε_w in Eq.(4.101) can be be calculated by the formula

$$\varepsilon_w = \frac{i\omega \displaystyle\int_z^\infty \left\{ A\omega - \hat{U}(z)\, e^{i\phi(z)} \right\} dz}{\dfrac{\partial}{\partial z}\left\{ A\omega - \hat{U}(z)\, e^{i\phi(z)} \right\}} \tag{4.103}$$

From Eq.(4.103), it can be seen that the eddy viscosity, which corresponds to the first harmonic component of $\tilde{U}(z,t)$, should be time–independent in the combined wave current flows. Fig.4.27 to Fig.4.29 show the vertical distributions of eddy viscosity calculated from the experimental data via Eq.(4.103).

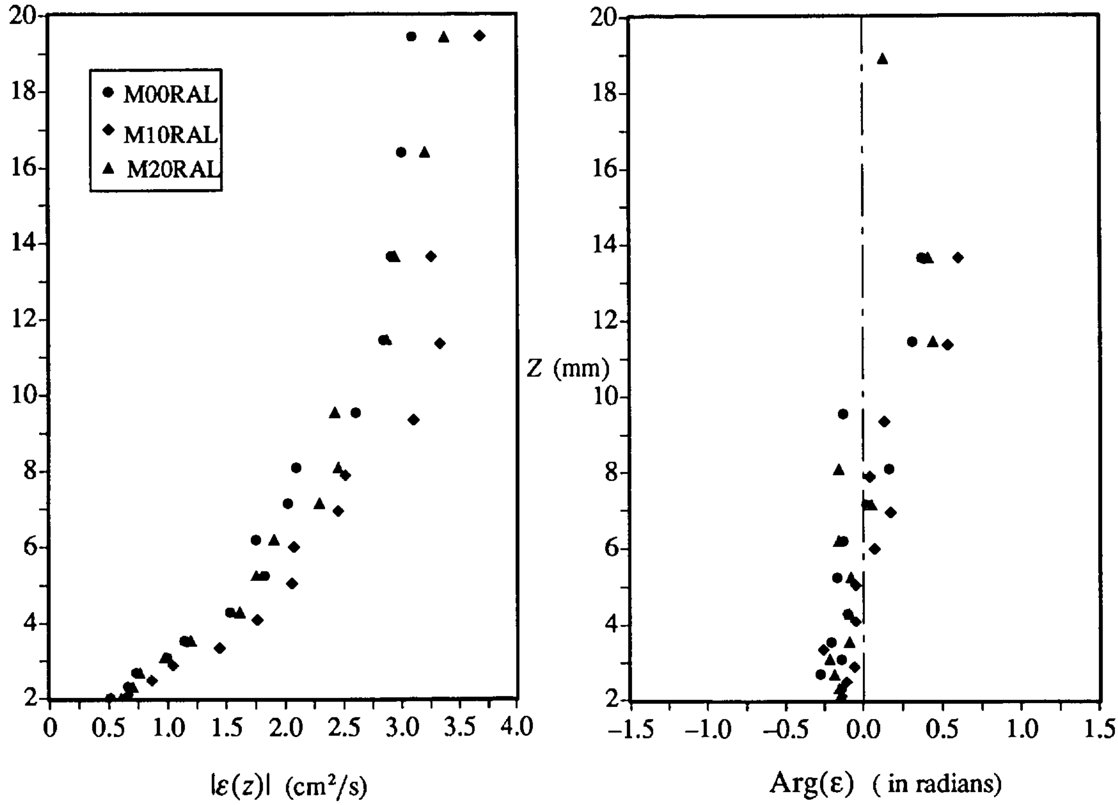

Fig.4.27 The eddy viscosity for the wave motion evaluated from van Doorn (1982) MRAL via Eq.(4.103)

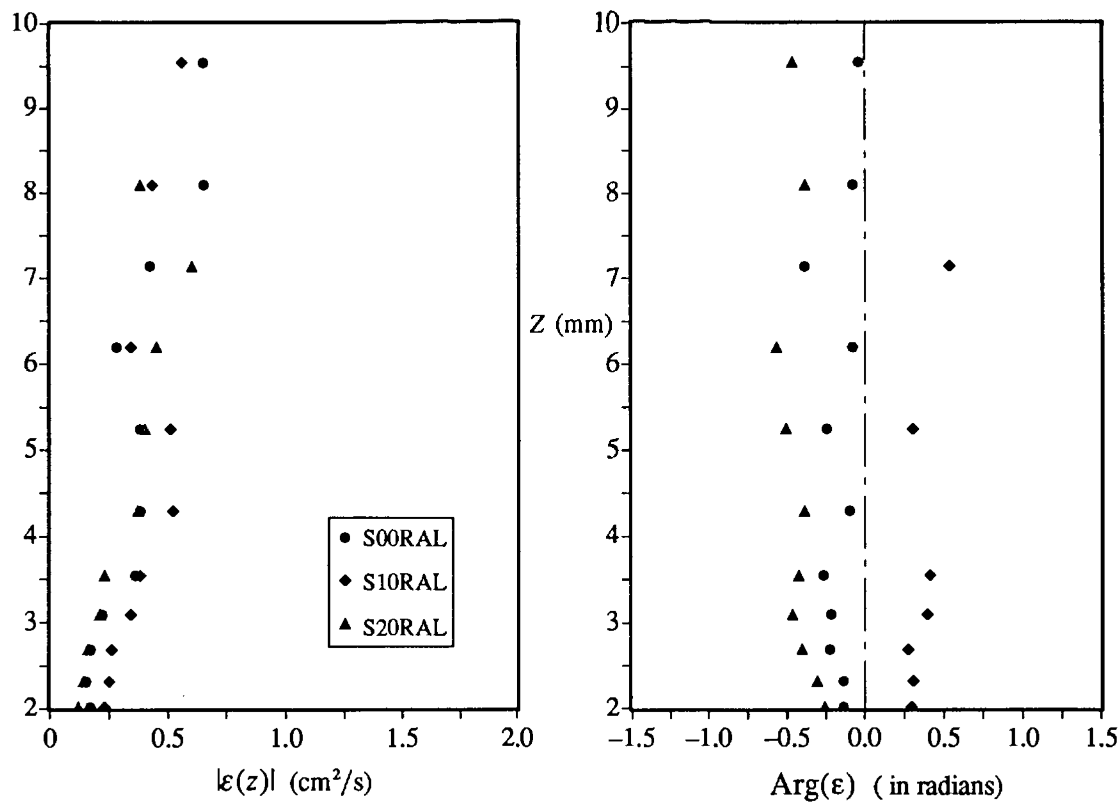

Fig.4.28 The eddy viscosity for the wave motion evaluated from van Doorn (1982) SRAL via Eq.(4.103)

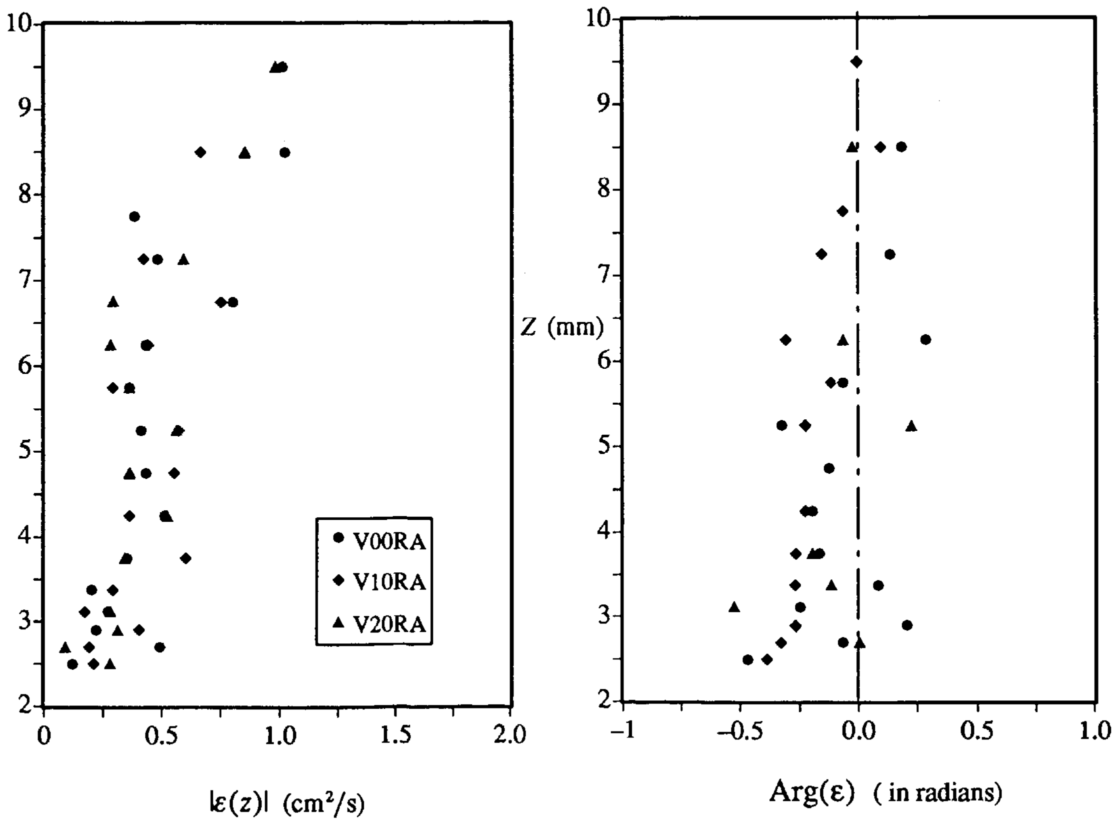

Fig.4.29 The eddy viscosity for the wave motion evaluated from van Doorn (1981) VRA via Eq.(4.103)

§4.5.3.2 Analysis of the Eddy Viscosity Data ε_w

§4.5.3.2.1 The influence of current strength on ε_w

Fig.4.27, in which the wave parameters are constant, shows that the eddy viscosity ε_w for the wave motion in the combined wave−current flows changes little when the depth−averaged current velocity is increased from 0.0cm/s to 20cm/s. Fig.4.27 and Fig.4.29, in which the wave parameters are also constant, again show that ε_w is little affected by current strength. Therefore, it seems reasonable to assume that ε_w is independent of current strength in wave dominated combined flows as suggested by You *et al.* (1991a).

§4.5.3.2.2 The effect of wave motion on ε_w

If we compare the values of ε_w evaluated from S10RAL [S20RAL] in Fig.4.28 with that calculated from M10RAL [M20RAL] in Fig.4.27, we find that the eddy viscosity for the wave motion in the combined wave–current flows increases with increasing the amplitude of the free stream velocity $A\omega$.

§4.5.3.2.3 Conclusions on ε_w

Combining the findings from Fig.4.27 to Fig.4.29 [$1.8 < \hat{U}^*_w/\bar{U}^* < 6.5$], we may draw the following conclusions regarding ε_w in the combined wave–current flows :

(1) ε_w is best described in terms of a time–independent and real–valued parameter.

(2) ε_w is dominated by the wave motion and affected little by the current strength in the wave–dominated combined flows.

§4.5.4 COMPARISON BETWEEN ε_w AND ε_c FROM DATA

Grant & Madsen (1979), Christoffersen & Jonsson (1985), Myrhaug & Slaattelid (1989) and Sleath (1991) all assumed that inside the boundary interaction zone [$z \leq \delta$] the eddy viscosity for the wave motion was the same as that for steady flow. However, Coffey & Nielsen (1986) claimed that the eddy viscosity for the steady component of the combined wave–current flow was much larger than the eddy viscosity for the oscillatory component. Recently, You *et al.* (1991a) argued on the theoretical grounds that the eddy viscosity for the steady flow should be different from that for the wave motion in the combined flows, see Section §4.4.9. Fig.4.30 and Fig.4.31 suggest that ε_c and ε_w are not the same in the boundary interaction zone [$z \leq \delta$] in terms of their magnitudes or distribution profiles. The other data sets V10RA, V20RA, S20RAL & M20RAL all indicates that ε_c is quite different from ε_w inside the boundary interaction layer.

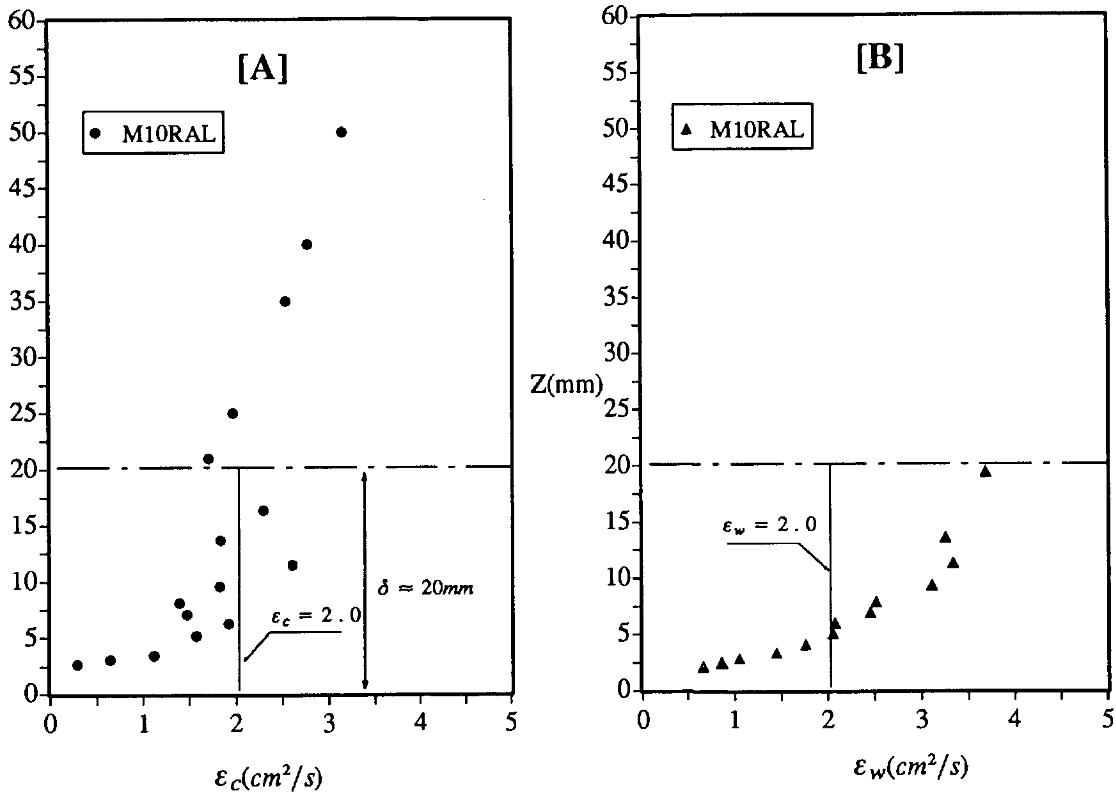

Fig.4.30 A comparison between ε_c and ε_w in the boundary interaction zone

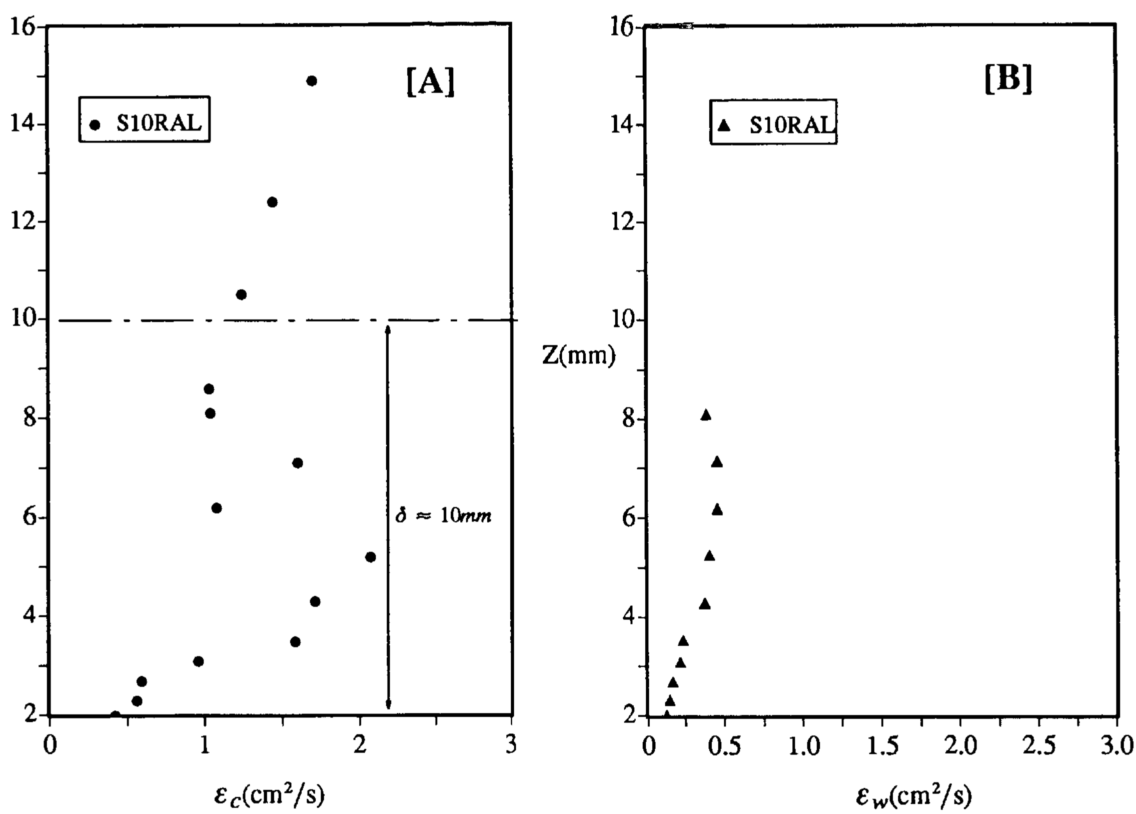

Fig.4.31 A comparison between ε_c and ε_w in the boundary interaction zone

§4.5.5 THE PRESENT EDDY VISCOSITY MODEL

It was concluded in Section §4.5.2.2.4 that inside the boundary interaction layer $[z \leq \delta]$ ε_c increases in the presence of waves while outside the boundary interaction zone $[z \geq \delta]$ ε_c is dominated by current strength $\overline{U}^*$. The distributions of ε_c shown in Fig.4.19 to Fig.4.24, may be described by the functional form

$$\varepsilon_c(z) = \varkappa \hat{U}^*_{cw} z \qquad z_o \leq z \leq \delta_1 \tag{4.104}$$

$$\varepsilon_c(z) = \varkappa \hat{U}^*_{cw} \delta_1 \qquad \delta_1 \leq z \leq \delta \tag{4.105}$$

$$\varepsilon_c(z) = \varkappa \overline{U}^* z \qquad \delta \leq z \leq h \tag{4.106}$$

as suggested by You *et al.* (1991a). Eq.(4.106) yields a logarithmic distribution of the current velocity outside the boundary interaction zone $[z \geq \delta]$, so that ε_c is similar to that in pure steady flow whereas inside the interaction zone $[z \leq \delta]$ ε_c exceeds that in pure steady flow as shown in Fig.4.32.

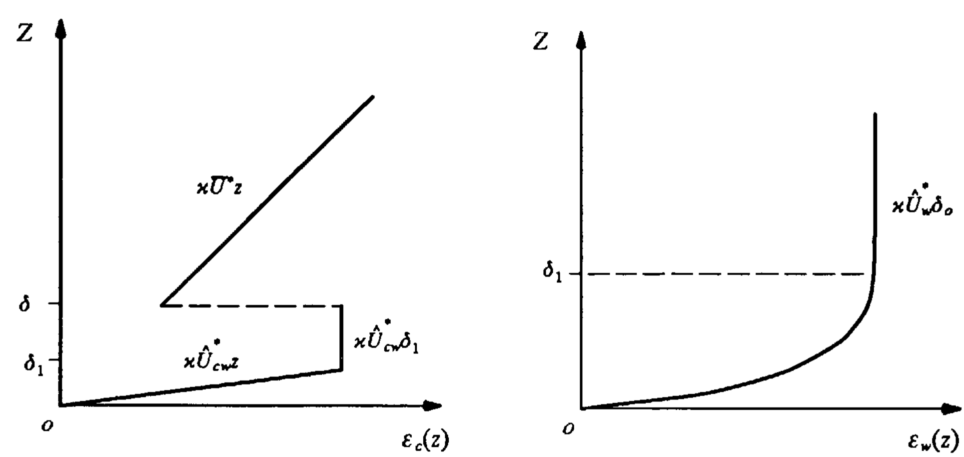

Fig.4.32 The eddy viscosities of the currents and waves suggested in the present model

In Section §4.5.3.2, it was argued that the eddy viscosity ε_w for the wave motion is independent of current strength $\overline{U}^*$ in the wave–dominated combined flow. Therefore, the eddy viscosity ε_w for the wave motion in the combined wave–current flow may be assumed as

$$\varepsilon_w(z) \;=\; \varkappa \hat{U}_w^* \delta_o \left\{ 1 - \left[1 - z/\delta_1 \right]^2 \right\} \qquad z_o \le z \le \delta_1 \qquad (4.107)$$

$$\varepsilon_w(z) \;=\; \varkappa \hat{U}_w^* \delta_o \qquad \delta_w \le z \le \delta_1 \qquad (4.108)$$

as suggested by You *et al.* (1991c). The eddy viscosity model for the wave motion described by Eqs.(4.107) and (4.108) is in close agreement with the eddy viscosity data derived from experimental data with the relative roughness at a wide range of $2.8 \times 10^{-4} < A/K_N < 2.5 \times 10^{-1}$ in pure wave motion as discussed in Chapter 2. A comparison of the present eddy viscosity model with eddy viscosity data calculated from experimental data via Eq.(4.103) is shown in Fig.4.33 to Fig.4.36.

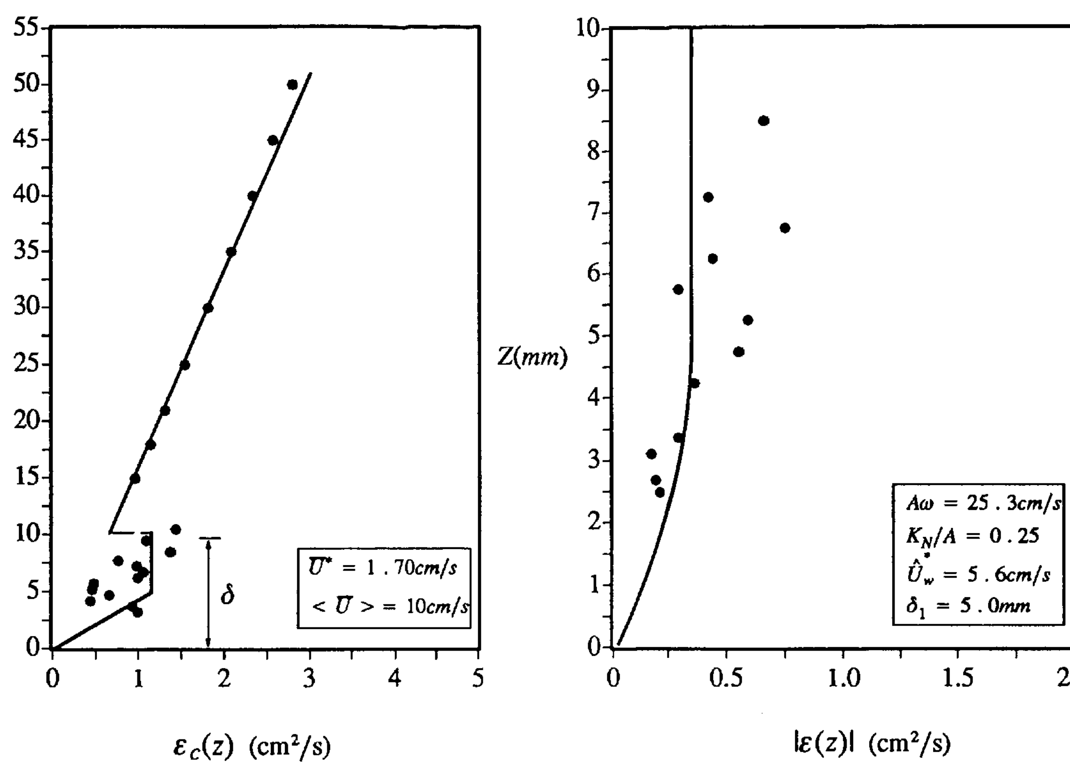

Fig.4.33 Comparison of the present eddy viscosity model with eddy viscosity data derived from V10RA

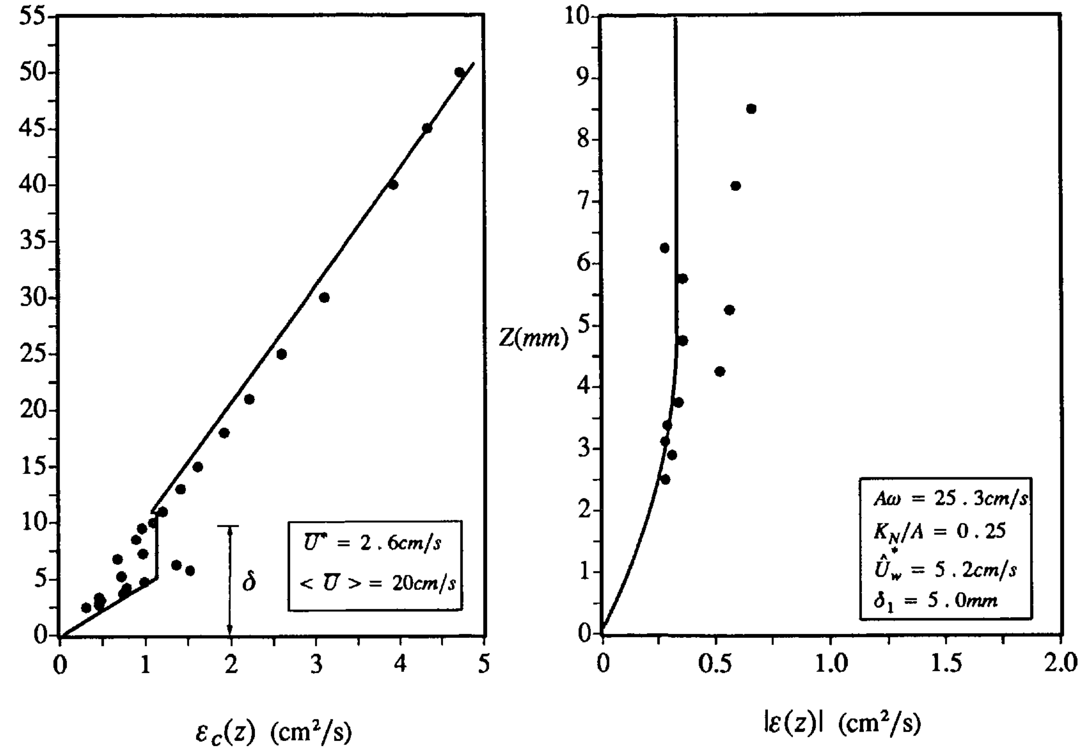

Fig.4.34 Comparison of the present eddy viscosity model with eddy viscosity data derived from V20RA

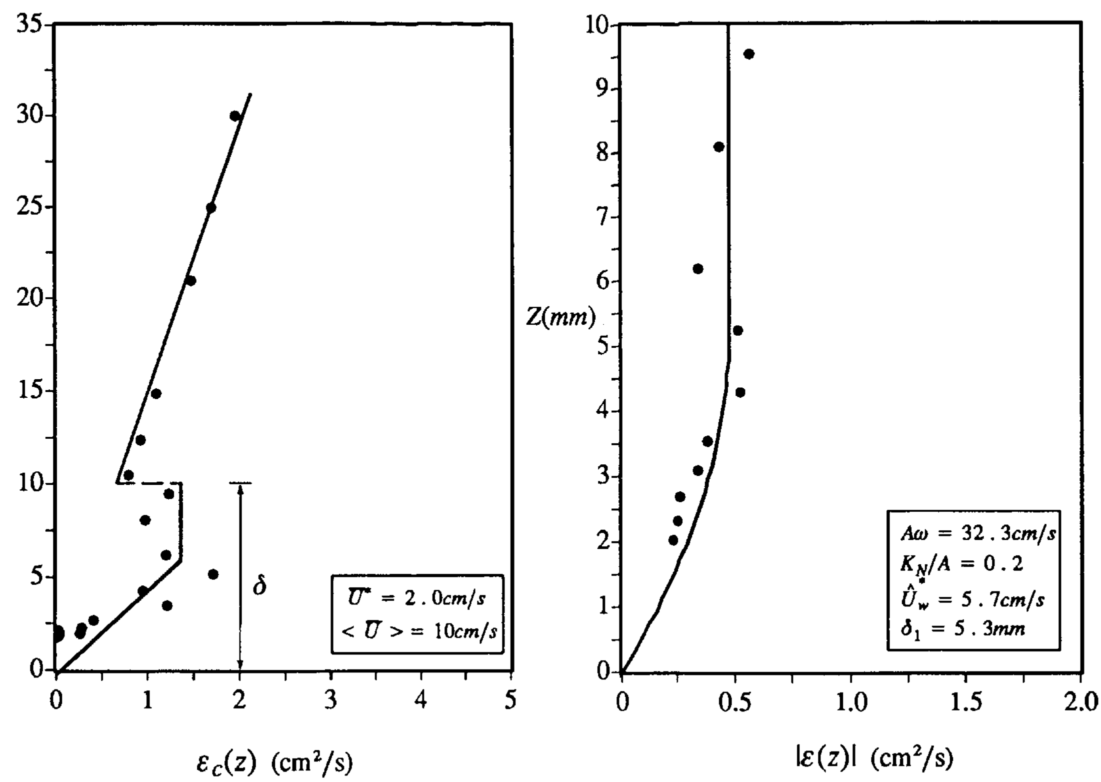

Fig.4.35 Comparison of the present eddy viscosity model with eddy viscosity data derived from S10RAL

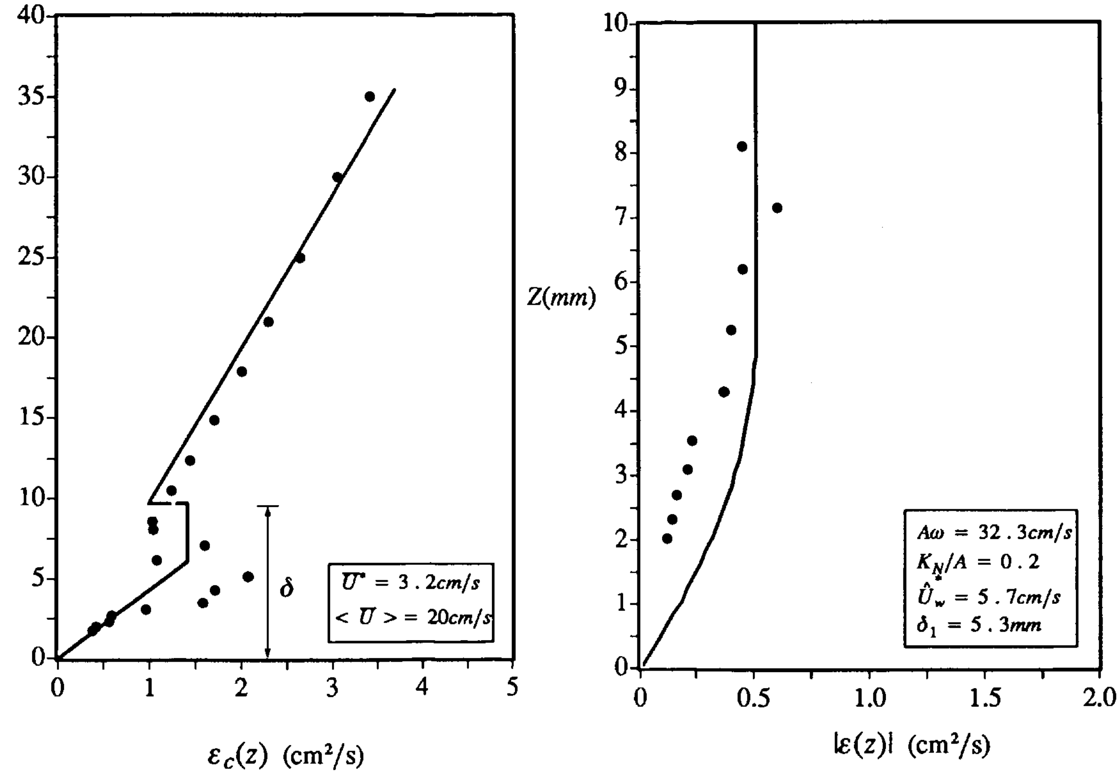

Fig.4.36 Comparison of the present eddy viscosity model with eddy viscosity data derived from S20RAL

§4.5.6 SOLUTION FOR $\overline{U}(z)$

Combining Eqs.(4.95) and (4.96), we will obtain

$$\overline{U}(z) \;=\; \int \frac{\overline{\tau}_b\left\{1 - \frac{z}{h}\right\}}{\varrho\ \varepsilon_c(z)}\, dz \qquad (4.109)$$

Furthermore, if we assume that the shear stress near the bed is constant, Eq.(4.109) can be further simplified to give

$$\overline{U}(z) \;=\; \int \frac{\overline{\tau}_b}{\varrho\ \varepsilon_c(z)}\, dz \;=\; \int \frac{\overline{U}^*\overline{U}^*}{\varepsilon_c(z)} dz \qquad (4.110)$$

Substituting the current eddy viscosity distributions given in Eqs.(4.104) and (4.105) into Eq.(4.110), and using the boundary conditions, we will obtain the current velocity profile inside the interaction zone $[z < \delta]$

$$\overline{U}(z) = \frac{\overline{U}^*}{\varkappa}\left\{\frac{\overline{U}^*}{\hat{U}^*_{cw}}\right\}\ln\frac{z}{z_o} \qquad z_o \le z \le \delta_1 \tag{4.111}$$

$$\overline{U}(z) = \frac{\overline{U}^*}{\varkappa}\left\{\frac{\overline{U}^*}{\hat{U}^*_{cw}}\right\}\left\{\frac{z}{\delta_1} + \ln\frac{\delta_1}{z_o} - 1\right\} \qquad \delta_1 \le z \le \delta \tag{4.112}$$

Similarly, substituting the eddy viscosity outside the interaction zone given by Eq.(4.106) into Eq.(4.110) and using the boundary conditions, we will obtain the current velocity profile outside the boundary interaction zone $[z \ge \delta]$

$$\overline{U}(z) = \frac{\overline{U}^*}{\varkappa}\ln\frac{z}{z_1} \qquad \delta \le z \le d_c \tag{4.113}$$

in which z_1 is given by

$$z_1 = 2\delta_1\left\{\frac{2.718\delta_1}{z_o}\right\}^{-\frac{\overline{U}^*}{\hat{U}^*_{cw}}} \tag{4.114}$$

Eq.(4.114) can be rewritten in no−dimensional form as

$$\frac{z_1}{z_o} = \left\{2 \times 2.718^{-\frac{\overline{U}^*}{\hat{U}^*_{cw}}}\right\}\left\{\frac{\delta_1}{z_o}\right\}^{1-\frac{\overline{U}^*}{\hat{U}^*_{cw}}} \tag{4.115}$$

The effect of waves on the current outside the interaction zone can be explained from Eq.(4.113), which can be rewritten as

$$\overline{U}(z) = \frac{\overline{U}^*}{\varkappa}\ln\frac{z}{z_o} - \frac{\overline{U}^*}{\varkappa}\ln\frac{z_1}{z_o} \qquad z \ge \delta \tag{4.116}$$

From Eq.(4.116), it is found that the first term represents the current velocity without waves while the second term indicates a reduction of the current velocity with waves. The amount of current reduction can be evaluated by

$$\Delta U_c = \frac{\overline{U}^*}{\varkappa}\ln\left\{\frac{z_o}{z_1}\right\} \tag{4.117}$$

which implies that the reduction in the current velocity results from an effective increase in the roughness from the Nikuradse roughness $K_N = 30z_o$ to the apparent roughness $K_1 = 30z_1$.

§4.5.7 SOLUTIONS FOR $\tilde{U}(z,t)$

The wave–induced velocity inside the wave boundary layer can be worked out by solving the equation for the wave motion

$$\frac{\partial \tilde{U}(z,t)}{\partial t} = \frac{\partial U_\infty(t)}{\partial t} + \frac{\partial}{\partial z}\left\{\varepsilon_w \frac{\partial \tilde{U}(z,t)}{\partial z}\right\} \tag{4.46}$$

with an assumed eddy viscosity distribution $\varepsilon_w(z)$. Since the eddy viscosity distribution ε_w given by Eqs.(4.107) and (4.108) and the equation for the wave motion (4.46) in a combined wave–current flow are identical to those in a pure wave motion, the procedures for derivation of the wave–induced velocity in a combined wave–current flow are exactly the same as were followed in Section §2.5.6 of Chapter2. Therefore, the wave–induced velocity in the inner layer can be expressed as

$$\tilde{U}(\xi,t) = \left\{1 - \frac{(p - \cos\lambda\pi)P_\lambda(\xi) + P_\lambda(-\xi)}{(p - \cos\lambda\pi)P_\lambda(\xi_o) + P_\lambda(-\xi_o)}\right\}U_\infty(t) \tag{4.118}$$

where $\xi = z/\delta_1 - 1$ and the wave–induced velocity in the outer layer is given by

$$\tilde{U}(z,t) = \left\{1 - \frac{(p - \cos\lambda\pi + 1)P_\lambda(0)}{(p - \cos\lambda\pi)P_\lambda(\xi_o) + P_\lambda(-\xi_o)}\exp[-\eta(1+i)(z-\delta_1)]\right\}U_\infty(t) \tag{4.119}$$

in which $P_\lambda(\xi)$ is called Legendre's function of the first order, and

$$p = \frac{\eta(1+i)\delta_1(\cos\lambda - 1) + (\cos\lambda\pi + 1)q}{\eta(1+i)\delta_1 + q} \quad \text{and} \quad \eta = \left\{\frac{\omega}{2\varkappa \hat{U}^*_w \delta_o}\right\}^{\frac{1}{2}}$$

$$q = \frac{1}{4\pi^2}\lambda^2 \sin\lambda\pi \left\{\Gamma\left\{\frac{\lambda}{2}\right\}\Gamma\left\{\frac{1}{2}-\frac{\lambda}{2}\right\}\right\}$$

$$\lambda = \frac{1}{2}\{1 - a\} - i\frac{\beta}{a} \quad \text{and} \quad a = \left\{\frac{1}{2}\left\{1 + \{1 + 16\beta^2\}^{\frac{1}{2}}\right\}\right\}^{\frac{1}{2}}$$

§4.5.8 THE BED FRICTION FACTORS

§4.5.8.1 The Wave Friction Factor

In order to evaluate the wave–induced velocities from Eqs.(4.118) and (4.119), it is necessary to first specify the friction velocity $\hat{U}_w^*$ or alternatively wave friction factor f_w. The maximum bed shear stress can be expressed by

$$\frac{\hat{\tau}_b(z_o)}{\varrho} = \left\{ \varepsilon_w(z) \frac{\partial \tilde{U}(\xi, t)}{\partial z} \right\}_{Max} \tag{4.120}$$

Substituting the wave–induced orbital velocity near the bed Eq.(4.118) and the wave eddy viscosity Eq.(4.107) into Eq.(4.120), it leads to

$$\frac{\hat{\tau}_b(z_o)}{\varrho} = 0.8\varkappa \hat{U}_w^* \left\{1 - \xi_o^2\right\} \left\{\hat{Z}(\xi_o)\ Z(\xi_o)\right\}^{\frac{1}{2}} A\omega \tag{4.121}$$

in which $\hat{Z}(\xi_o)$ denotes the complex conjugate of $Z(\xi_o)$, which is given by

$$\hat{Z}(\xi_o) = \frac{(p - \cos\lambda\pi)P'_\lambda(\xi_o) - P'_\lambda(-\xi_o)}{(p - \cos\lambda\pi)P_\lambda(\xi_o) + P_\lambda(-\xi_o)} \tag{4.122}$$

where

$$P'_\lambda(x) = \frac{\lambda + 1}{x^2 - 1}\left\{P_{\lambda+1}(x) - xP_\lambda(x)\right\} \tag{4.123}$$

The maximum bed shear stress can also be expressed as

$$\frac{\hat{\tau}_b(z_o)}{\varrho} = \frac{1}{2} f_w \{A\omega\}^2 \qquad \text{and} \qquad \frac{\hat{\tau}_b(z_o)}{\varrho} = \hat{U}_w^* \hat{U}_w^* \tag{4.124}$$

Combining Eqs.(4.121) and (4.124) and simplifying, the wave friction factor f_w can be written as

$$f_w = 0.0512\left\{1 - \xi_o^2\right\}^2 Z(\xi_o)\hat{Z}(\xi_o) \tag{4.125}$$

Although the wave friction factor f_w is explicitly expressed in Eq.(4.125), f_w can not be directly obtained since the variables ξ and p are a function of the wave friction factor. The wave friction factor must be obtained by iterating Eq.(4.125) based on the required accuracy of the iteration.

§4.5.8.2 The Current Friction Factor

After evaluating the wave friction velocity $\hat{U}_w^*$, it is necessary to determine the current friction velocity $\overline{U}^*$ in order to determine the current velocity by using Eqs.(4.111), (4.112) and (4.113). We define the current friction factor f_c as

$$\frac{\overline{\tau}_b}{\varrho} = \frac{1}{2} f_c < \overline{U}_{dc} > < \overline{U}_{dc} > \text{ and } \qquad \frac{\overline{\tau}_b}{\varrho} = \overline{U}^* \overline{U}^* \tag{4.126}$$

as suggested by Christoffersen & Jonsson (1985), Myrhaug & Slaattelid (1989) and You *et al.* (1991a). The depth–averaged current velocity $< \overline{U}_{dc} >$ is defined as a velocity averaged from the bed level $z = z_o$ to a upper level $z = d_c$ which the current velocity profile still follows a logarithmic distribution, see Fig.4.37.

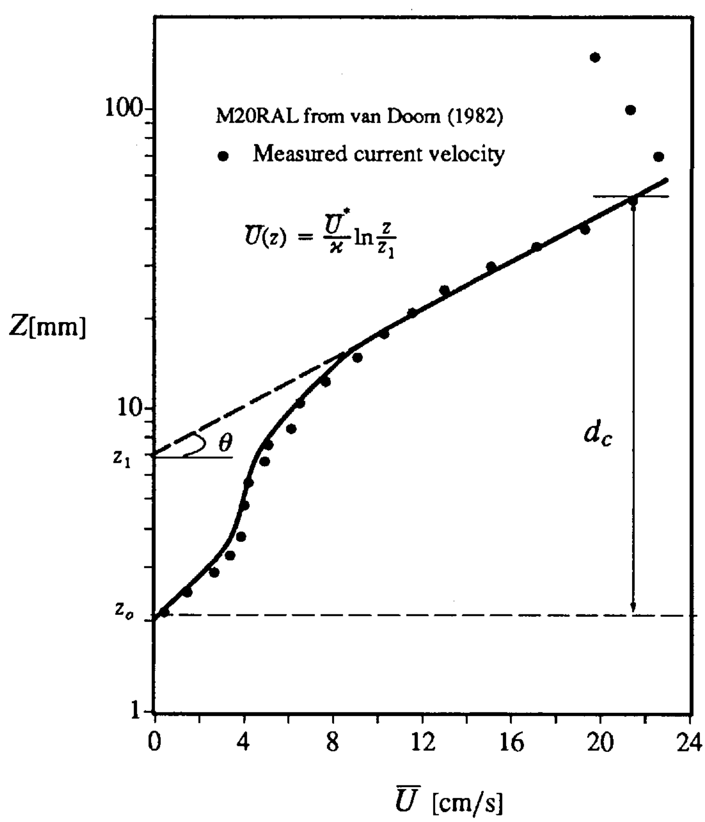

Fig.4.37 The definition of the depth–averaged current velocity in a combined flow

Therefore, the depth−averaged current velocity in a combined flow can be evaluated in terms of Eqs.(4.111), (4.112) and (4.113)

$$< \overline{U}_{dc} > d_c \;=\; \int_{z_o}^{\delta_1} \overline{U}(z)dz \;+\; \int_{\delta_1}^{\delta} \overline{U}(z)dz \;+\; \int_{\delta}^{d_c} \overline{U}(z)dz \qquad (4.127)$$

The sum of the first two terms in the right side of Eq.(4.127) is considerably smaller than the last term when $\delta \ll d_c$. Therefore, Eq.(4.127) can be approximated by

$$< \overline{U}_{dc} > \;\approx\; \frac{1}{d_c} \int_{z_1}^{d_c} \overline{U}(z)\; dz \qquad (4.128)$$

Substituting Eqs.(4.113) into (4.128) and simplifying, the depth−averaged current velocity in the range of $z_1 \le z \le d_c$ is given by

$$< \overline{U}_{dc} > \;=\; \frac{U_c^*}{\varkappa} \ln\left\{\frac{11\; d_c}{K_1}\right\} \qquad (4.129)$$

Based on Eqs.(4.129) and (4.126), the current friction factor can be determined by

$$\left\{\frac{2}{f_c}\right\}^{\frac{1}{2}} \;=\; \frac{< \overline{U}_{dc} >}{\overline{U}^*} \;=\; \frac{1}{\varkappa}\; \ln\left\{\frac{11 d_c}{K_1}\right\} \qquad (4.130)$$

which can be rewritten as

$$f_c \;=\; 2.0\left\{\frac{1}{\varkappa}\; \ln\left\{\frac{11 d_c}{K_1}\right\}\right\}^{-2} \qquad (4.131)$$

In Eq.(4.131), the current friction velocity f_c can not be explicitly calculated since the apparent roughness K_1 is a function of f_c and therefore must be evaluated iteratively.

§4.5.9 THE PROCEDURES OF CALCULATION

The velocities $\tilde{U}(z,t)$ and $\overline{U}(z)$ can be evaluated assuming that the following parameters are known

$$A\omega, \qquad T, \qquad K_N, \qquad \overline{U}_{dc}, \qquad d_c$$

where $A\omega$ is the free stream wave–induced velocity amplitude, or the first harmonic component, T the wave period, K_N the Nikuradse roughness, $\overline{U}_{dc}$ the reference current velocity at the level $z = d_c$, see Fig.4.37. The calculation proceeds as follows

(1) Calculate the wave friction factor f_w by iterating Eq.(4.125) until the required accuracy of f_w is obtained.

(2) Calculate the current friction factor f_c by iterating Eq.(4.131) until the current velocity calculated from Eq.(4.113) at the level $z = d_c$ is approximately equal to the reference current velocity $\overline{U}_{dc}$.

(3) Calculate the wave and current velocities by using Eqs.(4.118), (4.119), (4.111), (4.112) and (4.113) respectively.

§4.5.10 COMPARISON WITH EXPERIMENTS

The present model described above has been compared with the following experimental data, V10RA & V20RA from van Doorn (1981), S10RAL & S20RAL and M10RAL & M20RAL from van Doorn (1982). The input parameters used in the present model are listed in Table.4.3 .

TESTS	Facility	$A\omega$ (cm/s)	T (s)	K_N (cm)	$\overline{U}_{dc}$ (cm/s)	d_c (cm)
V10RA	Flume	25.3	2.0	2.1	9.0	9.0
V20RA	Flume	24.3	2.0	2.1	24.9	10.0
S10RAL	Tunnel	32.3	2.0	2.1	9.5	3.5
S20RAL	Tunnel	32.3	2.0	2.1	18.0	4.2
M10RAL	Tunnel	106	2.0	2.1	12.0	5.5
M20RAL	Tunnel	106	2.0	2.1	22.5	7.0

Table.4.3 Measurements of combined wave–current flows conducted by van Doorn (1981 & 1982)

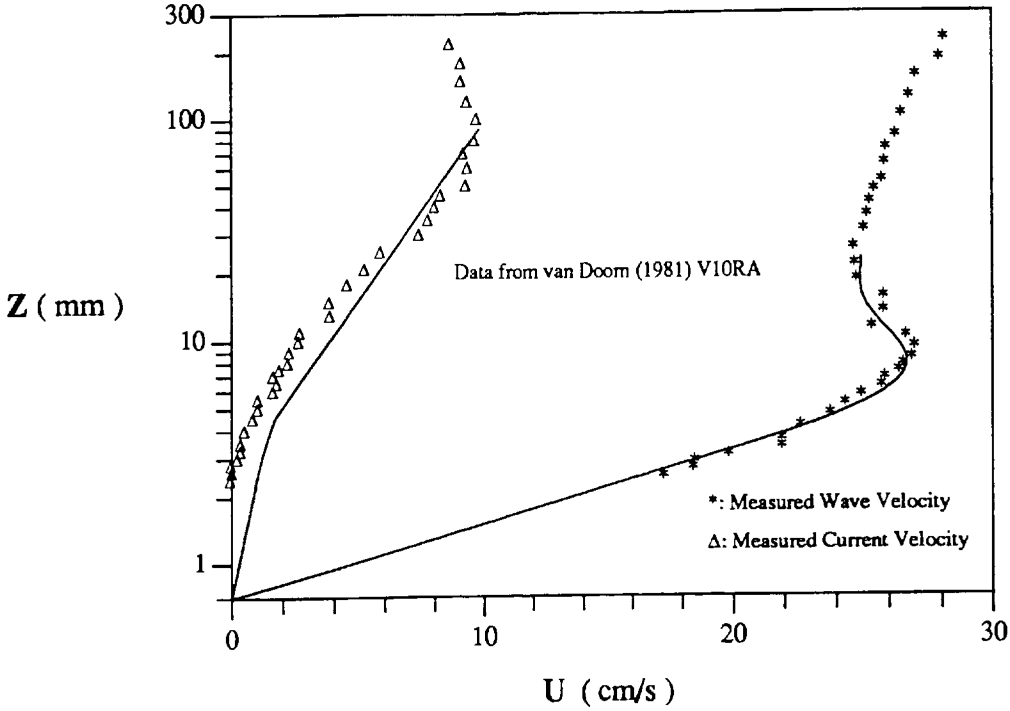

Fig.4.38 The comparison of the present model with experimental data V10RA from van Doorn (1981)

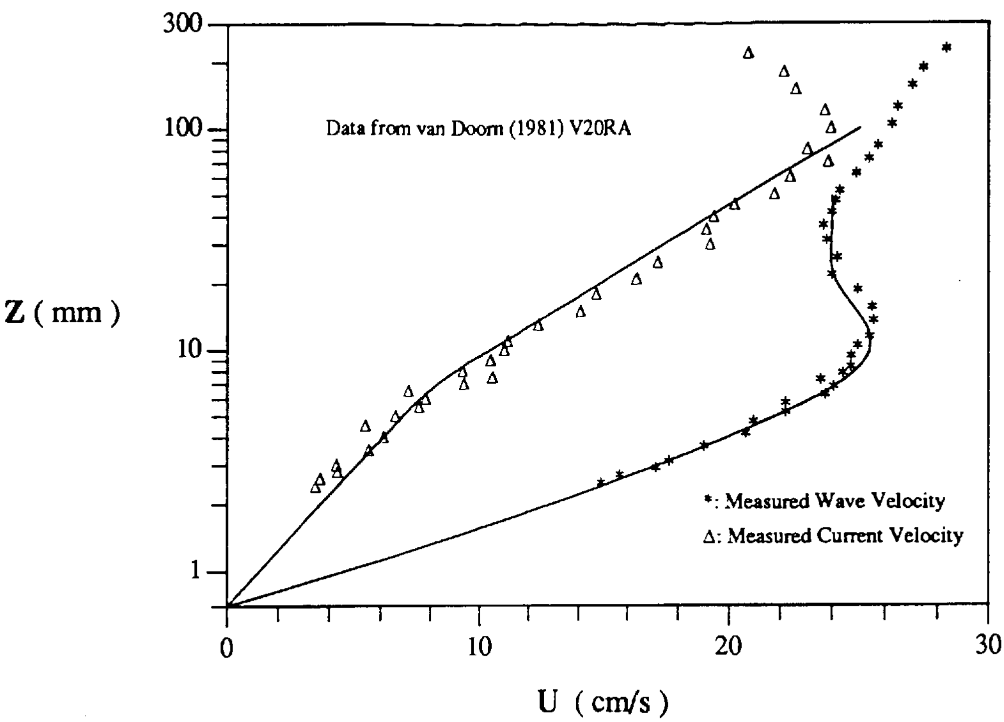

Fig.4.39 The comparison of the present model with experimental data V20RA from van Doorn (1981)

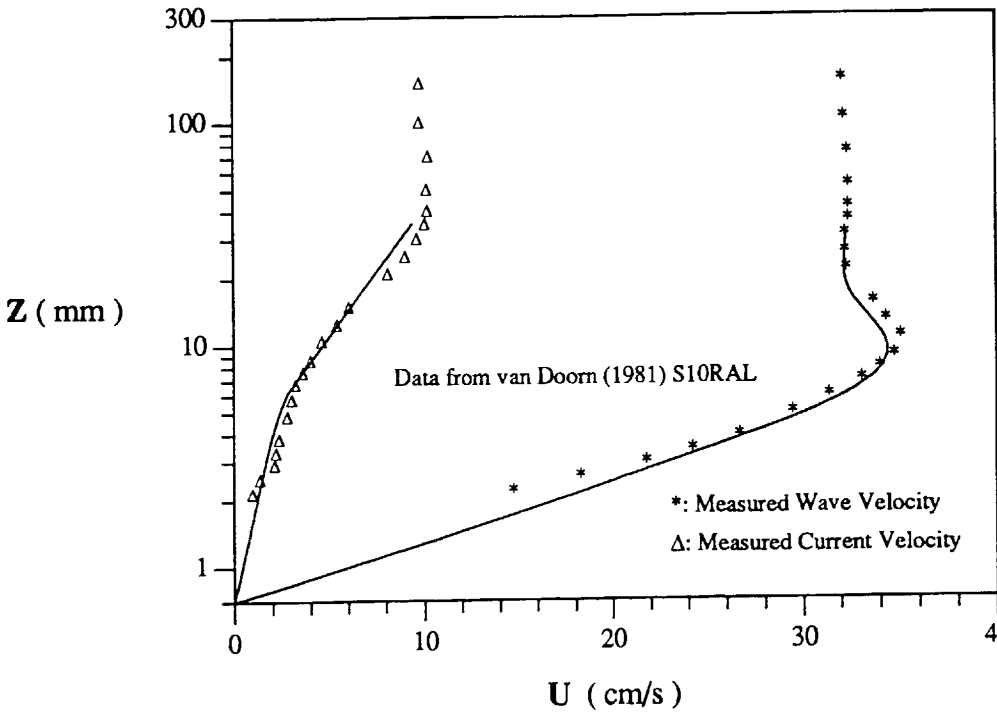

Fig.4.40 The comparison of the present model with experimental data S10RAL from van Doorn (1982)

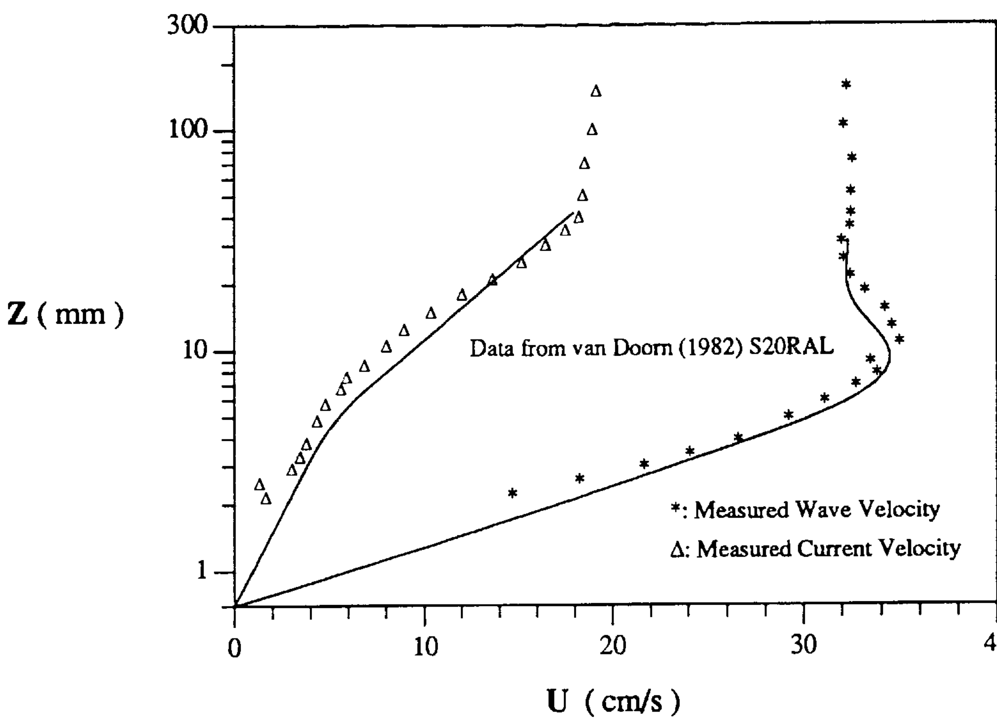

Fig.4.41 The comparison of the present model with experimental data S20RAL from van Doorn (1982)

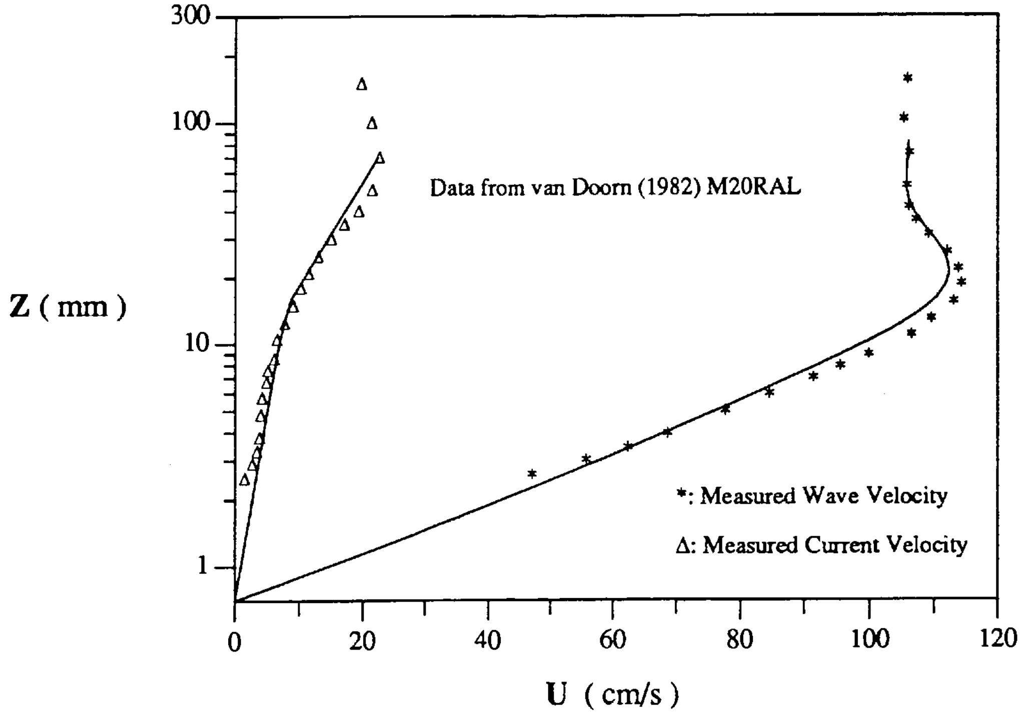

Fig.4.42 The comparison of the present model with experimental data M10RAL from van Doorn (1982)

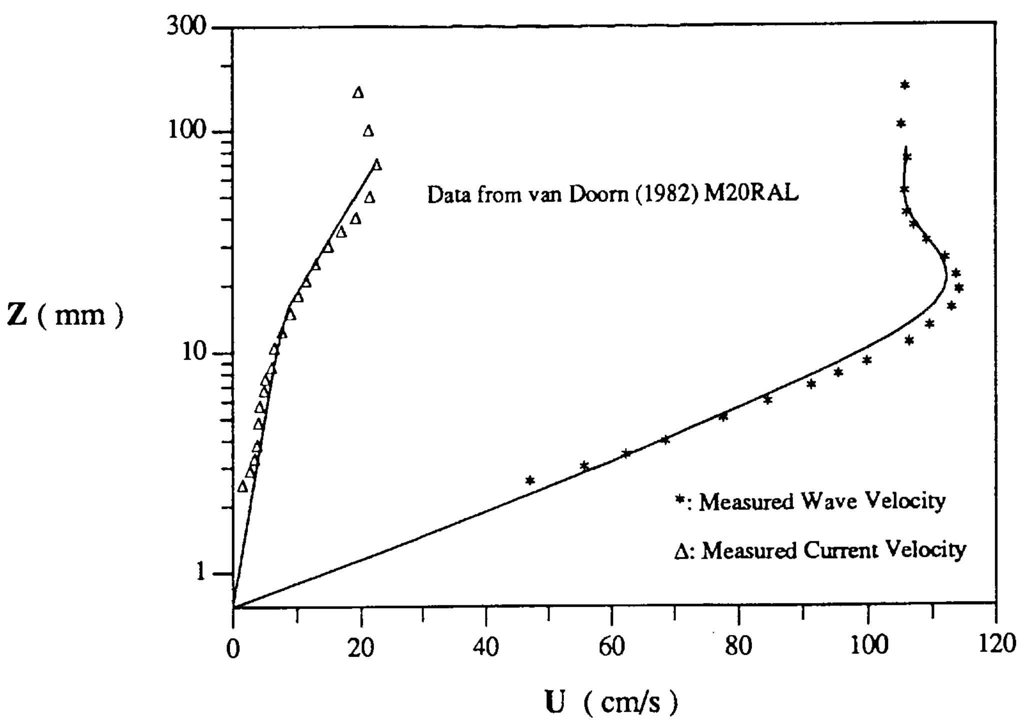

Fig.4.43 The comparison of the present model with experimental data M20RAL from van Doorn (1982)

§4.5.11 CONCLUSIONS

From the study of the eddy viscosities in combined wave–current flows within the range $1.8 < \overline{U}^{*}/\hat{U}_{w}^{*} < 6.5$, the following conclusions can be drawn :

(1) The current eddy viscosity outside the interaction layer is affected little by the wave motion while inside the interaction layer it is increased by the presence of the waves.

(2) The wave eddy viscosity inside the wave boundary layer is independent of current strength $\overline{U}^{*}$

(3) The current eddy viscosity is quite different form the wave eddy viscosity in the boundary interaction layer either from a qualitative view or from a quantitative view.

(6) The present eddy viscosity model gives a good prediction of the velocity fields of combined wave–current flows.

CHAPTER 5

A PRACTICAL EXAMPLE

An Example

As an example, consider the experiment V20RA from van Doorn (1981). The parameters of the combined wave–current flow are : wave height $H = 9.64cm$, wave period $T = 2.0s$, water depth $h = 30cm$, current friction velocity $U_c^* = 2.6cm/s$ and the bed roughness $K_N = 2.1cm$.

[1] What is the amplitude of the free stream velocity just outside the boundary layer?

Based on small–amplitude wave theory, the amplitude of the free stream velocity can be evaluated from the formula

$$|U_\infty(t)| = A\omega = \frac{H\omega}{2\sinh kh} \tag{5.1}$$

Iterating the equation

$$L = \frac{gT^2}{2\pi}\tanh\left\{\frac{2\pi}{L}h\right\} \tag{5.2}$$

we obtain $L \approx 330cm$. Therefore,

$$|U_\infty(t)| = A\omega = \frac{9.64 \times \frac{2\pi}{2}}{2\sinh\left\{\frac{2\pi}{330} \times 300\right\}} \approx 26.3 \text{ cm/s}$$

[2] What is wave friction factor f_w ?

The wave friction factor in the combined flow can be obtained by iterating Eq.(4−125), but here we directly use an explicit formula, which was deduced by You *et al.* (1991a)

$$f_w = 0.108\{A/K_N\}^{-0.343} \qquad \hat{U}^* = \sqrt{0.5f_w}A\omega \tag{5.3}$$

Fig.5.1 shows that the wave friction velocity is well predicted by Eq.(5.3). The details of the measurements given in Fig.5.1, see Table.5.1.

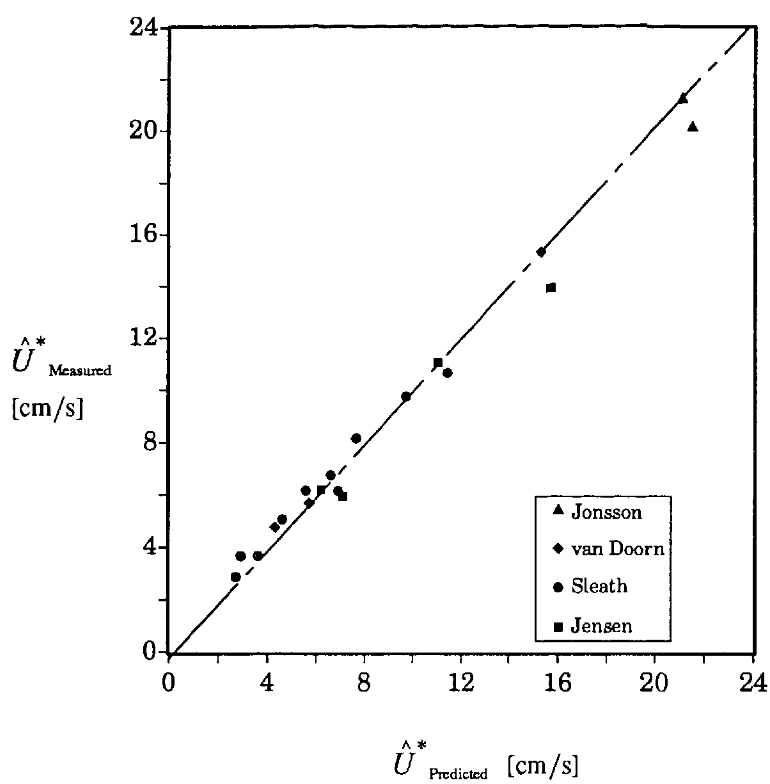

Fig.5.1 The wave friction velocity $\hat{U}^*$ in oscillatory boudnary layer flows calculated via Eq.(5.3)

INVESTIGATORS	TESTS	Log−Fit $\hat{U}^*$ [cm/s]	Integrated f_w $\hat{U}^* = \sqrt{0.5f_w}A\omega$ [cm/s]	$f_w = 0.108(A/K_N)^{-0.343}$ $\hat{U}^* = \sqrt{0.5f_w}A\omega$ [cm/s]
Jonsson & Carlsen (1976)	Test No.1	21.1		21.3
	Test No.2	21.5		20.2
Doorn (1981 &1982)	V00RA	4.3		4.8
	S00RAL	5.7		5.7
	M00RAL	15.3		15.4
Sleath (1986)	Test−3	6.6	6.2	6.8
	Test−4	5.6	5.5	6.2
	Test−5	4.6	4.5	5.1
	Test−6		3.7	3.6
	Test−7		2.9	2.7
	Test−9	7.6	7.2	8.2
	Test−10	6.9	6.7	6.7
	Test−11		3.7	2.9
	Test−14		10.7	11.4
	Test−15		9.8	9.7
Jensen (1989)	Test−12	6.2		6.2
	Test−13	11.0		11.1
	Test−14	6.0		7.1
	Test−15	14.0		15.7

Table.5.1 Comparison of measured wave friction velocities with those predicted by Eq.(5.3)

Therefore,

$$f_w = 0.108 \times \left\{26.3 \times \frac{2.0}{2\pi} \times \frac{1}{2.1}\right\}^{-0.343} = 0.0672$$

$$\hat{U}^* = \sqrt{0.5f_w}A\omega = \sqrt{0.5 \times 0.0672} \times 26.4 = 4.88 \text{ cm/s}$$

[3] What is the apparent roughness K_1 in the combined flow ?

The apparent roughness $K_1 = 30z_1$ can be evaluated from Eq.(4−115)

$$\frac{z_1}{z_o} = 2 \times 2.718^{-\frac{\overline{U}^*}{\hat{U}^*_{cw}}} \left\{\frac{\delta_1}{z_o}\right\}^{1-\frac{\overline{U}^*}{\hat{U}^*_{cw}}}$$

in which

$$\delta_1 = \frac{0.5\varkappa\hat{U}^*}{\omega}$$

Since,

$$\hat{U}^*_{cw} = \left\{\hat{U}^{*2} + \overline{U}^{*2}\right\}^{0.5} = \{4.88^2 + 2.60^2\}^{0.5} = 5.52 \text{ cm/s}$$

$$\delta_1 = \frac{0.5\varkappa\hat{U}^*}{\omega} = 0.5 \times 0.4 \times 4.88 \times \frac{2.0}{2\pi} = 0.31 \text{ cm}$$

Therefore,

$$\frac{z_1}{z_o} = 2 \times 2.718^{-\frac{2.60}{5.52}}\left\{0.31 \times \frac{30}{2.1}\right\}^{1-\frac{2.60}{5.52}} \approx 2.74$$

That is

$$K_1 = 30z_1 = 2.74 \times 2.1 = 5.76 \text{ cm}$$

[4] The current velocity profile in the combined flow ?

The current velocity profile can be calculated from Eqs.(4−111) to (4−113)

$$\overline{U}(z) = \frac{\overline{U}^*}{\varkappa}\left\{\frac{\overline{U}^*}{\hat{U}^*_{cw}}\right\}\ln\frac{z}{z_o} \qquad z_o \le z \le \delta_1$$

$$\overline{U}(z) = \frac{\overline{U}^*}{\varkappa}\left\{\frac{\overline{U}^*}{\hat{U}^*_{cw}}\right\}\left\{\frac{z}{\delta_1} + \ln\frac{\delta_1}{z_o} - 1\right\} \qquad \delta_1 < z \le 2\delta_1$$

$$\overline{U}(z) = \frac{\overline{U}^*}{\varkappa}\ln\frac{z}{z_1} \qquad 2\delta_1 \le z < h$$

The comparison of current velocities calculated by Eqs.(4−111) to (4−113) with experimental data V20RA from van Doorn (1981) is shown Fig.5.2. It is shown that a simple application used above gives a good prediction on the current velocity profile of V20RA for the lower 25% of the water depth.

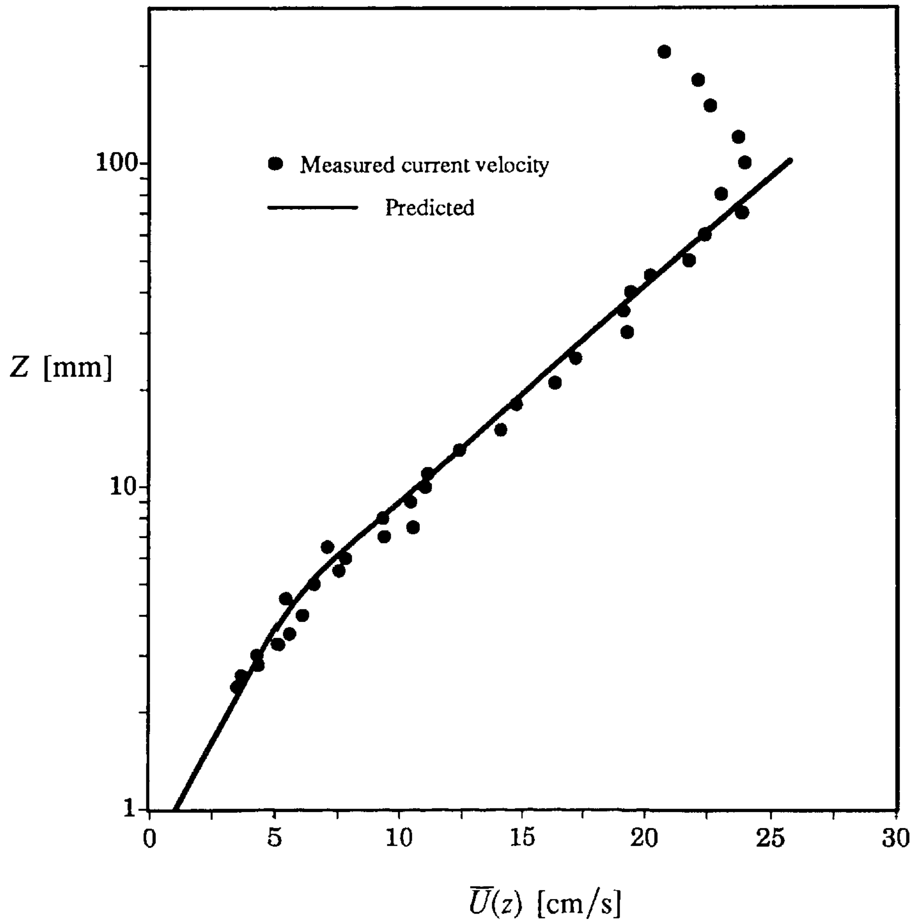

Fig.5.2 A simple application of the present model on experimental data van Doorn (1981) V20RA

CHAPTER 6

CONCLUSIONS AND FURTHER RESEARCH SUGGESTIONS

§6.1. CONCLUSIONS

Through the study of turbulent oscillatory boundary layers without and with currents, new insights into oscillatory boundary layers have been obtained. The conclusions reached in each chapter are as follows:

§6.1.1 OSCILLATORY BOUNDARY LAYERS WITHOUT CURRENTS

(1) The eddy viscosity in turbulent oscillatory boundary layers can be taken as a time–independent and real–valued parameter when a simple harmonic solution is sought for the equation of motion.

(2) For the presently available experimental data with relative roughness K_N/A in the range of $2.8 \times 10^{-4} \sim 2.5 \times 10^{-1}$, the eddy viscosity in the boundary layer has been found to have a distribution which is reasonably described by

$$\varepsilon(z) = \varkappa \hat{U}^* \delta_o \left\{ 1 - \left\{ 1 - \frac{z}{\delta_1} \right\}^2 \right\} \qquad z_o \le z \le \delta_1$$

$$\varepsilon(z) = \varkappa \hat{U}^* \delta_o \qquad \delta_1 \le z \le \delta_w$$

in which

$$\delta_1 = \frac{0.5\varkappa\hat{U}^*}{\omega} \qquad \text{and} \qquad \delta_o = 0.4\delta_1$$

(3) This eddy viscosity model gives an improved prediction of measured velocity fields and bed shear stress in comparison with the former models.

§6.1.2 MASS TRANSPORT VELOCITY UNDER PROGRESSIVE WAVES

(1) The experiments indicated that the maximum Lagrangian mass transport velocity near the bed decreases with increasing bed roughness when $R_\delta < 160$. This is opposite trend to that found by Brebner *et al.* (1966).

(2) The maximum mass transport velocity is approximately proportional to $H^{\frac{4}{5}}$ rather than H^2 as predicted by Longuet–Higgins (1953) for laminar flow.

§6.1.3 OSCILLATORY BOUNDARY LAYRS WITH CURRENTS

(1) Based on experimental data, the current eddy viscosity outside the boundary interaction zone has been found to be independent of the wave motion while inside the boundary interaction zone the current eddy viscosity is increased by the presence of waves.

(2) For presently available experimental data [$1.8 < \hat{U}^*/\overline{U}^* < 6.5$ and $\Phi = 0$], the wave eddy viscosity in the boundary interaction zone is found to be independent of the current strength.

(3) The current eddy viscosity is quite different from the wave eddy viscosity in the boundary layer with respect to both magnitudes and distribution shapes.

(4) Based on experimental data [$1.8 < \hat{U}^*/\overline{U}^* < 6.5$ and $\Phi = 0$], the current eddy viscosity has been found to have a distribution which is reasonably described by

$$\varepsilon_c(z) = \varkappa\hat{U}^*_{cw}z \qquad\qquad z_o \le z \le \delta_1$$

$$\varepsilon_c(z) \;=\; \varkappa \hat{U}^{*}_{cw}\delta_1 \qquad\qquad \delta_1 \le z \le 2\delta_1$$

$$\varepsilon_c(z) \;=\; \varkappa \overline{U}^{*} z \qquad\qquad 2\delta_1 \le z \le d_c$$

and the wave eddy viscosity

$$\varepsilon_w(z) \;=\; \varkappa \hat{U}^{*} \delta_o \left\{ 1 \;-\; \left\{ 1 - \frac{z}{\delta_1} \right\}^2 \right\} \qquad\qquad z_o \le z \le \delta_1$$

$$\varepsilon_w(z) \;=\; \varkappa \hat{U}^{*} \delta_o \qquad\qquad \delta_1 \le z \le \delta_w$$

(5) The present eddy viscosity model gives better predictions of $\overline{U}(z)$ and $\tilde{U}(z,t)$ than the former models.

§6.2. FURTHER RESEARCH SUGGESTIONS

Through the present study, it is found that there are still many aspects worthwhile investigating in the areas of turbulent oscillatory boundary layers. The following suggestions for further research work may be suggested.

(1) For a pure wave motion, good measurements of the velocity amplitude $|U(z,t)|$ and phase shift $\phi(z)$ are needed in order to obtain more reliable eddy viscosity data in the region of $z > \delta_1$ from the formula

$$\varepsilon(z) \;=\; \frac{i\omega \displaystyle\int_z^{\infty} \{A\omega \;-\; |U(z,t)|e^{i\phi(z)}\}\,dz}{\dfrac{\partial}{\partial z}\{A\omega \;-\; |U(z,t)|e^{i\phi(z)}\}}$$

(2) For the mass transport due to progressive waves, there is an urgent need to develop a model for finite amplitude wave conditions in the interior flow.

(3) For the combined wave–current flows, more measurements are needed in order to study the effect of Φ on ε_c and the apparent roughness K_1.

REFERENCES

Abramowitz, M. and Stegun, I. A. (1964). Handbook of mathematical Functions. National Bureau of Standard, Washington, DC.

Agnew, R. (1965). A two layer theory for unsteady flow. *Proc. 2nd Australas. Conf. Hydraul. Fluid Mech.*, pp. 137–157.

Asano, T. and Iwagaki, I. (1984). Bottom turbulent boundary layer in wave–current coexisting system. *Proc. 19th Conf. Coastal Eng.* Houston., pp. 2397–2431.

Baddour, R. E. and Song, S. (1990). On the interaction between waves and currrents. *J. Ocean Eng.*, pp.1–21.

Bagnold, R. A. (1947). Sand movement by waves : some small scale experiments with sand of very low density. *J. Inst. Civ. Eng.,* pp. 447–469.

Bakker, W. T. (1974). Sand concentration in oscillatory flow. *Proc. 14th Conf. Coastal Eng.* Copenhagen, pp. 1129–1148.

Bakker, W. T. and van Doorn, T. (1978). Near bottom velocities in waves with a current. *Proc. 16th Conf. Coastal Eng.* Hamburg, pp. 1394–1413.

Bijker, E. W. (1967). Some considerations about scales for coastal models with movable bed. *Delft Hydraulics Lab.* Pub. No.50.

Bijker, E. W., Kalkwijk, J. P. T., and Pieters, T. (1974). Mass transport in gravity waves on a sloping bottom. *Proc. 14th Conf. Coastal Eng.* Copenhagen, pp. 447–465.

Brebner, A., Askew, J. A., and Law, S. W. (1966). Effect of roughness on mass transport of progressive gravity wave. *Proc. 10th Conf. Coastal Eng.* Tokyo, pp. 175–184.

Brevik, I. (1980). Flume experiment on waves and currents. 1: Rippled bed. *Coastal Eng.*, 3 : 149–177

Brevik, I. (1980). Flume experiment on waves and currents. 2. Smooth bed. *Coastal Eng.*, 4 : 89–110.

Brevik, I. (1981). Oscillatory rough turbulent boundary layers. *J. Waterways, Harbors and Coastal Eng.* Div., ASCE, 107(WW3), pp. 175–188.

Christoffersen, J. B. (1982). Current depth refraction of dissipative water waves. Inst. Hydrodyn. Hydraul. Eng. Tech. Univ. Denmark. Series paper 30.

Christoffersen, J. B. and Jonsson, I. G. (1985). Bed friction and dissipation in a combined current and wave motion. *J. Ocean Eng.*, 12 (5) : 387–423.

Coffey, F. C. and Nielsen, P. (1984). Aspects of wave current boundary layer flows. *Proc. 19th Conf. Coastal Eng.* Houston, pp. 2232–2245.

Coffey, F. C. (1987). Current profiles in the presence of waves and the hydraulic roughness of natural beaches. Ph.D thesis. Dept. of Geography, University of Sydney.

Collins, J.I. (1963). Inception of turbulence at the bed under periodic gravity waves. *J. Geophys. Res.*, 68 (21) : 6007–6014.

Collins, J.I. (1964). Effect of currents on mass transport of progressive water waves. *J. Geophys. Res.*, 69 (6) : 1051–1056.

Davies, A. G. (1986a). A model of oscillatory rough turbulent boundary flow. *Est. Coast. Shelf Sci.*, 23 (3) : 353–374.

Davies, A. C. (1986b). A numerical model of the wave boundary layer. *Cont. Shelf Res.*, 6 (6) : 715–739.

Dean, R. G. (1965). Stream function representation of nonlinear ocean waves. *J. Geophys. Res.*, 70 (18) : 4561–4572.

Doorn, Th. van (1981). Experimental investigation of near–bottom velocities in water waves without and with a current. Report Investigation, Delft Hydraul. Lab. Rep. M1423, Part 1.

Doorn, Th. van (1982). Experimenteel onderzoek naar het snelheidsveld in de turbulente bodemgrenslaag in een oscillerende stroming in een golftunnel. (Experimental investigation of the velocity field in the turbulent bottom boundary layer in an oscillatory water tunnel). *Delft Hydraul. Lab. Rep. No. M1562–1b* (in Dutch).

Dore, B. D. (1982). On the second approximation to mass transport in the bottom boundary layer. *Coastal Eng.*, 6 : 93–120.

Du Toit, C. G. and Sleath, J. F. A. (1981). Velocity measurements close to rippled beds in oscillatory flow. *J. Fluid Mech.*, 112 : 71–96.

Dyke, P. P. G. and Barstow, S. F. (1981). Wave induced mass transport : Theory and experiment. *J. Hydr. Res.*, 19 (2) : 89–106.

Fredsoe, J. (1981a). Mean current velocity distribution in combined waves and currents. Inst. Hydrodyn. Hydraul. Eng. Tech. Univ. Denmark, Prog. Rep.53.

Fredsoe, J. (1981b). A simple model for the wave boundary layer. Inst. Hydrodyn. Hydraul. Eng. Tech. Univ. Denmark, Prog. Rep.54.

Fredsoe, J. (1984). calculation of mean current profile in combined wave–current motion by application of the momentum equation. Inst. Hydrodyn. Hydraul. Eng. Tech. Univ. Denmark, Prog. Rep.55–56.

Fredsoe, J. (1984). Turbulent boundary layers in wave–current motion. *J. Hydraul. Eng.*, ASCE, 110(HY8) : 1103–1120.

George, C. B. and Sleath, J. F. A. (1979). Oscillatory laminar flow above a rough bed. *Proc. 16th Conf. Coastal Eng.* Hambug, pp. 898–910.

George, C. B. and Sleath, J. F. A. (1979). Measurements of combined oscillatory and steady flow over a rough bed. *J. Hydraul. Res.*, 17 (4) : 303–313.

Gradshteyn, I. S. and Ryzhik, I. M (1980). Table of integrals, series and products. Corrected and enlarged edition. Academic Press, New York.

Grant, W. D. (1977). Discussion of Friction factors under oscillatory waves by Kamphuis, J. W. *J. Waterways, Harbors and Coastal Eng.* Div., ASCE, 101(WW4) : 466–467.

Grant, W. D. and Madsen, O. S. (1979). Combined wave and current interaction with a rough bottom. *J. Ceophys. Res.*, 84 (C4) : 179–1808.

Grant, W. D. and Madsen, O. S. (1982). Moveable bed roughness in unsteady oscillatory flow. *J. Geohys. Res.*, 87 (C1) : 469–481.

Grant, W. D. and Madsen, O. S. (1982). Movable bed roughness in unsteady oscillatory flow. *J. Geophys, Res.* 87 (C1) : 469–481.

Grant, W. D. and Madsen, O. S. (1986). The continental shelf bottom layer. *Ann. Rev. Fluid Mech.*, 18 : 265–305.

Hino, M., Kashiwayanagi, M., Nakoyama, A. and Hara, T. (1983). Experiments on the turbulence statistics and the structure of a reciprocating oscillatory flow. *J. Fluid Mech.,* 131 : 363–400.

Horikawa, K. and Watanabe, A. (1968). Laboratory study on oscillatory boundary layer flow. *J. Coastal Eng. Jap.*, 11 : 13–28.

Hsu, J. R. C. (1986). Rough turbulent boundary layer in short–crested waves. *Proc. 20th Coastal Eng.*, pp. 271–285.

Hsu, J. R. C., Tsuchiya, Y. and Silvester, R. (1979). Third–order approximation to short–crested waves. *J. Fluid Mech.*, 90 : 179–196.

Hsu, J. R. C., Silvester, R. and Tsuchiya, Y. (1979). Boundary layer velocities and mass transport in short–crested waves.. *J. Fluid Mech.*, 90 : 179–196.

Hunt, J. N. (1952). Viscous damping of waves over an inclined bed in a channel of finite width. La Houille Blanche. No.7, pp. 836–842.

Inman, D. L. (1957). Wave generated ripples in nearshore sands. Tech. Memo. 100, USCE, Beach Erosion Board.

Inman, D. L. and Bowen, A. J. (1962). Flume experiments on sand transport by waves and currents. *Proc. 8th Conf. Coastal Eng.* Mexico, pp. 137–150.

Isaacson, M. de St. Q. (1976a). Mass transport in the bottom boundary layer of cnoidal waves. *J. Fluid Mech.*, 74 : 401–413.

Isaacson, M. de St. Q. (1976b). The second order approximation of cnoidal waves. *J. Fluid Mech.*, 78 : 445–457.

Iwagaki, Y. and Asano, T. (1980). Water particle velocity in wave–current system. *Coastal Eng. Japan.* 23 : 1–14.

Jacobs, S. J. (1984). Mass transport in a turbulent boundary layer under a progressive water wave. *J. Fluid Mech.,* 146 : 303–312.

Jackson, P. S. (1981). On the displacement height in the logarithmic velocity profile. *J. Fluid Mech.*, 111 : 15–25.

Jensen, B. L. (1989). Experimental investigation of turbulent oscillatory boundary layers. Series Paper 44. Technical University of Denmark, Institute of Hydrodynamics and Hydraulic Engineering. Lyngby, Demark.

Jensen, B. L., Sumer, B. M. and Fredsoe, J. (1989). Turbulent oscillatory boundary layers at high Renolds numbers. *J Fluid Mech.*, 206 : 265–297.

Johns, B. (1970). On the mass transport induced by oscillatory flow in a turbulent boundary layer. *J. Fluid Mech.,* 43 : 177–185.

Johns, B. (1975). The form of the velocity profile in a turbulent shear wave boundary layer. *J. Geophys. Res.*, 80 (36) : 5109–5012.

Johns, B. (1977), Residual flow and boundary shear stress in the turbulent bottom layer beneath waves. *J. Phys. Oceanogr.*, 7 : 733–738.

Jonsson, I. G. (1963). Measurements in the turbulent wave boundary layer. *Proc. 10th Congr. IAHR.* London, pp. 85–92.

Jonsson, I. G. (1966). Wave boundary layer and friction factor. *Proc. 10th Conf. Coastal Eng.*, Tokyo, pp. 127–148.

Jonsson, I. G. and Carlsen, N. A. (1976). Experimental and theoretical investigations in an oscillatory turbulent boundary layer. *J. Hydraul. Res.*, 14 (1) : 45–60.

Jonsson, I. G. (1980). A new approach to oscillatory rough turbulent boundary layers. *J. Ocean Eng.*, 7 : 109–152.

Justesen, P. (1988). Turbulent wave boundary layers. Series Paper 43. Technical University of Denmark, Institute of Hydrodynamics and Hydraulic Engineering. Lyngby, Demark.

Justesen, P. (1988). Prediction of turbulent oscillatory flow over rough beds. *Coastal Eng.,* 12 : 257–284.

Kajiura, K. (1964). On the bottom friction in an oscillatory current. Bull. Earthquake Res. Inst., Univ. Tokyo. 42 : 147–74.

Kajiura, K. (1968). A model of the bottom boundary layer in water waves. *Bull. Earthquake Res. Inst.*, Vol.46, pp.75–123.

Kalkanis, G. (1957). Turbulent flow near an oscillating wall. Beach Erosion Board. Tech. Memo. 97.

Kalkanis, G. (1964). Transportation of bed material due to wave action. U.S. Army C.E.R.C. Tech. Memo. 2.

Kamphuis, J. W. (1974). Determination of sand roughness for fixed beds. *J. Hydr. Res.*, 12 (2) : 193–203.

Kamphuis, J. W. (1975). Friction factors under oscillatory waves. *J. Waterway, Harbors and Coastal Eng.* Div., ASCE, 101(WW2) : 135–144.

Kemp, P. H. and Simons, R. R. (1982). The interaction between waves and a turbulent current. Wave propagating with the current. *J. Fluid Mech.*, 116 : 227–250.

Kemp, P. H. and Simons, R. R. (1983). The interaction between waves and a turbulent current. Wave propagating against the current. *J. Fluid Mech.,* 130 : 73–89.

Kesteren, W. G. M. van and Bakker, W. T. (1984). Near bottom velocities in waves with a current. *Proc. 19th Conf. Coastal Eng.* Houston, pp. 1161–1177.

Lamb, H. (1932). Hydrodynamics. Cambridge University Press.

Launder, B. E. and Spalding, D. B. (1972). Mathematical models of turbulence. Academic Press, New York.

Liu, P. L–P. (1977). Mass transport in water waves propagated over a permeable bed. *Coastal Eng.*, 1 : 79–96.

Lofquist, K. E. B. (1978). Sand ripple growth in an oscillatory flow water tunnel. C.E.R.C. Tech. Paper No. 78–5.

Lofquist, K. E. B. (1980). Measurements of oscillatory drag on sand ripples. *Proc. 17th Conf. Coastal Eng.*, Sydney, pp. 623–634.

Longuet–Higgins, M. S. (1953). Mass transport in water waves. Philos. Trans. Roy. Soc. Ser. A., Vol. 245, pp. 535–581.

Longuet–Higgins, M. S. (1956). The mechanics of the boundary layer near the bottom in a progressive wave. *Proc. 6th Conf. Coastal Eng.,* Miami, pp. 184–193.

Lundgren, H. (1972). Turbulent currents in the presence of waves. *Proc. 13th Conf. Coastal Eng.,* Vancouver, pp. 623–634.

Madsen, O. S. and Grant, W. D. (1977). Quantitative description of sediment transport by waves. *Proc. 15th Conf. Coastal Eng.*, pp. 1093–1112.

Manohar, M. (1955). Mechanics of bottom sediment movement due to wave action. Beach Erosion Board. Tech. Memo. 75.

Mei, C. C., Liu, P. L–F and Carter, T. G. (1972). Mass transport in water waves. M.I.T. Dept. Civil Eng. Ralph M. Parsons Lab. Rep. 146.

Myrhaug, D. (1982). On a theoretical model of rough turbulent wave boundary layers. *J. Ocean Eng.,* 10 : 190–220.

Myrhaug, D. and Slaattelid, O. H. (1989). Combined wave and current boundary layer model for fixed rough seabeds. *J. Ocean Eng.,* 16 : 119–142.

Myrhaug, D. (1989). A rational approach to wave friction coefficients for rough, smooth and transitional turbulent flow. *Coatal Eng.,* 13 : 11–24.

Nakato, T., Locher, F. A., Clover, J. R. and Kennedy, J. F. (1977). Wave entrainment of sediment from rippled beds. *J. Waterw. Port Coastal Ocean* Div. ASCE. 103 (WW1) : 83–99.

Nielsen, P. (1979). Some basic concepts of wave sediment transport. Inst. of Hydrodyn. Hydraul. Eng. Tech. Univ. of Denmark. Series Paper 20.

Nielsen, P. (1985). On the structure of oscillatory boundary layer. *Coastal Eng.,* 9 : 261–276.

Nielsen, P., Sena, R.N. and You, Z.J. (1990). Discussion on The Roughness Height under Waves by Raudkivi, A.J. *J. Hydr. Res.,* 28 (5) : 645–647.

Nielsen, P. (1992). Coastal bottom boundary layers and sediment transport. World Scientific Publishers, Singapore. (in press)

Nikuradse, J. (1933). Laws of flow in rough pipes. National Advisory Committee on Aeronautics, Tech. Mem. 1292.

O'Connor, B. and Yoo, D. (1988). Mean bed friction of combined wave–current flow. *Coastal Eng.*, 12 : 1–21.

Prnatl, L. (1927). Uber den reibungswiderstand stromender luft. Ergebn. d. Aerodyn. Versuchsanstalt zu Cottingen, III Lief.

Prantl, L. and Tietjens, O. G. (1934). Fundamentals of hydro and aeromechanics. McGraw–Hill, New York.

Raudkivi, A. J. (1963). Study of sediment ripple formation. *J. Hydraul. Div.* ASCE. 89 (HY2) : 15–33.

Raudkivi, A. J (1976). Loose Boundary Hydraulics. 2nd ed. pergamon Press, Great Britain.

Raudkivi, A. J. (1988). The roughness height under waves. *J. Hydr. Res.,* 26 : 569–584.

Russell, R. C. H. and Osorio, J. D. C. (1958). An experimental investigation of drift profile in a closed channel. *6th Conf. on Coastal Eng.*, pp. 293–305.

Schlichting, H. (1960). Boundary Layer Theory. McGraw–Hill Book Co. Inc., U.S.A.

Sheng, Y. P. (1986). Modeling turbulent bottom boundary layer dynamics. *Proc. 20th Conf. Coastal Eng.*, pp.1496–1508.

Simons, R. R., Grass, A. J. and Kyriacou, A. (1988). The influence of currents on wave attenuation. *Proc. 21st Conf. Coastal Eng.* Spain, pp. 363–376.

Sleath, J. F. A. (1970). Measurements close to the bed in a wave tank. *J. Fluid Mech.*, 42 : 11–123.

Sleath, J. F. A. (1973). Mass transport in water waves of very small amplitude. *J. Hydr. Res.*, 11 (4) : 369–383.

Sleath, J. F. A. (1974). Mass transport over a rough bed. *J. Mar. Res.* 32 (1) : 13–24.

Sleath, J. F. A. (1982). The effect of jet formation on the velocity distribution in oscillatory flow over flat beds of sand or gravel. *Coastal Eng.,* 6 : 151–177.

Sleath, J. F. A. (1984). Measurements of mass transport over a rough bed. *Proc. 19th Conf. Coastal Eng.*, pp. 1149–1159.

Sleath, J. F. A. (1984). Sea Bed Mechanics. John Wiley, New York.

Sleath, J. F. A. (1987). Turbulent oscillatory flow over rough beds. *J. Fluid Mech.*, 182 : 369–409.

Sleath, J. F. A. (1990). Velocities and bed friction in combined flows. *Proc. 22nd Conf. Coastal Eng.* Delf Netherlands, pp. 450–463.

Sleath, J. F. A. (1991). Velocities and shear stress in wave–current flows. *J. Geophys. Res.*, 96 (8) : 15,237–15,244.

Smith, J. D. (1977). Modeling of sediment transport on continental shelves. In the Sea, Vol.6, ed. Goldberg, E.K., McCave, I. N., O'Brien, J. J. and Steele, J. H. Wiley Interscience, New York. pp. 539–577.

Stokes, G. G. (1847). On the theory of oscillatory waves. Trans. of the Camb. Phil. Soc. Vol. VIII.

Swan, C. (1989). Convective within an experimental wave flume. *J. Hydr. Res.*, 28 (3): 273–282.

Swan, C. and Sleath, J. F. A. (1990). A second approximation to the time–mean Lagrangian drift beneath a series of progressive gravity waves. *J. Ocean Eng.*, 17 : 65–79.

Swart, D. H. (1974). Offshore sediment transport and equilibrium beach profiles. Delft Hydraulics Lab. Publ. No.131.

Swart, D. H. (1976). Coastal sediment transport. Computation of longshore transport. Delft Hydraulics Lab. Rep. R968.

Tanaka, H. and Shutom N. (1981). Friction coefficient for a wave–current coexistent system. *Coastal Eng. Japan.*, 24 : 105–128.

Tanaka, H., Chian, C. S. and Shuto, N. (1983). Experiments on an oscillatory flow accompanied with a unidirection motion. *J. Coastal Eng. Japan.*, 26 : 19–36.

Thomas, G. P. (1981). Wave–current interactions : an experimental and numerical study. Part 1. Linear waves. *J. Fluid Mech.*, 110 : 457–474.

Trowbridge, J. and Madsen, O. S. (1984). Turbulent wave boundary layers. 1. Model formulation and first order solution. *J. Geophys. Res.*, 89 (C5) : 7989–7997.

Trowbridge, J. and Madsen, O. S. (1984). Turbulent wave boundary layers. 2. Second order theory and mass transport. *J. Geophys. Res.*, 89 (C5) : 7999–8007.

Ullah, M. H. and Sharp, B. B. (1989). Eulerian mean velocity under large amplitude waves. *Proc. 9th Australasian Coastal and Ocean Eng.* Adelaide, pp. 74–77.

Unluata, U. and Mei, C. C. (1970). Mass transport in water waves. *J. Geophys. Res.*, 75 (36) : 7611–7618.

Vincent, G. E. (1957). Contribution to the study of sediment transport on a horizontal bed due to wave action. Proc. 6th Conf. Coastal Eng. Florida, U.S. pp.

Visser, P. J. (1986). Wave basin experiments on bottom friction due to current and waves. Proc. *20th Conf. Coastal Eng.*, pp. 807–821.

Wang, H., Sunamura, T. and Hwang, P. (1982). Drift velocity at the wave breaking point. *Coastal Eng.,* 6 ; 121–150.

Wang, H. and Liang, S. S. (1975). Mechanics of suspended sediment in random waves. *J. Geophys. Res.*, 80 (24) : 3488–3494.

Yoo, D. and O'Connor, B. A. (1987). Bed friction model of wave–current interacted flow. *Proc. Spec. Conf. Coastal Hydrodynamics*, ASCE. pp. 93–106.

You, Z.J., Wilkinson, D.L and Nielsen, P. (1991a). Velocity distributions of waves and currents in combined flow. *Coastal Eng.,* 15: 525–543.

You, Z.J., Wilkinson, D.L and Nielsen, P. (1991b). Near bed net drift under waves. *10th Australasian Conference on Coastal and Ocean Engineering.* Auckland, pp. 183–187.

You, Z.J., Nielsen, P. and Wilkinson, D.L (1991c). Velocity distribution in turbulent oscillatory boundary layer. *Coastal Eng.,* 16.(– –) (in publish)

You, Z.J. (1992). Eddy Viscosities and Velocities in Combined Wave–Current Flows. *Ocean Eng.*, (in publish)

You, Z.J. (1992). Discussion on an Evaluation of Expressions for Wave Energy Dissipation due to Bottom Friction in the Presence of Currents by Tolman, H. L. (1992). *Coastal Eng.*, 16 : 165–179. (in publish)

APPENDIX

Smooth Bed [perspex]		Sand Bed [d = 2mm]		Gravel Bed [d = 25mm]	
H [mm]	$\overline{U}$ [mm/s]	H [mm]	$\overline{U}$ [mm/s]	H [mm]	$\overline{U}$ [mm/s]
2.4	0.8	2.5	0.6	2.5	0.5
2.5	0.7	3.3	0.8	3.1	0.6
3.4	1.1	4.0	0.8	3.7	0.7
3.7	1.2	4.9	1.0	5.1	0.8
4.1	1.1	5.6	1.2	7.0	1.2
4.6	1.2	7.5	1.5	8.9	1.4
5.0	1.4	8.2	1.6	10.0	1.7
6.8	1.6	9.1	1.8	14.0	2.0
8.7	2.0	10.0	2.0	21.0	2.7
12.0	2.5	11.5	2.2	29.0	3.0
12.3	2.7	12.0	2.3	35.0	3.8
14.9	3.1	13.0	2.4	39.0	4.0
15.0	3.4	14.0	2.5	50.0	4.0
21.0	4.0	17.0	2.9	55.0	4.1
24.0	4.4	21.0	3.4		
27.0	5.3	26.0	3.6		
31.0	5.4	34.0	4.4		
38.0	5.9	39.0	4.7		
38.3	6.7	45.0	4.8		
44.0	8.0	51.0	5.0		
52.0	8.6	60.0	4.5		
Wave Period T = 1.0s Water Depth h = 0.30m					